Sensitivity Analysis of Fine Sediment Transport in the Humber Estuary

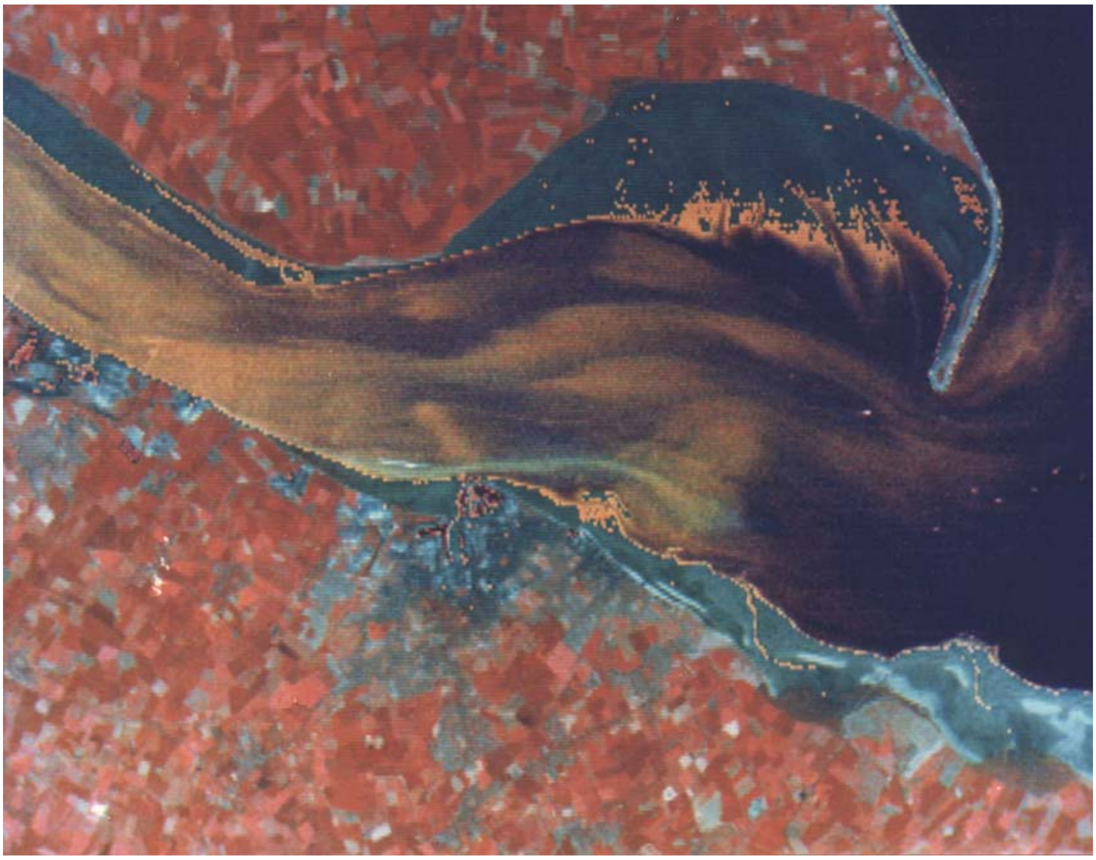

M.Sc. Thesis Report, Delft, October 2003

T.J. Vermeulen

Supervisors:

Prof. dr. M.J.F. Stive,	Delft University of technology		
dr. J.C. Winterwerp,	Delft University of technology	&	WL | Delft Hydraulics
dr. Z.B. Wang,	Delft University of technology	&	WL | Delft Hydraulics
dr. J.A. Roelvink,	Delft University of technology	&	WL | Delft Hydraulics

TU Delft
Delft University of Technology

WL | delft hydraulics

Preface

This report describes the study 'Sensitivity analysis of fine sediment transport in the Humber estuary', which has been carried out as a master thesis, as part of the study Civil Engineering at Delft University of Technology. The study concerns the net-upward transport mechanisms of fine sediment transport.

I would like to thank my supervisors from the WL | Delft Hydraulics and Delft University of technology, dr. ir. J.C. Winterwerp, dr. ir. Z.B. Wang, dr. ir. J.A. Roelvink, and Prof. dr. ir. M.J.F. Stive for sharing their knowledge and support during this study.

Special thanks goes out to Han Winterwerp and Johan Boon from WL | Delft Hydraulics for the regular exchange of experiences and results during this sensitivity study. Last words of thanks go out to M.M. Bedaux de Jonge for sharing her interest and experience in writing 'Oxford' English.

Tjaard Vermeulen
October 2003, Delft

Contents

Appendices

List of Figures

List of Tables

List of Symbols

Symbol	Units	Meaning
S	psu	Salinity, practical salinity unit
CL	‰	Salinity weight ratio
k_s	m	Nikuradse roughness height
C	$kg.m^{-2}$	Mass sediment concentration
T	$kg.s^{-1}.m^{-2}$	Mass sediment flux
d	m	Depth to bed from reference datum (positive down)
z	m	Vertical Cartesian coordinate
IM1	$g.m^{-3}$	Concentration of inorganic matter number one
IM1S1	g	Inorganic matter in sediment layer number one
IM1S1M2	$g.m^{-2}$	Inorganic matter in sediment layer number one
w_s	$m.s^{-1}$	Sediment fall velocity
Θ	°Celsius	Temperature
ρ	$kg.m^{-3}$	Local fluid density (including salinity and temperature)
τ_b	$N.m^{-2}$	Bed shear stress
Hs	m	Significant wave height
ξ	m	Water surface elevation above reference datum
S_b	$kg.m^{-2}\,s^{-1}$	Bed-load sediment transport
u, v, w	$m.s^{-1}$	Eularian velocity components in Cartesian coordinates
Notation: $\bar{\ }$	-	Depth averaged value
Notation: ´	-	Difference between the depth averaged and the actual value at that level
Notation: ˆ	-	Amplitude

List of Abbreviations

Abbreviations	Meaning
CD	Chart datum, level of lowest astronomical tide
EstProc	Estuary Research Project
ETM	Estuarine turbidity maximum
FSI	Fresh-salt water interface
HESMP2	Humber Estuary Shoreline Management Plan 2
ISE-model	Initial sedimentation and erosion model
MLWS[1]	Mean low water spring
MHWS	Mean high water spring
MLWN	Mean low water neap
MLWS	Mean low water spring
HWS	High water slack period
LWS	Low water slack period
ΔWS	Difference in slack water period (HWS – LWS)
SPM	Suspended particle matter
ES-processes	Erosion and sedimentation processes
E	Erosion
D	Deposition
LCMS	Low-concentration mud suspensions
HCMS	High-concentration mud suspensions
ZUNO-model	(in Dutch) Zuiderlijk Noordzee model
Delft3D-Delwaq	Water Quality Module within the Delft3D framework
Delft3D-Flow	Hydrodynamic module within the Delft3D framework

[1] The values of MHWS, MLWS, MHWN and MLWN vary from year to year with a cycle of approximately 18.6 years.

Summary

The ability to predict the movement of cohesive sediments within estuarine waters has a significant economical and ecological importance in development of new engineering works and the maintenance of existing installations. Therefore, the ‘Department for Environment, Food & Rural Affairs’ funds the Estuary Research Project (EstProc). The aim of EstProc is to innovative and fundamental research in estuarine hydrodynamics, sediments and biological interactions. Within the EstProc project the Humber estuary is chosen as study area, to improve the understanding of the processes involved in transport and furthermore improve the modelling of fine sediments.

This report describes a study on the processes relevant for the up-estuary transport of fine sediment in the Humber estuary. The aim of this study is to improve the knowledge of the influence of three key processes on the net up-estuary transport of fine grained sediment in the Humber estuary. The key processes that will be focused on are:

1. Tidal asymmetry
2. Gravitational circulation
3. Channel - Shoal interaction

After the calibration of the hydrodynamic model Delft3D-Flow and the set-up of the initial sedimentation and erosion model Delft3D-Delwaq, the key processes are studied in the form of a sensitivity analysis.

Non-linear interactions of tidal components are of paramount importance to the sediment transport, since they can give rise to a net, tide averaged, sediment flux. The tidal asymmetry depends on the sea-boundary conditions and the local generation of higher components. Depending on the bed status, an asymmetry in slack water periods or in combination with an asymmetry in peak velocity magnitude is of importance to net up-estuary sediment transport. This analysis describes the sensitivity of the tidal asymmetry with respect to slack periods and peak velocities on small changes in the M_4 sea-boundary condition. Tidal asymmetry usually refers to the distortion of the predominant semi-diurnal tide with its overtides. Therefore we restrict ourselves in the first analysis to the asymmetry due to the semi-diurnal (M_2) tide and its first overtide (M_4). This asymmetry can be described by the relative phase-difference and the amplitude ratio of the depth averaged velocity components of M_2 and M_4. Slack water period asymmetry in the second analysis is derived from the difference in periods of low velocity magnitude during high water slack and low water slack.
Peak velocity asymmetry is flood-dominant throughout the estuary and increases in magnitude up-estuary. Slack water period asymmetry due to tidal components M_2 and M_4 shows a different result than analysis of low velocity magnitude. Thus it can be concluded that analysis of only components M_2 and M_4 is not sufficient to describe slack water period asymmetry in the Humber estuary. Slack water period analysis of low velocity magnitude reproduces a flood dominant asymmetry in the outer estuary and in the inner estuary. The high sensitivity of tidal asymmetry for M_4 boundary conditions in the outer estuary is consistent with results found in a morphological model (WL | Delft Hydraulics (z3451)). Tidal asymmetry in the inner estuary is primarily locally generated and therefore less sensitive to small changes in the M_4 sea-boundary condition.

Horizontal density gradients can generate a vertical circulation in the system resulting in a net up-estuary sediment transport. Three factors can cause this gravitational circulation: salinity differences, temperature differences and differences in concentration of solid matter. During this sensitivity study the effect of gravitational circulation on net up-estuary fine sediment transport is limited to density gradients due to salinity.
Integrating of the gross discharges and transport in longitudinal direction gives the net distribution of discharge and fine sediment transport. From this analysis follows that in longitudinal direction gravitational circulation results in a net up-estuary fine sediment transport.

In the Humber estuary-channel, and especially -mouth, large longitudinal gross ebb (export) and flood (import) transports of fine sediments occur. If part of the sediments entering the system during flood is deposited in intertidal areas, a net import of fine sediments is the possible result. In the intertidal areas, bedshear stresses play an important role in the overall sediment import. The sensitivity of net up-estuary transport on channel-shoal interaction is analyzed by a change in bed roughness in the SE-processes. The main conclusion from this analysis is that, as bed roughness increases, a lower amount of fine sediments is net imported. Whereas, -with the exception of the areas Skeffling clays and Easington clays- the net transport in transversal direction increases for the ‘rough bed’-simulation. This process can be explained by a lower deposition in the deeper parts of the estuary, resulting in a higher amount of material that reaches the intertidal areas.

Besides the three key processes that are focused on, several other processes can be of importance. The literature survey shows the high variability in conditions due to biological, chemical and seasonal processes. Knowledge of the influence of this variability on net fine sediment import and distribution can be improved by additional work that needs to be done.

The understanding of the separate fine sediment transport processes should lead to an integrated model where the insight of the relative effects can be applied. Eventually different grain sizes, with different trapping mechanisms, can be combined to model a more realistic estuarine system that can be used as a management tool.

1 Introduction

1.1 Problem definition

1.1.1 Problem analysis

The ability to predict the movement of cohesive sediments within coastal, estuarine or inland waters has a significant economical and ecological importance in development of new engineering works and the maintenance of existing installations. Furthermore, government politics have become increasingly aware of the immense ecological value of delicate estuarine systems. In attempts to improve the ecological value of the system and to combat tidal flooding of lowland coastal areas, 'managed retreat' of sea defences can be taken into consideration in shoreline plans. On several formally reclaimed salt-marshes the coast line is then allowed to recede to a more natural line of defence, thus creating wetlands. The ecological value of the wetlands is partly determined by the presence and the physics of cohesive fine sediments. Successful development, e.g. 'managed retreat', depends on thorough knowledge of fine sediment dynamics in estuaries. In order to predict the response of complicated systems, process-based computer programs have to be used as a helping hand. At this moment modelling of the complete process of fine sediment transport in shallow water, characteristic for wetlands needs further improvement.

1.1.2 Field of research

WL | Delft Hydraulics participates in the Estuary Research Project (EstProc) funded by the Department for Environment, Food & Rural Affairs. The aim of EstProc is to innovative and fundamental research in estuarine hydrodynamics, sediments and biological interactions. The main objectives of EstProc are:

- Acquiring improved understanding of hydrodynamic processes in estuaries
- Undertaking investigations into sedimentary processes in estuaries
- Investigating interactions between biological and sedimentary processes in estuaries.

This fundamental new research will stimulate further development of the management tools for estuary morphology, water quality and ecology.

In order to improve the understanding of the processes involved in transport of fine sediments and furthermore improve the modelling, we will first focus on a single estuary. It was agreed that WL | Delft Hydraulics would focus on the Humber estuary, as ample data and knowledge is available. Moreover, WL | Delft Hydraulics carried out some studies on the Humber estuary in the past.

Observations in several estuaries established the existence of gradients of fine-grained suspended sediments from the tidal inlets, where concentrations are comparatively low, up-estuary. Hence, up-estuary transport mechanism must exist to keep this gradient intact when the estuaries have the following characteristics:

- no net erosion within the estuary,
- the water masses are rapidly refreshed by tidal motion (i.e. days or weeks) and
- a net export of water due to river inflow.

Several authors (e.g. Van Straaten and Kuenen (1957), Postma (1967), Dronkers (1985) and many others) identified processes that could trap fine sediments -even with a high flushing rate- and a net down-estuary discharge.

- tidal asymmetry
- gravitational circulation and
- channel shoal interaction

Other processes that can be of importance are:

- sedimentation and erosion processes in combination with lag effects,
- waves that stir up sediments, especially from shallow areas and
- large-scale horizontal circulations differentiating in ebb and flood paths.

Besides the complicated interaction between large-scale en small scale processes that can cause the import of fine sediments there is a lack of insight in the relative importance of the processes.

1.1.3 Objective

The objective of this study is to improve the knowledge of the influence of three key processes on the net up-estuary transport of fine grained sediment in the Humber estuary.

The key processes that will be focused on are:

1. Tidal asymmetry
2. Density effects / River flow
3. Channel - Shoal interaction

Besides these three key processes there are several other processes that may have influence on the main phenomena. However, their effect will not be explicitly accounted for instead it will be assessed by induction.

1.2 Set-up of the study

Approach of the study

At first a literature study was performed in order to discover the relevant knowledge about the Humber estuary. After this site analysis the possible mechanisms that can influence net sediment transport were studied.

In order to study the influence of the three key processes on the net transport of fine sediments, the study is carried out in the form of a sensitivity analysis. After studying the literature, the model previously used in a morphological study is tested. If necessary the model is adjusted to new demands of the sensitivity analysis and validated against measurements. The aim of calibration is to get the hydrodynamic conditions (tide, river discharge and currents) in agreement with the data measured at several stations. This can be done based on earlier model calibrations.

Sensitivity analysis
The processes focussed on are mentioned in section 3.2 'Literature survey of transport processes of cohesive sediments'. In the sensitivity analysis a calibrated Delft3D model is used to study various processes that can drive fine-grained sediment import. The main interest of the analysis is to study the relative effect of a process on fine-grained sediment import into the system. Depending on the phenomenon to be studied, process parameters are varied and a choice will be made in modelling solely the hydrodynamics or in collaboration with the sediment module in Delft3D-Delwaq. The most important processes for fine sediments transport in shallow basins are discussed in section 3.2 'Literature survey of transport processes of cohesive sediments'. From these processes, the following are studied in the sensitivity analysis.

Tidal asymmetry;

- By studying the sensitivity of tidal asymmetry on a M_2 tide sea boundary condition combined with its first overtide M_4. In this study only the asymmetry in peak velocity and slack water period is studied, by analyzing the relative phase and amplitude ratio of astronomical components M_2 and M_4 throughout the estuary.

Gravitational circulation;

- By comparing net sediment transport, between homogeneous and non-homogeneous density simulations, insight can be gained on the effect of gravitational circulation on the net sediment transport. If a 3D simulation with homogeneous density and a 2Dh simulation show comparable results, these simulations are used to study the effect of gravitational circulation. Else two 3D simulations with homogeneous and non-homogeneous density are used.

Channel - Shoal interaction;

- By comparing simulations with changing global roughness values in the ES-processes, the sensitivity of net sediment transport on the storage on intertidal areas can be studied. In this study 2Dh and 3D reference runs are compared with simulations with equal hydrodynamics and a higher global roughness in the ES-processes.

1.2.2 Outline of the report

The first chapter describes the problem definition which consequently results in the aim of this study.

In the second chapter a description is given of the Humber estuary in ecological and physical terms, followed by a literature survey on the sediment transport in the Humber.

Chapter three elaborates on the literature survey, focusing on small and large scale processes of cohesive sediments in shallow basins. Besides a description of the key processes mentioned in section 1.1.3 ‘Objective’, a number of transport processes that could be of influence are described as well.

Chapter 4 ‘Model set-up’ describes the numerical model used in a previous morphological study. Additionally the adjustments and the calibration of the model used in this study are described. In section 4.3 ‘Set-up of the Sediment Transport Model’ the set-up of the sediment transport model is described.

The model developed in Chapter 4 is used for the sensitivity analyses. The sensitivity analyses of the three key processes are described in chapter 5.

In the last chapter 6 ‘Conclusions and recommendations’ the conclusions of the studies are summarized and recommendations for possible follow-up studies are listed.

2 The Humber estuary

2.1 Description of the Humber estuary

Introduction
The United Kingdom lies on a wide continental shelf bordering the North Atlantic Ocean and possesses a coastal zone of great physical and ecological diversity, with many large centres of population, commerce and industry. Natural factors have caused the physical environment of the coastal zone to change markedly with time. These changes include for example, cliff erosion and estuarine filling by sediment.

The Humber estuary on the east coast of England is one of the largest UK estuaries with a tidal intrusion of 120 km and a maximum width of 15 km. The estuary receives drainage principally from the rivers Trent and Ouse, draining an inland area of more than 24,000 km^2 which is almost one/fifth of England. The tidal wave inside the estuary is highly asymmetrical, with strong flood currents bringing sediment into the estuary from the North Sea. Most of the 'marine' sediments come from erosion of the Holderness Cliffs, just north of the estuary-mouth (see Figure 2-1 Location map Humber). Besides the 'marine' sediments the rivers deposit 'riverine' sediments as well.

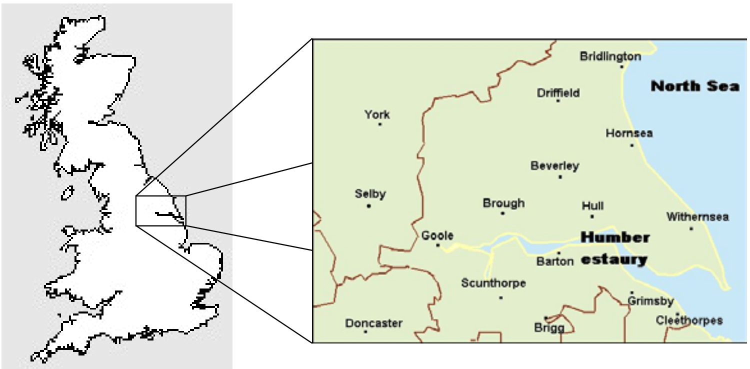

Figure 2-1 Location map Humber estuary

From medieval times onward, the low-lying areas in the Humber Estuary and in adjoining rivers experienced a number of drainage improvements and reclamation. Reclamation was accompanied by various phases of port development and industrialisation, culminating in the current configuration of the estuary. Hull on the north side of the Humber is the UK's leading timber port, and is the only passenger port on the Humber estuary, handling some 15,000 ship movements and 500,000 passengers every year.

Morphological development
Detailed bathymetric evidence available over the past 150 years has demonstrated that a period of sediment accretion ended in the 1950's and was superseded by net erosion in the estuary. Whether this transition is the result of natural processes or of anthropogenic interference is subject of ongoing research. Fragmentary evidence may be interpreted as showing a damped oscillation between flood and ebb asymmetry in the Humber estuary over the Holocene period. The oscillations occur with an increasing frequency towards the present, suggesting a movement towards a tidal symmetrical equilibrium (Pethick, 1994 from Hardisty, 1999). Knowledge on this evolution would be of great importance since it could be used to predict the future development of the estuary.

2.2 Physical description of the Humber estuary

2.2.1 Bathymetry

A schematisation of the bathymetry of the Humber estuary is shown in Figure 2-2. A 6 km long spindly peninsula of sand and shingle that hooks into the northern mouth of the Humber estuary was built. After construction, flats of muddy sands have been a built up in its shelter. The bed of the Humber consists of sand gravel, silt and bed rock. In shallow areas along the banks of the estuary bed, material consists mainly of silt, whereas in the centre of the estuary it consists of sand.

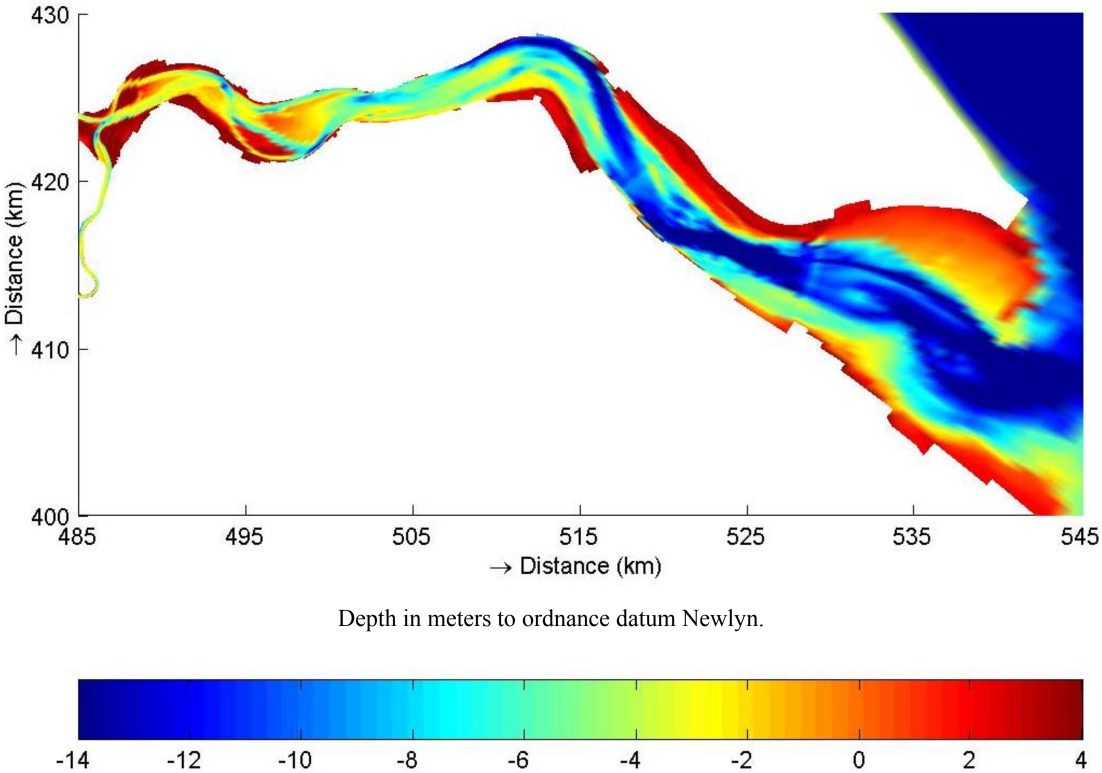

Figure 2-2 Bathymetry Humber estuary

In Figure 2-3 the wet surface area is plotted against the depth, where the horizontal lines show the average spring- and neap-tidal range.

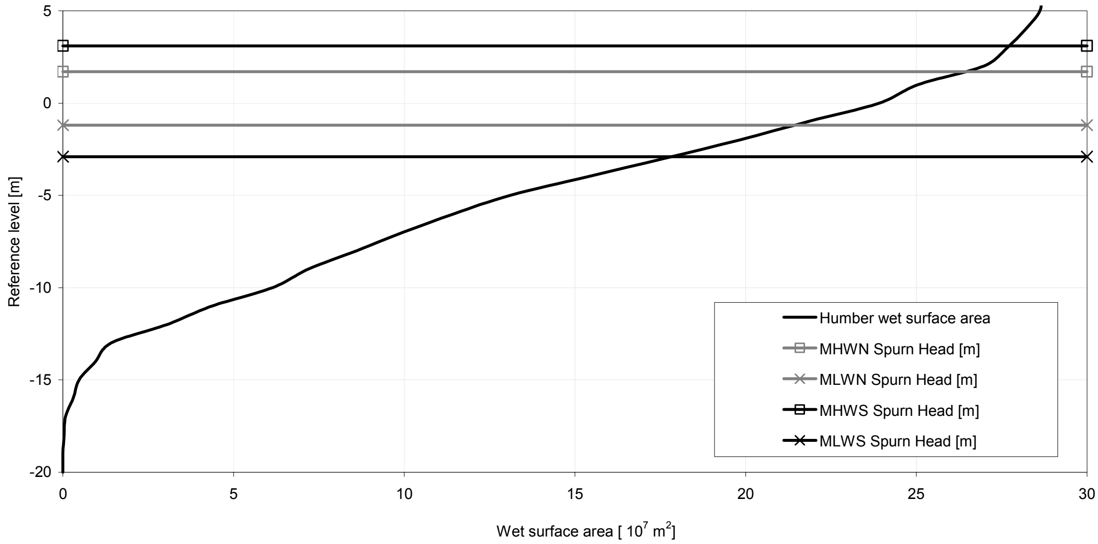

Figure 2-3 Wet surface area and tidal limits with respect to ordnance datum Newlyn.

2.2.2 Catchment area

The River Ouse catchment area is divided into five sub-basins: Don, Aire, Wharfe, Ouse and Derwent. The River Trent and the estuary itself are subject to extensive industrial waste water, sewage inputs and agricultural runoff.

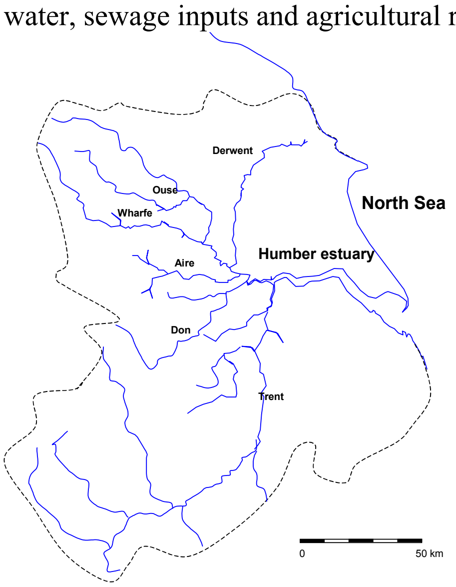

Figure 2-4 Catchment area Humber estuary

Although the six river catchments (see Figure 2-4) represent only 71% of the total drainage area (24,054 km^2) of the Humber estuary, they represent 90% of the total mean freshwater flow (250 m3 s-1) to the estuary. In order to measure riverine input exclusively some of the monitoring sites are located, close to but, above the tidal limit and at many upstream sites within the catchment (see Table 2-1).

Table 2-1Mean river discharges

River:	Monitoring site:	Area [km^2]	Percentage of area draining into Humber	Flow [m^3/s]	Percentage of flow entering Humber
Ouse	Skelton	3,315	14%	49	20%
Wharfe	Flint Mill	759	3%	18	7%
Derwent	Buttercrambe	1,586	7%	17	7%
Aire	Beal Weir	1,932	8%	36	14%
Don	Doncaster	1,256	5%	16	6%
Trent	North Muskham	8,231	34%	90	36%
	Total:	17,079	71%	225	90%

Source: Natural Environment Research Council, 1998

In winter the discharge of the rivers is much higher than in summer (see Table 2-2).

Table 2-2 Average seasonal discharges

River:	winter [m^3/s]	spring [m^3/s]	summer [m^3/s]	autumn [m^3/s]
Ouse, Skelton	90	61	27	75
Trent, North Muskham	140	124	58	128

Source Table 2-2 Average discharges [01-12-1997, 01-11-2000], see Appendix C 'River discharges'.

2.2.3 Tide

The tide in the Humber is mainly semi-diurnal. Characteristic water levels at high water spring (HWS), low water spring (LWS), high water neap (HWN) and low water neap are measured above Chart Datum in Table 2-3.

Table 2-3 Water levels during spring and neap tide

Location	MHWS [m]	MLWS [m]	MHWN [m]	MLWN [m]
Spurn Head	+3.1	-2.9	+1.7	-1.2
Blacktoft (near falls)	+4.2	-1.5	+2.4	-0.9

Source Table 2-3: International chart series, England - East coast, River Humber and Rivers Ouse and Trent. Levels are with respect to ordnance datum Newlyn. Chart datum of Spurn Head (local lowest astronomical tide) is 3.9m and Chart Datum of Blacktoft is 1.5m below ordnance datum.

Hardisty (1999), gives a summary of characteristic velocities at maximum flood and maximum ebb velocity; both during spring and neap tide (see Table 2-4).

Table 2-4 Maximum velocities during spring and neap tide

Location	MFVS [m/s]	MEVS [m/s]	MFVN [m/s]	MEVN [m/s]
Spurn Head	+1.9	-2.2	+0.9	-1.3
Immingham	+1.6	-2.2	+0.9	-1.4

Source Table 2-4: Hardisty (1999)

The astronomical tide can be described in terms of a number of harmonic components of which the frequency is astronomically determined (from the motion of celestial bodies).

Table 2-5 Tidal constituents at station 'Spurn Point Level'

	A0	M2	S2	N2	K2	O1	K1	L2	M4	MS4
Amplitude [m]	0.19	2.07	0.78	0.30	0.24	0.19	0.16	0.15	0.01	0.01
Phase [degrees]	-	154	209	137	209	108	267	160	277	135

Source Table 2-5: ABP Research 'Humber Tidal Data 1998 - 2000', period 01/01/2000 to 31/12/2000

As shown in Table 2-5, the M_2 tidal constituent is the main driving force of the occurring tide. Observe that the tide is mainly semi-diurnal with diurnal variation of about 10%. In the following section Co-tidal charts are studied to verify the extreme low M_4 component.

The ZUNO model simulates the astronomic tidal movement in the southern North Sea. The calibration of the ZUNO model focused mainly on the east coast of the southern North Sea. Along the west coast only a few stations in the area of interest were included (e.g. North Shields, Inner Dowsing, see Brummelhuis et al. (1998)). For this reason the ZUNO output is only used as a clarification of the extreme low values of M_4. The ZUNO co-tidal chart M_2 agrees with the earlier developed co-tidal chart given in Appendix D 'Co Tidal charts M_2 and S_2'. The amphidromic systems of M2 and M4 as calculated by the ZUNO model are shown in Figure 2-5.

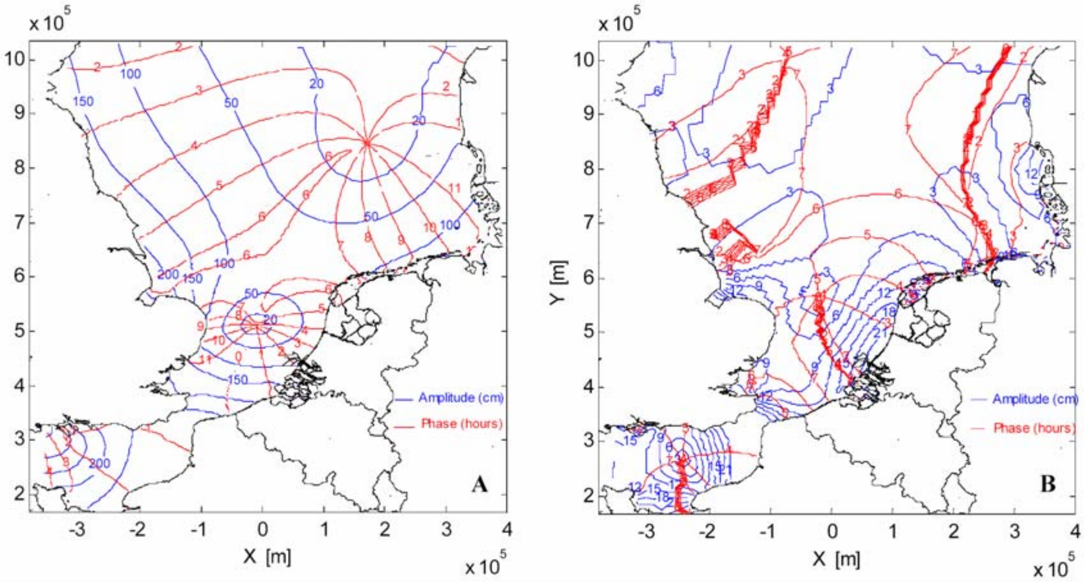

Figure 2-5 Co-tidal chart of the M_2 (A, left) and M_4 (B, right) constituent in the ZUNO model

Source: Results from ZUNO model, which is nested in the Delft 3D, Continental Shelf Model. The calibration of an early version of the model (e.g. ZNZ model) is described by Brummelhuis et al. (1998).

The term amphidrome refers to elevation nodal points where the amplitude tends to zero. In each amphidromic system, co-tidal lines can be defined, which link all the points where the tide is at the same stage (or phase) of its cycle. The tidal waves of amphidromic systems tend to rotate anticlockwise in the Northern Hemisphere and thus also in the North Sea. Co-range lines, which join places having an equal tidal range, cut across co-tidal lines at approximately right angles to them. Co-range lines form more or less concentric circles around the amphidromic point, representing larger tidal ranges further away. As can be seen an M_4 amphidromic point lies near the Humber estuary, explaining the extreme low M_4-amplitude.

2.2.4 Wind and wave climate

In the report of Van Ormondt and Roelvink (WL | Delft Hydraulics, 2002), the following description of the wind and wave climate of the Humber estuary is given.

Wind climate

The wind climate over the Humber Estuary is dominated by westerly to south-westerly winds. Typical wind speeds are 5 to 10 m s^{-1}. Figure 2-6 is a probability plot of the wind climate. The data was derived from the results of the UK MetOffice wind model at point 433.

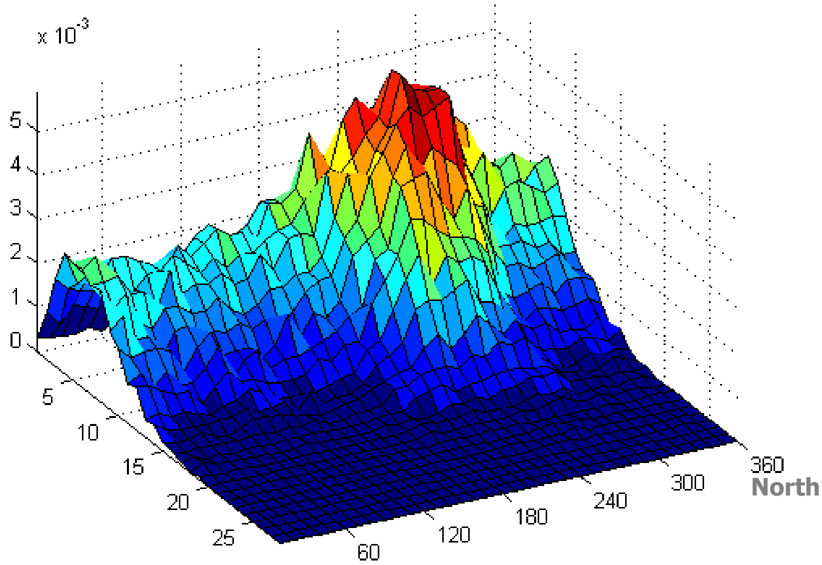

Figure 2-6 Wind climate

Source: MetOffice model [15-10-1986 until 31-03-2002]. On the vertical axis the probabilities (in percentages) of combinations of wind speed and direction are plotted. On the right hand horizontal axis, the wind direction is given and on the left hand axis the wind velocities.

A typical wind from the southwest with a velocity of 7.5 m s^{-1} generates waves inside the estuary with significant wave heights up to 0.5 m. These waves are too low to affect the sediment transport in deeper parts of the estuary, but they do, in the long term, prevent excessive growth of shoals.

Wave climate

The wave conditions in the North Sea near Spurn have been analysed in this study on the basis of data from the UK MetOffice wave model. Wave data was provided over the period 1986-1999 at point 433. Figure 2-7 is a probability plot of the wave climate. The data was derived from the results of the UK MetOffice wave model at point 433. Figure 2-7 Wave climate

Source: Metoffice model [15-10-1986 until 31-03-2002]. On the vertical axis the probabilities (in percentages) of combinations of wave height and direction are plotted. On the right hand horizontal axis, the wave direction is given and on the left hand axis the wave heights.

Table 2-6 contains the probabilities over 8 directional and 8 wave height bins.

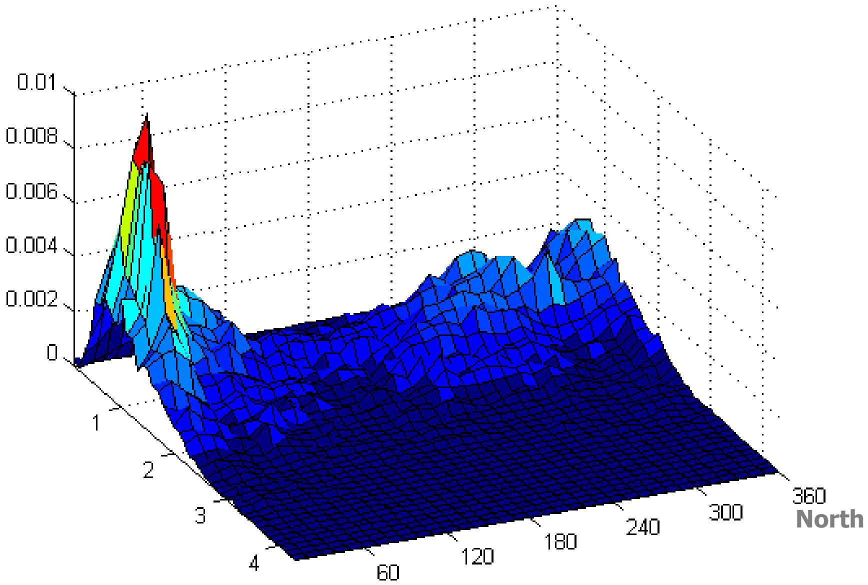

Figure 2-7 Wave climate
Source: Metoffice model [15-10-1986 until 31-03-2002]. On the vertical axis the probabilities (in percentages) of combinations of wave height and direction are plotted. On the right hand horizontal axis, the wave direction is given and on the left hand axis the wave heights.

Table 2-6 Wave conditions, probability of occurrence

	0-45	45-90	90-135	135-180	180-225	225-270	270-315	315-360	Sum %
0.0-0.5 m	4.831	2.445	0.886	0.502	0.578	0.691	0.765	1.862	12.559
0.5-1.0 m	13.269	5.627	2.391	1.862	2.748	4.278	3.874	5.614	39.663
1.0-1.5 m	7.073	3.301	1.724	1.680	3.210	4.111	3.687	3.774	28.558
1.5-2.0 m	2.757	1.626	1.028	0.821	1.849	1.883	1.316	1.744	13.023
2.0-2.5 m	1.184	0.763	0.315	0.339	0.426	0.386	0.491	0.640	4.543
2.5-3.0 m	0.348	0.174	0.060	0.083	0.076	0.094	0.138	0.216	1.189
3.0-3.5 m	0.141	0.098	0.016	0.005	0.007	0.025	0.009	0.076	0.375
> 3.5 m	0.025	0.031	0.009	0.000	0.000	0.002	0.000	0.013	0.080
Sum (%)	29.626	14.065	6.428	5.291	8.893	11.469	10.280	13.940	100

Source: MetOffice model [15-10-1986 until 31-03-2002]

The data from the MetOffice wave model clearly shows that most of the wave energy in the North Sea near Spurn Point comes from the north to northeast. The spit of Spurn Head provides shelter from these waves to most of the outer estuary.

2.3 Literature survey on sediments transport in the Humber estuary

In the following section a literature survey on the sediment transport in the Humber estuary is described. A subdivision has been made between measurements, and an enumeration of estimations of sediment transport.

2.3.1 Measurements in the Humber estuary

The British Transport Docks Board issued a report on silt movement in the Humber estuary in 1970. At that time the concentration of silt in suspension was monitored continuously at five stations between Bull Fort, at the mouth of the estuary, up to Goole, which is situated on the Yorkshire Ouse. A number of regression analyses have been carried out in order to determine the relative importance of various factors on the concentration of silt in suspension. From this analysis the author concluded the following. ‘The monthly average concentrations of silt in suspension for Hull and Immingham can be predicted with temperature alone, whilst at Goole the major factor is freshwater discharge. At Brough, in the upper Humber, both the temperature and freshwater flow are important.’

Although the conclusions seem to be premature, this regression study has established the existence of a remarkable change in suspended matter in time. The data collected in this study can still be used to give insight into the Humber estuary system. A more detailed study of continuous records of the silt meter data showed the hysteresis in the silt concentration during a spring neap cycle.

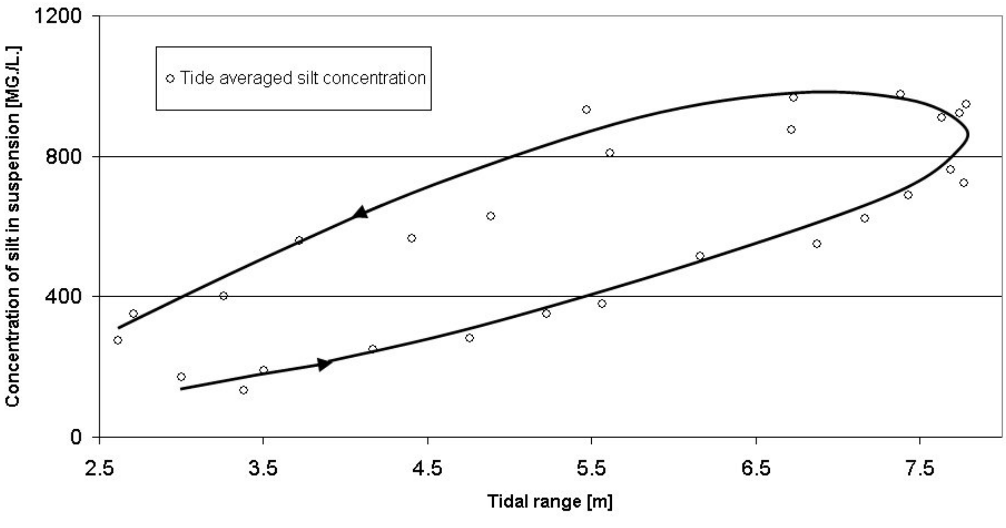

Figure 2-8 Development of silt concentration during a neap-spring-neap cycle in Alexandra Dock Hull
Source: The British Transport Docks Board (1970) in Alexandra Dock Hull from 02/03/1966-16/03/1966

When the average silt concentration (averaged over one tide) is plotted against the tidal range over a tidal cycle from neap through spring and back to neap, it usually (in general) takes the form of an anti-clockwise loop (see Figure 2-8). Although the anti-clockwise loop or the linear relationship is the general rule, there are occasions where other factors mask this effect and a reversal of this pattern, namely a clockwise loop, occurs e.g. during the large sustained freshwater flood in December 1965.

The Humber-Ouse is a very turbid estuary which has a marked localised region of the lower Ouse and the upper Humber of very high suspended particulate matter (SPM) concentrations. In an estuarine turbidity maximum, sediment concentrations can be much greater than in the in-flowing rivers and coastal zone. Boat measurements, described by Uncles et al (2001), in the Ouse at high water during a spring tide in November 1995, showed that the turbidity maximum occurred over a fairly restricted region between 20 and 50 km below the tidal limit. During strong currents the turbidity maximum's sediment load was largely suspended in the water column, while during high and low water slack the SPM rapidly settled in a thin layer close to the bed. The SPM within the turbidity maximum comprised very fine-grained material and its low organic content demonstrated that the SPM was essentially mineral, derived originally from erosion and decay of crustal rock.

2.3.2 Transport of sediments in the Humber estuary

Sediment transports in the Humber estuary have been studied by many authors. In the following section a brief overview is given of the different views of authors on the sediment transport. Hardisty (1999) recommended not to compare the different values since the assumptions differ strongly. Nevertheless a list is given of the estimations of several authors.

- Milliman and Syvitski, (from Hardisty, 1999) found an annual total sediment flux from rivers to the ocean of 18 - 24 10^9 metric tons. Usually 90 to 99% of which is delivered as suspended load rather than bed load.
- O'Conner (1987), (from Hardisty, 1999) has estimated that most of the sediment entering the Humber comes from the flooding marine tide, 2.2 10^6 m^3 a^{-1}, compared with riverine input of $0.3*10^6$ m^3 a^{-1}.
- Hardisty (1999) on the other hand estimated 430 to 710 tons of marine sediments entering per tide and a riverine input of 300 to 500 kT a year.
- Hardisty & Rousse (1996) found that $1.6*10^6$ tonnes of suspended sediment is transported in and out the Humber estuary during a typical spring tide.
- Ward (1985) (from Christy, 1999) shows that erosion rates of this order (compared with journal data: 17 mg $cm^{-2}h^{-1}$, mean value during first four hours of the flood) are indicative of massive erosion, resulting from superposition of the tidal- and wind driven currents, combined with wind induced waves and the pressure fluctuations of storms.
- Clayton (1989) (from Hardisty (1999)) found that the Holderness Cliffs that reach 25 metres in height have been formed by unconsolidated Quaternary sediments consisting of chalk. Under natural conditions these cliffs are eroding with an average rate of retreat of approximately 1m a year.
- Dyer and Moffat (1994), estimated the annual supply of eroded fine sediments from Holderness Cliffs as 2.6 Mton a year and 6.3 Mton a year for the cliffs along the east Anglian coast.

3 Transport processes of cohesive sediments in shallow basins

3.1 Literature survey of cohesive sediment characteristics

The public perception is that mud is a dirty, sticky, dark coloured and evil smelling nuisance. These characteristics can partly be explained. The stickiness is a defining characteristic of muds, which are technically classed as cohesive sediments. Generally speaking a sediment containing more than about 10% by mass of fine material (i.e. sieved material finer than 63 μm) may exhibit cohesive properties. The dark colour and the smell arise from anaerobic[2] decomposition of organic matter, which is often a major constituent of muds.

Historically, sediments have been treated as either mud or sand because the characteristics and resultant behaviour are very different. Whereas in sandy sediment it is the particle size of the bed sediment which controls the mobility of sediment, with cohesive sediments it are the bulk properties of the admixture that determine the behaviour of the sediment. Cohesive sediment characteristics vary due to chemical and biological processes. Due to the complexity of sediment characteristics the following section can only be used as a brief overview of cohesive sediment characteristics. Whitehouse et al (2000a), provide an overview of the current knowledge and research on cohesive sediments that is used in this study.

3.1.1 Small scale processes

Cohesive sediments can be considered to exist in four states. The small scale processes linking these states are indicated schematically in Figure 3-1. These processes may be described as; a mobile suspended sediment, a high concentration near bed layer which is sometimes referred to as fluid mud, a newly deposited or partially consolidated bed, and a settled or consolidated bed.

Of primary interest to the engineer are four small scale processes: erosion and transport, deposition and consolidation. In the next sections these processes will be studied. Besides a description, a brief overview is given of the modelling method that is used.

[2] *The absence of free oxygen*

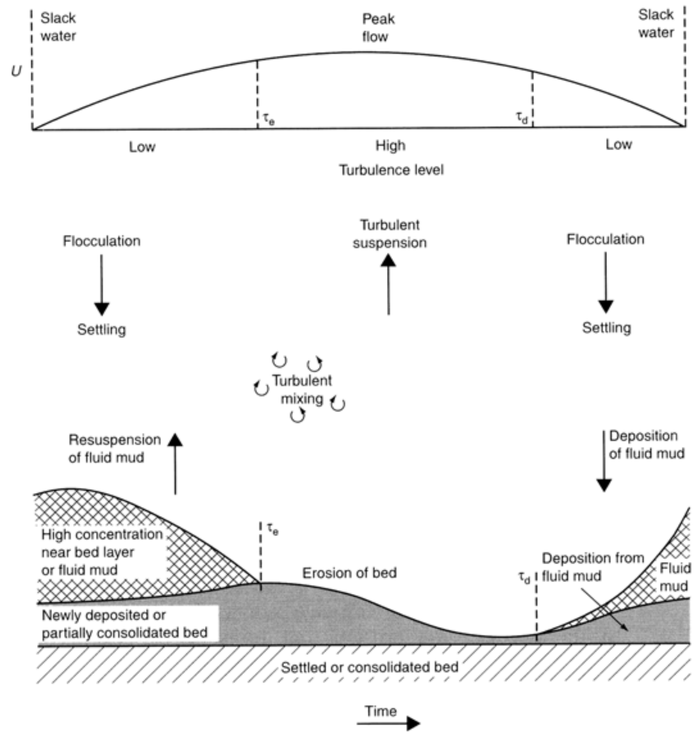

Figure 3-1 States of cohesive sediments

Source: Whitehouse et al. (2000a) p. 16.

Erosion

Erosion (or resuspension) is the removal of sediment from the surface of the bed due to the stress of the moving water above the bed. Erosion is proportional to the excess of the applied shear stress over the critical erosive bed shear stress.

Modelling of erosion in Delft3D-Delwaq

The method that is used in Delft3D-Delwaq to model upward mass transport of bed material is based on Partheniades (1962):

$$f_{res} = E_0 \, \mathrm{P}_{res} \qquad (3.1)$$

With the limitation that the erosion in one model time step cannot exceed the available amount of substances in the bed layer.

$$\mathrm{P}_{res} = \max\left(0, \frac{(\tau_b - \tau_{cr})}{\tau_{cr}}\right) \qquad (3.2)$$

With:

f_{res}	:	resuspension flux	[kg.m^{-2}.s^{-1}]
E_0	:	sedimentation flux	[kg.m^{-2}.s^{-1}]
P_{res}	:	erosion probability	[-]
τ_b	:	bed shear stress	[Pa]
τ_{cr}	:	critical shear stress for erosion	[Pa]

Sedimentation

Sedimentation involves the settling of sediment through the water column and on to the bed.

Modelling of sedimentation in Delft3D-Delwaq

Delft3D-Delwaq uses the sedimentation formula derived by Krone (1962). The rate of downwards mass transport is equal to the product of near bed velocity, the concentration and the probability that a settling particle becomes attached to the sea bed. The sediment flux derived by Krone (1962) is given by:

$$f_{sed} = \mathrm{P}_{sed} \cdot w_s \cdot C \qquad (3.3)$$

With the limitation that the sedimentation in one model time step cannot exceed the available amount of substances in the water column.

$$\mathrm{P}_{sed} = \max\left(0, \frac{\left(\tau_{c,sed} - \tau\right)}{\tau_{c,sed}}\right) \qquad (3.4)$$

With:

f_{sed}	:	sedimentation flux	[g.m^{-2}.s^{-1}]
P_{sed}	:	sedimentation probability	[-]
V_{set}	:	settling velocity of SPM	[m.s^{-1}]
C	:	concentration of SPM	[g.m^{-3}]
τ_b	:	bottom shear stress	[Pa]
$\tau_{c,sed}$	:	critical shear stress for sedimentation	[Pa]

Winterwerp (2003-01) found that in general, the sedimentation rate appears to be much larger (an order of magnitude!) than predicted by the classical formula of Krone, where the following arguments are elaborated. The so-called 'probability of deposition' in Krone's formula is in fact a resuspension term. Hence, Krone's formulation contains both a deposition and an erosion term, and Krone's sedimentation formula cannot be used together with an erosion formula like the one by Partheniades. The sedimentation rate for low-concentrated cohesive sediment suspensions simply reads ($w_s \cdot C$). In order to omit the probability term, the critical shear stress for sedimentation is set to a value much higher than the maximum value that will be reached.

Transport

According to Whitehouse et al. (2000a), transport is the movement of suspended mud and high concentrations layers on or near the bed by the flow. The transport rate of suspended mud per unit width can be obtained from the product of the concentration profile and the velocity profile, integrated over the depth. (Whitehouse et al.):

$$Q_{smud} = \int_{z=0}^{z=h} C_M(z)U(z)\partial z \qquad (3.5)$$

With:

Q_{smud}	:	transport rate of suspended mud	[kg.m^{-2}.s^{-1}]
$C_M(z)$	:	mass concentration (dry density) of mud at height z	[kg.m^{-3}]
$U(z)$	:	flow velocity at height z	[m.s^{-1}]
h	:	water depth	[m]

Modelling of transport in Delft3D-Delwaq

Fine sediment transport is simulated in Delft3D-Delwaq by solving the advection diffusion equation numerically (WL | Delft Hydraulics, 1999):

$$\frac{\partial C}{\partial t} = -\vec{u}\cdot\vec{\nabla}C + \vec{\nabla}\left(\vec{\vec{D}}\cdot\vec{\nabla}C\right) + f_R(c,t,\vec{u}) \qquad (3.6)$$

With:

$\vec{u}$	:	(u_x, u_y, u_z)	flow velocity	[m.s^{-1}]
$\vec{\nabla}C$	:	$(\frac{\partial C}{\partial x}, \frac{\partial C}{\partial y}, \frac{\partial C}{\partial z})$	concentration gradient	[kg.m^{-3}s^{-1}]
$\vec{\vec{D}}$	:	$\begin{matrix} D_{xx} & D_{yx} & D_{zx} \\ D_{xy} & D_{yy} & D_{zy} \\ D_{xz} & D_{yz} & D_{zz} \end{matrix}$	Diffusion tensor	
$f_R(c,t,\vec{u})$	:	Sedimentation and erosion processes in lower layer (see equations 3.1 and 3.3).		

The volume balance is computed by Delft3D-Flow.

Consolidation

Consolidation of a deposit is the gradual expulsion of interstitial water by the self weight of the sediment accompanied by an increase in both the density of the bed and its strength with time. In the following analysis the effect of consolidation is not taken into account.

Biological and Chemical processes

The presence and activity of the benthic[3] community in the sediment mass can affect the sediment characteristics in a number of different ways.

Biostabilisation

- Biostabilisation can vary from the large scale such as mangrove roots to in tropical swamps to microscopic fungi and bacteria threads which act to bind individual grains together.

Biodestabilisation

- Alternatively but to a smaller extent in general, biological activity can result in the sediment being more susceptible to erosion. The activity of digging and burrowing can weaken the sediment structure and create zones of weakness around which erosion will preferentially occur.

Microtopography and bottom roughness

- The biological activity of benthic sediments can have pronounced effects on the bottom topography. Biological communities also move around in response to tidal forcing, light levels and diurnal processes and it is likely that the roughness of natural sediment will vary in space and time depending on the prevailing ecological processes.
- Furthermore the chemical environment and mineralogy can be of great importance as well.

Flocculation and settling

- Due to collision and cohesion particles can stick together, forming flocs. The size and settling velocity of the flocs may be much larger than that of the individual particles. The size of flocs is limited by the maximum rate of internal shear and by several factors among which are size, concentration, pH, hydrodynamic parameters as velocity, turbulence structure, internal shear and bed shear stresses.

Sediment-induced buoyancy

Around slack water, when the flow velocity becomes small, the sediment suspension may become saturated. As a result, sediment-induced buoyancy effects start to play a role. This may be the case in particular during falling water, when the water depth over intertidal areas is decreasing rapidly. These buoyancy effects affect the deposition process as follows:

- As a result of a positive feed-back between the sediment suspension and turbulence mixing, sediment-induced buoyancy effects result in a total collapse of the mixing capacity of the flow, hence rapid sedimentation and the formation of small-scale sediment-induced density currents,
- Toorman (1999, from Winterwerp (2001)) proposes that the boundary conditions for flow and turbulence equations should be modified to account for buoyancy effects properly, as a result of which these effects may be even larger than elaborated by Winterwerp (2001).

[3] *On bottom*

The positive feed-back mentioned before also affects the impact of waves:

- the wave-boundary layer is affected, decreasing the contribution of this layer to the overall mixing capacity of the flow,
- the waves are damped in the viscous, high-concentrated near-bed sediment suspension (fluid mud layer), decreasing their effect, and
- earlier deposited sediment is protected from wave-induced erosion by aforementioned near-bed suspension.

3.2 Literature survey of transport processes of cohesive sediments

3.2.1 Abstract

The net transport of fine sediment is the result of interactions between water motion, sediment transport and bed topography. The processes that are of main importance in shallow basins will be discussed in the following sections. Many studies have been published in the literature to explain the observed high turbidity in shallow areas. In Appendix G 'Literature survey, tide induced residual fine sediment transport', articles of Postma (1954 from Postma(1961)), van Straaten & Kuenen (1957), Groen (1967) and Dronkers (1984) that describe fine sediment import in the Wadden Sea are summarized. In these articles causes are suggested for the established existence of fine-grained suspended sediments gradients.

3.2.2 Tidal asymmetry

An important factor causing net sediment transport is the distortion of the tidal wave, known as tidal asymmetry. Non-linear interactions of tidal components lead to sub-harmonic tides (e.g. spring-neap cycle, $M_2 \pm S_2$), as well as super-harmonic tides. Super-harmonic tides (known as overtides e.g. M_4, S_4, M_6, etc.) are developed due to the interaction of a constituent with itself. Combined overtides are developed by interaction between different constituents. Non-linear interactions between tidal components are of paramount importance to the sediment transport, since they can give rise to a net, tide averaged, sediment flux. Tidal asymmetry usually refers to the distortion of the predominant semi-diurnal tide with its overtides. In this analysis we restrict ourselves to the discussion of the asymmetry due to the semi-diurnal tide and its first overtide.

The magnitude of the asymmetry depends on the ratio between the amplitude of the overtide and the semi-diurnal tide and the lag effects, as described in Appendix D 'Literature survey, tide induced residual fine sediment transport'. The ebb or flood dominance depends on the relative phase-difference of the overtide and the semi-diurnal tide. The relative phase difference of M_4 is defined as derived in Appendix H 'Relative phases', see equation (3.8).

$$\text{Amplitude ratio:} \quad \widehat{U}_{M2M4} = \widehat{U}_{M4} / \widehat{U}_{M2} \tag{3.7}$$

$$\text{Relative phase difference } M_4\text{:} \quad \varphi_{M2M4} = \varphi_{M4} - 2\varphi_{M2} \tag{3.8}$$

With:

$\widehat{U}_{M2}$	:	amplitude of tidal component velocity M_2	[$m.s^{-1}$]
$\widehat{U}_{M4}$	:	amplitude of tidal component velocity M_4	[$m.s^{-1}$]
φ_{M4}	:	phase of tidal component velocity M_2	[°]
φ_{M4}	:	phase of tidal component velocity M_4	[°]

In the further analysis relative phase differences of the constituents are all relative to the M_2 constituent and flow velocity is defined as positive when the direction is up-estuary.

Sediment transport can be divided into two types of transport, bed-load transport and suspended-load transport. Suspended-load transport is the main driving force of fine sediment transport. Bed-load transport is assumed to be proportional to a higher power of the local instantaneous flow velocity than one, which is used in modelling of suspended-load transport. The asymmetry in peak flow velocities is considered to be of main importance for the residual transport of coarse sediment. The asymmetry of the slack water periods during a tidal cycle has always been considered to be of main importance for the residual-transport of fine-grained sediment suspensions.

By a schematization of the asymmetry, insight into the M_2 and M_4 asymmetry can be gained. When we assume that the velocity can be described by two cosines components (see equation H.5). We can calculate what combination of amplitude and phase of the cosiness result in a high peak velocity asymmetry (see Figure 3-2 Tidal asymmetry for peak velocities).

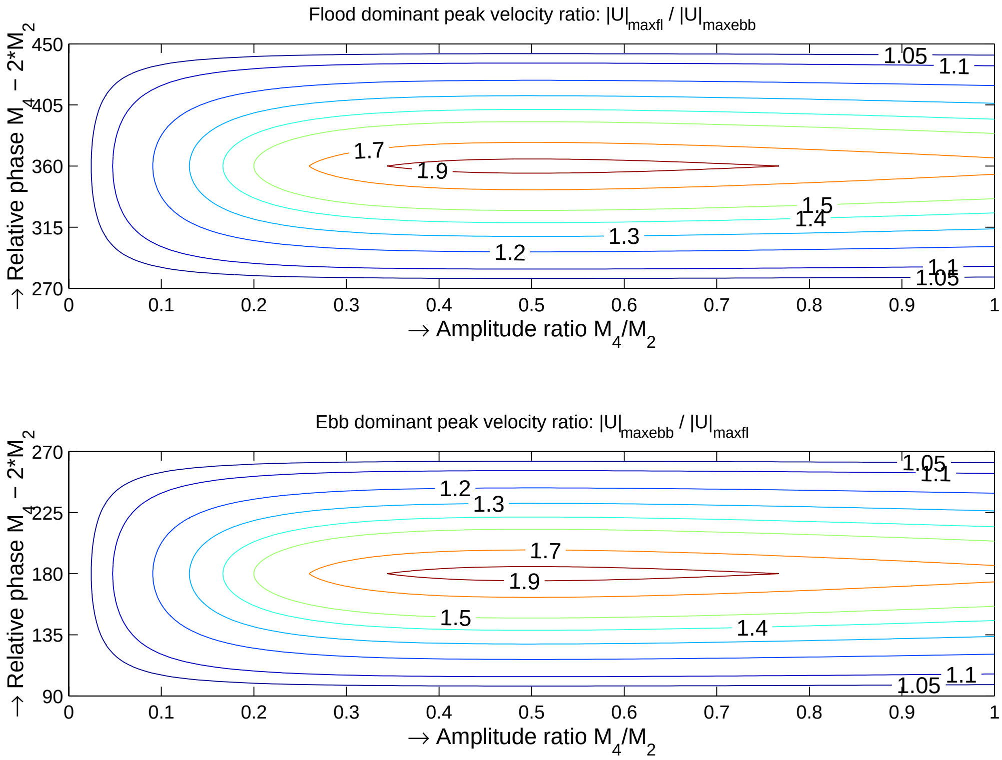

Figure 3-2 Tidal asymmetry for peak velocities, dominant net transport direction for relative phase M4

Explanation: On the horizontal axis, the amplitude ratio of M4 is given and on the left hand axis the relative phase and the contour lines show the ratio of the peak velocity dominance.

Source: Contour line plot of peak velocity asymmetry has been published in Friedricks and Aubrey (1988).

Flood dominant slack period asymmetry occur when the period of high water slack (HWS) is longer than the period of low water slack (LWS). A relative longer HWS period will have a lower steepness of the velocity in time at zero velocity. Therefore gives the ratio of the velocity derivative at zero velocity insight in the magnitude of dominant slack water period asymmetry. In Figure 3-3 Tidal asymmetry slack periods the values of flood and ebb-dominant slack period asymmetry ratio are given for all possible relative phases and relative amplitudes zero till one.

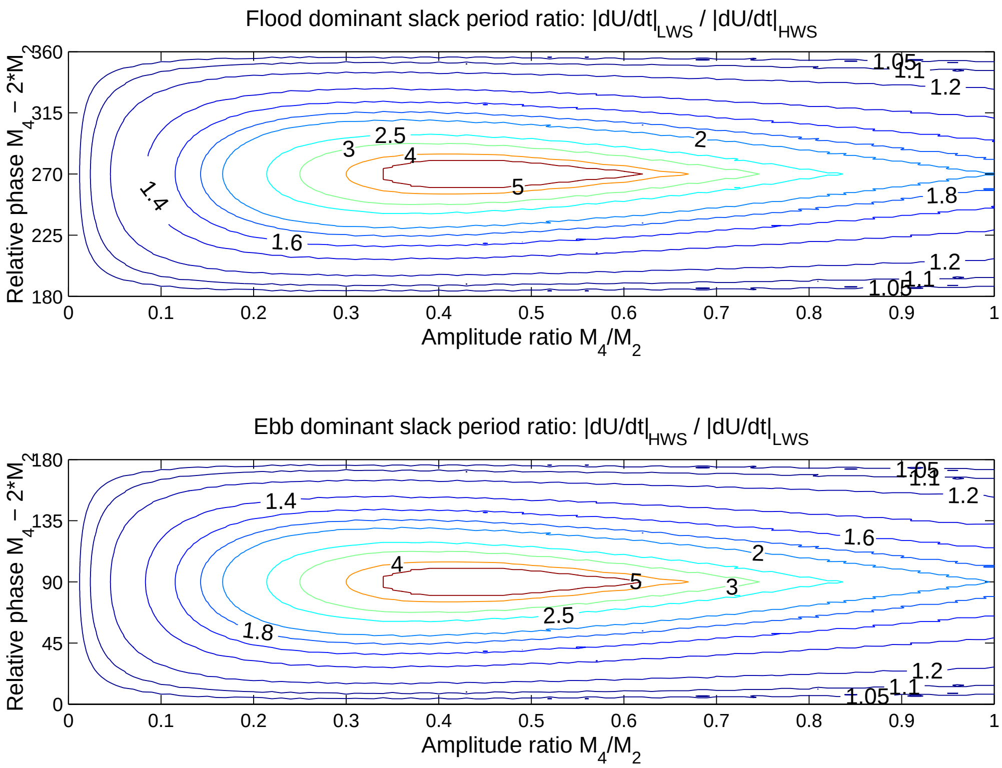

Figure 3-3 Tidal asymmetry slack periods, dominant net transport direction for relative phase M_4

Explanation: On the horizontal axis, the amplitude ratio of M_4 is given, on the vertical axis the relative phase and the contour lines show the ratio of slack period dominance.

The extreme values around amplitude ratio = 0.5 and relative phase = 90º and 270º show the existence of a table near U=0. For this reason the figure has been clipped for maximum values of 5 in order to view only the relevant contours for slack period dominancy.

In Appendix D.2 'Tidal asymmetry and estuarine morphology, Dronkers (1985)', Dronkers derives conditions for a landward net sediment flux as follows. A landward net sediment flux direction is favoured if:

- the channel depths decrease in landward direction (as demonstrated by Van Straaten & Kuenen (1957)) and/or,
- the velocity variation is slower around slack before ebb (High water slack, HWS): $\left|\partial U/\partial t\right|_{\mathrm{HWS}} < \left|\partial U/\partial t\right|_{\mathrm{LWS}}$ (or as in Figure 3-3: flood dominant if the ratio has a value above one, $\left|\partial U/\partial t\right|_{\mathrm{LWS}} / \left|\partial U/\partial t\right|_{\mathrm{HWS}} > 1$).

This last condition can be realized by a distortion of the tidal wave or by a landward decrease of the current velocity. Insight into the generation of tidal asymmetry in the

Humber and its influence on the net sediment transport can help us understand the net transport of fine sediments.

Winterwerp (2003-07) on the other hand, suggests that, depending on the bed status, peak velocities in conjunction with lag effects are often of importance for fine sediment transport. The following situations are distinguished:

- Low-concentration mud suspensions (Clean bed conditions) occur when:
  - the bed contains little or no erodible cohesive sediment,
  - erosion rate (E) exceeds the sedimentation rate (D) and
  - the actual erosion rate is limited by the amount of erodible material

  Or:
  - tide averaged erosion rate (E) is about equal to the sedimentation rate (D). Such conditions can occur at large flow velocities (~1m/s) and/or low C (~several 10 mg/l).

  The net transport of fine sediments, for clean bed conditions, depends on the asymmetry in slack periods.
- Low-concentration mud suspensions (starved bed conditions) occur when:
  - the bed does contain fine sediments but too little for capacity conditions. E and D are of the same order of magnitude, though either can be larger. In this situation the suspended sediment concentration is a function of the erosion rate (and the deposition rate which is not effected by the flow conditions) generally proportional to the bed shear stress, hence U^2.

  The net transport of fine sediments, for starved bed conditions, depends on the asymmetry in peak velocities.
- High-concentration mud suspensions (capacity flow conditions) occur when:
  - sediment availability is abundant. Such conditions are encountered in the turbidity maximum of estuaries and coastal areas, above mud banks and in very turbid systems like the Severn estuary.

  In this case, the effect of asymmetry in slack water periods is probably much smaller than the effects of an asymmetry in peak velocities because of the prominent effects of sediment-fluid interaction, which starts to dominate the flow and suspended sediment structure at high concentrations.

3.2.3 Gravitational circulation

Horizontal density gradients can generate a vertical circulation in the system. Many factors can cause non-homogeneous density, among them are: salinity differences, temperature differences and differences in concentration of solid matter. For sea water the density can be approximated by the following equation:

$$\rho = 1000 + 1.455 \cdot CL - 0.00065(\Theta - 4 + 0.4Cl)^2 \qquad (3.9)$$

With:

ρ	:	density of sea water	[kg.m^{-3}]
CL	:	salinity weight ratio	[‰]
Θ	:	temperature	[C°]

Source: Abraham (1982)

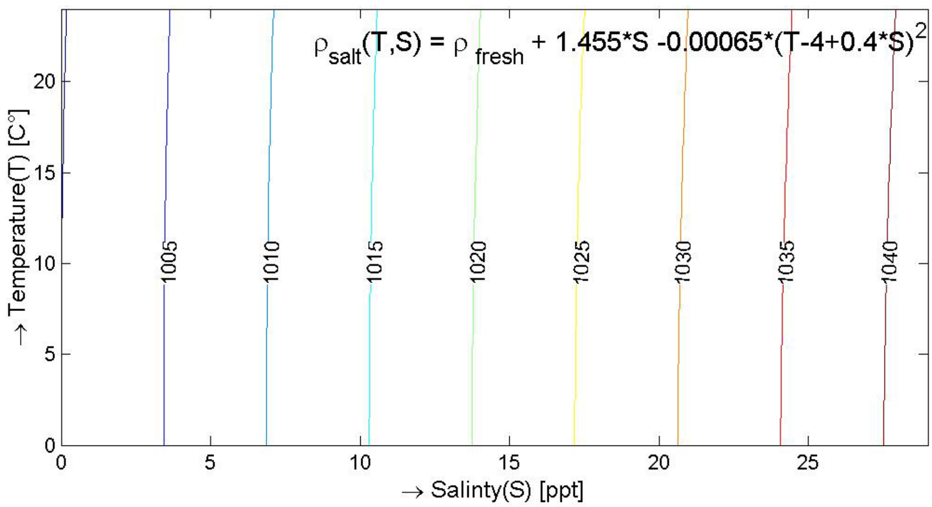

Figure 3-4 Sea water density as function of temperature and salinity

Source: equation 3.9 by Abraham (1982)

The effect on the density due to temperature difference is far smaller than the effect due to salinity differences, as shown in Figure 3-4. For this reason the gravitational circulation study is limited to density gradients due to salinity. Note that the gradients of salinity and temperature do not need to have the same direction. The effect on viscosity is larger for temperature differences in comparison with the effect of salinity differences. Winterwerp (2003-07) wrote the following, ‘especially the settling velocity of the sediment will alter throughout the season because of temperature-induced variations in viscosity (Θ = 6º C, Viscosity = 1.45 mPa and Θ = 16º C, Viscosity = 1.10 mPa).’

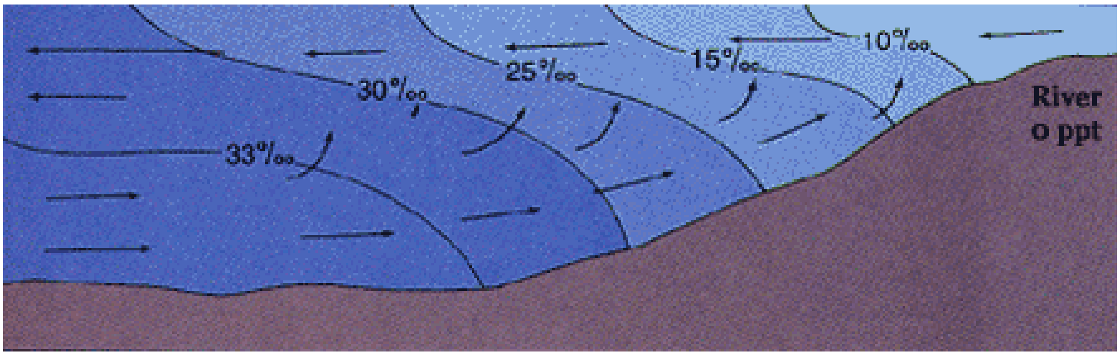

Figure 3-5 Net sea and river discharge combined with the salinity intrusion for a partially mixed estuary

Source: internet address (MARE)

Continuing with Winterwerp (2003-07), ‘Fresh water outflow in estuaries and lagoons generate horizontal density gradients resulting in a vertical circulation in the system with a net landward near-bed current. As the near-bed sediment concentration tends to be larger than the concentration higher in the water column, gravitational circulation causes a net landwards sediment transport. When the salinity structure is stratified, the landward transport will increase. This mechanism plays a role mainly in the (deeper) channels of the system, and is stronger for fine sediment with a larger grain size, as this depicts a more pronounced vertical concentration gradient.’

3.2.4 Channel-Shoal interaction

Estuaries, tidal lagoons and inlets are often characterised by large longitudinal gross ebb (export) and flood (import) transports of fine sediment, in particular in their mouth. If part of the sediments entering the system during flood is deposited on intertidal area, a net import of fine sediments is the result.

In many cases bathymetry data do not represent the shallow area accurately. If bed forms cannot be modelled explicitly at sufficient detail, their effect has to be parameterized through the bed friction coefficient. Water movement is commonly represented by an augmented hydraulic roughness coefficient (form drag).Whitehouse et al. (2000b) discussed the influence of mudflat-bed forms on the hydrodynamics and the sediment processes.

Winterwerp (2003-07) discussed the parameterization of sub-grid effects on fine sediment transport. The relevant bed shear stresses for sediment transport should be based on the local skin friction coefficient. This effect is in particular of importance on intertidal areas, where skin friction can be large, and which can play an important role in the overall sediment import.

3.2.5 Other transport processes

Some processes that can be expected to be of influence but are not accounted for explicitly in this study are described in the following section, as summarized in Winterwerp (2003-07).

Lag effects

Generally, two lag effects are distinguished:

- Settling lag: Around slack water, when the flow is no longer able to keep sediment in suspension, the sediment will settle. However, settling takes time, as a result of which the sediment is transported beyond the point where the flow falls below its transport capacity. Hence, sediment settling velocity and (local) water depth governs the magnitude of settling lag.
- Scour lag: Following slack water, the flow accelerates and will re-erode the sediment deposited during slack water. However, flow velocities (bed shear strength) to re-erode sediment deposits are larger in general than the flow velocity to keep the sediment in suspension. Hence, bed strength, erosion rate and vertical mixing time govern the magnitude of scour.

These lag effects determine the magnitude of the net transport, its direction is governed by asymmetry effects (and possibly gravitational circulation).

Water level effects

The mean water depth in systems with pronounced intertidal areas is smaller during HWS than during LWS, as a result of which a larger fraction of sediment will settle during HWS than at LWS. Moreover, during HWS, the shallow parts, situated near the head of the system, are flooded. Hence, the landward transport during flood is not, or only partly balanced by a seaward transport during ebb. The magnitude of the net landward transport is determined by the bathymetry of the system and the lag-effects discussed above.

Interaction of these mechanisms often results in flood-dominated transport over the intertidal areas and ebb-dominated transport in the estuary channel. However, the estuary channel in the Humber is probably flood-dominated as well.

Wave effects

Waves stir up sediment deposits and/or prevent the sediment from settling. It is noted that on shallow areas only little wave action is required to have a major effect, as small waves in shallow water induce bed shear stresses much larger than those induced by the tidal flow. It is indeed observed that, in particular near the mouth of the Humber estuary, and of other estuaries, the intertidal areas are quite sandy. Note that De Jonge & Beusekom (1995, from Winterwerp (2003-07)), report that a doubling in wind speed is up to five times more effective at resuspending bottom sediments than a doubling in current velocity in the Ems Estuary. This would imply that accumulation of fine-grained sediment on shallow areas can only occur during calm weather conditions, and/or in spring/early summer, when biological activity stabilises sediment deposits.

Gravitational circulation and tidal asymmetry (if flood dominant), in conjunction with lag effects, generate a net import of marine sediment and/or trapping of riverine sediment in estuaries, lagoons and inlets. The accumulating sediment is continuously settling on and re-eroding from the bed, which explains the high turbidity levels in the channels of these systems. On intertidal areas, flow velocities are very small in general, often below critical threshold values, which would yield large net deposition rates. The large concentrations on these intertidal areas can be explained from the fact that:

- small erosion rates can already result in large sediment concentrations on intertidal areas, as the local water depth is very small.
- small waves can generate relatively large bed shear stresses, which may erode the intertidal areas rapidly, consequently prevent sediment from deposition.

The wave activity in shallow areas like intertidal flats, however, is often so large, that net sedimentation on these flats seems impossible. Indeed, many flats in estuaries, lagoons and inlets are mainly sandy. However, many muddy intertidal flats are frequently encountered as well, and such mudflats play an important role in the overall mud balance of estuaries, lagoons and inlets. So, how can such mudflats survive? Only in very sheltered areas, or do we miss one or more processes?

Seasonal effects

Physical and biological seasonal effects can be distinguished:

1. Physical seasonal effects
   - The seasonal variability of wind and wave conditions play an important role, as large areas with deposits of fine-grained sediment can be eroded under storm conditions: it has been suggested for instance (Eisma, from Winterwerp (2003-07)) that the Wadden Sea exports fine-grained sediments during storm conditions. However, significant wave effects on intertidal areas occur already at moderate wind conditions (Beaufort 4 to 5), prevailing almost throughout the year.
   - Another seasonal effect concerns temperature fluctuations: an increase in temperature lowers the fluid viscosity, hence augments the sediment settling velocity.

2. Biological effects
A number of biological effects can be distinguished with their typical seasonal cycle:

- fixation by micro-phyto benthos and bacteria, in particular from mid spring to mid summer, sometimes with a second peak in autumn,
- pelletisation by filter feeders; these organisms filter the sediment from the water column at a large rate and pelletise the mineral components of the sediment, increase their effective settling velocity by a few orders of magnitude,
- burial: a number of organisms bury fine-grained sediments during their activities.

These biological effects are summarised nicely in a diagram by J. Widdows (from Winterwerp 2003-07), shown in Figure 3-6.

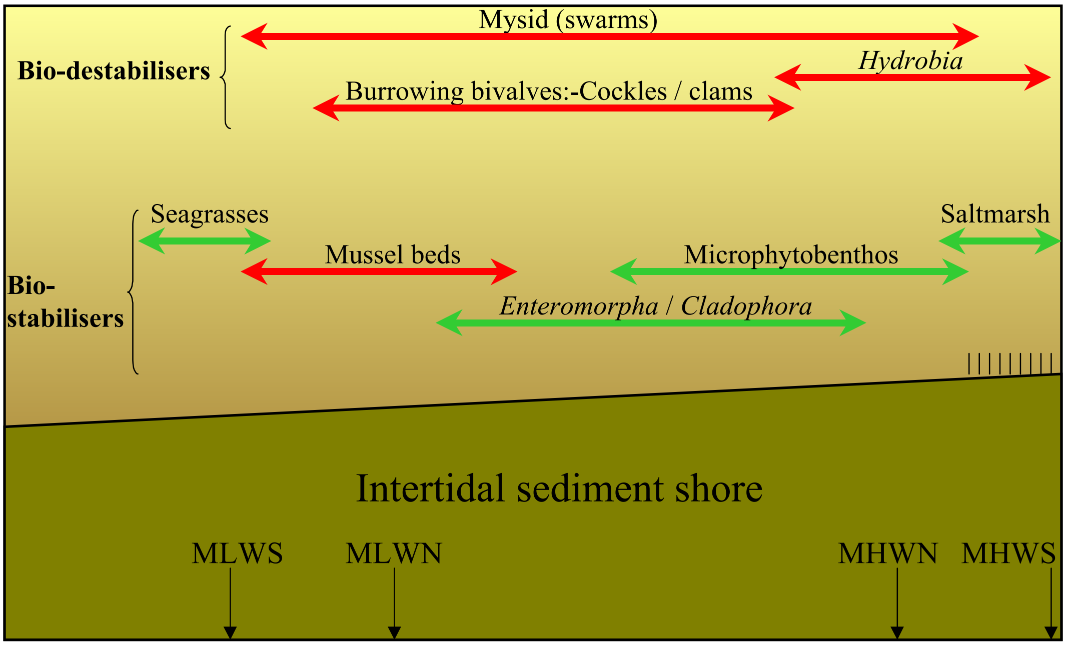

Figure 3-6 Classification scheme of biological effects on intertidal sediment dynamics

Such effects are for instance observed during spring season in the Dollard estuary, The Netherlands, when sediment deposits are stabilised by biological activity, as a result of which the overall turbidity in the system decreases substantially.

Horizontal circulation

Generally, the filling and emptying of tidal basins does not occur in a symmetrical way. For instance, an intertidal flat can be surrounded by a relative deep channel at one side, and a relative shallow channel at its other side. As a result of non-linear effects (friction), a net circulation around that flat will be generated.
Also asymmetrical shapes of intertidal areas may result in different paths of the flood and ebb currents over such flats. This is in particular the case in drainage systems often depicting a fractal structure, such as many Wadden Sea basins, where the small channels have been formed by drainage flow (ebbing) and where the flood current enters the basin as a front. But also in more elongated estuaries, like the Humber, this may occur, for instance in the middle estuary and along its shallow shores.
Phase differences between horizontal and vertical tide (HWS a bit (one hour) later than HW, etc.) may also augment longitudinal dispersion considerably, often bringing the fine sediments further into the system. One result may be that the net sediment transport in the deeper part of a channel may be seawards, whereas the transport on shallow parts on either side of the channel may be landward (van Rijsewijk (2002), from Winterwerp (2003-07)). All these net transport effects may be augmented by the spring-neap cycle.

The spring-neap cycle also causes considerable hysteresis in the suspended sediment concentration: towards neap tide suspended sediment concentrations are generally larger than towards spring tide because of the effects of consolidation of the fine-grained sediment deposits. In concert with the channel-shoal interaction and water level effects, lag effects and bathymetrical effects mentioned above this hysterisis may also result in net residual sediment transport in the system.

Wind-driven currents may further enhance horizontal circulations and dispersion, in particular over irregular bathymetries

Flocculation

Flocculation of cohesive sediments may be important in shallow basins like the Humber estuary:

- Riverine sediments are transported by the fresh water rivers into the estuary, where the sediments come in contact with a saline environment. It is well known that already at moderate salinities, cohesive sediments tend to flocculate if the physical conditions are appropriate (Metha, 1986).
- On the other hand, riverine sediments may flocculate in fresh water environments as well, because of chemical and biological effects. Observations in the Rhine for instance suggest that large fragile flocs of riverine sediments are broken in the high shear zones around the turbidity maximum in the river near Rotterdam (Van Leussen, 1994).
- The turbulence level in estuaries is often high, and the residence time of the sediment in the estuary is large as well. As a result, not only the riverine sediments, mentioned above, but also marine sediments may flocculate.

Hence, one may conclude that the settling velocity of cohesive sediment varies over the estuarine reach. In fact, the settling velocity may also vary with the seasons, as biological activity increases with higher (water) temperature.

4 Model set-up

4.1 Process based numerical model

Process based models consist of a number of modules which describe waves, currents and sediment transport. When the dynamic interaction of these processes with the bed topography is taken into account, these modules are used in a time loop. Such models are called Medium Term Morphodynamic models (MTM). Process based models that do not take bed topographic changes into account are called Initial Sedimentation - Erosion models (ISE). ISE models are used when only the short time-scale processes, like sedimentation and erosion rate, at a given bed topography need to be described.

In this study the package of WL | Delft Hydraulics will be used, containing a hydrodynamic module Delft3D-Flow and an ISE model Delft3D-Delwaq to simulate sedimentation and erosion.

In Appendix B.1 'Hydrodynamic module' a module description, application areas of the model and last but not least, possible couplings of the hydrodynamic module with other modules of Delft3D are described. In Appendix B.2 'Water quality module' a module description, application areas of the model and, the specific sedimentation and resuspension formula that are used in DELWAQ are given.

4.2 Calibration Delft3D-Flow Humber model

4.2.1 Previous calibration Delft3D Humber model

Geometrical schematization
WL | Delft Hydraulics calibrated and validated a fine and a coarse-grid model for stage 2 of the Humber Estuary Shoreline Management Plan (HESMP2). The grid dimensions of the coarse (fine) model were 210 (339) x 25 (46) with 2738 (8914) active cells. The average grid resolution is 2-4 (1-2) km seaward of Spurn, reducing to approximately 100-200 (50-150) m in the rivers.

Boundary conditions
The seaward boundary conditions consist of the eight major tidal constituents that were derived by the UK Admiralty Hydrographic Office. This analysis was based on observations of tidal records at Spurn for a period of a year. Along the seaward boundaries a salinity of 35 ppt was used for the hydrodynamic calibration. A mean monthly discharge for the year 2000 was used as the river boundary condition of the rivers Ouse (including discharge of rivers Foss and Wharf), Trent, Aire, Derwent, and Don. For the upstream boundaries a salinity of 0 ppt was applied representing fresh water.

Calibration standards
The calibration standards that needed to be achieved for 90 % of the position/time combinations were:

- Water levels within 15 % of spring tidal range.
- Timing of high water within ±15 minutes at the mouth and ±20 minutes at the head.
- Speeds to within 10-20 % of the observed speeds.
- Directions to within ±20 degrees.
- Salinity within ±1 psu at the mouth and head, ±5 psu or more in the region of most rapid change.

Calibration parameters
The main calibrations parameters used to improve tidal propagation were:

a) bathymetry,
b) bed roughness, and
c) the seaward boundary conditions.

a) The scale of channel meandering is typically less than the longitudinal grid spacing, thus the interpolation of depths from the survey data onto the grid results are a poor representation of the low water channel. This problem was overcome with the use of maximum value approach in the interpolation stage resulting in a schematic representation of the channel meanders.

b) In both the coarse and the fine models, the final calibration applied the same spatially varying map of bed roughness with higher friction towards the sea (Manning (n) = 0.025 s $m^{-1/3}$), and lower friction in the upper river reaches (Manning (n) = 0.015 s $m^{-1/3}$).

c) During model calibration the amplitudes and phases were further adjusted to represent more adequately the observed values throughout the estuary. The necessary adjustments were determined by comparing harmonic constituents from the model with constituents derived from the observed data.

Calibration of tidal constituents
A consistent error was found initially in all calibration stations for the amplitudes and phases of the O_1 and K_1 constituents. The adjustments made after the calibrations tests resulted in further improvement of the model results. The comparison of water levels predicted from harmonic constituents from the model, and from observations showed that the amplitudes were predicted adequately to within 5%. The computed and observed phase and amplitude of the main tidal component M_2, S_2, K_1, O_1 and M_4 reproduced within ± 10%.

Calibration of water levels
Both the coarse and fine grid models were demonstrated to have achieved an adequate level of calibration in terms of water level according to requirements stated in Calibration standards.

Validation of currents
Recent data (post 1980) were only available for locations downstream of Hull. The only information available upstream of Hull was recorded in 1966. Validation of tidal currents was quantified by assessing differences in peak flood and peak ebb speeds and comparing these to the recommended standards. Similarly the direction during flood and ebb were compared with observations. More than 90% of the peak ebb speeds lie within the ±20% error-band, the upper limit of +20% (+0.4 m/s) is exceeded on approx. 20 % of locations. The calibration is considered reasonable according to requirements stated in Calibration standards.

Conclusions previous calibration
- Both coarse and fine grid models are demonstrated to have achieved an adequate level of calibrations in terms of water levels and current speeds. The fine grid model provides a better calibration against measured currents than the coarse grid model. Water levels appear to have a slightly higher level of accuracy within the coarse grid.
- A higher level of calibration was consistently achieved by the fine compared with the coarse grid model. This can be attributed to the improved level of resolution enabling the fine grid models to resolve the smaller scale channels more precise, particular in the rivers.

4.2.2 Adjustments in previous Delft3D Humber model

The above described fine and coarse models used in the HESMP2 will be used in the sensitivity analysis of the current study. A few adjustments will be made to the existing model, which will make a further validation of the model necessary. In the previous calibration of the hydrodynamic model a local Manning roughness (n) was calibrated. This value varies in three areas; from the upper reaches to the inner estuary, in the outer estuary and outside the Humber estuary. Note that in this case the changing roughness is not a changing physical characteristic but was used as a calibration parameter in order to improve the water levels and velocities. In succession of the previous calibration, a constant Chezy value has been prescribed in the morphological study (WL | Delft Hydraulics (z3451)) after a brief check on water levels in three observation stations.

Roughness terms

Roelvink (2003) wrote the following: 'For a constant Chezy value, the friction is constant with depth, whereas for constant Nikuradse roughness or Manning value, the friction coefficient increases rapidly with decreasing depth. This will tend to shift the flow to deeper water and to reduce velocities in the near shore, with important consequences for the long shore transport. For a constant Chezy friction coefficient, the Nikuradse roughness (k_s) increases linearly with depth. This 'simple' Chezy model at least represents the situation often found where tidal flats and shallow coastal areas are relative smooth and channels and deeper areas exhibit dunes and or wave ripples.'

Therefore, in the current study, several constant Chezy values are used to calibrate the model on the three major astronomical components of the water levels in 13 observation stations. See Appendix G 'Hydrodynamic calibration' for the detailed figures.

Table 4-1 Piecewise Manning roughness coefficient

Area of constant Manning coefficient	Averaged depth [m]	Calibrated Manning coefficient $[s \cdot m^{-1/3}]$	Corresponding Chezy coefficient $[m^{1/2} s^{-1}]$
Inner estuary	2	0.015	75
Outer estuary	8	0.020	71
Outside the estuary:	20	0.025	65

Note: the estimated average depth has great influence in the corresponding Chezy coefficient.

Table 4-1 suggest that the Chezy value is constant throughout the cross-section, regardless of the depth. If a constant Chezy value is prescribed, the roughness height (k_s) is a fixed portion of the water depth. The effect of this is that if the overall cross-sectional average of the shear stress is about the same in both cases, the shear stress in the case of a Manning roughness will be greater on shallow areas and less in the channels than for the case of constant Chezy value.

Boundary conditions

The average discharges over the period 1997-2000 of the rivers Trent and Ouse are chosen as the upstream flow boundary condition. Density differences are not taken into account in the 2Dh model. See 'Table 2-2 Average seasonal discharges'. The tide is modelled by a water elevation boundary, built up by the seven major tidal constituents: M_2, S_2, N_2, K_2, O_1, K_1, and L_2. For the year 1997 a coarse and a fine grid depth file exists. The existing depth files of year 1997 were locally adjusted to prevent unrealistic high velocity gradients. For the year 2000 only a fine depth file could be retrieved, as a result of which a new coarse depth file was made out of the fine grid version of year 2000.

Model approach during calibration

In Table 4-2 a summary is given of the simulations that are developed in order to calibrate the hydrodynamics on the three major constituents M_2, S_2 and M_4.

Table 4-2 Model approach, calibration hydrodynamics on global roughness

Code	Calibration of the global roughness	Model type	Sea boundary
CH01	previous local manning roughness	coarse grid, 2D	8 TC*
CH02	global Chezy 70	coarse grid, 2D	8 TC*
CH03	global Chezy 75	coarse grid, 2D	8 TC*
CH04	global Chezy 80	coarse grid, 2D	8 TC*
CH05	global Chezy 85	coarse grid, 2D	8 TC*
CH06	global Chezy 90	coarse grid, 2D	8 TC*
CH07	previous local manning roughness	fine grid, 2D	8 TC*
CH08	global Chezy 70	fine grid, 2D	8 TC*
CH09	global Chezy 75	fine grid, 2D	8 TC*
CH10	global Chezy 80	fine grid, 2D	8 TC*
CH11	global Chezy 80	fine grid, 2D	8 TC*
CH12	global Chezy 70, depth 2000 minus 5dm	fine grid, 2D	8 TC*

* : Eight major tidal constituents (see Table 2-5 on page 9)

In order to save computing time, a maximum time step was estimated by calculating the Courant number. The maximum Courant numbers were computed for the coarse model with a time step of 30 seconds.

Table 4-3 Courant number

Area	Courant nr. [-]	Area	Courant nr. [-]
Outer estuary	3.55	Lower part of the Ouse	16.45
Inner estuary	10.83	Upper part of the Trent	23.25
Lower part of the Trent:	14.17	Upper part of the Ouse:	47.03

Source: Courant numbers calculated from reference run, using software package: Delft3D–Quickin.

The values in the estuary are within the desired range. The high Courant number in the upper reaches of the rivers make it unwise to increase the time step to save computing time. The fine model shows proper results with a time step of 15 seconds.

4.2.3 Observed water level analysis

In June and July 2000, water levels were measured at 13 observation stations, see Figure 4-1. At some stages in this period, drying occurred in station ‘06 Humber Bridge’. Unfortunately, drying in this water level station makes the data invalid as input for an astronomical analysis.

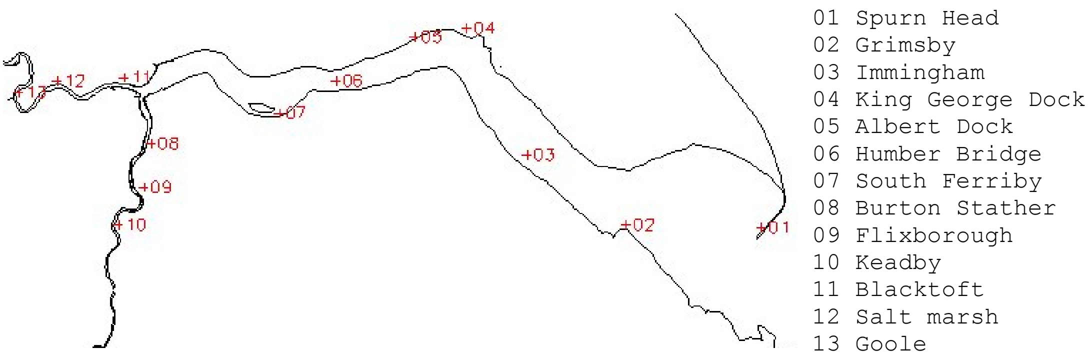

Figure 4-1 Water level observation stations in Humber estuary

The remaining data, from 12 observation stations, is used to calculate for each of the 12 stations 32 tidal constituents. From now on, the set of these constituents is called the ‘hindcast observation’. Tidal analysis has filtered out distortions that do not follow the 32 tidal periods (e.g. atmospheric pressure differences, discharges, other astronomical components, etc.). The ‘observation’, the ‘hindcast observation’ and the ‘residual observation’ are plotted for stations Spurn Head, Albert Dock, Blacktoft, South Ferriby and Burton Stather. See Figure 4-2 and Figure G-1 to G-5.

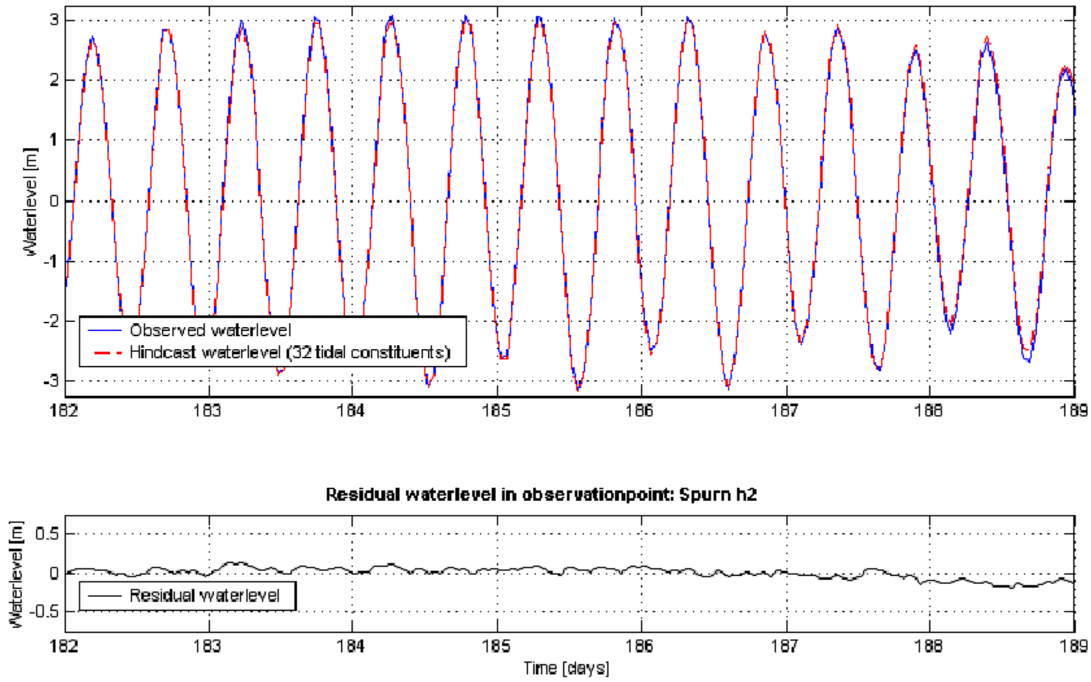

Figure 4-2 Observed and hindcast water level in Spurn Head, 01/07/2000 - 07/01/2000

Source: Hindcast observations consisting of 32 tidal constituents derived from observations in June 2000.

4.2.4 Calibration Delft3D hydrodynamic Humber model

As a first check, computed water levels were compared with the hindcast observations. The water levels were computed for July 2000 for the fine as well as the coarse Delft3D model. The plots for stations Spurn Head, Albert Dock, Blacktoft, South Ferriby and Burton Stather are shown in Figure 4-3 and Figure G-6 to G-10. As can be concluded from the results, the water levels in the outer and inner estuary were computed well by the fine and the coarse model.

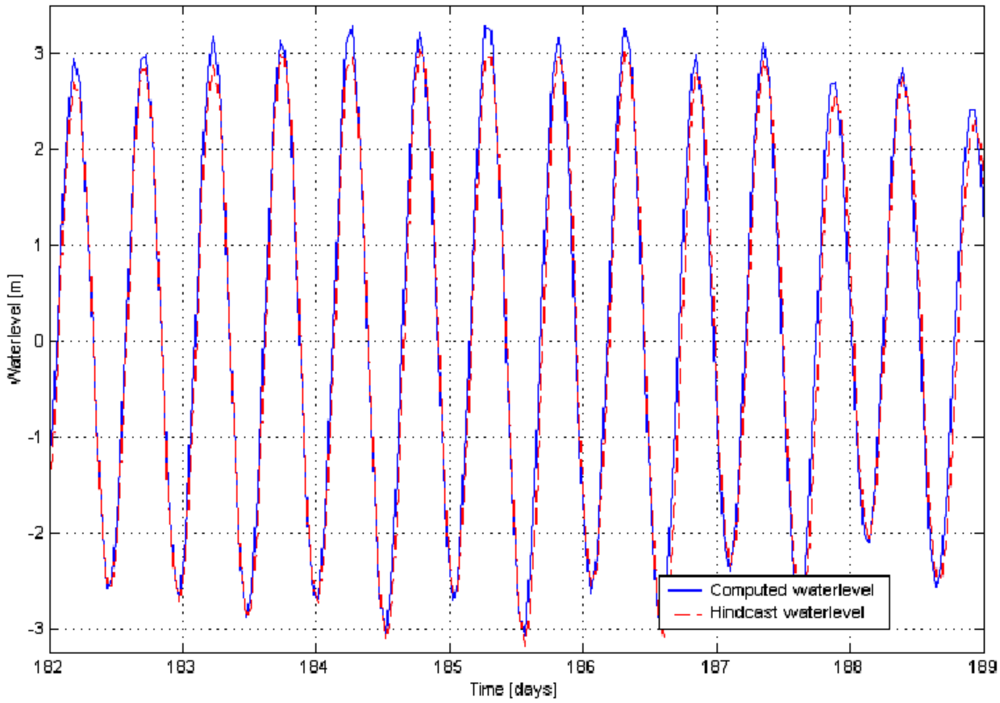

Figure 4-3 Hindcast and computed coarse-grid water level in Spurn Head, 01/07/2000 - 07/01/2000

Source: Hindcast observations consisting of 32 tidal constituents derived from observations in June 2000.

The computed water levels further upstream show a larger error compared with the hindcast observations. At several stations (Keadby wk 1-3, Flixborough wk 2-3, South Ferriby wk 2-3, Burton Stather wk 2-3) the computed low waters are persistently lower than the hindcast observations, while the high waters show good correspondence. A possible explanation could be that the scale of channel meandering is typically less than the longitudinal grid spacing, thus the interpolation of depths from the survey data onto the grid results are a poor representation of the low water channel. This was described in the previous calibration, and it was suggested that this can be solved by using a maximum value approach during the interpolation stage of the depth. Unfortunately the low waters show that the schematic representation of the channel meanders could still be improved. Due to the high sensitivity of the interpolation method of depth surveys a test was done by running the coarse model with a depth profile that is 0.5m deeper than the existing profile. A deepening was chosen with the aim to reduce the error in the phases. The phases M_2 and S_2 show a small improvement, however the absolute error in phase M_4 increases considerable and all three amplitudes deteriorated. Since the area of poor low-water representation is not within the area of main interest, only a recommendation is made for future use of this model at the end of this section.

A more detailed analysis was done by comparing the three major astronomical components in a tidal analysis on data of computed and observed water levels in 2000.

Validation of M_4

A tidal analysis throughout the estuary was made. The local generation of M_4 shows a good representation of it's amplitude but not of it's phase, especially near the mouth of the estuary. Attempts were made to reproduce the M_4 phase more precisely by adding a small M_4 in the sea-boundary. As can be shown in Figure 2-5 'Co-tidal chart of the M_2 (A, left) and M_4 (B, right) constituent in the ZUNO model' an M_4-amphidromic point is located near the seaward boundary of the model, which explains the extremely low amplitude of M_4 in the sea-boundary near Spurn Head. Based on the analysis of observations at Spurn Head for a period of a year, ABP Research derived an amplitude of 1 cm and a phase of 277 degrees for M_4. Thus, M_4 is modelled by enforcing an amplitude of 1 cm and a phase developing along the eastern sea-boundary from 176 to 236 degrees. This adjustment reduces the absolute mean error in the phase of M_4.

Calibration of the global Chezy roughness

By running the models with a varying roughness coefficient, an optimum can be found in representing tidal components. In this analysis the three major components M_2, S_2 an M_4 are used. (M_4 is locally generated from 1 cm in Spurn Head up to 51 cm in Goole).

As shown in Figure G-10 Hindcast and Computed Burton Stather, the model does not reproduce the water levels in the river mouths as well as in the estuary. When we divide the area in two (the inner estuary and the river mouths) the mean average error can be calculated separately. Since the inner estuary is of main importance the seven observation stations in the inner estuary will be analyzed first. This analysis is described in Appendix G. After this analysis, the focus will be on the total area (all 12 observation stations). The average errors in water level of the runs with a global Chezy of 70 and 75 lie near each other. The mean absolute value of the relative error and the absolute error phase are within acceptable error-range for both roughness values. See Table 4-4.

Table 4-4 Mean error in tidal constituents M2, S2 and M4 in inner estuary

D3D model: Roughness:	Coarse, Chezy70	Coarse, Chezy75	Fine, Chezy70	Fine, Chezy75
Mean absolute relative error in amplitude M_2	3%	2%	5%	4%
Mean absolute relative error in amplitude S_2	5%	8%	7%	8%
Mean absolute error amplitude M_2	0.073 m	0,043 m	0,107 m	0.081 m
Mean absolute error amplitude S_2	0.035 m	0,054 m	0,044 m	0.054 m
Mean absolute error amplitude M_4	0.033 m	0,029m	0,021 m	0.016 m
Mean absolute error phase M_2	9°	10°	11°	12°
Mean absolute error phase S_2	7°	5°	6°	6°
Mean absolute error phase M_4	20°	22°	13°	14°

Source: Mean relative absolute error amplitude, mean (|Hc-Ho|)/Ho). Where, Hc = computed amplitude and Ho = observed amplitude.

Since the M_4 is only a centimetre at Spurn Head, a relative mean error in amplitude would not give useful information on the accuracy of the model; for this reason this value is not given.

Conclusion and recommendation

- When the river area is of main interest the representation of channel meandering needs improvement.
- Since the area of poor low-water representation is not within the area of main interest, only a recommendation is made for future use of this model.
- By a global deepening of the estuary by half a meter, the propagation speed of M_2 and S_2 increases (as intended) and the local generation of M_4 decreases. The overall effect is not an improvement since all three the amplitudes deteriorated.
- With the focus on the inner estuary,
  - a global Chezy of 70 $m^{½}$ s^{-1} has been chosen for the coarse model. Amplitudes and phases show acceptable results in the inner estuary as well as in the total area,
  - a global Chezy of 75 $m^{½}$ s^{-1} has been chosen for the fine model, since the output shows acceptable results in both areas.

4.3 Set-up of the Sediment Transport Model

4.3.1 Spatial aggregation of model results

In order to evaluate the general sediment transport fluxes within the estuary, the model results are spatially aggregated according to the following zones. The Humber estuary is divided in longitudinal direction in 6 sections. The sections are sub-divided in zones where distinction has been made between tidal flats and channels. The output of the model contains fluxes through the interfaces between different zones. Attention has been paid to minimize the amount of interfaces between the different zones. See Figure 4-4.

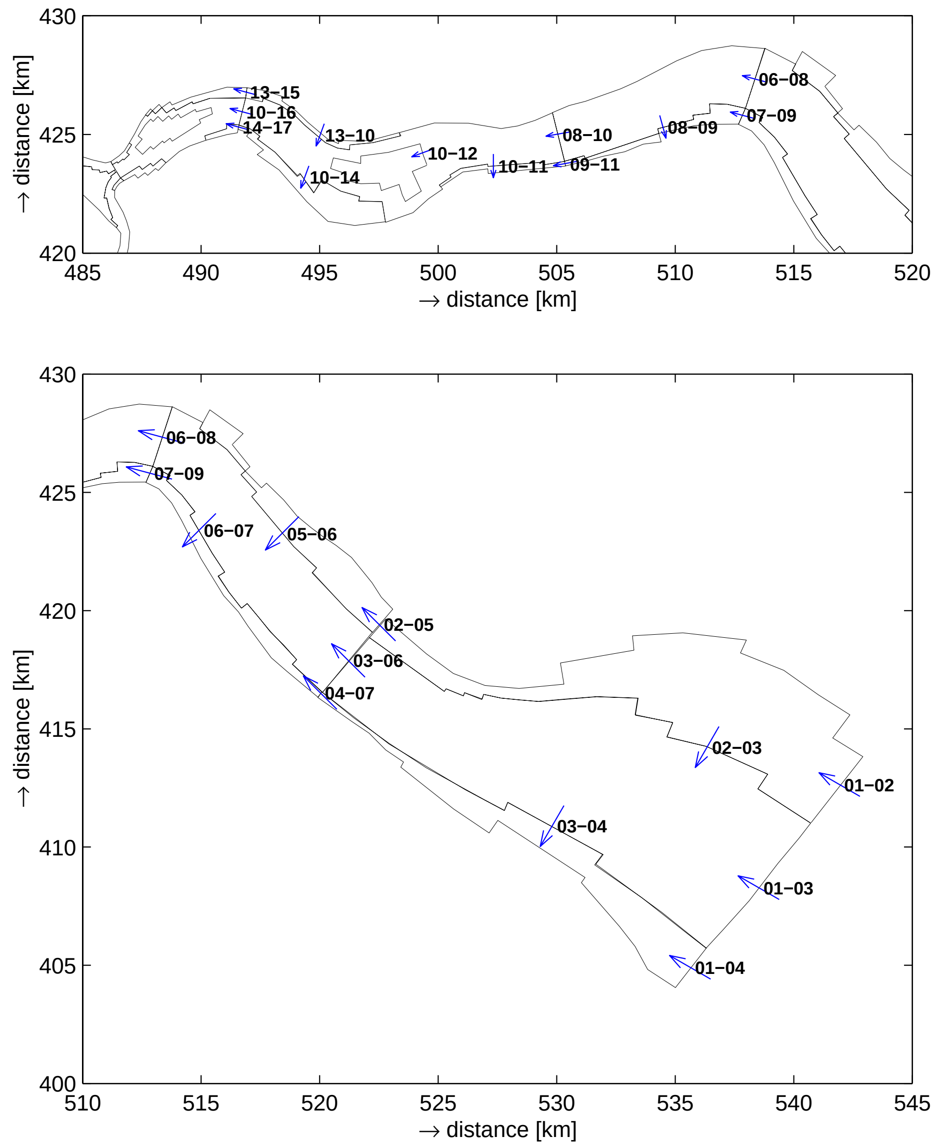

Figure 4-4 Aggregated grid Humber estuary

Explanation: Numbers refer to exchange fluxes between zones.

4.3.2 Coupling of the hydrodynamics

Conversion of hydrodynamic results is required for coupling the off-line hydrodynamic database of Delft3D-Flow to the Delft3D-Delwaq framework. In order to reduce the size of the hydrodynamic database results are stored every 30 min. The reference run has a sea boundary consisting of only the M_2 tide. For this run a coupling period of six M_2 periods is used to minimize the differences in water levels in the beginning and the end of the coupling period (mean coupling error in water level throughout the estuary ≈ 0.0025m). A second check has been done on the mass balance of each cell. The error in the mass balance lies within acceptable error range of +/-1% (e.g. minimum value: -0.6 ‰ and maximum value: +0.8 ‰).

4.3.3 Calculation average concentration

One of the outputs Delft3D-Delwaq produces is cumulative fluxes through the interfaces between different zones. An approximation of the average concentrations through these cross sections can be obtained by dividing the cumulative transport by cumulative discharge. However, extreme and unrealistic values can occur when the fluxes over a period consist of both import as well as export. In this case, the average concentration does not correspond with the transport divided by the discharge. A possible explanation for this is given with the help of an example.

> *A period is chosen with the intention that during the first phase import and the second phase export occurs and that the net flow discharge over the full period tends to zero. The concentration after the change in direction (during the second phase of the period) is probably lower since during the period in-between no large bed shear stresses occur and some of the sediments in suspension has settled. Therefore, the import of sediments during the first phase will be larger than the export in the second phase.*

As the example above shows, it is possible to have a net transport value that is several orders of magnitude larger than the value of net discharge and secondly a sediment concentration that does not correspond with this order of magnitude. With the intention of keeping the values within realistic range, a mathematic exception-rule has been made for situations as described in the example and opposite directions. The exception rule used during this analysis calculates the average concentration of the concentration values before and after the period.

4.3.4 Sediment transport model set-up reference run

In the following section all relevant model characteristics are given for the reference run. In a first attempt to set-up the model a large difference in 2Dh and 3D bed shear stresses attracted the attention. An adjustment in the bed shear stress formulation in DELWAQ for 3D models was necessary. See Appendix M.5 'Bed shear stress formulation in previous DELWAQ version'. In the following analysis the new version of Delft3D-Delwaq (version 450.05) has been used.

Sediment properties

Table 4-5 presents the sediment parameters that are used in the reference run GC01C. In order to omit the probability term, the critical shear stress for sedimentation is set to constant value of 100 Pa. This value is two orders higher then the bed shear stress that occur, by which the probability term in equation 3.3 has the value one.

Table 4-5 Fine sediment properties in sediment transport model Delft3D-Delwaq module

	Parameter	SI value	SI Unit
Sedimentation velocity	w_s	$0.5\ 10^{-3}$	$m\ s^{-1}$
Critical shear stress resuspension	τ_e	0.5	Pa
Critical shear stress sedimentation	τ_s	100	Pa
Roughness White Colebrook[4] in the sedimentation and erosion processes.	k_s	10^{-3}	m
Zeroth order resuspension flux	M	$1\ 10^{-4}$	$kg\ m^{-2}\ s^{-1}$

Explanation: In Winterwerp (2003-01) A re-analysis of Krone's deposition experiments lead to omit the probability term, for this reason the critical shear stress for sedimentation is set to a constant value of 100 Pa (See Appendix B.3 Sedimentation and resuspension).

Boundary conditions

The marine sediments entering the Humber are schematized as a concentration of 100 g/m^3. Note that O'Conner (1987, from Andrews (2000)) as well as Hardisty (1999) have estimated that most of the sediment entering the Humber comes from the flooding marine tide compared with riverine input.

Salinity has been taken into account by 31 ppt at the sea-boundary and 0 ppt at the river boundary. Since the sea boundary is located far from the area of interest no 'Thatcher and Harleman time lag' has been prescribed.

Initial conditions

At the beginning of the computation initial concentrations must be given for all substances to be able to solve the advection-diffusion equation. Initially there is no sediment trapped in the system ('cold start'-initial condition). Another approach could have been by initially starting the model with an overall layer of sediment on the bottom. After the spin up time the same amount of residual import should be found. On the other hand the dry cells that are not involved in the hydrodynamics will show a sediment layer on the bottom only due to the initial conditions. For this reason a clean-bed start has been chosen in order to have a direct relation between the amounts of material on the bed and the sedimentation and erosion (SE) processes, instead of a combination of initial conditions and SE -processes.

[4] *The roughness of the hydrodynamics and the SE-processes is not the same.*

Dispersion and turbulent diffusion

Transport of fine sediments takes place through advection or dispersion. Dispersion, as defined here, differs from the physical concept of molecular diffusion as it stands for all transport that is not described by the advective velocities. This implies that dispersion is much larger than molecular diffusion. First of all, small scale chaotic movement of water parcels (due to density fluctuations in the water column) will lead to turbulent diffusion. Still this term can be small. More dispersion enters the modelling effort by small scale eddies that are not resolved by the hydrodynamics and the underlying computational grid. In the hydrodynamic calculation some cells on tidal flats become temporarily dry. Then, the process of dispersion must stop to prevent artificial transport on land. For this reason dispersion is set to zero when the flow velocity is zero.

Numerical scheme

The WAQ interface allows the user to choose a numerical scheme to fit the desired stability, convergence and consistence criteria for there model approach. In order to avoid relative differences in the runs due to numerical diffusion, all simulations were computed with the same numerical scheme.

Given the primary aim of this study modelling experts at WL Delft advised to test a numerical scheme that uses an implicit upwind scheme in horizontal direction and in vertical direction a centrally discretised scheme. A brief summary is given below; the method is:

- computational efficient,
- not strictly positive, nor monotone,
- there is no stability criterion for Δt for transport, therefore relative large time-steps may be used, the size being restricted by accuracy and stability criteria for processes,
- first order accurate in the horizontal but second order accurate in vertical direction,
- artificial mixing due to numerical diffusion.

In order to determine the influence of the numerical scheme used in the SE-model, several simulations with different numerical set-up are analysed. First the time step is investigated on the applied scheme. Secondly a 2Dh run is compared with a numerical scheme that corrects for numerical diffusion (run GC05A). Table 4-6 presents the runs made especially for this study.

Table 4-6 Description numerical scheme runs

Runid	Model type	Numerical scheme	Time-step WAQ	Dispersion coefficients	Density difference
GC01A	2Dh, coarse grid	#16	30 min	1.0 m^2/s	homogeneous
GC05A	2Dh, coarse grid	#05	10 sec	1.0 m^2/s	homogeneous
GC16A	2Dh, coarse grid	#16	5 min	1.0 m^2/s	homogeneous

Explanation Table 4-6: In the manual of Delft3D-DELWAQ (1999) the numerical schemes are discussed. Numerical scheme #05: Flux correct transport method and numerical scheme #16: Implicit upwind scheme in horizontal and centrally discretised vertically, with an iterative solver.

In the course model the minimum residence time of a water particle (or sediment particle due to only advective transport) in a computational grid-cell is 45 sec. After trial and error a time step of only 10 seconds was stable enough to complete the run. When an implicit scheme is used a much larger time step is allowed within the stability criteria. Note that the total computing time of GC05A is far larger than run GC01A.

Results reference run

Figure 4-5 presents the maximum and minimum salinity intrusion for a simulation with an M_2 and M_4 sea-boundary condition and a three years' average discharge from River Trent and River Ouse. Since differences between top and bottom layer are small, the dept averaged values are given.

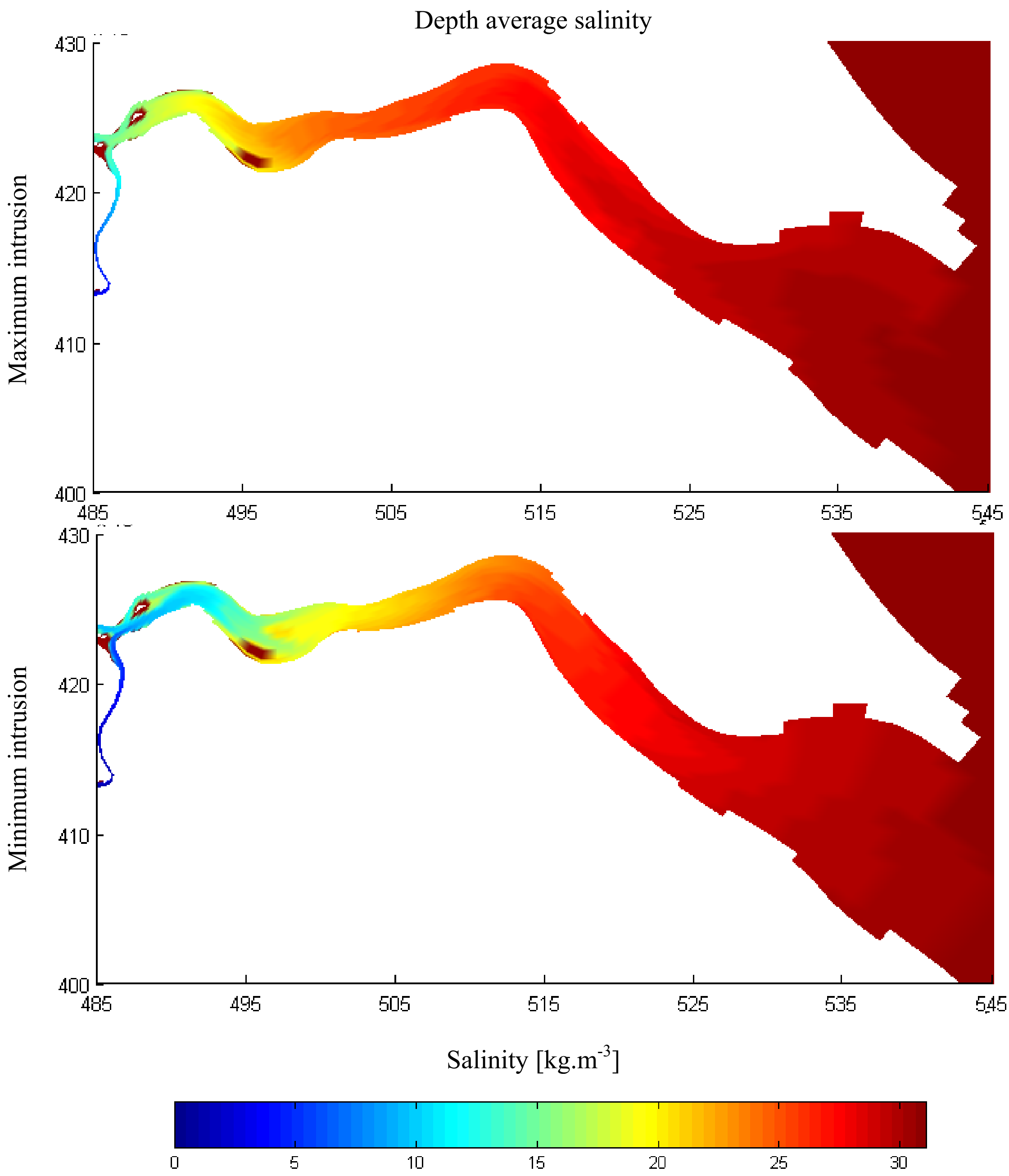

Figure 4-5 Salinity intrusion

In the inner estuary, three spots of high salinity are shown. Note that these values are determined by initial conditions because the tide cannot reach these cells.

The distribution of fine sediments is presented at maximum and minimum concentration in Figure 4-6.

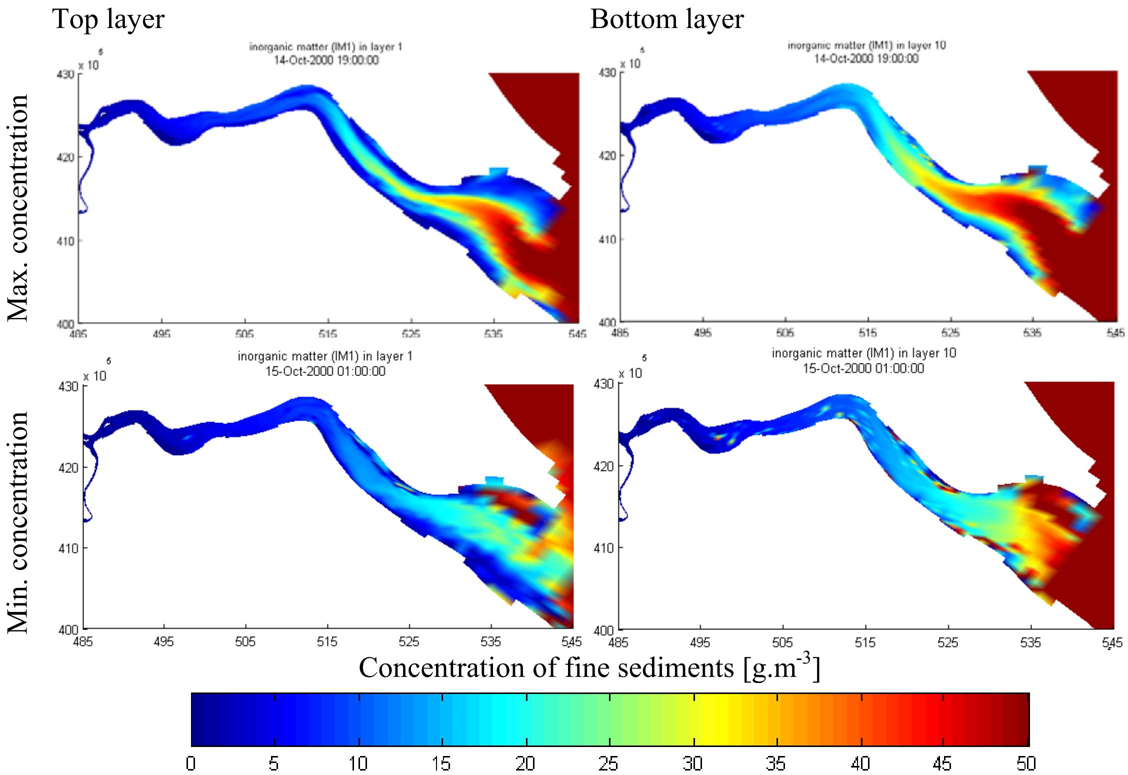

Figure 4-6 Minimum and maximum concentration of top and bottom layer

Along the estuarine channel the computed concentrations of fine sediments and salinity is monitored. The locations of the observation points in the aggregated grid are given in Figure 4-7. After a period of two months, sediment erosion processes show a returning development for all locations in the estuary, see Figure 4-9. Note that the spin–up time for observations in Figure 4-7 is less then in locations furhter up-estuary.

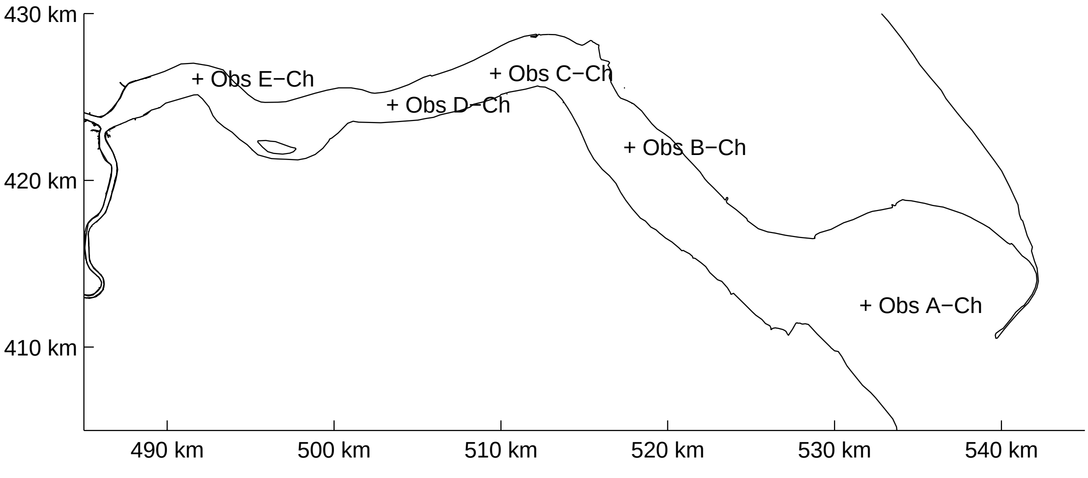

Figure 4-7 Observation points in the Humber estuary

Figure 4-8 presents the development of concentration and salinity.

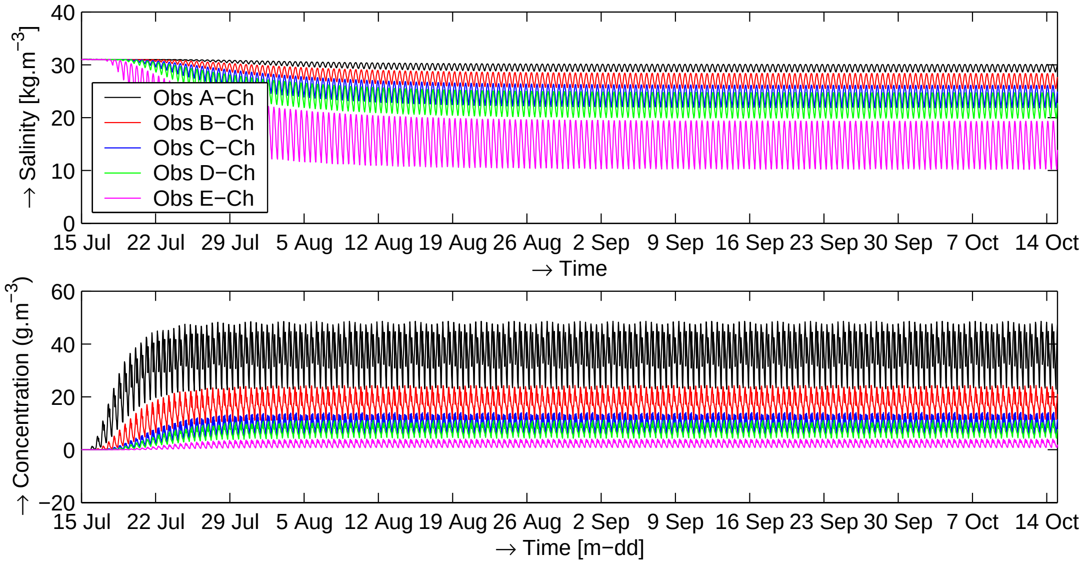

Figure 4-8 Salinity and fine sediment concentration development after ‘cold-start’

After a period of two months, sediment erosion processes show a returning development in the whole estuary, see Figure 4-9.

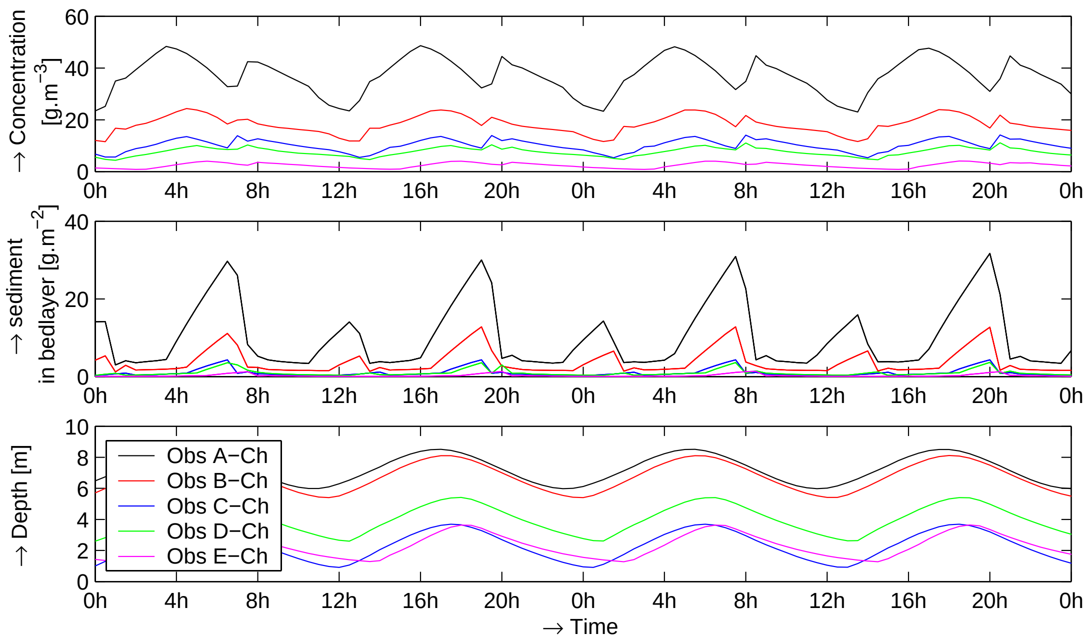

Figure 4-9 Development of salinity, fine sediment concentration, mass of sediments settled in the bed layer and local depth after spin-up time.

Conclusions of the numerical scheme study

Significant decrease in time step (GC16A versus GC01A) shows in the outer estuary no difference in concentration development in time whereas up-estuary the values of run GC16A show lower values. Furthermore, the relative difference in net sediment transports is very small in the outer estuary whereas up-estuary the relative differences increase considerably. A possible explanation for this difference in net transport is the smaller amount of material that reaches this area. The described differences could be explained by the difference in applied simulation time-step of the hydrodynamic integration and by a higher numerical diffusion in simulation GC01A due to the larger time step. Although, only during the spin up time a higher gradient can be seen outside the Humber mouth for run GC16A.

Comparison of runs GC01A and GC05A shows that the concentrations, especially up-estuary, are higher for run GC01A than for GC05A. This can be explained by the higher gradient in run GC01A due to numerical diffusion at equal dispersion terms.

Considering the objective of the study, improve the knowledge of processes on net landwards transport, the relative difference in net transport is of importance. Since the time efficient numerical scheme ‘Flux correct transport method’ describes the concentration gradient of the fine sediment concentration realistic for run GC01A, this set-up will be used in the following study.

Recommendations of the numerical scheme study

When in a future project SE processes need to be calibrated, numerical scheme #5 can be used with a higher numerical dispersion value to represent lower gradients in concentration. This dispersion value could then be calibrated against measured salinity data.

5 Sensitivity analysis

5.1 Experimental program

The experimental program is divided in three subjects:
1) Sensitivity analysis of tidal asymmetry.
2) Sensitivity analysis of gravitational circulation.
3) Sensitivity analysis of channel – shoal interaction.
An overview of the experimental program is given in Appendix A ‘Experimental program’, furthermore at the start of each new subject a summary is given of the simulations used.

5.2 Tidal asymmetry study

5.2.1 Set-up of the tidal asymmetry study

The main objective for this study is to determine the influence of tidal asymmetry on the net up- estuary transport of fine sediments. Tidal asymmetry inside the Humber estuary depends on the local generation and the sea-boundary conditions. In a previous morphological study of the Humber estuary executed by WL | Delft Hydraulics (z3451) net coarse sediment transport has shown to be sensitive for M_4 sea-boundary conditions. Whether fine sediment transport is sensitive for small changes in M_4 sea-boundary condition is a second objective of the following sensitivity study.

As discussed in section 3.2.2 'Tidal asymmetry', fine sediment transport can be less sensitive to the velocity magnitude than coarse sediment transport. Moreover, fine sediment transport can be more sensitive to slack water periods due to lag effects, depending on the bed conditions.

A number of Delft3D-Flow 2Dh runs have been made (see Table 5-1) to study the sensitivity of the tidal-asymmetry-driven fine sediment transport on changes in the sea-boundary condition. All runs are done with a coarse model grid, a 2Dh model with homogeneous density, a three-year average discharge and the year 2000 bathymetry. In Table 5-1 the various runs are summarized. In the reference run a M_4 sea-boundary condition is used that follows from the previous calibration of waterlevels inside the estuary. In Table 5-1 are the phases given relative to this calibrated value and are the M_4 amplitudes given relative to the calibrated M_2 amplitude.

Table 5-1 Model approach, sensitivity analysis tidal asymmetry

Code	Sea-boundary condition		Model type	Sea-boundary condition
	Phase M_4	Relative amplitude M_4		
TA01A	No overtide M_4	-	Coarse grid, 2D	M_2
TA01B	0°	5 %	Coarse grid, 2D	M_2 & M_4
TA01C	-20°	5 %	Coarse grid, 2D	M_2 & M_4
TA01D	+20°	5 %	Coarse grid, 2D	M_2 & M_4
TA01E	0°	10 %	Coarse grid, 2D	M_2 & M_4
TA01F	-20°	10 %	Coarse grid, 2D	M_2 & M_4
TA01G	+20°	10 %	Coarse grid, 2D	M_2 & M_4
TA01H	$0°^{RR}$	1 cm^{RR}	Coarse grid, 2D	M_2 & M_4
TA01I	$0°^{RR}$	1 cm^{RR}	Coarse grid, 2D	8 $T.C.^{RR}$

Explanation: The phases of constituent M4 in this table are given relative to the phase used in the reference run (CH02). The 'Amplitude M_4' percentage is given relative to the amplitude of M_2.
RR: Values as used in the reference run, calibration of the hydrodynamics (CH02), as described in Table 4-2 on page 35.

The study is set up as follows. First, an astronomical component analysis of tidal components of M_2 and M_4 is set-up and carried out on 21 observation points in the model (section 5.2.1 till 5.2.2). Secondly the described theory on peak velocities and slack water periods is applied by using the output of the astronomical analysis (section 5.2.3 till 5.2.5) and thirdly, slack water periods are derived from the velocity magnitude (section 5.2.6). After each subject the conclusions are listed in a table. The last section describes the conclusions and the difference between the two analyses of slack periods.

5.2.2 Astronomical components analysis

Every run of the tidal asymmetry study has been evaluated by a tidal analysis (in 21 observation points) concerning depth average velocity in u and v direction. Unfortunately the local u or v directions (e.g. local grid directions) are not always defined in channel direction. In order to obtain the main flow-direction along the channel instead of along the grid, the direction of the maximum amplitude of the velocity ellipses is used. The combination of tidal phases and amplitudes in u and v are used to create velocity ellipses of M_2 and M_4. The phases and amplitudes of theses ellipses are the basis of the comparison of asymmetry of horizontal tide in the first part of the sensitivity analysis.

The 21 observation points start at Obs01, at the mouth of the estuary, to obs21 at Trent Fall, near the conjunction of the two rivers River Trent and River Ouse. In the inner estuary, near the conjunction, the amplitude of M_4 increases strongly. For this reason observation points at this part of the estuary are placed closer together (See Figure 5-1 and Figure 5-2).

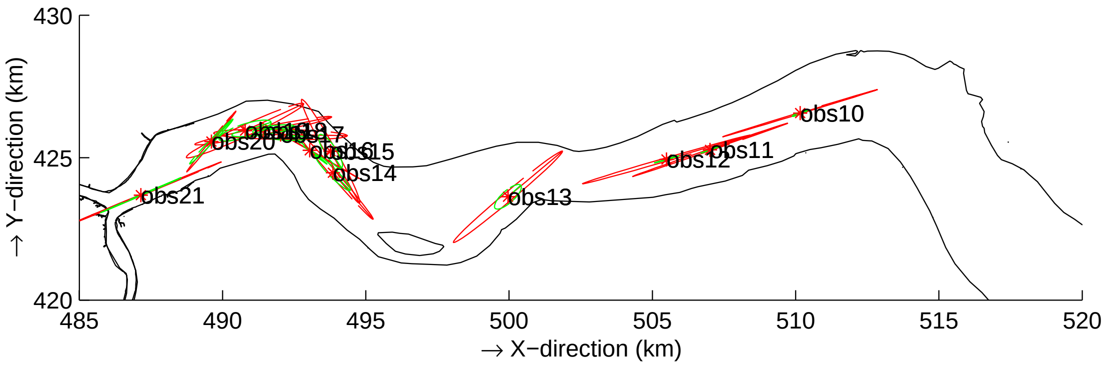

Figure 5-1 Velocity ellipse in the inner estuary for run TA01B, M_2 (red) and M_4 (green)

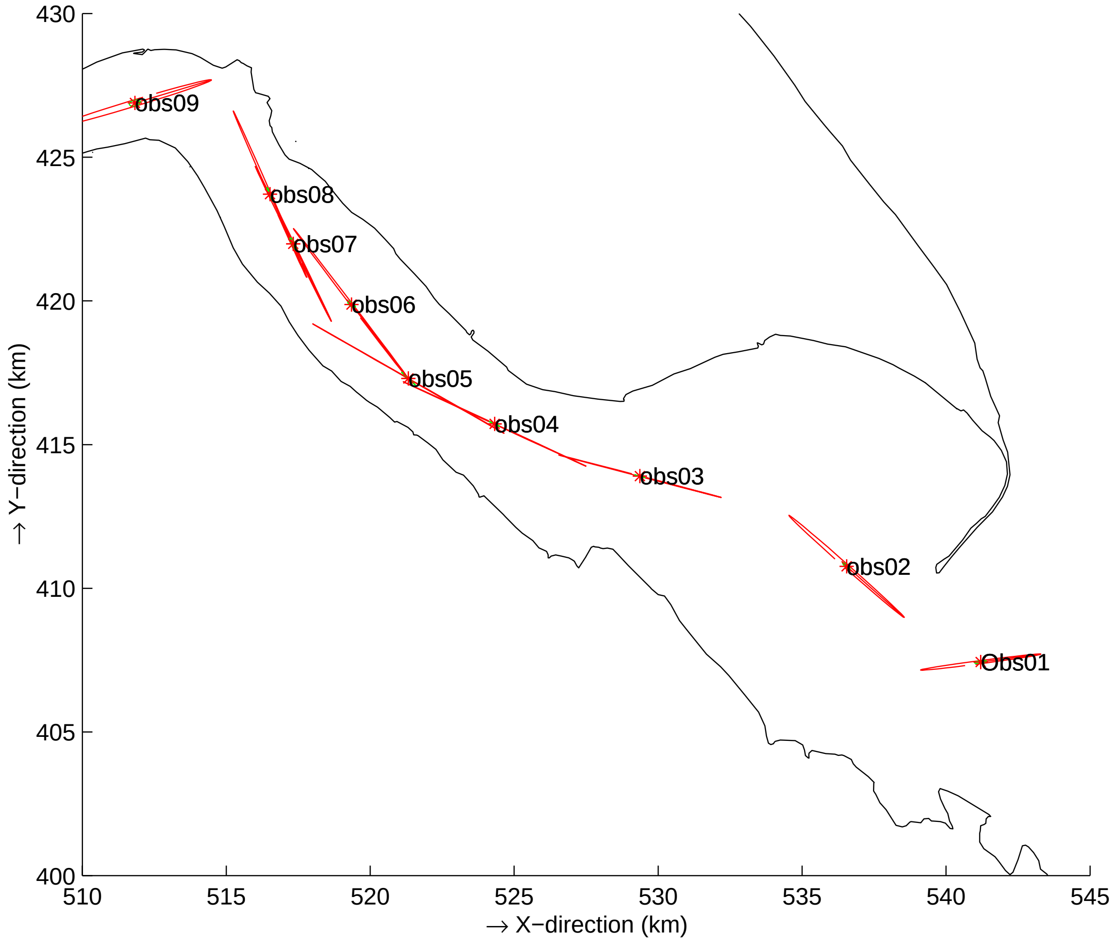

Figure 5-2 Velocity ellipse in the outer estuary for run TA01B, M_2 (red) and M_4 (green) is very small in the outer estuary

When we assume that the major axis of the M_4 velocity ellipse has the same direction as the major axis of the M_2 velocity ellipse and the minor axes are negligible compared with the major axes, the amplitude ratio and the relative phases can be calculated (see Figure 5-3 and Figure 5-4). The difference between inclination[5] of the M_2 and M_4 component are small enough for the assumption of mutual major current axes. From analysis not presented here, the values of average absolute inclination differences are for runs TA01B, C, D, E, F and G ± 4 degrees. Larger differences in inclination are found in Obs06 for TA01A, TA01H and TA01I (16, 16 and 13 degrees).

Unfortunately drying of cells occurs in obs16 and obs20, see figure I-28 and I-32 where the velocity magnitude is given for runs TA01I. Due to drying of these cells the observation points are excluded from the following tidal analysis.

In the following analysis the relative phase of M4 is used to determine dominant transport direction. Figure 5-3 presents the phase of M_2 and M_4 in the observation points. Out of the phases of velocity components M_2 and M_4, the relative phase is derived. In Figure 5-4 the amplitudes of M_2 and M_4 are given. The amplitude ratio is used in the following analysis to determine the magnitude of the asymmetry.

[5] *Angle between the semi-major axes and u-axis of the local grid cell*

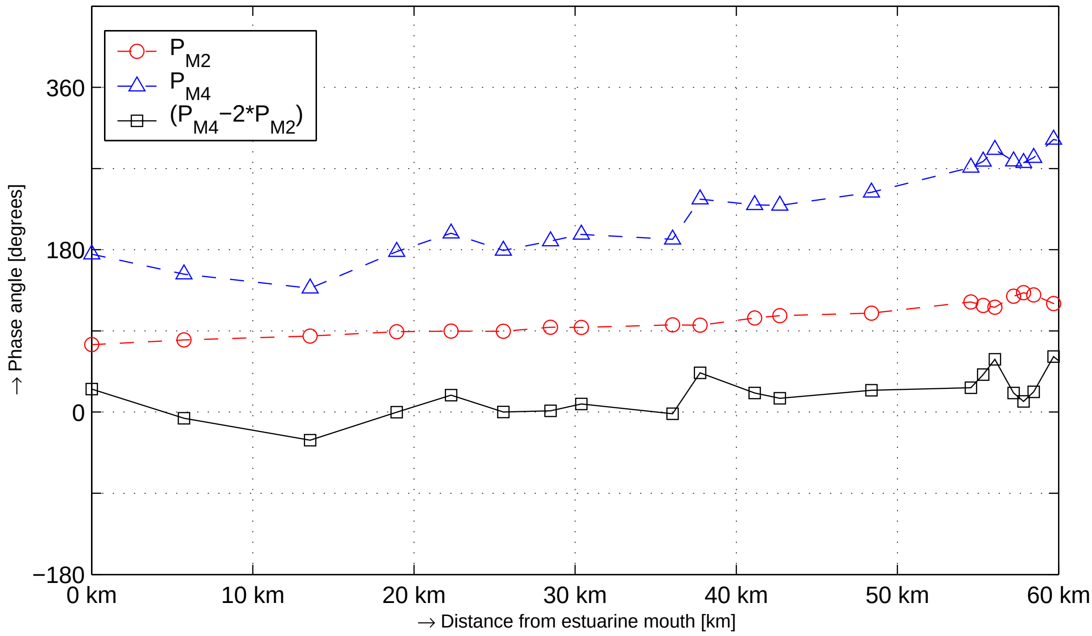

Figure 5-3 Relative phase velocity ellipse M2 and M4 along the estuarine channel for run TA01B
Description: The values of depth average velocity are computed for runs TA01A, B, C, D, E, F, G H, I. Phase differences in Figure 5-3.B have been minimized by adding (or subtracting) 360 degrees to the calculated values.

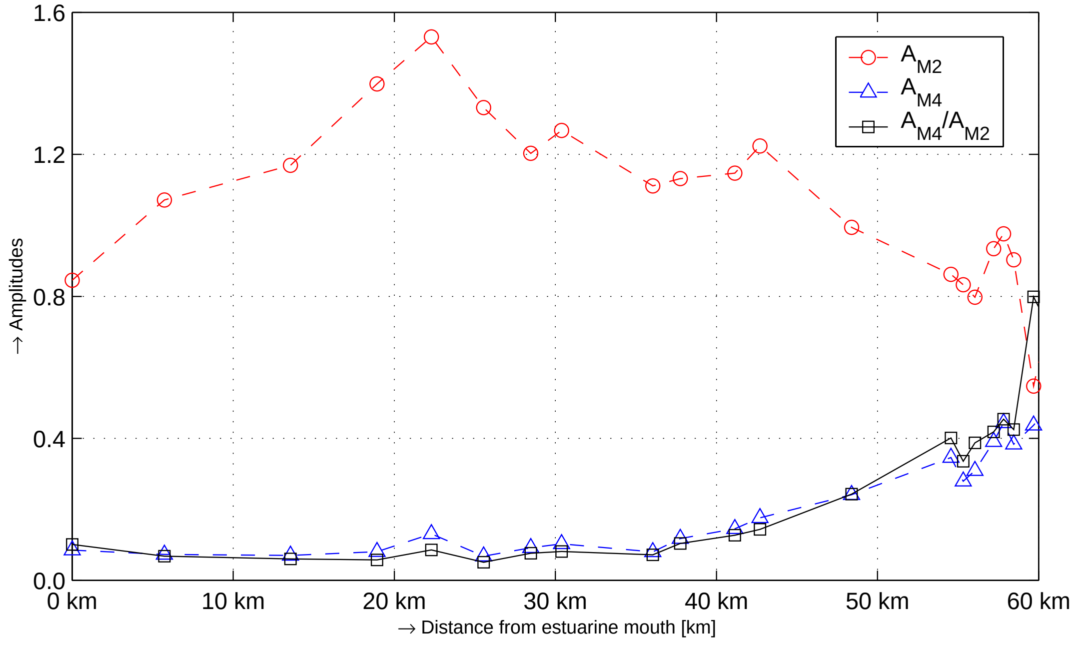

Figure 5-4 Amplitude ratio of velocity ellipse M_2 and M_4 along the estuarine channel for run TA01B

In Appendix I 'Tidal Asymmetry' the relative phase and amplitude ratio of the velocity ellipse along the estuarine channel is given for runs TA01A to TA01I. Now that when the phase and amplitude of M_2 and M_4 are calculated the magnitude and direction of the tidal asymmetry with respect to both peak velocities and slack water periods can be derived.

5.2.3 Magnitude tidal asymmetry by astronomical components analysis

The magnitude of the tidal asymmetry can be described by the parameter amplitude ratio, (see equation (3.7)). This ratio is given in Appendix I for runs TA01A to TA01I in Figure I-1 to Figure I-9.

Distinction has been made between runs with varying amplitude of M_4 in the in the sea-boundary condition and varying amplitude (see Figure 5-5) and runs with equal amplitude and varying phase (see Figure 5-6).

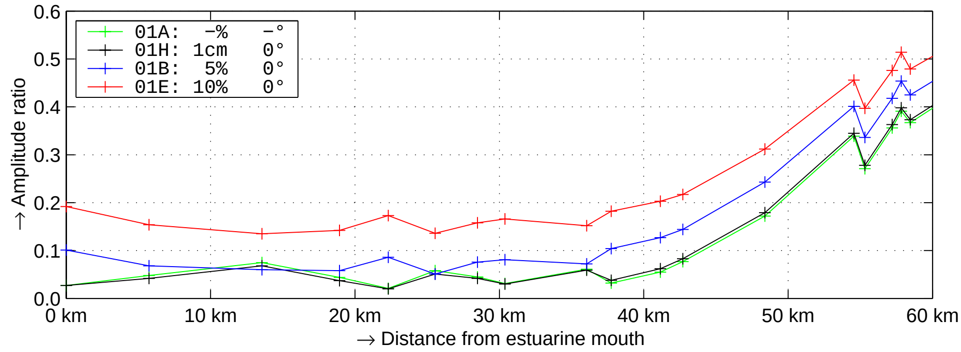

Figure 5-5 Velocity ellipse Amplitude ratio along the estuarine channel for runs with equal phases in the sea-boundary condition

All runs show an increasing ratio in the inner estuary (38 - 60 km, Obs10 – obs21). This behaviour can be explained by run TA01A. TA01A has no M_4 tidal component in the water elevation at the open sea-boundary, so that all the M_4 (in the horizontal tide) is generated locally. As can be shown in Figure 5-6 the M_4 amplitude is relatively low in the outer estuary and starts to increase rapidly at app. 40 km into the inner estuary. This increase is possibly generated by the decreasing depth. A possible explanation is described by Wang et al. (2002): 'In shallow tidal area that are characterised by large spatial velocity gradients a generation of M_4 is likely to occur as a result of the auto-interaction of M_2 via the bottom friction term and the advective inertia term.'.

When comparing the amplitude ratio between runs with an equal phase and a M_4 amplitude of 0 and 1 cm (Runs 01A and H, as shown in Figure 5-5), the amplitude ratio shows a minor difference over the full length of the estuary. Runs TA01E with an amplitude of 10 % shows a comparable development as TA01B along the estuary, only at a higher level.

The amplitude ratio of the depth averaged velocity ratio in the estuary mouth is a factor two higher for runs TA01B and TA01E than the enforced percentage of M_4 amplitude of the water elevation (see Figure 5-5). Note that if:

$$h(t) = +\hat{h}_{M2}\cos(wt) + \hat{h}_{M4}\cos(2wt - \Delta\varphi_{M2M4}) \qquad (5.1)$$

and:

$$U(t) \sim \partial h / \partial t \qquad (5.2)$$

then:

$$U(t) \sim -w\hat{h}_{M2}\sin(wt) - 2w\hat{h}_{M4}\sin(2wt - \Delta\varphi_{M2M4}) \qquad (5.3)$$

This may explain that an increase in water level of M_4 in the sea-boundary condition, results in a double increase in the velocity of M_4 at the estuary mouth.

Figure 5-6.A) Water elevation M_4 sea boundary condition: 5% of M_2

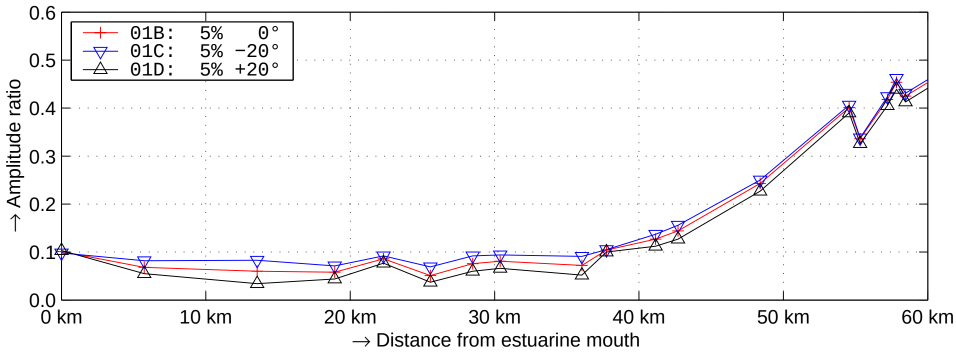

Figure 5-6.B) Water elevation M_4 sea boundary condition: 10% of M_2

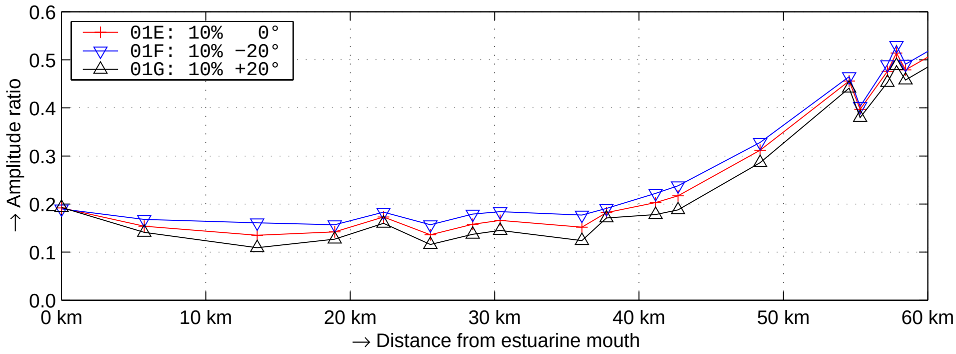

Figure 5-6 Amplitude ratio velocity ellipse M_4 along the estuarine channel for runs with equal M_4 water elevation amplitude in the sea-boundary condition

When we compare the amplitude ratio between runs with equal amplitude in the sea-boundary condition and varying phase (as shown in Figure 5-6.A and B), the amplitude ratio shows a small variation throughout the full estuarine length. The amplitude ratio throughout the estuarine channel is slightly higher for the runs with a phase of -20 degrees (TA01C and TA01F), and lower for a phase of +20 degrees (TA01C and TA01G).

Asymmetry magnitude of the horizontal tide seems more sensitive for M_4 sea-boundary condition amplitude variation than for a small variation in phase. The value of the amplitude ratio in the outer estuary depends mainly on the amplitude of M_4 in the sea-boundary condition.

Table 5-2 Overview of sensitivity of tidal asymmetry magnitude on small changes in the sea-boundary conditions

Sea-boundary condition:		Subject:	Outer estuary (0-35 km from estuarine mouth):	Inner estuary (35-60 km from estuarine mouth):
M_4 amplitude 0% and 1cm	Reference values of M_4-phase	Magnitude:	weak	medium
		Sensitivity of magnitude:	Highly dependent on amplitudes of M4 in the sea-boundary conditions.	Mainly locally generated thus not sensitive for sea boundary conditions
M_4 amplitude 5% & 10%	Reference value, small increase and decrease in relative phase M_4	Magnitude:	medium	strong
		Sensitivity of magnitude:	Highly dependent on amplitudes of M4 in the sea-boundary conditions.	Partially locally generated thus not very sensitive for sea-boundary conditions.

With respect to the amplitude ratio ($\hat{U}_{M4}/\hat{U}_{M2}$) we conclude that:

- The high amplitude of M_4 in the inner estuary is mainly locally generated and consequently not sensitive to the amplitude of the M_4 sea-boundary condition. The magnitude of the tidal asymmetry in the outer estuary on the other hand is mainly determined by the M_4 component in the water elevation in the sea-boundary condition (see Table 5-2).
- For runs with a sea-boundary condition with a M_4 amplitude of 5 or 10%, small phase differences are of minor importance on the possible magnitude of the horizontal tidal asymmetry (see Table 5-2).

5.2.4 Peak velocities asymmetry by astronomical components analysis

Tidal asymmetry with respect to peak velocities has been discussed in section 3.2.2 'Tidal asymmetry'. In Appendix H 'Relative Phase' the relative phase difference between U_{M2} and U_{M4} (φ_{M4}-$2\varphi_{M2}$) is derived. The dominant transport direction for peak velocity asymmetry is given by:

$$\text{Flood dominant peak velocities:} \qquad -90^{o} < \varphi_{M4} - 2\varphi_{M2} < +90^{o} \tag{5.4}$$

$$\text{Ebb dominant peak velocities:} \qquad +90^{o} < \varphi_{M4} - 2\varphi_{M2} < 270^{o} \tag{5.5}$$

Figures I-1 to I-9 in Appendix I 'Tidal asymmetry' show the relative phase development and the amplitude ratio of M_4 along the estuarine channel for runs TA01A to TA01I. When the development of the M_4 phase is studied a clear distinction is shown between the runs with a small M_4 amplitude in the sea-boundary condition (TA01A, H) and runs with a larger amplitude in the sea-boundary condition (TA01B, C, D, E, F and G).

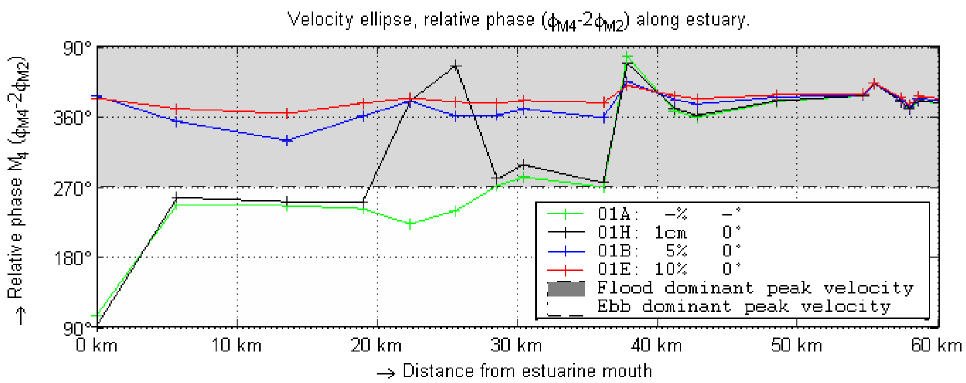

Figure 5-7 Relative phase M_4 of the velocity ellipse along the estuarine channel for runs TA01A, H, B and TA01E

Runs with a small M_4 amplitude in the sea-boundary condition (TA01A (0 cm) and TA01H (1 cm)) show a discontinuous development of the M_4 phase at the two transitions, North Sea to estuary mouth (0-5 km, obs01-obs02) and outer to inner estuary (35-40 km, obs09-obs11). Consequently, the relative phase shows a discontinuous development as well, see Figure 5-7. The relative phases in these runs lie in the inner estuary around 360 degrees and in the outer estuary around 270 degrees, with the exception of run H, which has a second area with values of app. 360 degrees at 19-28 km. In the estuary mouth and the beginning of the outer estuary, the relative phase differences of M_4 lie within ebb dominant range for peak velocities. However the amplitude ratio in the outer estuary (especially for these runs) is very small (see Figure 5-5). In the inner estuary the relative phases lie within the range of flood dominant peak velocities. Together with a high amplitude ratio this suggests that a notable dominance of the effect of flood peak velocities can be expected.

On the other hand, runs with M_4 amplitudes in the boundary condition of 5 % and 10 % of the M_2 amplitude (TA01B, C, D, E, F and TA01G) have a M_4 phase that increases gradually throughout the estuarine channel (with a relative phase angle in the region of -45 to 80 degrees), see Figure 5-8. This is over the full length of the estuary within the range of dominant peak flood velocities; combined with the increasing amplitude ratio this suggests that the peak flood velocities are dominant especially at the inner estuary.

Figure 5-8.A M4 sea-boundary condition: TA01B (5%, 0°), TA01C (5%, -20°) & TA01D (5%, +20°).

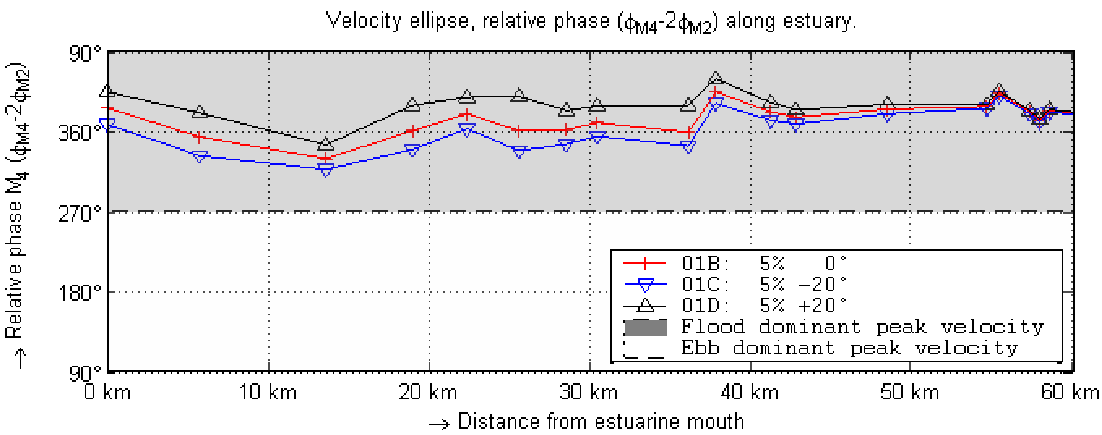

Figure 5-8.B M4 sea-boundary condition: TA01E (10%, 0°), TA01F (10%, -20°) & TA01G (10%, +20°).

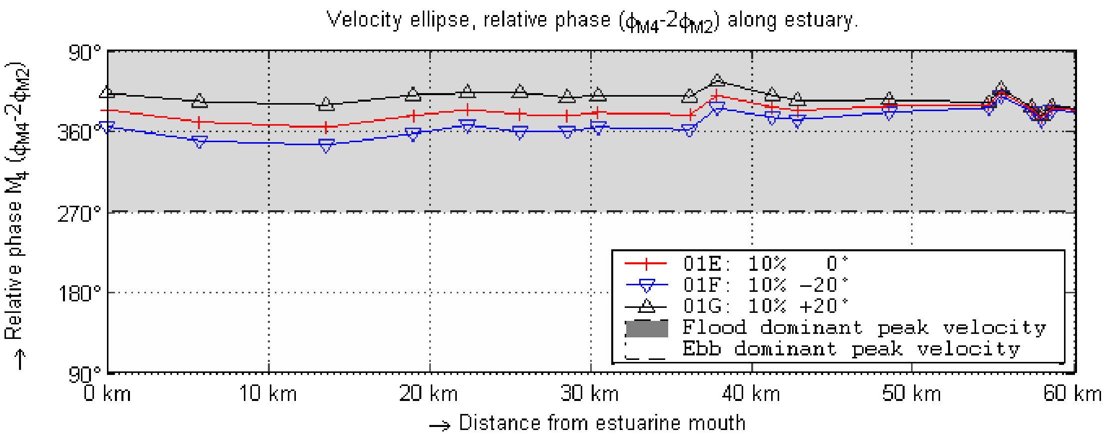

Figure 5-8 Relative phase velocity ellipse M4 along the estuarine channel for runs TA01B, C, D, E, F and TA01G

Note that, run TA01I (see Figure I-9,) does not show a notable difference in amplitude ratio and relative phase compared to run TA01H (see Figure I-8, with two components, M_2 and M_4 in the sea-boundary condition and equal phase and amplitude as simulation TA01I). Whereas TA01I has eight major tidal components in the sea-boundary condition, while TA01H has only components M_2 and M_4 in the sea boundary condition.

The conclusions with respect to peak velocity asymmetry are listed in Table 5-3.

Table 5-3 Overview of sensitivity of peak velocity asymmetry on small changes in the sea-boundary conditions, by astronomical component analysis

Sea-boundary condition:		Topic of TAPV:	Outer estuary (0-35 km from estuarine mouth):	Inner estuary (35-60 km from estuarine mouth):
M_4 amplitude 0% and 1cm	Reference values of M_4-phase	Dominant direction TAPV:	Fluctuating dominant direction, but mainly in ebb-direction	Flood-direction
		Sensitivity of dominant direction TAPS:	Relative phase near 270°-limit, therefore weak TAPV and is the dominant direction highly sensitive for small changes in sea-boundary conditions.	Relative phase near 360°-limit maximum for flood TAPV and therefore a low sensitivity for small changes in the sea-boundary.
M_4 amplitude 5% & 10%	Reference value, small increase and decrease in relative phase M_4	Dominant direction TAPV:	Flood dominated TAPV.	Flood dominated TAPV.
		Sensitivity of dominant direction TAPV:	Not very sensitive	Not sensitive

Explanation: TAPV = Tidal Asymmetry with respect to ebb and flood peak velocities. Magnitude of TAPV is calculated by the amplitude ratio of M_4 ($\hat{U}_{M4}/\hat{U}_{M2}$) see Figure 5-8.A & B. Dominant direction of TAPV follows from the relative phase of M_4 (Figure 5-5) and Figure 3-2 on page 22.

With respect to the peak velocity asymmetry we conclude that:

- The dominant direction of tidal asymmetry, with respect to peak velocities, is sensitive for small (or even absence of) amplitudes of M_4 in the sea-boundary condition in the outer estuary.
- The relative phase of M_4 in the inner estuary is for all runs within the flood dominant range with respect to peak velocities. Thus, a high amplitude ratio in the inner estuary suggests a notable effect of flood-dominant peak velocity asymmetry.
- When amplitudes of 5 and 10 % are enforced the whole estuary is flood dominant for peak velocities.

5.2.5 Slack water period asymmetry by astronomical components analysis

Tidal asymmetry with respect to slack water periods has been discussed in section 3.2.3. The dominant transport direction for slack water period asymmetry is given by:

Ebb dominant slack water periods: $$0^{\circ} < \varphi_{M4} - 2\varphi_{M2} < 180^{\circ} \tag{5.6}$$

Flood dominant slack water periods: $$180^{\circ} < \varphi_{M4} - 2\varphi_{M2} < 360^{\circ} \tag{5.7}$$

In Figure 5-9 and Figure 5-10 the relative phase M_4 of the velocity ellipse along the estuarine channel is represented. At the estuary mouth (0 km) and in the inner estuary (38-60 km) the relative phase is for all runs in the ebb dominant range. Again the runs are divided into runs with small M_4 amplitude and runs with a sea-boundary condition of 5 and 10% of the M_2 amplitude. The variation of relative phase throughout the estuarine channel varies strongly for runs with small (or even absence of) M_4 amplitude in the sea boundary conditions.

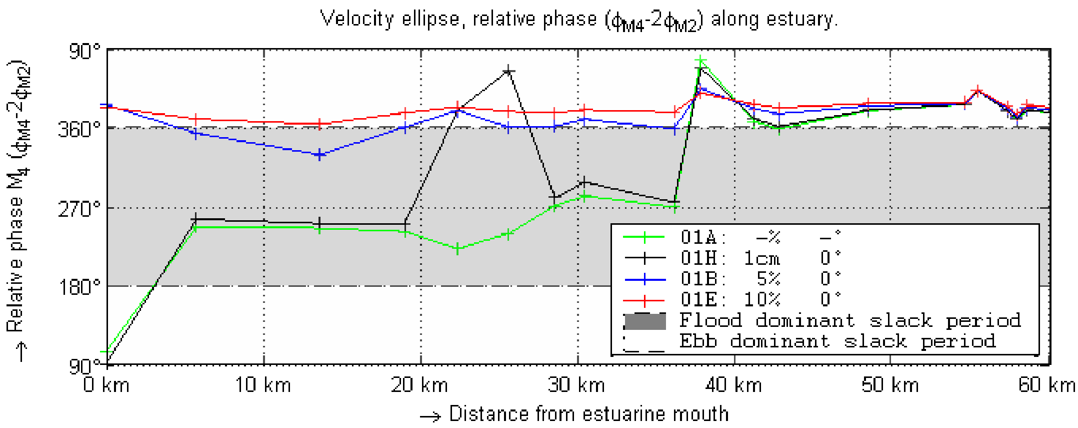

Figure 5-9 Relative phase M4 of the velocity ellipse along the estuarine channel for runs TA01A, H, B and TA01E

First runs with small M_4 amplitudes are studied. Runs TA01A, and 01H have a relative phase in the outer estuary within the range 180 to 360 degrees. Therefore, in this part the flood dominant slack water periods should dominate, see Figure 5-9. As concluded in the previous section, the amplitude ratio in the outer estuary is sensitive for changes in the sea-boundary condition. The relative phase of M_4 in Obs10 (at 38 km), just after the transition of inner to outer estuary (and in obs05 and obs06 in runs 01H and 01I) shows a sudden increase out of the flood dominant slack range into the ebb dominant range. In the inner estuary the relative phase is just above 360 degrees, except for locations obs10 (at 38 km) and 15 (at 55 km) which seem to be near 450 degrees with fluctuating high amplitude ratios.

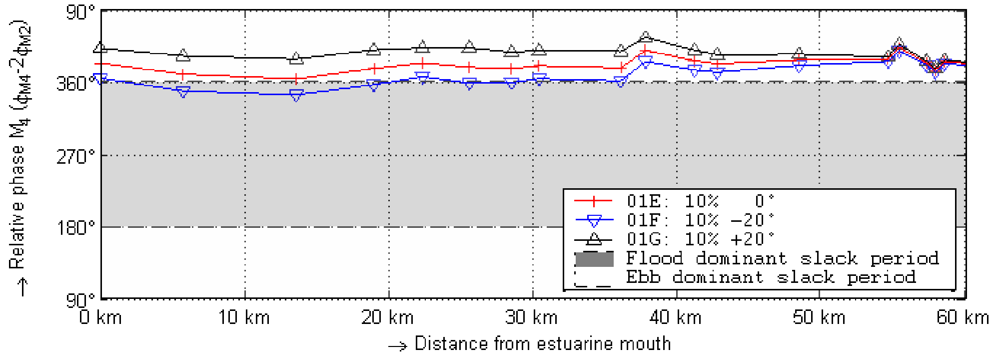

Figure 5-10 Relative phase velocity ellipse M_4 along the estuarine channel for runs TA01E, F and TA01G
M4 sea-boundary condition: TA01E (10%, 0°), TA01F (10%, -20°) & TA01G (10%, +20°).

Next, the runs with a 5% and a 10% amplitude ratio are studied, see Figure 5-10. The dominant direction of the asymmetry with respect to the slack periods is less clear at first sight, since the relative phase difference varies around the 0°-limit. Except for TA01G where the relative phase is for all observation points within the range of ebb dominant slack periods (0 to 180 degrees). Slack period asymmetry in the outer estuary can shift in dominant direction when a small change is made in the phase of M_4 in the sea-boundary condition, as shown by the difference between run TA01F and TA01G. On the other hand in Figure 3-3 on page 23 is shown that the asymmetry in dU/dt and therefore in slack water periods is small for values near the 0°-limit.

The conclusions with respect to slack water period asymmetry in combination with the conclusions regarding the tidal asymmetry magnitude are listed in Table 5-4.

Table 5-4 Overview of sensitivity of slack water period asymmetry on small changes in the sea-boundary conditions, by astronomical component analysis

Sea-boundary condition:		Topic of TASW:	Outer estuary (0-35 km from estuarine mouth):	Inner estuary (35-60 km from estuarine mouth):
M_4 amplitude 0% and 1cm	Reference values of M_4-phase	Dominant direction TASW:	Outside the Humber mouth in ebb-direction, whereas inside the outer estuary in flood–dominant direction.	A fluctuating dominant direction, but mainly flood dominated.
		Sensitivity of dominant direction TASW:	Sensitivity of TASW on absence of or small amplitude is large.	Relative phase near 360°-limits and therefore a low sensitivity for sea-boundary changes.
M_4 amplitude 5% & 10%	Reference value, small increase and decrease in relative phase M_4	Dominant direction TASW:	Fluctuating dominant direction of TASW	Ebb dominant TASW.
		Sensitivity of dominant direction TASW:	High sensitivity because the dominant direction dependents on the sea-boundary condition.	Not sensitive for small sea boundary changes.

Explanation: TASW = Tidal asymmetry with respect to slack water periods.

5.2.6 Slack water period asymmetry by slack water period analysis

The computed velocity magnitude has a far more erratic development than can be estimated by a tidal analysis of only two tidal constituents. Therefore, one would suggest that the period of slack water can give more insight in the asymmetry. When we calculate the period of the HWS and LWS, we can check if the applied theory on ebb and flood dominant slack periods due to the semi-diurnal tide and its first overtide is adequate. For convenience, we focus on the variation of the flow velocity magnitude instead of the bed shear stress. The definition of a water slack period has been chosen as the period that the magnitude of the depth average flow velocity is below a critical velocity value (u_{cr}) of 0.35 m/s, which corresponds with a bed shear stress of approximately 0.3 Pa. HWS and LWS periods are computed for 14.7 days (e.g. a full spring neap cycle in run TA01I). In Figure 5-11 two M_2 tidal periods and their slack periods are given for run TA01I in obs01, and in section I.2 of Appendix 'Tidal asymmetry' all 21 observation stations are plotted for run TA01I.

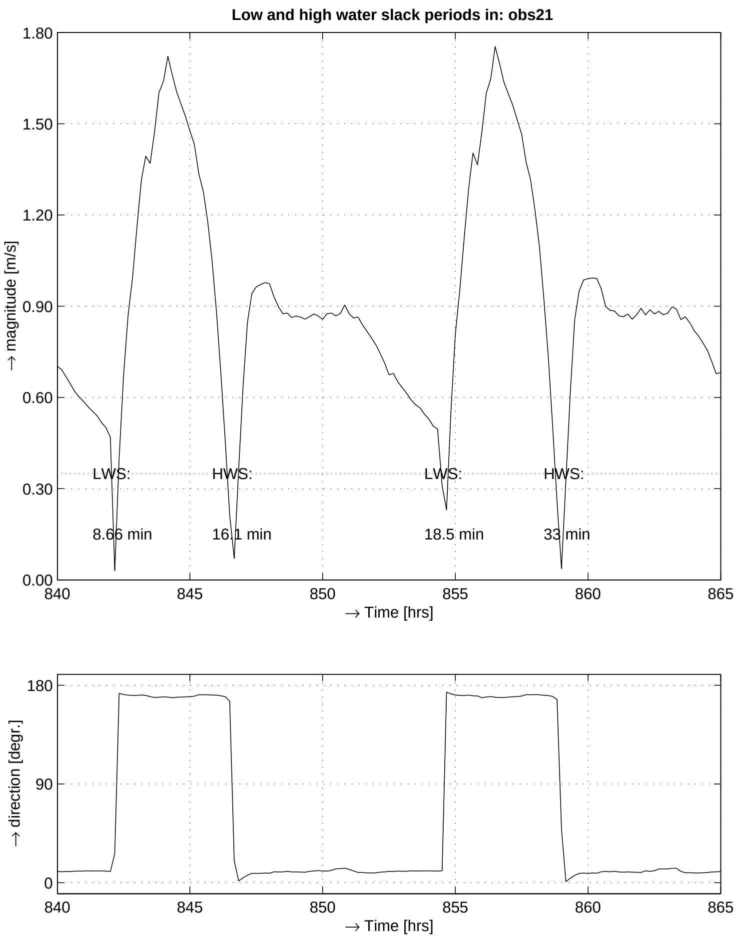

Figure 5-11 Depth average velocity magnitude, and derived HWS & LWS periods in obs01 for run TA01I
Explanation: Flood velocities are near directions of 180°, ebb velocities are near directions of 0°.

The average HWS and LWS periods in all observations points for runs TA01A to TA01I are used to derive the 'tidal averaged' slack water dominance (ΔWS=HWS-LWS). In Appendix I.2 'Slack water period analysis' the average values of HWS, LWS and ΔWS in observations along the estuarine channel are plotted for run TA01A to TA01I in Figure I-10 to I-11. This ratio gives insight in tidal asymmetry with respect to the slack water periods. When parameter ΔWS has a positive value, a fine sediment particle will have a longer period to deposit after flood during HWS than after ebb during LWS, this can result in a flood dominant fine sediments transport. See Figure 5-12 where an overview is given of the dominant direction of slack water asymmetry for each tidal asymmetry run.

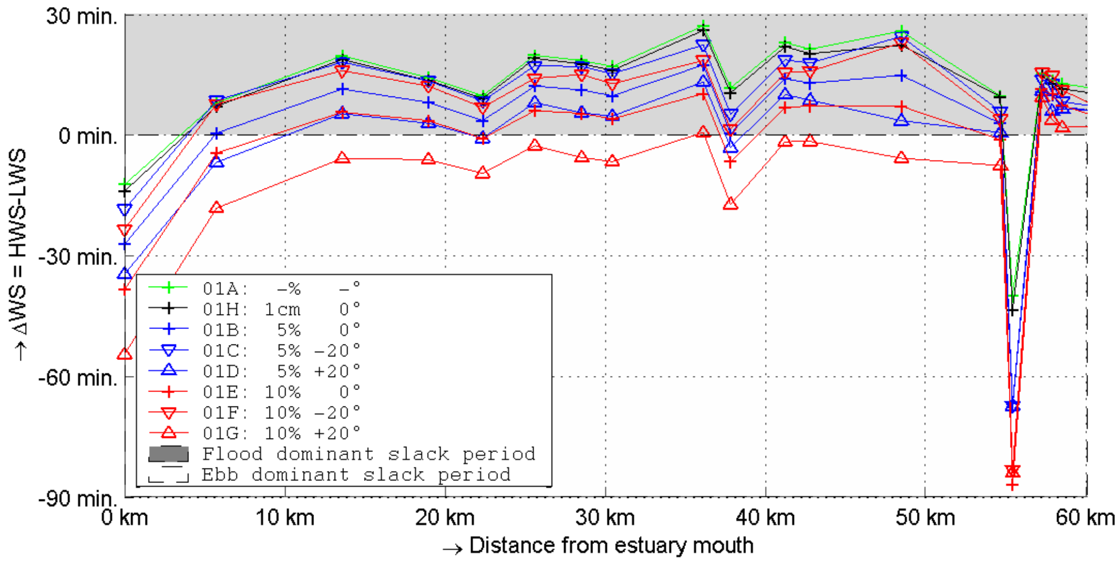

Figure 5-12 Slack water period asymmetry along estuarine channel
Explanation: Flood-dominant (ebb-dominant) slack water period asymmetry is represented by a positive (negative) value of ΔWS. Note that observation points 16, and 20 are not included in this figure because drying occurs in these cells.

In the previous section 5.2.5, the relative phase of the velocity M_4 is described. At the transition from outer to inner estuary, runs TA01A, TA01H, TA01I show a sudden increase out of the flood dominant slack range into the ebb dominant range (see Figure 5-9 at 38 km). In Figure 5-12 the transitions from outer to inner estuary (at 38 km) does not show a change in dominant direction.

During all runs, drying of cells occurs in ‘obs16’ and ‘obs20’ (see Figures I-28 and I-32). This is the explanation of the low value of the slack ratio shown in Figure I-12 and the reason why these observation points are not included in the analysis. In Figure 5-12, obs15 shows a stronger ebb-dominance than the neighbouring observation points. An analysis of all (non-drying) cells in the hydrodynamic grid is done to investigate this high difference. Figures I-37 till I-43 show the slack water dominance for runs TA01A till TAO1H and Figure 5-13 for the reference run TA01H. Figure 5-12 shows a higher sensitivity of the slack water period asymmetry in the inner estuary on small sea-boundary changes than is shown in the analysis of only the M_2 and M_4 tidal component.

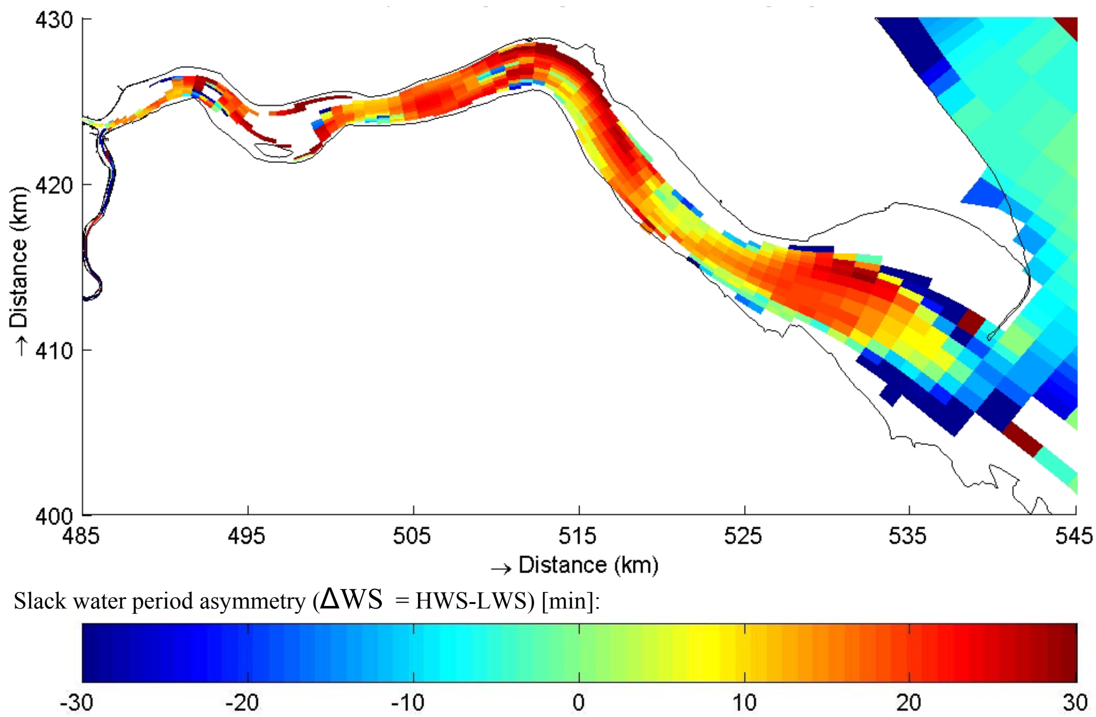

Figure 5-13 Slack water period asymmetry of reference simulation TA01H
Explanation: Flood-dominant (ebb-dominant) slack water period asymmetry is represented by a positive (negative) value of ΔWS. Note that observation numbers 16, and 20 are placed in cells were drying occurs.

From the variation of slack dominance in the inner and outer estuary it can be concluded that (as relative phase plots suggested earlier) the magnitude of the slack periods in the upper parts of the inner estuary is less sensitive to the sea-boundary than the outer estuary. Observations in Figures I-37 till I-44 show similar results; when a high ebb-dominant tide is enforced the outer estuary is forced to become ebb-dominant. This conclusion corresponds with conclusions from the astronomical constituent analysis of the velocity ellipse. An increase of phase M_4 (φ_{M4}: ↑) will decrease the relative phase ($2\varphi_{M2}$-φ_{M4}: ↓). Since the relative phase in the outer estuary for runs TA01B, C, D, E, F and G are all near the slack dominance 0°-limit, might a decrease of the relative phase, result in a switch from HWS to LWS dominance ($2\varphi_{M2}-\varphi_{M4}<0$), see Figure 3-3 on page 23.

Shallow area in the outer estuary show a relative longer low water slack period than the deeper parts of the estuary. This is explained by the difference in water level during HWS and LWS. In the shallow area is the water depth during HWS much higher then during LWS. Due to the smaller water depth at LWS, the velocity is smaller at LWS than during HWS. Whether sediment-deposit-asymmetry on the shallow area during HWS and LWS result in ebb dominant transport is beyond the scope of this analysis. In the sensitivity analysis of Channel-Shoal interaction, a more detailed analysis of the shallow area is done with a model that simulates sedimentation and erosion processes.

The conclusions with respect to slack water period asymmetry by analysing the velocity magnitude are listed in Table 5-4.

Table 5-5 Overview of sensitivity of slack water period asymmetry on small changes in the sea-boundary conditions by velocity magnitude analysis

Sea-boundary condition:		Topic of TASW:	Outer estuary (0-35 km from estuarine mouth):	Inner estuary (35-60 km from estuarine mouth):
M_4 amplitude 0% and 1cm	Reference values of M_4-phase	Dominant direction TASW:	Outside the Humber mouth and on shallow area in ebb-direction, whereas inside the deeper parts of the outer estuary in flood–dominant direction.	A fluctuating dominant direction, but mainly flood dominated.
		Sensitivity of dominant direction TASW:	Dependent on the sea boundary conditions.	Dependent on the sea boundary conditions, only the most upper reaches of the inner estuary near the Trent Falls are not sensitive for small M_4 sea boundary changes.
M_4 amplitude 5% & 10%	Reference value, small increase and decrease in relative phase M_4	Dominant direction TASW:	Flood dominant TASW direction	Flood dominant TASW direction
		Sensitivity of dominant direction TASW:	High sensitivity because the dominant direction dependents on the sea-boundary condition.	Not sensitive for small sea boundary changes.

Explanation: TASW = Tidal asymmetry with respect to slack water periods.

5.2.7 Conclusions and recommendations

In the following paragraph ‘Comparison slack period analyses’ the conclusions of the ‘Slack period asymmetry by tidal components analysis’ and ‘Slack period asymmetry by slack water period analysis’ are given. Furthermore, in section ‘Discussion’ the differences between the analyses are studied and used to estimate the influence of other components than M_2 and M_4 on the asymmetry in slack periods. The main conclusions from the previous analyses will end this section on the horizontal tidal asymmetry.

Comparison slack period analyses

Slack water period asymmetry by tidal components analysis (see Table 5-4)

- At the estuary mouth (0 km) and at the total inner estuary (35-60 km) the ebb-dominant direction seems insensitive for small sea-boundary condition changes. The relative phase of M_4 lies near the 0-limit for the outer estuary, which can mask the effect of the high amplitude ratio in the inner estuary, as shown in Figure 3-3.
- The tidal asymmetry magnitude, with respect to slack water periods, is sensitive in the outer estuary for small (or even absence of) amplitudes of M_4 in the sea-boundary condition.
- When amplitudes of M_4 water elevation in the sea-boundary condition of 5 and 10% are enforced, the direction of tidal asymmetry with respect to slack water periods varies around the 0°-limit throughout the estuarine channel. The dominant direction is therefore sensitive for changes in the phase of M_4 in the sea boundary condition.

Slack period asymmetry by slack water period analysis (see Table 5-5)

The conclusions of the tidal component analysis and the elaborated slack period analysis that are not equal are listed.

- In the inner estuary the dominant direction of tidal asymmetry with respect to slack water periods is in flood direction. A possible explanation for this difference in dominant direction could be given by effects of tidal components besides the M_2 and its first overtide M_4.
- The differences in slack water periods of the sensitivity runs are large throughout the whole estuary. In the previous analysis (of components M_2 and M_4) only the sensitivity in the outer estuary was noted for runs with small (or even absence of) M_4 amplitude of in the sea-boundary condition.

Discussion

Driving forces other than M_2 and M_4 in the sea-boundary condition on tidal asymmetry is beyond the scope of this study. Whether other components influence the M_2 and M_4 asymmetry is evaluated in the following discussion. The sea-boundary condition of simulation TA01H consists of components M_2 and M_4. Simulation TA01I has besides M_2 and M_4, 6 other large tidal components in the sea-boundary conditions. In the astronomical component analysis of M_2 and M_4 run TA01H and TA01I do not show notable differences in phases and amplitudes in the horizontal tide.

Besides the influence of other tidal constituents on M_2 and overtide M_4, higher overtides of M_2 can drive an asymmetry in slack or peak velocity as well. Wang (2002) mentioned the possible influence of the sixth-diurnal tide on the asymmetry in slack periods for the Westerschelde estuary. Only the second slack period analysis does take the influence of other components than M_2 and M_4 into account such as higher orders of the tidal components (e.g. M_6) and combined overtides (e.g. MS_4). The effect of higher overtides becomes clear when we compare the asymmetry in the first and second slack period analysis. A huge difference is found between these two analyses. The analysis of M_2 and M_4 suggest a ebb dominant slack period whereas, the second analysis shows a flood dominant slack period.

When we compare run TA01H and TA01I (in the second analysis of slack periods), the small difference in slack period asymmetry could suggest that the M_2 and its overtides are the main driving force of the tidal asymmetry with respect to slack periods. Since the spring-neap averaged values of the slack water ratio could give a distorted view no conclusion can be made. In Figure 2-8 an example is given of the 'Development of silt concentration during a neap-spring-neap cycle'. This figure clearly shows the huge influence of the spring neap cycle on the SPM.

As the amplitude ratio and the relative phase suggest (see Figure I-1 and I-9), the asymmetry difference between obs01 and obs21 are distinct in velocity magnitude. See Figure I-13 and I-33 where an extreme flood dominant peak velocity can be observed in obs21.

The influence of modelling 2Dh instead of 3D (with density differences) on tidal asymmetry is beyond the scope of this study. Gravitational circulation due to fresh water discharges may cause an asymmetry in the bed shear stress. Bed shear stresses at flood will increase due to this mechanism and decrease at ebb. A study on possible effects is described in a report by WL | Delft Hydraulics (1978).

According to Winterwerp (2002), slack period asymmetry in conjunction with lag effects or combined with peak velocity asymmetry can be of importance for fine sediment transport, depending on the bed status. Above mud banks and at the ETM up-river, the area can be classified as high-concentration mud suspensions (capacity flow condition). In this case the prominent effect will be the sediment- fluid interaction which starts to dominate the flow and suspended sediment at high concentrations. Most of the area of interest in this study can be classified as low-concentration mud suspensions (Clean bed conditions). As stated before in section 3.2.2 'Tidal asymmetry' the net transport of fine sediments, for clean bed conditions, depends mainly on the asymmetry in slack periods.

Conclusions of the Tidal Asymmetry Study

Both peak velocity and slack period asymmetry in the outer Humber estuary seem more sensitive to sea-boundary condition differences in M_4 than the inner estuary. A possible explanation is that the tidal asymmetry at the inner estuary is primarily locally generated and therefore less sensitive to changes in the sea-boundary condition.

In view of the fact that a small M_4 amplitude and small phase differences in sea-boundary conditions can have notable effects on the tidal asymmetry direction in the outer estuary, even though the amplitude ratio is small. It is recommended to investigate more precisely how the amplitude and the phase of M_4 develop, since small net effects over long periods are of importance.

When a relatively high M_4 amplitude in the sea-boundary condition is enforced, the dominant direction of the peak velocity is flood dominant in the whole estuarine channel. For slack period asymmetry the direction is more sensitive when relatively high M_4 amplitude in the sea-boundary condition is enforced.

The astronomical and the slack water period analysis in the estuarine channel give comparable results in the outer estuary. However, in the inner estuary the dominant direction of transport that follows from both analyses is not the same. This difference shows that higher harmonics play an important role in slack period asymmetry in the inner estuary. It is suggested that M_6 could influence the slack period asymmetry.

Recommendations of the Tidal Asymmetry Study

For convenience, the depth averaged velocity from the 2Dh model has been used instead of the bed shear stress to determine the slack periods. In this sensitivity analysis only the deeper parts of the estuary, referred to as estuarine channel, are studied. With a model simulating SE-processes the sensitivity of the area outside the estuarine channel can also be studied, since the analysis used in this study is inappropriate for drying cells.

The relative phase and amplitude ratio theory has a shortcoming for slack water periods since the derivative of depth averaged velocity components M_2 and M_4 is not a precise tool to measure the slack periods. Especially when a point of inflection is near the HWS or LWS period the derivative can underestimate the magnitude of the slack periods.

5.3 Gravitational circulation

5.3.1 Abstract

In the following section the sensitivity analysis of fine sediment transport on gravitational circulation is presented. Theory on gravitational circulation has been described in section 3.2.3. The density differences in the analysis are limited to those driven by salinity differences. Figures J-1 to J-17 in Appendix J ‘Gravitational Circulation’ support the analysis in this section.

Whether the density differences influence the hydrodynamics in horizontal plane or the vertical direction as well, can be estimated from the degree of stratification. Estuaries can range from well mixed to strongly stratified. Completely mixed systems are characterised by a constant density in vertical sense, while the density varies in horizontal sense. Partly mixed systems are characterised by gradually varying density both in horizontal and vertical direction.

Stratification
Hardisty (1999) analysed the stratification in the Humber estuary for a range of freshwater flow inputs and a spring neap tide. Depending on the Volume ratio (a) and the Estuary Froude Number the estuary can be classified as strongly stratified (a>1 & E<0.005), partially stratified (0.1<a<1 &, 0.005<E<0.2) or well mixed (a<0.1 &, E>0.2).

Volume ratio (a): $$a = Q_\mathrm{R} T / V_\mathrm{F} \tag{5.8}$$

Estuary Froude Number ($\mathrm{F_o}$): $$F_\mathrm{o} = U_{\max} / (gh)^{0.5} \tag{5.9}$$

Estuary Number (E): $$\mathrm{E} = F_\mathrm{o}^{\,2} / a \tag{5.10}$$

With:

E	:	Estuary Number	[-]
F_o	:	Estuary Mouth Froude number	[-]
a	:	Volume ratio, the volume of water entering the estuary during each tidal cycle divided by the flood volume of the tide	[-]
Q_R	:	river discharge	[m^3.s^{-1}]
T	:	duration of the tidal cycle	[s]
V_F	:	volume of sea water entering the estuary at the mouth on the flood tide	[m^3]
$U_{\max}$	:	maximum cross section average flow during flood at the estuary mouth	
h	:	cross section averaged water depth below mean sea level at the estuary mouth	[m]

Table 5-6 Estuary Number during spring and neap tide

Freshwater [$m^3.s^{-1}$]	Volume ratio (a) Spring [-]	Volume ratio (a) Neap [-]	Estuary Number (E) Spring [-]	Estuary Number (E) Neap [-]
50	1.3 10^{-4}	2.8 10^{-4}	698.8	146
250	6.6 10^{-4}	13.9 10^{-4}	139.8	29.2
2500	65.6 10^{-4}	139.5 10^{-4}	14	2.9

Source Hardisty (1999)

The results confirm that the Estuary Froude number ranges from 0.2 to 0.3 over the neap to spring cycle and that both the Volume Ratio and the Estuary Number indicate that very well mixed conditions prevail at extremely low fresh water discharges and small tides.

5.3.2 Set-up of the gravitational circulation study

Before net sediment transport is studied in the sensitivity analysis, a summary is given of the model approach. Secondly a description is given of the aggregated grid used in the following analyses.

In first attempt, a 2Dh and 3D model were used to study the effect of gravitational circulation on fine sediment transport. Attention was paid to minimize differences in the hydrodynamics other than due to density differences. In order to make sure that a comparison between 2Dh and 3D models agrees with the aim described above a check has been done. In a comparison between two homogeneous density runs in 2Dh (GC01A) and 3D (GC01E) the bed shear stresses appeared erroneous. An adjustment in the Delft3D-Delwaq software solved this error (the encountered problem is described in Appendix O 'Previous Delft3D-Delwaq version'). All runs used in the following analysis are made with the correct DELWAQ (version 450.05).

Besides the small differences in hydrodynamics in 2Dh and 3D, a difference in sediment transport exists. Therefore, the effect of gravitational circulation only is studied by 3D simulations. This is done by comparison of a homogeneous density simulation with a non-homogeneous density simulation (GC01E versus GC01C). Besides the difference due to gravitational circulation the effect of modelling 2Dh instead of 3D is studied by comparison of a 2Dh simulation with a 3D homogeneous density simulation (GC01A versus GC01E).

Table 5-7 Model approach, sensitivity analysis gravitational circulation

Runid	Model type		Discharge
GC01A	2D	homogeneous density	3 years average
GC01C	3D	fresh – salt	3 years average
GC01E	3D	homogeneous density	3 years average

The hydrodynamics used in run GC01A is equal to reference run CH02. In case of a 3D model 10 evenly distributed layers in depth are used.

In order to study the process of gravitational circulation the tide is modelled by a sea-boundary condition consisting of tidal components M_2 and M_4 (tidal components as in reference run TA01H, see Table 5-1). Fluctuations due to a spring neap cycle are out of the scope of this study. At the end of this section a recommendation is done to study the effects of a spring neap cycle on the net up-estuary sediment transport.
In the following study, the horizontal transport profile in vertical direction is of interest. For this reason the transport fluxes are calculated in 10 equally distributed layers in depth for

transects that cover the longitudinal direction of the estuary. In Figure 4-4 on page 41, the aggregated grid together with the transect-names is shown that is used here.

5.3.3 Depth averaged transport

From Figure J-1 follows that the simulations described in Table 5-5 have a similar gross water discharge through cross-section '01->03'. The classification of the estuary as 'well mixed' already suggested that the influence of density differences in the vertical plane - possibly effecting the turbulent mixing capacity and therefore the friction- has no notable effect on the gross discharge. The gross discharge through section '01-04' is approximately 1 percent of the gross discharge through section '01-03'. From mass balance principles it follows that the depth averaged net discharge through a cross section over the full width of the estuary ought to be equal to discharges emptied by River Ouse and River Trent in the estuary (see Table 5-8).

Note that net discharges through the aggregated grid are calculated from the Delft3D-Delwaq output, which are coupled periods of hydrodynamics originally calculated by the Delft3D-Flow module. A coupling period of six tides has been chosen to minimize the error induced by the output time-step of half an hour. A similar approach will be used to calculate the net discharge and net fine sediment transports. Table 5-8 shows that the difference between the net discharge and the river discharge, of minus 176 m^3/sec, decreases up-estuary. A possible reason for this error may be found in a small coupling error of the hydrodynamics, since gross discharge increases down-estuary. An error induced by the output time step of half an hour results in an over estimation of six M_2 tide periods by 59 seconds. On start and end point of the integration period (see Gross discharge on 15 Oct 14:30 in Figure J-1) the gross importing discharge through '01-03' was approximately +8 10^4 m^3s^{-1} resulting in a lower net export (averaged over 6 M_2 tidal periods) of approximately 17 m^3s^{-1} through cross section 01-03.

Although net discharges can be of great importance since they are able to drive a net transport of sediments, the error in net discharges in the Humber mouth is acceptable small compared with the relatively high values of net fine sediment transport.

Table 5-8 Net depth averaged discharge and net transport of fine sediment along the estuary

Cross-section	Net discharge [m^3s^{-1}]			Net fine sediment transport [kTa^{-1}]		
	GC01A	GC01E	GC01C	GC01A	GC01E	GC01C
Import						
01 -> 02	0	0	0	0	0	0
01 -> 03	-312	-259	-216	1.0E+04	1.1E+04	1.2E+04
01 -> 04	+153	+94	+53	2.0E+02	1.1E+02	3.7E+01
	-159	**-166**	**-163.4**	**1.0E+04**	**1.1E+04**	**1.2E+04**
A -> B						
02 -> 05	+13	+21	14	-7.5E+00	4.2E+00	-2.4E-01
03 -> 06	-184	-196	-188	5.3E+02	5.3E+02	8.2E+02
04 -> 07	0	0	0	0	0	0
	171	**175**	**-174**	**5.2E+02**	**5.4E+02**	**8.2E+02**
B -> C						
06 -> 08	-191	-196	-119	1.8E+02	1.7E+02	2.4E+02
07 -> 09	+15	19	-58	2.4E+00	7.4E+00	-2.3E+01
	-175	**-178**	**-177**	**1.9E+02**	**1.8E+02**	**2.2E+02**
C -> D						
08 -> 10	-209	-212	-207	9.9E+01	1.1E+02	1.3E+02
09 -> 11	+32	+33	+29.6	1.5E+00	5.3E+00	-2.0E+00
	-176	**-178**	**-177**	**1.0E+02**	**1.2E+02**	**1.3E+02**

Source: Net transport of fine sediment over a period of 6 semi-diurnal tides (12-Oct-2000 02:00 to 15-Oct-2000 04:30). Up-estuary is defined as the positive direction. Figure J-8 till J-12 present the distribution of the net discharge. Figure J-15 till Figure J-17 present the net transports in the aggregated grid. 'Figure 4-4 Aggregated grid Humber estuary' on page 41 shows the aggregated grid together with the transect names.

Note that the gross discharge through 01-04 is approximately 1% of the value in 01-03, whereas the net importing discharge through cross-section 01-04 is up to 50% (for GC01A) of the net exporting discharge through cross section 01-03. Nevertheless, the difference in net transport of fine sediments through 01-04 (and other tidal flats) is much smaller than the cumulative difference between the runs that we are interested in. For this reason the following analysis will only focus on the channel cross-sections (the cross-sections of main interest are high-lighted in Table 5-8 and shown in Figure 5-14).

Concentration

When we study the concentration development, a large difference can be found between the ebb (18:30-00:30) and flood (15:00-18:30 & 00:30-03:30), see Figure 5-14. Logically, a higher average concentration exists at the Humber mouth during flood than during ebb. This is the consequence of modelling marine sediments that can only settle inside the Humber estuary.

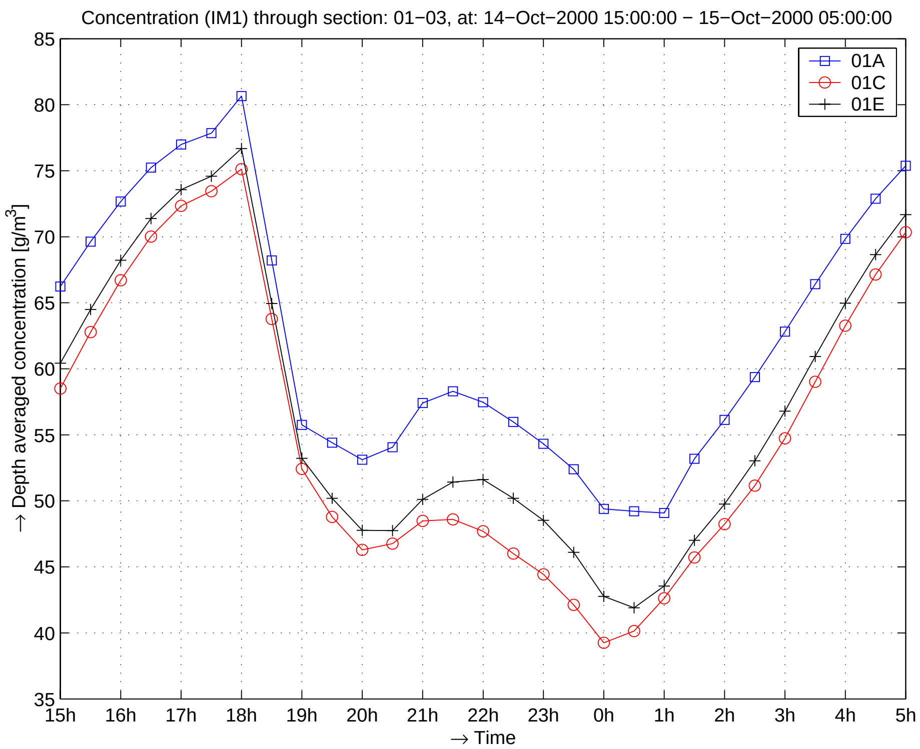

Figure 5-14 Concentration in cross section 01 -> 03

Explanation: the computation method of average concentration through cross section that is used in the sensitivity analysis is described in section 4.3.3. For an explanation of the WAQ runs see Table 5-7 on page 70.

When we compare the two 3D runs we can see that over the full period of the M_2 tide the concentration in cross section '01-03' is higher for run 01E than for 01C. Especially during part of the ebb tide (20:30 - 00:00), the difference between the depth averaged concentrations in 2Dh (01A) and 3D runs (01C and 01D) is significant. The difference between 2Dh and 3D computations is explained using a mental experiment described in Appendix J.2 'Experiment 2Dh and 3D transport'. From this analysis follows that when the depth averaged concentration is equal, the deposition term is larger for 3D than for 2Dh computations. This is why the depth averaged concentration after a few time steps will be larger for 2Dh than for 3D computation.

Net fine sediment transport
The depth averaged net fine sediment transport is computed for the gravitational circulation runs that are described in the previous section. See Table 5-8 (in the previous section) and Figure 5-15.

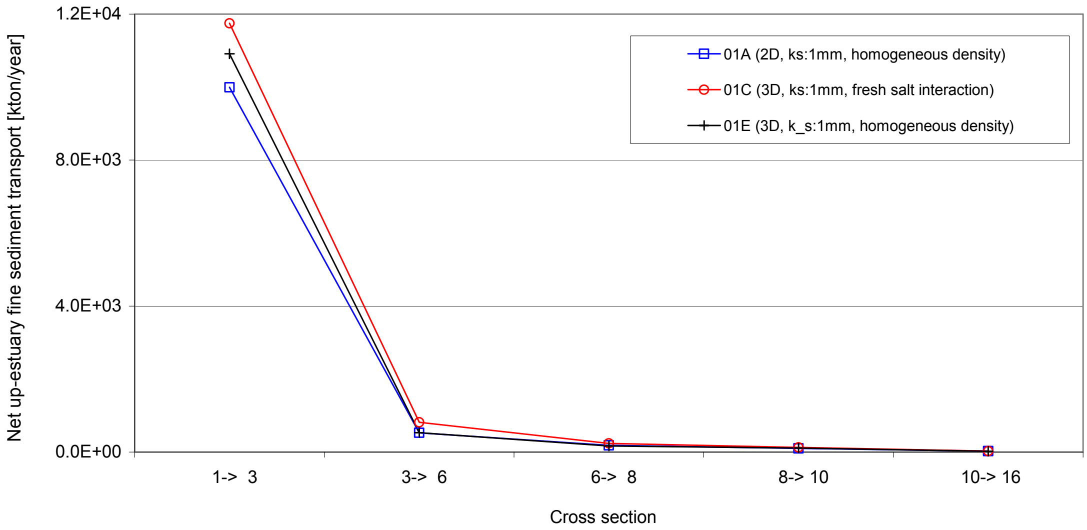

Figure 5-15 Net up-estuary transport of fine sediment through the main channel a tide

The three dimensional simulation GC01C with gravitational circulation shows a higher net fine sediment import than simulation GC01E. Note that the relative difference due to gravitational circulation is of the same order of magnitude as the difference between two and three dimensional simulations, except for section ‘03-06’ where a relative large difference is found (see Table 5-8). In this region a high salinity gradient moves up- and down-estuary with the tidal motion. This salinity gradient in horizontal direction co-exists with a density gradient. Therefore, gravitational circulation in run GC01C is a possible explanation for the relatively large net fine sediment transport. To analyse the difference between the three runs in Figure 5-15, the layers’ averaged transports in a profile along the relative depth are studied (see section 0).

Discussion depth averaged transport in 2Dh and 3D
In the previous section a distinct difference was found in depth averaged transport between the two and three dimensional runs with homogenous density. In Table 5-9 a list is given of the observations regarding depth averaged transport.

Table 5-9 Overview of depth averaged discharge, concentration, gross transport and net transport

Area:	GC01C		GC01E		GC01A	
Depth averaged gross discharge (Q_{gross})	$Q_{gross01C}$	≈	$Q_{gross01E}$	≈	$Q_{gross01A}$	(Figure J-1)
Depth averaged concentration (C)	C_{01C}	<	C_{01E}	<	C_{01A}	(Figure 5-14)
Depth averaged fine sediment transport (T_{gross})	$T_{gross01C}$	<	$T_{gross01E}$	<	$T_{gross01A}$	(Figure J-2)
Depth averaged fine sediment transport (T_{net})	T_{net01C}	>	T_{net01E}	>	T_{net01A}	(Figure 5-15)

The differences in 2Dh and 3D computation are elaborated in Appendix J ‘Gravitational Circulation’. The first experiment describes that -under the assumption of an equal depth averaged concentration in 2Dh and 3D mode- the deposition term in 3D is higher than in

2Dh mode. Since the near bed concentration of the 3D simulation is higher than the depth averaged concentration.

A second experiment is done to describe the differences in concentration and in gross transport (see Appendix J.2 for a description of the second experiment). Under the assumption of an equal depth averaged concentration and an equal depth averaged velocity, the observed difference between sediment transport in 2Dh and 3D is explained in Appendix J.2. The conclusions from these analyses are summarized as follows.

$$\begin{aligned} &c_{\text{2Dbottom}} (= \overline{c_{\text{2D}}}) < c_{\text{3D bottom}} \\ &D = w_s c_{\text{bottom}}, \\ &D_{\text{3D}} > D_{\text{2D}} \end{aligned} \tag{5.11}$$

When the depth averaged components of velocity ($\overline{u}$) and concentration ($\overline{c}$) are separated from the profile, the difference between 2Dh and 3D becomes clear.

$$\begin{aligned} T_{\text{2D}} &= \overline{u} \cdot \overline{c} \\ T_{\text{3D}} &= \overline{u} \cdot \overline{c} + \overline{u'c'} \end{aligned} \tag{5.12}$$

Considering the profile of sediment transport and the profile of velocity it appears that the right hand term of equation (5.12) has a negative value, which results in a higher gross transport of fine sediments for 2Dh simulations.

5.3.4 Distribution of transport in the vertical direction

Gross transport distribution

In Figure J-4 to J-7, discharge, concentration and gross transport is given for section ‘01-03’ on October 14th at the following time steps: near maximum flood (15:30), in between max flood and max ebb, approaching HWS (18:30) near maximum ebb velocity (21:00) and in between maximum ebb and maximum flood, approaching LWS (00:30).

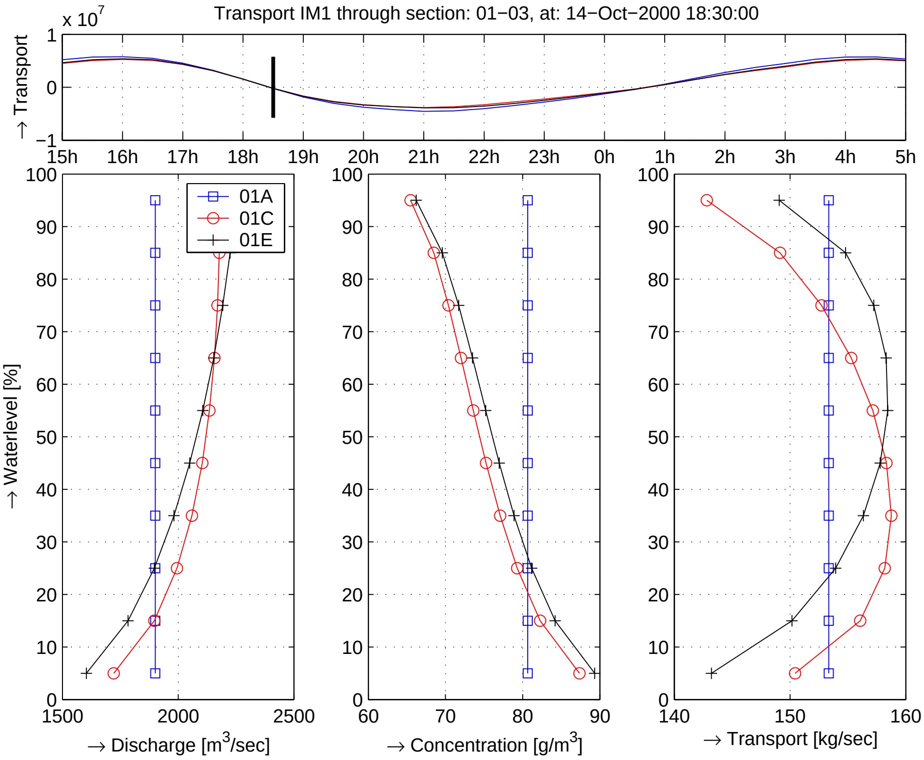

Figure 5-16 Profile of gross discharge, concentration and gross sediment transport over depth in section 01-03 approaching HWS

Explanation: the figure at the top represents gross transport of fine sediments and a marked time step below, indicating the phase of the sediment transport of the three figures below.

It is hard to draw conclusions from the figures J-4 to J-7, since a small phase difference in hydrodynamics could result in large differences in gross sediment transport. A possible difference in hydrodynamics in 3D (GC01E) versus 2Dh (GC01A) due to inertia is a more early turn in tide near the bottom for 3D. Note that the two 3D runs (GC01C and GC01E) show a clear difference in hydrodynamics near the slack periods. When approaching HWS (Figure 5-16), the decreasing flood velocity near the bed will have a higher value for GC01C than for GC01E, whereas the opposite will occur at decreasing ebb velocity when approaching LWS (see J-7).

Net transport distribution

Net discharge and transport through channel cross-sections are computed for every layer separately, see Figures J-8 to J-12 in Appendix 'Gravitational Circulation' and for section 03-06, see Figure 5-17. The net discharge of simulation GC01C shows an up-estuary bottom residual flow and a down-estuary surface residual flow. The net transport of fine sediments shows a higher import near the bottom, as suggested by the theory.

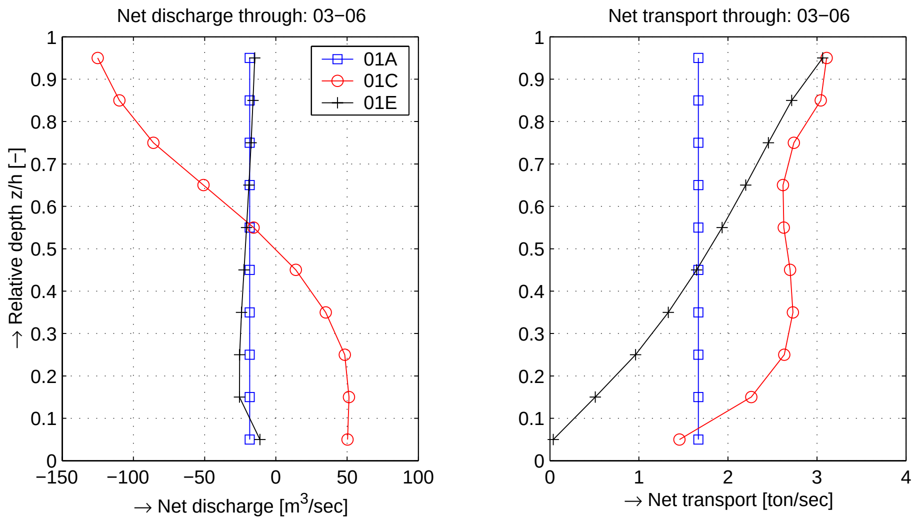

Figure 5-17 Net discharge and transport profile through cross section 03-06
Source: Cumulative discharges every 30min, integration period: 12-Oct-2000 02:00 to 15-Oct-2000 04:30

In Table 5-8 is shown that the depth averaged value of net transport through cross section 03-06 is highest for simulation GC01C. Whether this maximum influence of gravitational circulation is shifted up-estuary when the concentrations in the inner estuary increase can be subject of further research.

5.3.5 Sedimentation areas

During the analysis distinction is made between gross cumulative sedimentation and net cumulative sedimentation. With help of the first quantity the areas where both settling and erosion occurs becomes clear. The latter quantity helps to analyse in which area net trapping of sediments occurs.

Gross cumulative sedimentation
In the Humber estuary the bed material on many shallow areas consists of fine sediments. Figure 5-18 represents the cumulative amount of fine sediment settled on the bed after three months of simulation. Charts of the Humber estuary and the output from the simulations show corresponding locations in the outer estuary where fine sediments settle.

Some difference can be found on the north tidal flat near the estuary mouth (e.g. Skeffling clays and the Easington clays). In the most upper part of the intertidal flat no net deposition seems to occur. A more detailed analysis shows that the tidal flat is inundated for about six hours by water containing small amounts of sediments in the water column. The velocities that occur in this area are low, but just high enough to erode the small amounts of settled material, resulting in zero net sedimentation.

Unfortunately, modelling of the inner estuary does not show a large correlation with measured concentrations. An explanation could be that the major part of the sediment is trapped in the outer estuary and therefore does not reach the inner estuary. Possible natural processes -that are not included in the model- which bring back more particles in suspension are: wave induced bed shear stresses and an increase in maximum bed shear stresses due to the spring-neap cycle. It is suggested by De Jong and Beusekom (1995 from Winterwerp 2003-07) that even small waves, which are not included in this model, could spread the matter more evenly over this sheltered shallow area.

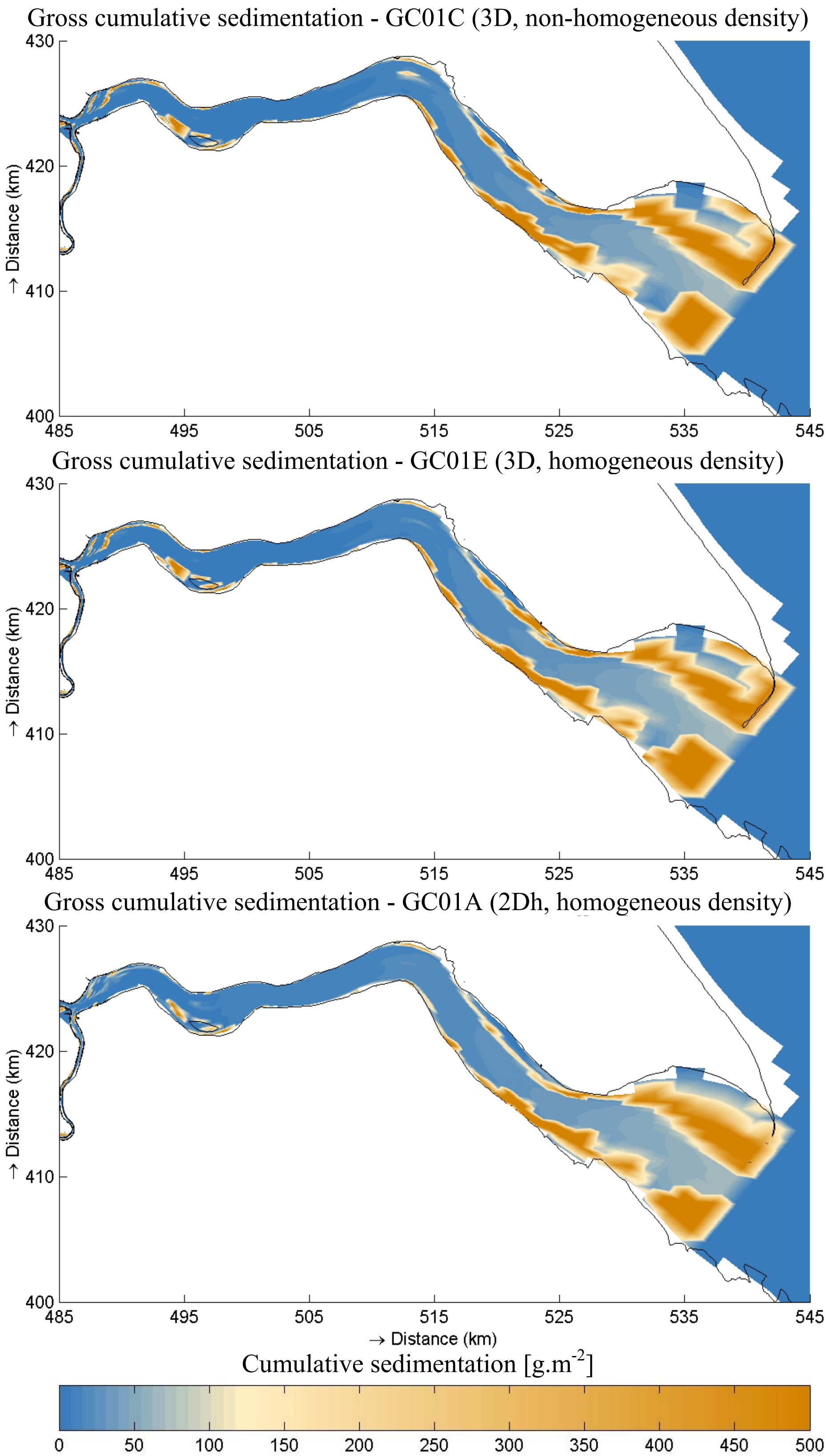

Figure 5-18 Gross cumulative sedimentation three months after 'cold-start' of runs GC01C, GC01E & GC01A
Explanation: note that the values have been clipped above 500 g.m^{-2} whereas the highest recorded value is 23 kg.m^{-2}.

Net fine sedimentation

Due to the initial ‘cold start’ bed-condition no net erosion is possible. Therefore, Figure 5-19 represents the net increase of the sediment in the bottom layer in [kg.a^{-1}.m^{-2}].

During the simulation no sediments net settle in the channel sections due to the high bed shear stresses that occur. Note that sediments do settle continuously in the channel, but they are eroded within the tidal cycle period (see Figure 5-18). Areas of net sedimentation are primarily located in the outer estuary on the tidal flats and that only a few cells determine the net import.

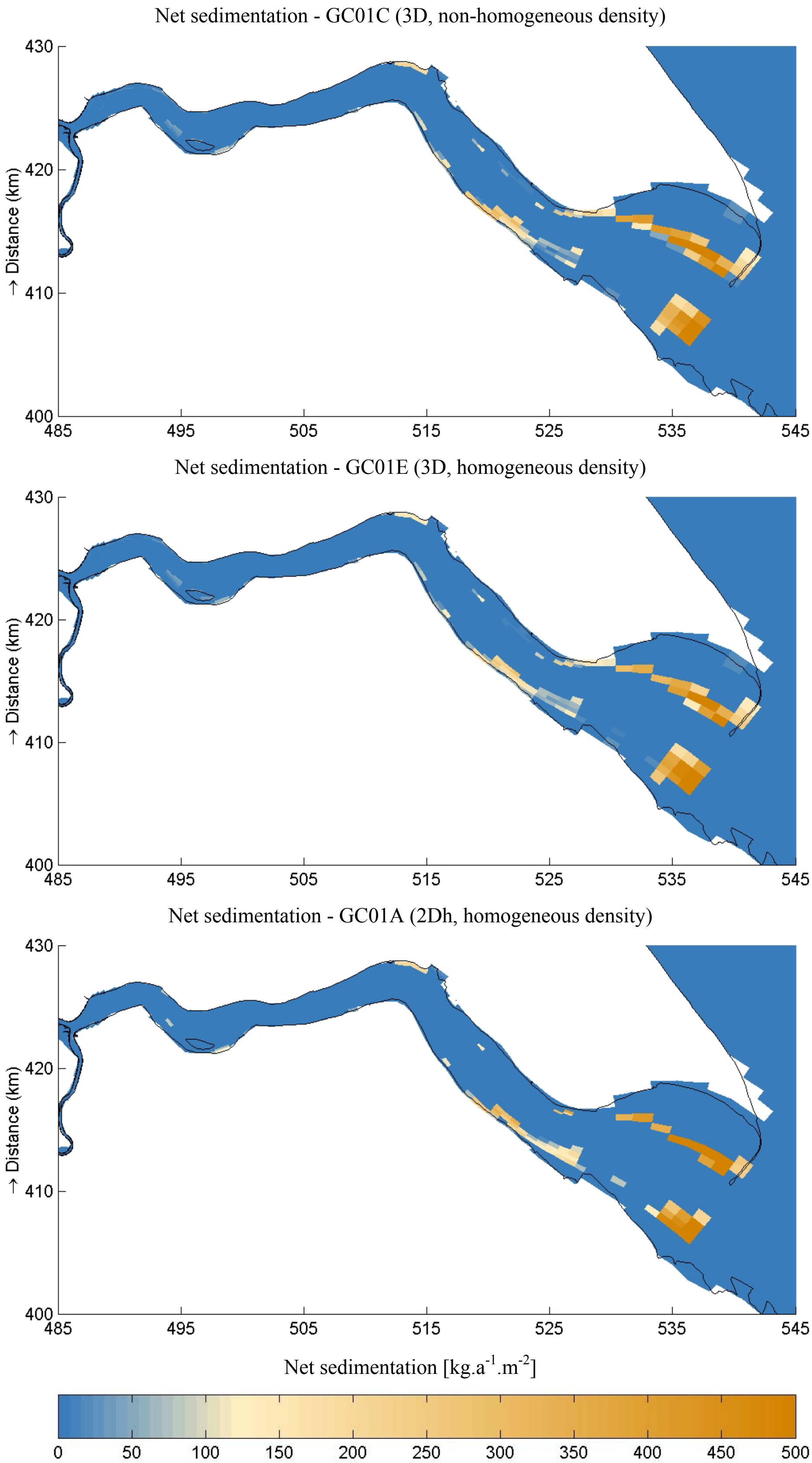

Figure 5-19 Net sedimentation of fine sediment of runs GC01C, GC01E & GC01A
Explanation: note that the values have been clipped above 500 kg.m^{-2} whereas the highest recorded value is 700 kg.m^{-2}

5.3.6 Conclusions and recommendations of the gravitational circulation study

Discussion
Gross transport is higher for simulations of homogeneous density than for non-homogeneous density simulations. However, the latter shows a slightly higher net import in the estuary due to gravitational circulation. The influence of horizontal density gradients on net discharge results in a profile as described in literature; net importing flow near the bottom and net exporting flow at the top of the water column, resulting in an increase of net import of fine sediments.

Conclusions

The settling area of fine sediments in the model shows a high correlation with admiralty charts of the outer estuary. This is not the case in the inner estuary.

Net fine sediment transport has not proven to be very sensitive to the non-homogeneous density. The difference in net transport due to gravitational circulation is in the order of 10% of the total net fine sediments import.

An unexpected conclusion is that the difference in net transport due to gravitational circulation and the difference between 2Dh and 3D simulations are of the same order of magnitude. Therefore no comparison of net transports should be made between 2Dh and 3D computations.

Recommendations

A spring neap cycle could affect the gravitational circulation by a combination of fluctuating suspended sediment concentrations and density gradients. Besides the effect of a spring-neap cycle on gravitational circulation its effect on net-landwards transport is unclear. Further study is needed to analyse the effect of a spring-neap cycle on gravitational circulation.

The inflow of rivers was modelled as a constant three years' average river discharge from River Trent and River Ouse. Natural conditions are that during winter a higher discharge enters the Humber then during summer. Further study is needed to analyse the effect of a higher and lower discharge and of a decreasing and increasing discharge on net sediment transport.

Further investigation is needed to evaluate if an adjustments in the current 2Dh SE-transport process simulation could result in an improvement of fine sediment transport. Note that with this adjustment the advantage of relative small computing time in 2Dh must not be lost.

Further study is needed in order to analyse what processes could enhance the sediment distribution along the estuary. It is suggested that this distribution could be enhanced by modelling wave action.

5.4 Channel-Shoal interaction study

5.4.1 Set-up of the channel-shoal interaction study

In section 3.2 the possible influence of intertidal areas on fine sediment net import is described. As suggested in this literature survey the interaction between channel and shoal are of importance to the net import. Note that results from the gravitational circulation study are consistent with the theory (see Figure 5-18).

The total friction can be divided in form drag and skin friction, where form drag is much higher than the skin friction. For the SE-processes the exchange of sediment between bed and water column is of main importance. Whitehouse (2000b) discussed the difference in parameterization of sub-grid effects with respect to fine sediment. According to Whitehouse (2000b) and others, the relevant bed shear stresses for sediment transport should be based on the local skin friction coefficient. Therefore, in the following analysis, the sensitivity of net sediment transport on bed roughness in the SE-processes is studied. Note that the bed roughness in the hydrodynamics is kept constant in the following runs. Figures in Appendix K 'Channel shoal interaction' support the analysis in this section.

In the following analysis the differences in net transport between two constant values of bed roughness in SE process are studied. Bed shear stress is more sensitive for changes in bed roughness in shallow areas than in the deeper parts. Therefore, a change in channel – shoal interaction is expected.

> *A higher Nikuradse roughness height (k_s) value results in a higher bed shear stress. Hence, a higher bed shear stress will result in higher (and longer period of) erosion when bed material is available. According to Winterwerp (2003-01) the probability of deposition in Krone's formula must not be used together with the erosion formula of Partheniades (as discussed in section 3.1.1). Therefore deposition in this model is not dependent on bed shear stress, but only on concentration near the bed and the particle fall velocity (e.g. constant at 0.5 $mm.s^{-1}$). However a higher bed shear stress will result in a higher amount of sediments in the water column. Due to the higher concentration is locally a higher deposition possible.*

The succession of influences as shown above makes the quantity of the net effect hard to predict beforehand. A numerical model enhances our insight in the sensitivity of SE-processes of fine sediments for a small change in bed roughness.

In Table 5-10 a summary is given of the numerical models that are developed to study the sensitivity on channel – shoal interaction. Note that GC01C and GC01A are equal to the runs described in the previous chapter 'Gravitational Circulation'.

Table 5-10 Model approach, sensitivity analysis channel-shoal interaction

Runid	Model type		Discharge	Roughness[6] (k_s):
GC01A	2D	homogeneous density	3 years average	1 mm
GC01B	2D	homogeneous density	3 years average	10 mm
GC01C	3D	fresh – salt	3 years average	1 mm
GC01D	3D	fresh – salt	3 years average	10 mm

The hydrodynamics used in runs GC01A, to GC01D are reference runs as in the calibration (Ch02). In case of a 3D model 10 evenly distributed layers in depth are used.

In the following two sections the gross and net sedimentation is studied of the runs described in Table 5-10. The gross sedimentation presents the area where sediment has settled at a certain phase of the tidal cycle. Secondly the net sedimentation is presented; this section shows the area where conditions of net aggregation prevail. Figure F-4 presents the names of the aggregated grid cells that will be used in the following analysis. In the following sections two and three dimensional simulations are analysed separately.

[6] *The roughness of the hydrodynamics and the SE-processes is not the same. The roughness given in Table 5-10 refers to the value used in the SE-processes. In the hydrodynamics the roughness is kept constant at the value that follows from the calibration study (see section 4.2).*

5.4.2 Fine sediment gross cumulative sedimentation

Gross sedimentation, 3D simulations

The model gives a reasonable representation of the settling area in the outer estuary, as described in section 5.3.5 for simulation GC01C. Figure 5-20 shows that on the tidal flats more sediment has settled for the 'smooth-bed' simulation. Figure 5-22 represents the net sedimentation after the concentration shows a repeating development (after the spin-up time is completed).

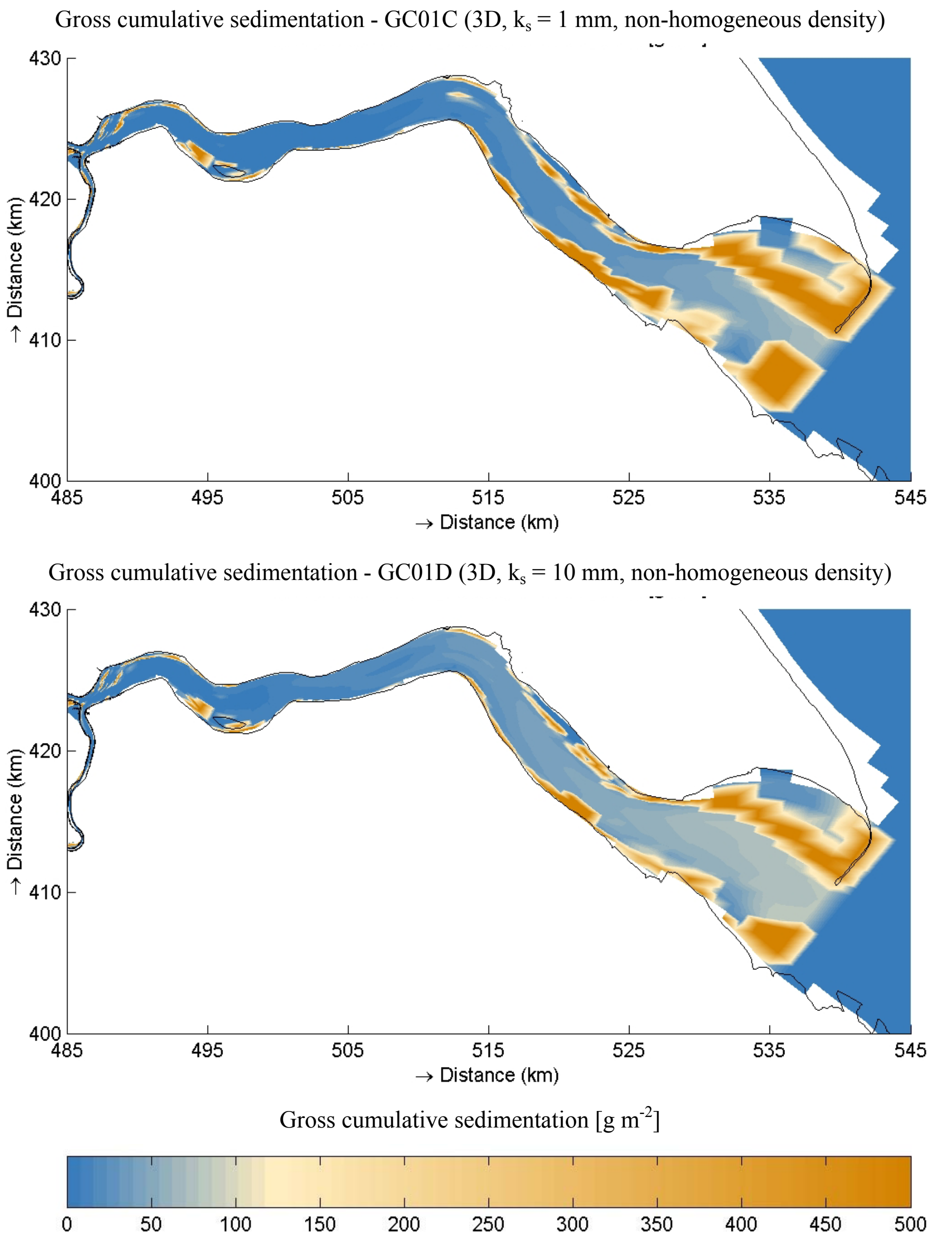

Figure 5-20 Gross cumulative sedimentation of 3D runs GC01C & GC01D three months after 'cold-start'
Explanation: Sedimentation in g m^{-2}, note that the values have been clipped above 500 g m^{-2} whereas the highest recorded value is 20 kg.m^{-2}.

Gross sedimentation, 2Dh simulations

Figure 5-21 presents the gross cumulative sedimentation after three months of simulation. Again, more sediment has settled in the intertidal area during the 'smooth-bed' simulation GC01A than during GC01B.

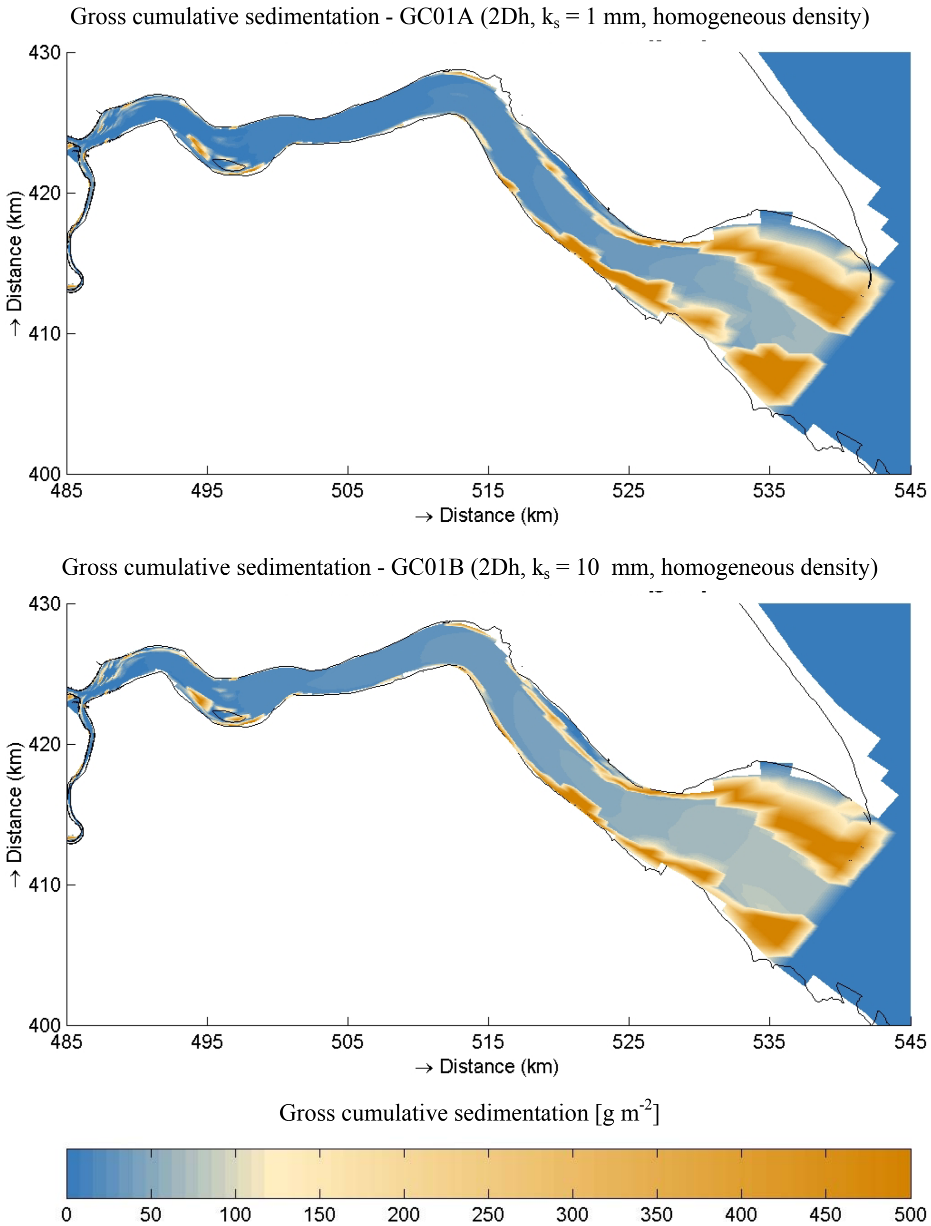

Figure 5-21 Gross cumulative sedimentation of 2Dh runs GC01A & GC01B three months after 'cold-start' Explanation: Sedimentation in g m^{-2}, note that the values have been clipped above 500 g m^{-2} whereas the highest recorded value is 25 kg.m^{-2}

5.4.3 Fine sediment net sedimentation

Net sedimentation, 3D simulations

Whether newly settled sediment (as shown in Figure 5-21) is eroded within a tidal cycle is studied by calculation of the net sedimentation. Figure 5-22 and Figure 5-23 present the net sedimentation of the two 3D (GC01C & GC01D) and the two 2Dh simulations (GC01A & GC01B). When a comparison is made between net and gross sedimentation, most area seem to have an equal deposition and erosion flux. Comparison of 2Dh and 3D show no large differences.

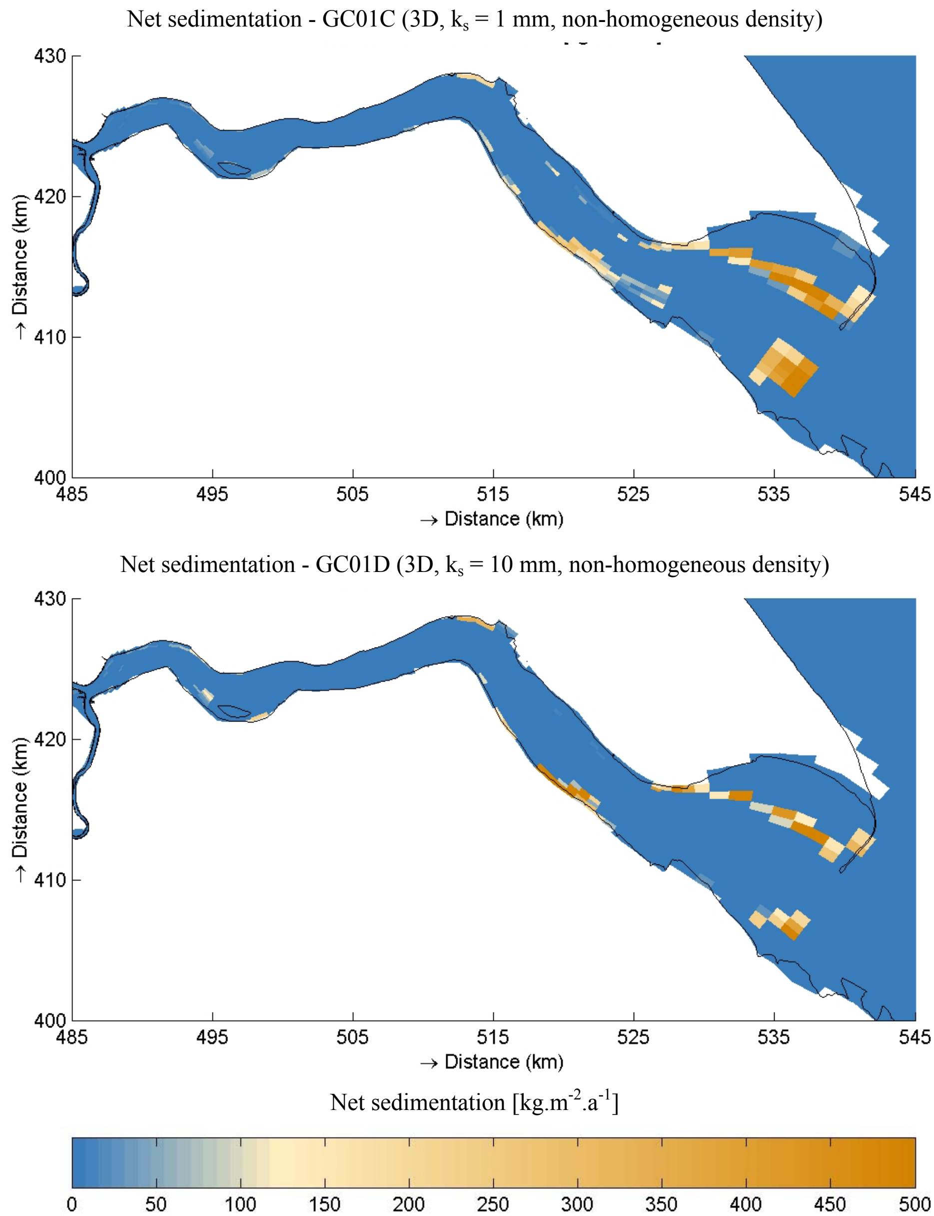

Figure 5-22 Net cumulative sedimentation of fine sediment in bed layer for 3D simulations GC01C & GC01D
Explanation: Net sedimentation in kg a^{-2} m^{-2} note that the values have been clipped above 500 kg.m^{-2} whereas the highest recorded value is 600 kg.m^{-2}.a^{-1}.

Net sedimentation, 2Dh simulations

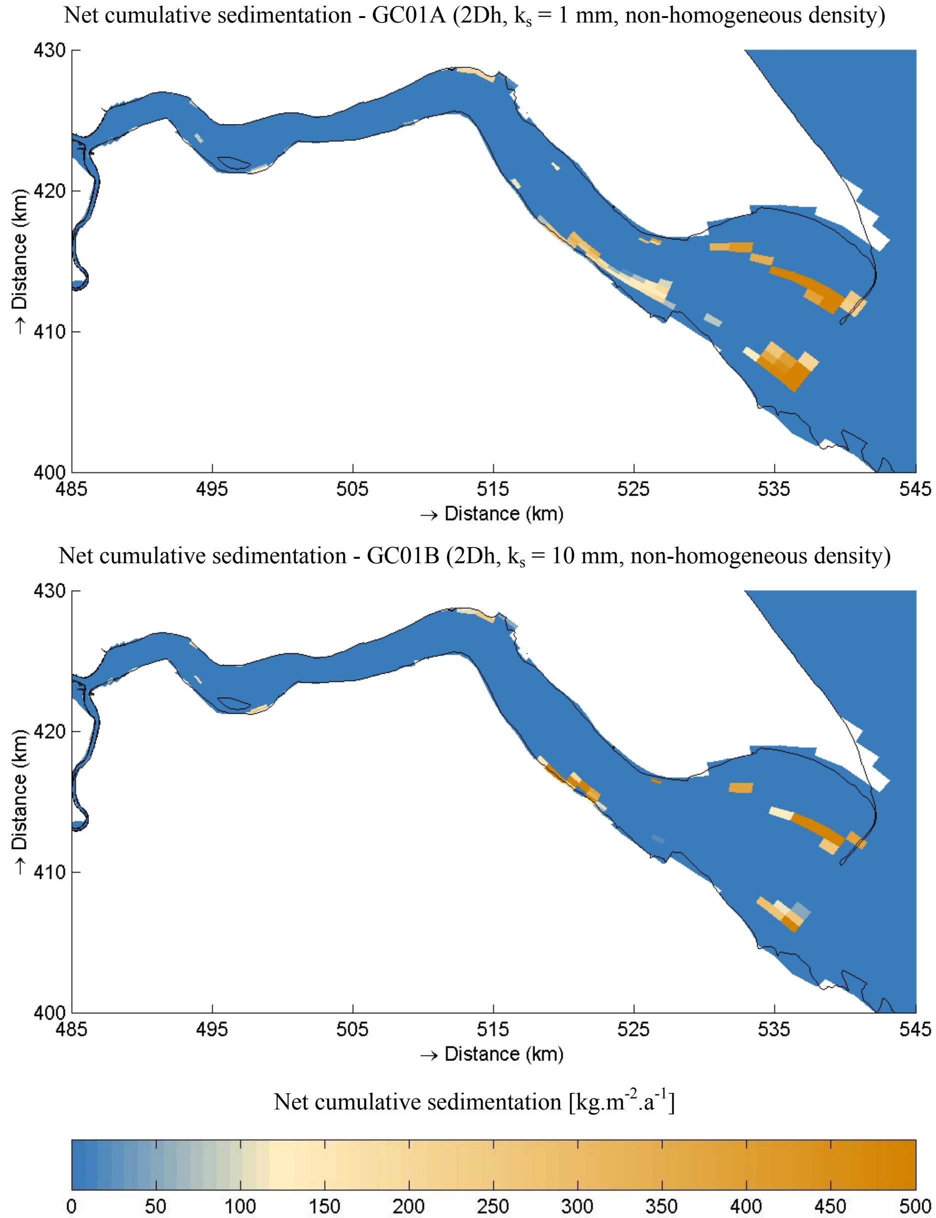

Figure 5-23 Net cumulative sedimentation of fine sediment in bed layer for 2Dh simulations GC01A & GC01B
Explanation: Net sedimentation in kg a^{-2} m^{-2} note that the values have been clipped above 500 kg.m^{-2}.a^{-1} whereas the highest recorded value is 800 kg m^{-2}.a^{-1}.

In Figure 5-23 the net cumulative sedimentation of fine sediments is presented. A small difference between 2D and 3D simulations can be found. In the previous section a brief description is given of the differences between modelling sediment transport in 2Dh and 3D mode. A combination of gravitational circulation and this difference in modelling between result in a higher import of fine sediments.

Since analysis of net sedimentation is difficult on the basis of Figure 5-22 and Figure 5-23. A more detailed comparison is made by studying the net fine sediment transports. What Figure 5-22 till Figure 5-23 do show us is that for the 'smooth-bed' simulations in a larger area net sedimentation occurs.

5.4.4 Net fine sediment transport

Before the net fine sediment transports through cross sections are studied, a definition is given of the quantities that are used. Besides the net transport and net sedimentation, trapping efficiency is introduced. Trapping efficiency (T_{eff}) is of great interest when due to a small change in bed roughness a large percentage of the sediment that enters an area is trapped.

$$T_{net} = \frac{\int_{t=t0}^{t=t_1} T_{gross}\, dt}{t_1 - t_0} \qquad (5.13)$$

$$T_{|cum|} = \frac{\int_{t=t0}^{t=t_1} \left|T_{gross}\right| dt}{t_1 - t_0} \qquad (5.14)$$

$$T_{eff} = \frac{T_{net}}{T_{|cum|}} \qquad (5.15)$$

With:

$t_1 - t_0$	:	Period in time (equal to a real number of tidal periods)	[s]
T_{gross}	:	Gross fine sediment transport	[kg.s^{-1}]
T_{net}	:	Net fine sediment transport	[kg.s^{-1}]
$T_{\|cum\|}$	:	Absolute cumulative gross transport of fine sediments	[kg.s^{-1}]
T_{eff}	:	Net trapping efficiency	[-]

For all simulations and in all cross section of the aggregated grid, the values of T_{net}, $T_{|cum|}$ and T_{eff} are calculated. Figure 5-24 presents an example of the calculation procedure for simulation GC01A in cross section ‘01-03’.

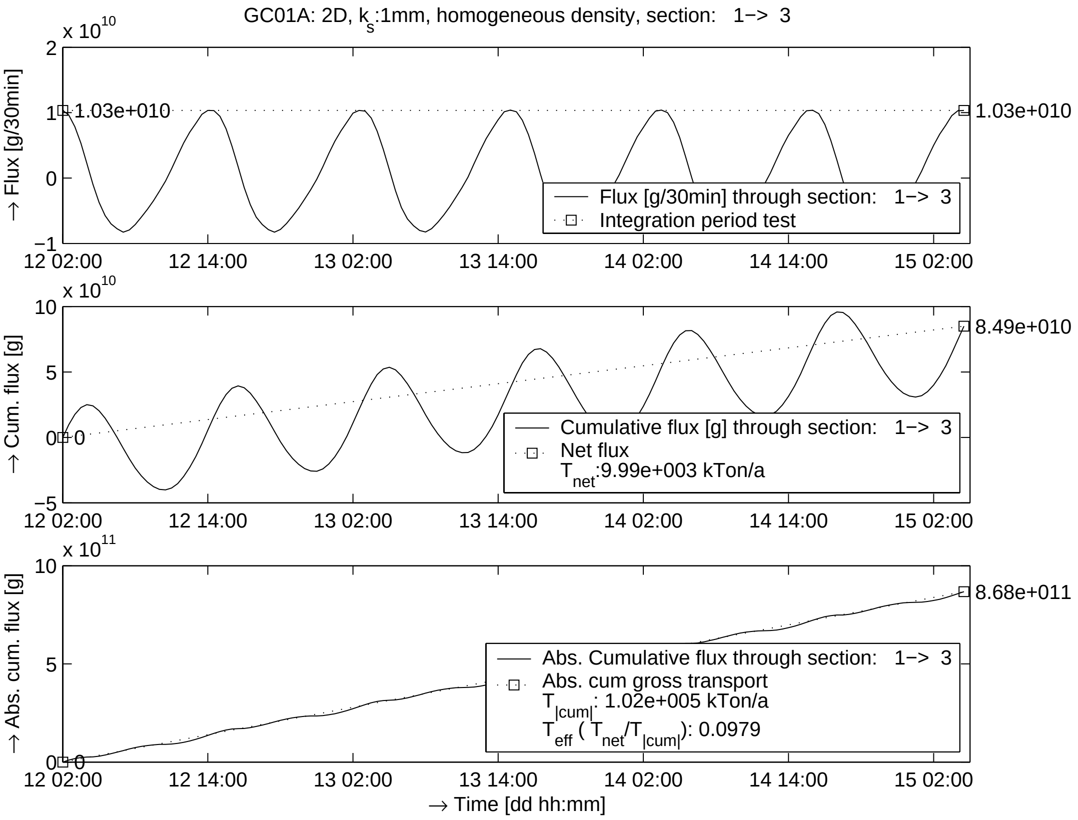

Figure 5-24 Calculation of net transport, absolute cumulative gross and net trapping efficiency

The upper panel of Figure 5-24 shows the gross flux of fine sediment through cross section '01-03' for a period of six M_2 tides. Start and end time of this integration period must have an equal value in gross transport, therefore a test is done (see the dotted line 'Integration period test'). Summation of the gross flux for the integration period gives the cumulative flux, (see the centre panel of Figure 5-24). The steepness of the trend line of cumulative flux is equal to the net transport (equation 5.12). The lower panel presents the summation of all sediment passing through the cross section (absolute cumulative transport; see equation 5.13). Now that T_{net} and $T_{|cum|}$ are derived the net trapping efficiency can be calculated (see equation 5.14). Figure 5-25 till Figure 5-28 show the net transports and the trapping efficiency through the cross sections in the aggregated grid.

For convenience, the net deposition is determined by a mass balance for each aggregated grid cell. Assume that an equal amount of sediment in the water column at start and end point of the integration period, then is the surplus in mass of each cell is equal to the net deposition in that cell. A comparison between the surplus in mass (as described above) and the output from Delft3D-Delwaq showed equal results.

Figure 5-25 and Figure 5-26 present the net transport of fine sediment between the aggregated grid cells for 3D simulations GC01C and GC01D. In Figure 5-27 and Figure 5-28 the two 2Dh simulations GC01A and GC01B are shown.

The net effect on sedimentation due to a higher bed shear stress is as expected for the channel sections. A higher bed shear stress results in a net decrease of fine sediment settling on the bed, thus the net import of material is lower.

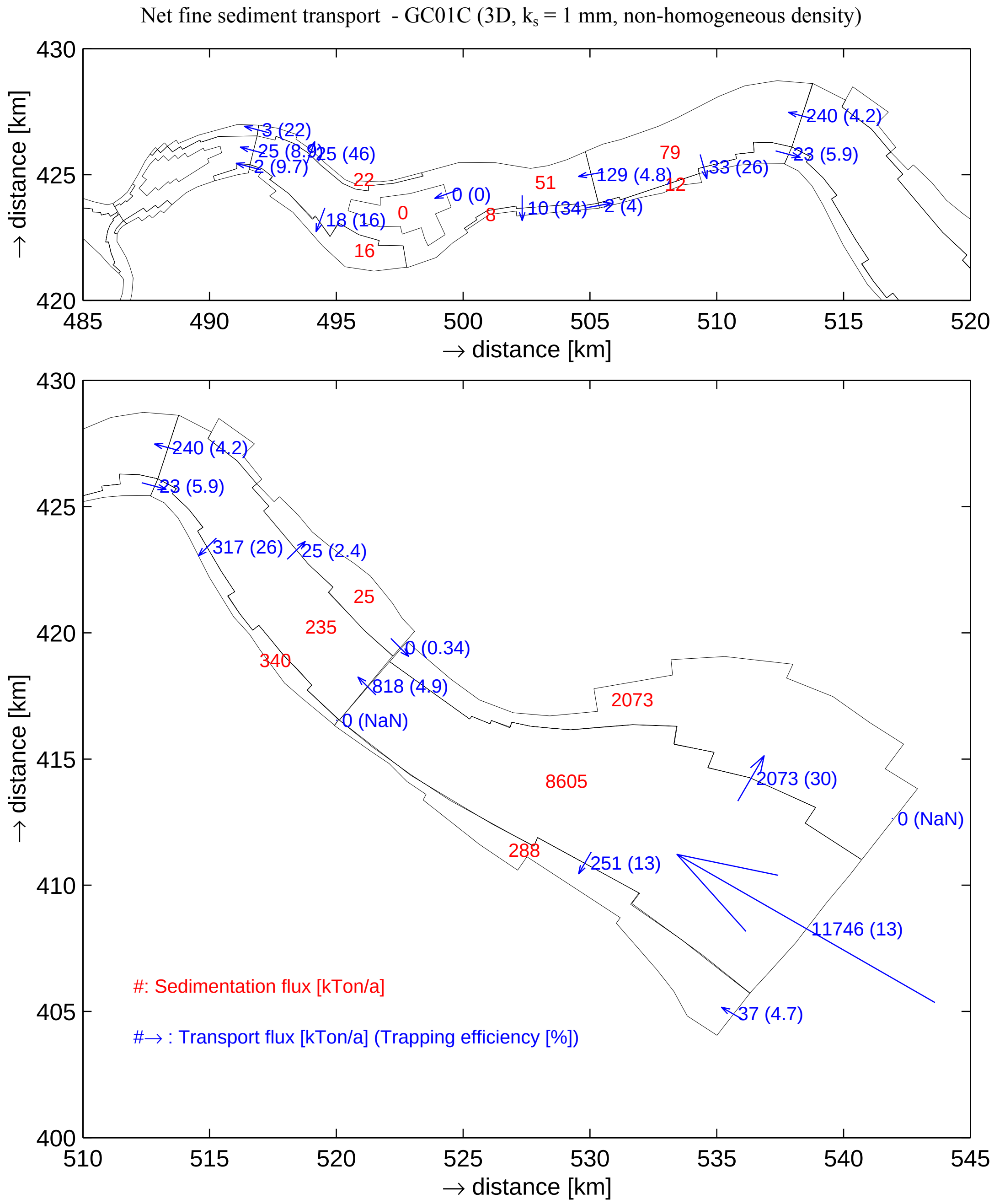

Figure 5-25 Net transport of fine sediment in aggregated grid for run GC01C

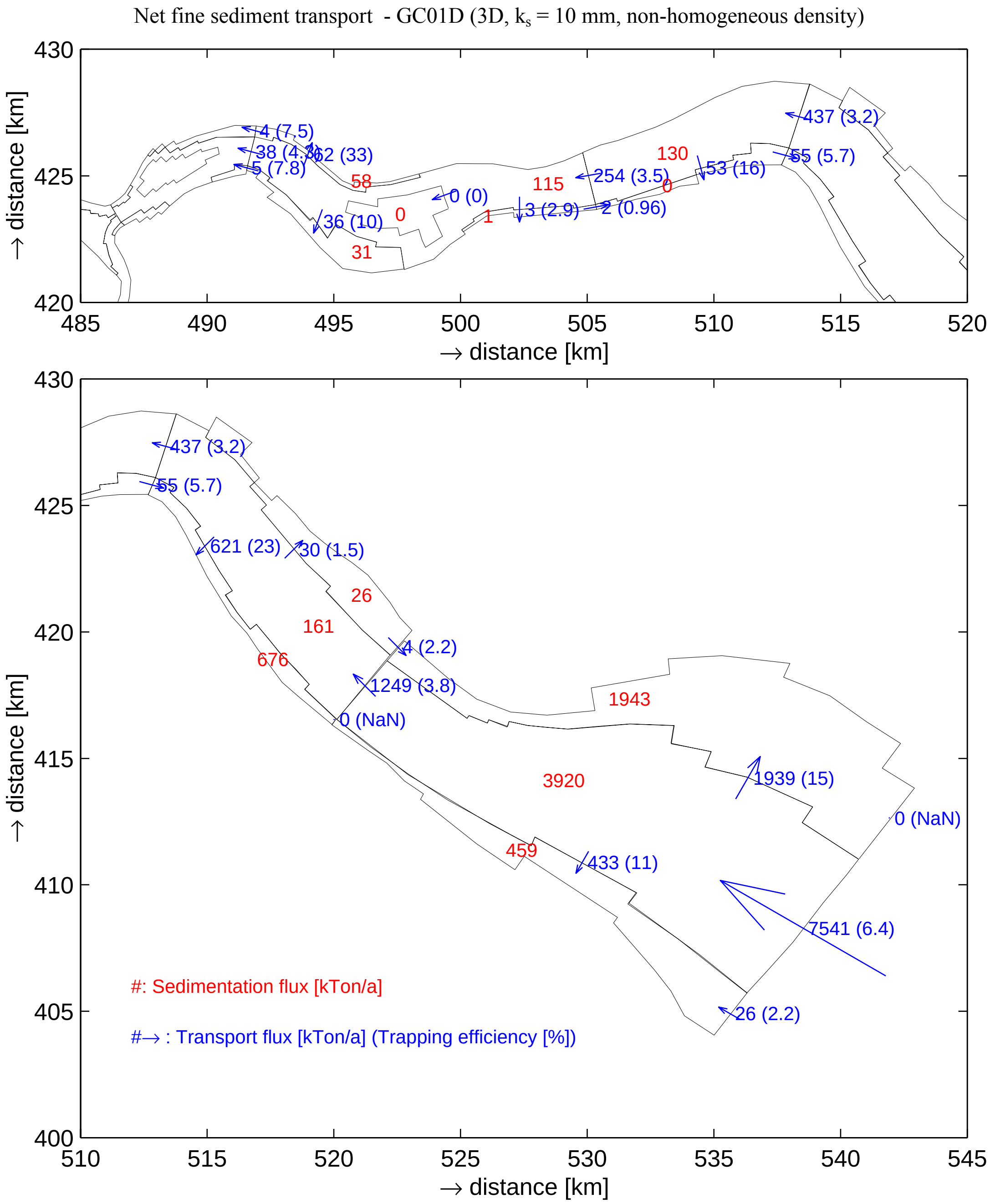

Figure 5-26 Net transport of fine sediment in aggregated grid for run GC01D

Net fine sediment transport - GC01A (2Dh, k_s = 1 mm, homogeneous density)

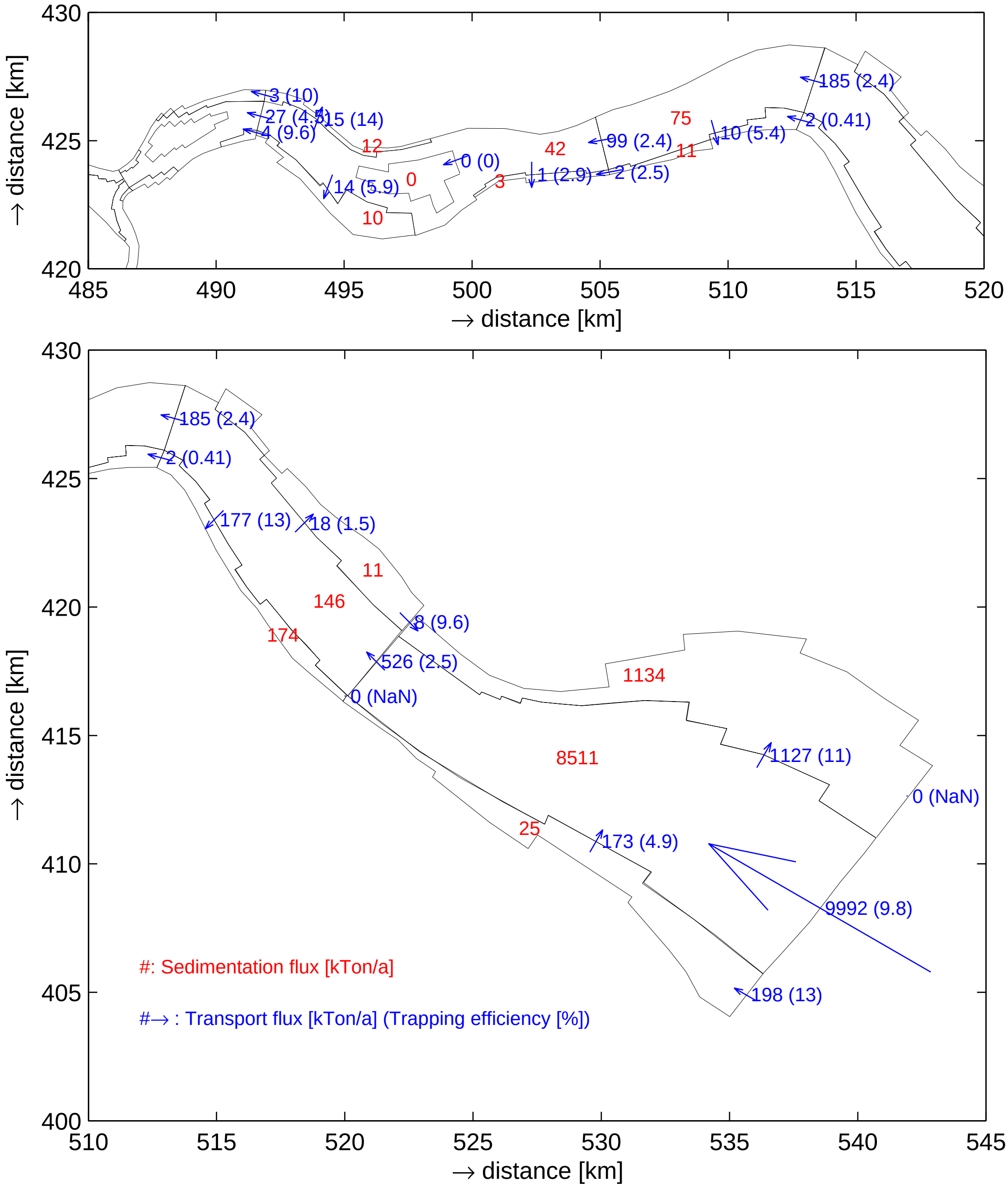

Figure 5-27 Net transport of fine sediment in aggregated grid for run GC01A

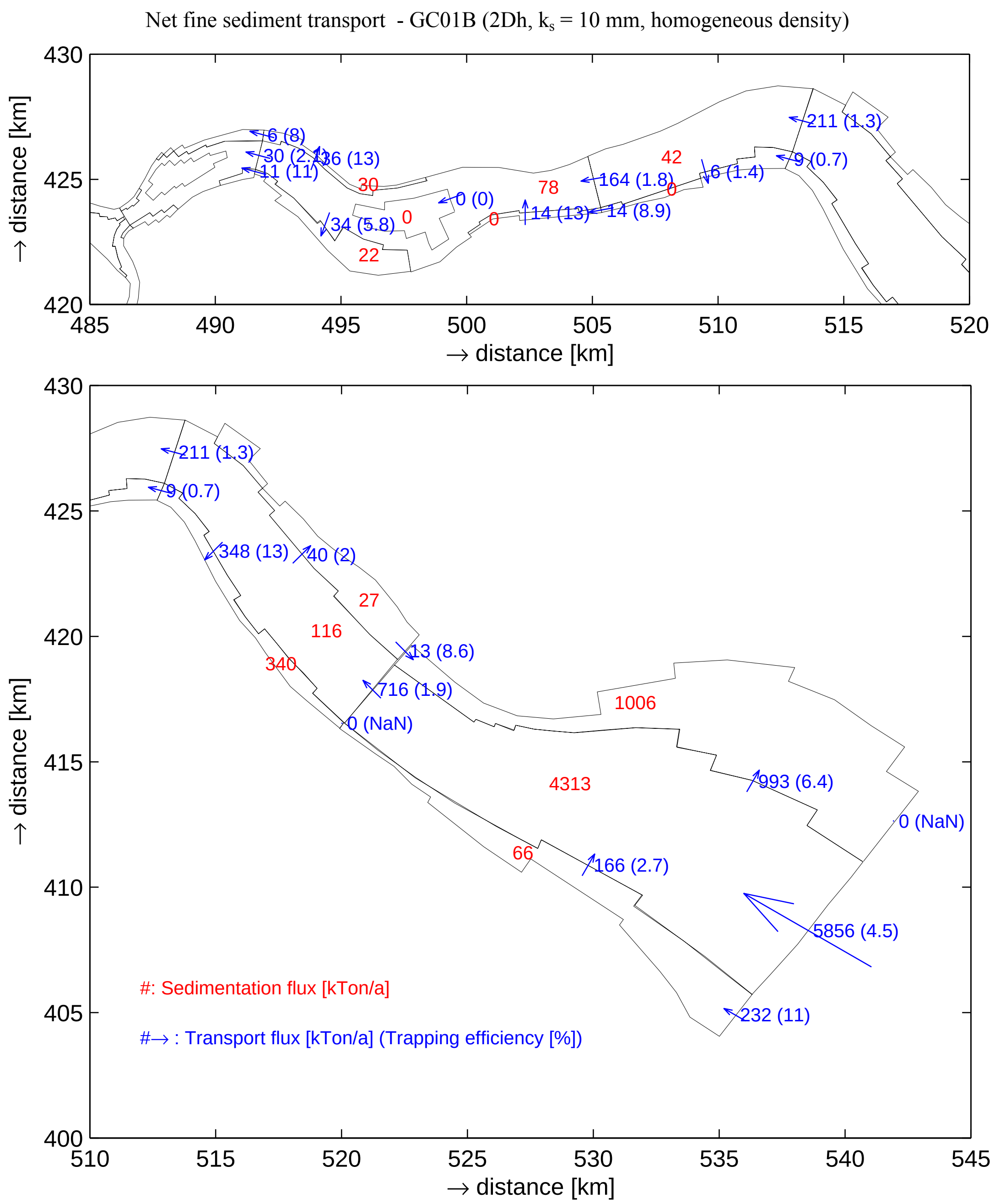

Figure 5-28 Net transport of fine sediment in aggregated grid for run GC01B

Discussion

When we compare the net transport between the simulations, the main differences occur in the outer estuary. For this reason this area will be focused on. Table 5-9 shows the relative net sedimentation of simulation GC01D in comparison to simulation GC01C.

Table 5-11 Comparison of net sedimentation in aggregated grid cells in the outer estuary

Aggregated grid cell name	Aggregated grid cell number	Classification	Deposition ratio 3D: $D_{ks\ 1mm}$ / $D_{ks\ 10mm}$ [-]	Deposition ratio 2D: $D_{ks\ 1mm}$ / $D_{ks\ 10mm}$ [-]
A-CH	03	deep	2.0	2.2
A-NT	02	shallow	1.1	1.1
A-ST	04	shallow	0.4	0.6
B-CH	06	deep	1.3	1.5
B-NT	05	shallow	0.4	1.0
B-ST	07	shallow	0.5	0.5

Explanation of aggregated grid cell name is shown in Appendix F, Figure F-4.

With the exception of the north tidal flat at the Humber mouth (A-NT), the following observation holds for the outer estuary:

> *Deep areas (see Table 5-11) have a lower net sedimentation rate when the bed roughness increases from k_s= 1 mm to k_s= 10 mm. Areas that are relative shallow seem to have a higher net sedimentation rate when the bed roughness increases from 1 mm to 10 mm.*

The observation sketched above can be explained as follows. Most particles enter the Humber estuary through the main channel. When the bed is relative smooth, the particle can settle there before the tidal flats are reached, resulting in a decrease of net fine sediment transport from the channel towards the tidal flats.

The largest difference in trapping efficiency between two simulation with different bed roughness is found at cross section '02-03' at the north tidal flat near the mouth of the estuary. For this cross section almost a doubling of trapping efficiency is gained due to a decrease in bed roughness.

5.4.5 Conclusions and recommendations

Conclusions of the Channel-Shoal interaction study

When net transports of fine sediments for simulations with different bed roughness are compared, a higher net import is observed during the 'smooth bed'-simulation. Besides the difference in longitudinal direction a shift in path of fine sediments is observed. During the 'rough bed'-simulation the sediments are eroded more easily, thus more sediment reach the tidal flat and the inner estuary.

Recommendations of the Channel-Shoal interaction Study

Fine sediment distribution along the estuary in the current model could use improvement, as discussed in section 5.3.6. An improved distribution of fine sediments is likely to affect the settling pattern as show in Figure 5-25 and Figure 5-26. When additional work is carried out attention must be paid to the value that is used for the Nikuradse Roughness height.

6 Conclusions and recommendations

Before the conclusions and the recommendations are given a summary is given of the aim of the study and the study set-up that is chosen.

The aim of the study is to improve the knowledge of the influence of three key processes on the net up-estuary transport of fine grained sediment in the Humber estuary. The three key processes that are focussed on in this study are:

- Tidal asymmetry with respect to slack periods and peak velocities.
  - The analysis focuses on the sensitivity of slack period and peak velocity asymmetry on the M_4 component in the sea boundary condition.
- Gravitational circulation due to the interaction of river run-off and the flushing by the tide.
  - The analysis focuses on the difference in net sediment transport between a homogeneous and a non-homogeneous density simulation.
- Channel shoal interaction due to settling of only a small percentage of the gross transports on intertidal area, a notable import of sediments can be the result.
  - The analysis focuses on the difference in longitudinal and transversal net transports between two simulations with different bed roughness in the sediment transport model.

6.1 Conclusions

The main conclusions of the study can be summarized as follows.

Tidal asymmetry

- Tidal asymmetry in the inner estuary is primarily generated locally and therefore less sensitive to changes in the sea-boundary condition.
- Both peak velocity and slack period asymmetry in the outer Humber estuary are more sensitive to sea-boundary condition differences in M_4 than the inner estuary.
- The high sensitivity for M_4 boundary conditions found in the outer estuary is consistent with results found in a morphological study (WL | Delft Hydraulics (z3451)).
- Peak velocity asymmetry is flood-dominant throughout the estuary and increases in magnitude up-estuary.
- Analysis of horizontal tidal components M_2 and M_4 only is not sufficient for a slack period asymmetry analysis.
- Slack period asymmetry is mainly flood-dominant throughout the estuary.

Gravitational circulation

- Gravitational circulation results in net up-estuary sediment transport.
- The magnitude of the effect of gravitational circulation on net import is in the order of 10% of the net transport of fine sediments.

Channel - Shoal interaction

- An increase of bed roughness in sedimentation and erosion processes results in a decrease of net up-estuary fine sediment transport.
- Besides the decrease in net fine sediment transport in longitudinal direction an increase in transversal direction towards the tidal flats is observed with increasing roughness.

Modelling of fine sediment transport

- Delft3D-Delwaq gives realistic results for net import of fine sediments in the estuary but concentrations of fine sediments needs improvement.
- In the outer estuary, the settling areas agree with data from admiralty charts.
- Measurements indicate higher concentrations of fine sediments than reproduced by the model.
- The aggregated grid effectively helps to analyze the interaction between channel and intertidal areas.

Recommendations

The main recommendations can be summarized as follows.

- The tidal asymmetry analyses on the hydrodynamics that are used are inappropriate for drying cells. Therefore only the deeper parts along the estuary are studied. With a model simulating sedimentation and erosion processes the asymmetry in sediment transports on the intertidal area can be studied.
- For convenience, the depth averaged velocity of the 2Dh model has been used instead of the bed shear stress to determine the slack periods. Actually, the bed shear stress itself or the velocity magnitude near the bottom (which implies a constant bed type) would give better insight in the fine sediment transport asymmetry.
- The modelling of the distribution of fine sediment along the estuary needs improvement. Further study is required to analyze what processes could enhance this distribution.
- Measurements indicate higher concentrations of fine sediments than reproduced by the model. The cause of this difference is not known. Whether this is the result of no sediment transport from up-river or the result of other processes can be part of new research.

Besides the three key processes that are focused on, several other processes can be of importance. The high variability in conditions due to biological, chemical and seasonal processes is discussed in the literature survey (section 3.2). Knowledge of the influence of this variability on net fine sediment import and distribution can be improved. We therefore suggest the following additional work to be carried out:

- It is likely that waves can affect the distribution of fine sediments throughout the system largely.

Possible parameters that can be studied are:

- The fixation of bed material by micro phyto-benthos and bacteria; by modelling a higher critical bed shear stress for erosion on the intertidal areas.
- The effect of bio-turbation; by modelling a lower critical bed shear stress for erosion on the intertidal areas.
- The effect of flocculation due to turbulence, and chemical and biological effects; by modelling a higher fall velocity for both riverine and marine sediments.

References

Abraham, G. (1982), ‘Reference notes on density currents and transport processes’, In: International course in hydraulic engineering (1982). Delft, The Netherlands.

Andrews, J.E.(2000) ‘Origin, abundance and storage of organic carbon and sulphur in the Holocene Humber Estuary: emphasizing human impact on storage changes’. In: Shennan, I. & J.E. Andrews (2000). ‘Holocene land- ocean interaction and environmental change around the North Sea’, The geological Society, London, UK, pp.145.

Black, K.S. (1998), ‘Suspended sediment dynamics and bed erosion in the high shore mudflat region of the Humber estuary, UK’, In: Marine Pollution Bulletin, Vol. 37 (1998), Great Britain, pp 122-133.

British Transport Docks Board (1970), ‘Silt movement in the Humber estuary’, Report No. R.221, 1970, Southall, Middx., Great Britain.

Brummelhuis et al. (1998), P.G.J. Brummelhuis & H. Gerritsen & D. Verploegh. ‘Calibration of the ZNZ model – Calibration on tidal water levels using WAQAD’. WL | Delft Hydraulics (1998), project number: Z2591.

Christy et al (1999), Christie, M. C. & K. R. Dyer & P. Turner , ‘Sediment Flux and Bed Level Measurements from a Macro Tidal Mudflat’. In: Estuarine, Coastal and Shelf science, Vol. 49 (1999), pp. 667-688.

Deckere et al (2001), Deckere, E.M.G.T. de & T.J. Tolhurst & J.F.C de Brouwer, ‘Destabilization of cohesive intertidal sediments by in fauna’, In: Estuarine, Coastal and Shelf science, Vol. 53 (2001), pp. 665-669.

Dronkers, J. (1984), ‘Import of fine marine sediment in tidal basins’. In: Netherlands Institute for Sea Research Publications Series 10 (1984), pp 83-105.

Dronkers, J. (1985), ‘Tide-induced residual transport of fine sediments’ In: J. van de Kreeke, ed. (1984) ‘Physics of shallow estuaries and bays’ Lecture notes on Coastal and Estuarine Studies16, New York, Springer verslag, pp228-244.

Dronkers, J. (1986) , ‘Tidal asymmetry and estuarine morphology’, Netherlands, Journal of sea research, pp.117-131.

Dyer (1988), Dyer, K.R., ’Fine sediment particle transport in estuaries’. In: ‘Physical processes in estuaries’ (1988), pp 295-310.

Dyer et al (2000), Dyer, K.R. & M.C.Christy & E.W.Wright. ‘The classification of intertidal mudflats’. In Continental Shelf Research 20 (2000) p 1039-1060, Pergamon Press.

Friedricks and Aubrey (1988), ‘Non-linear Tidal distortion in Shallow Well mixed Estuaries: a Syntehis’. In: ‘Estuarine, Coastal and Shelf Science’, pp 51-545

Groen, P. (1967), ‘On the residual transport of suspended matte by an alternating tidal current’, Netherlands, Journal of Sea Research (1967), pp.564-574

Hardisty J. (1999), ‘Physical processes in the Humber estuary’, paper submitted to the Environment Agency

HR Wallingford (2002), ‘Data gathering exercise for Offshore Boundary conditions – paper for discussion within HESMP2’, HR Wallingford, Project number: HESMP2.

Huntley et al (1998), Huntley, D. & J. Blewett, ‘Measurement of suspended sediment transport processes in shallow water of the Holderness coast, UK’. In: Marine Pollution Bulletin, Vol. 37 (1998), Great Britain, pp 134-143.

Krone (1962), From Delft3D_Delwaq manual

Leusen (1994) From Winterwerp (2003-07)

Metha, A.J (1986), ‘Characterization of cohesive sediment properties and transport processes in estuaries’. In: Lecture Notes on Coastal and Estuarine Studies’ Vol. 14 (1986), pp 92-325.

Partheniades, E (1962) , ‘A study of erosion and deposition of cohesive soils in salt water.’, PhD. thesis University of California, Berkely.

Postma (1961), ‘Transport and accumulation of suspended matter in the Dutch Wadden Sea’. In: Netherlands Journal of Sea research, 1961, Den Helder, The Netherlands, pp 148-190

Proctor et al (1999), Proctor, R & J. Holt & J. Harris & A. Tappin & D. Boorman 'Modelling the Humber Estuary catchment and coastal zone.' In: Malcolm & L. Spauling & H. Lee Butler (1999). In: Estuarine and coastal Modelling - Proceedings of the sixth international conference-, The American Society of Civil Engineers, New Orleans, Louisiana, pp.1259

Roelvink (2003), 'On Morphological modelling'.

Smits, J.G.C (2003), 'Sediment – water exchange of substances – Modelling of the interactions of organisms and sediment' (2003), WL | Delft Hydraulics, Project number: Z2845/Q2935.

Speer et al (1985), Speer, P.E.,& D.G. Aubrey, 'A study of non-lineaire tidal propagation in shallow inlet / estuarine systems - part II: theory', In: Estuarine, Coastal and Shelf science, Vol. 21 (1985), pp. 207-224.

Van Straaten & Kuenen (1957), van Straaten, L.M.J.U. & PH. H. Kuenen, 'Accumulation of fine grained sediments in the Dutch Wadden Sea.' Geologie en Mijnbouw 1957, pp.329-354

Uncles et al (1999), Uncles, R.J. & J.A. Stephens, 'Suspended sediment fluxes in the tidal Ouse, UK'. In: Hydrological Processes, Vol. 13 (1999), pp. 1167-1179.

Uncles et al (2001), Uncles, R.J. & S.J. Lavender & J.A. Stephens 'Remotely sensed observations of the turbidity maximum in the highly turbid Humber estuary, UK', In: Estuaries, Vol. 24 (2001), pp745-755.

Walling et al (2000), Walling, D.E. & P.N. Owens & B.D. Waterfall & G.J.L. Leeks & P.D. Wass, 'The particle size characteristics of fluvial suspended sediment in the Humber and Tweed catchments, UK' .In: the Science of the Total Environment, Vol. 251-252 (2000), pp. 205-222.

Wang, Z.B. & C. Jeuken & H.J.de Vriend (2002, 'Morphology and asymmetry of the vertical tide in the Westerschelde estuary', Continental Shelf Research 22 (2002), pp.2599-2609.

Whitehouse et al (2000a), Whitehouse, R. & R. Soulsby & W. Roberts & H. Mitchener, 'Dynamics of Estuarine muds: a manual for practical applications', Thomas Telfort Publishing (2000), London, UK

Whitehouse et al (2000b), Whitehouse, R. & P. Bassoullet & K.R.Dyer & H.J.Mitchener & W.Roberts, 'The influence of bedforms on flow and sediment transport over intertidal mudflats'. In: 'Continental Shelf Research 20' (2000) pp. 1039-1060, Pergamon Press.

Winterwerp, J.C. (2001), 'Stratification effects by cohesive and non-cohesive sediment', In: Journal of Geophysical Research Vol. 106 (2001), pp. 22,559 22,574.

Winterwerp (2002-11), 'The transport of sediment in the Wadden Sea – set up of the study', WL Delft Hydraulic (2002), project number: Z3385.

Winterwerp, J.C. (2003-01), 'A re-analysis of Krone's deposition experiments', submitted to INTERCOH-2003

Winterwerp, J.C. (2003-07), 'The transport of fine sediment in the Humber estuary', WL | Delft Hydraulics (2003), project number: Z3040-ESTPROC.

WL | Delft Hydraulics (1978), 'Een dimensionale numerieke berekeningen van getijbeweging en zoutverdeling in de getijgoot'.

WL | Delft Hydraulics (1999), 'Delft3D-Delwaq user manual', Version 3.01

WL | Delft Hydraulics (2003), 'Wave-induced bed shear stresses in shallow water', WL | Delft Hydraulics (2003), Project number: Z3385.

WL | Delft Hydraulics (2002), 'Humber estuary Shoreline management Plan –stage2 Hydrodynamic Calibration Report', WL | Delft Hydraulics and ABP mer, Project number: Humber SMP2.

WL | Delft Hydraulics (z3451), 'Humber Estuarine Shoreline Management plan Phase 2', project number: Z3451.

Internet references

Internet address (MARE). 'Marine and Aquatic Research Experience', [http://schc.sc.edu/MARE/estuaries.htm]

Appendices

Sensitivity analysis of fine sediment transport in the Humber Estuary

Delft University of Technology

WL | delft hydraulics

A Experimental program

The experimental program is divided in four subjects: calibration, sensitivity analysis of tidal asymmetry, gravitational circulation and the last subject is the sensitivity analysis of channel shoal interaction.

Calibration of hydrodynamics

In Table A-1 a summary is given of the numerical models that are developed in order to calibrate the hydrodynamics on the three major constituents M_2, S_2 and M_4.

Table A-1 Model approach, calibration hydrodynamics on global roughness

Code	Calibration of the global roughness	Model type	Sea boundary
CH01	previous local manning roughness	coarse grid, 2D	8 TC*
CH02	global Chezy 70	coarse grid, 2D	8 TC*
CH03	global Chezy 75	coarse grid, 2D	8 TC*
CH04	global Chezy 80	coarse grid, 2D	8 TC*
CH05	global Chezy 85	coarse grid, 2D	8 TC*
CH06	global Chezy 90	coarse grid, 2D	8 TC*
CH07	previous local manning roughness	fine grid, 2D	8 TC*
CH08	global Chezy 70	fine grid, 2D	8 TC*
CH09	global Chezy 75	fine grid, 2D	8 TC*
CH10	global Chezy 80	fine grid, 2D	8 TC*
CH11	global Chezy 80	fine grid, 2D	8 TC*
CH12	global Chezy 70 depth 2000 minus 1dm	fine grid, 2D	8 TC*

8 TC*: eight major tidal constituents (see Table 4-2)

Tidal asymmetry

In Table A-2 a summary is given of the numerical models that are developed in order to study the sensitivity analysis on tidal asymmetry, again by changing the sea boundary conditions.

Table A-2 Model approach, sensitivity analysis tidal asymmetry

Code	Sea boundary Phase M_4	Amplitude M_4	Model type	Sea boundary
TA01A	No overtide M4	-	Coarse grid, 2D	M_2
TA01B	0°	5 %	Coarse grid, 2D	M_2 & M_4
TA01C	-20°	5 %	Coarse grid, 2D	M_2 & M_4
TA01D	+20°	5 %	Coarse grid, 2D	M_2 & M_4
TA01E	0°	10 %	Coarse grid, 2D	M_2 & M_4
TA01F	-20°	10 %	Coarse grid, 2D	M_2 & M_4
TA01G	+20°	10 %	Coarse grid, 2D	M_2 & M_4
TA01H	RF	RF	Coarse grid, 2D	M_2 & M_4
TA01I	RF	RF	Coarse grid, 2D	RF*

RF* stands for reference values, as used in the calibration of the hydrodynamics (CH02).

Gravitational circulation

In Table A-3 a summary is given of the numerical models that are developed in order to study the sensitivity analysis on gravitational circulation.

Table A-3 Model approach, sensitivity analysis gravitational circulation

Runid	Model type		Discharge	Roughness (k_s):
GC01A	2Dh	homogeneous density	3 years average	1 mm
GC01C	3D	fresh – salt	3 years average	1 mm
GC01D	3D	homogeneous density	3 years average	1 mm

The hydrodynamics used in runs GC01A, GC01C and GC01D are reference runs as in the calibration (Ch02). Incase of a 3D model 10 evenly distributed layers in depth are used.

Channel - Shoal interaction

In Table A-4a summary is given of the numerical models that are developed in order to study the sensitivity on channel – shoal interaction.

Table A-4 Model approach, sensitivity analysis channel-shoal interaction

Runid	Model type		Discharge	Roughness (k_s):
GC01A	2Dh	homogeneous density	3 years average	1 mm
GC01B	2Dh	homogeneous density	3 years average	1 cm
GC01C	3D	fresh – salt	3 years average	1 mm
GC01D	3D	fresh – salt	3 years average	1 cm

The hydrodynamics used in runs GC01A, to GC01D are reference runs as in the calibration (Ch02). Incase of a 3D model 10 evenly distributed layers in depth are used.

B Delft3D Modelling

B.1 Hydrodynamic module

The hydrodynamic module, Delft3D-FLOW, is a multi-dimensional hydrodynamic simulation program that calculates non-steady flow and transport phenomena resulting from tidal and meteorological forcing on a curvilinear, boundary-fitted grid. In 3D simulations, the hydrodynamic module applies the so-called sigma co-ordinate transformation in the vertical, which results in a smooth representation of the bottom topography. It also results in a high computing efficiency because of the constant number of vertical layers over the whole computational domain.

Module description

The hydrodynamic module is based on the full Navier-Stokes equations with the shallow water approximation applied. The equations are solved with a highly accurate unconditionally stable solution procedure. The supported features are:

- three co-ordinate systems, i.e. rectilinear, curvilinear and spherical in the horizontal directions and a sigma co-ordinate transformation in the vertical;
- domain decomposition both in the horizontal and vertical direction
- tide generating forces (only in combination with spherical grids);
- simulation of drying and flooding of inter-tidal flats (moving boundaries);
- density gradients due to a non-uniform temperature and salinity concentration distribution (density driven flows);
- for 2D horizontal large eddy simulations the horizontal exchange coefficients due to circulation's on a sub-grid scale (Smagorinsky concept);
- turbulence model to account for the vertical turbulent viscosity and diffusivity based on the eddy viscosity concept;
- selection from four turbulence closure models: k-ε, k-L, algebraic and constant coefficient;
- shear stresses exerted by the turbulent flow on the bottom based on a Chézy, Manning or White-Colebrook formulation;
- enhancement of the bottom stresses due to waves;
- automatic conversion of the 2D bottom-stress coefficient into a 3D coefficient;
- wind stresses on the water surface modelled by a quadratic friction law;
- space varying wind and barometric pressure (specified on the flow grid or on a coarser meteo grid), including the hydrostatic pressure correction at open boundaries (optional);
- simulation of the thermal discharge, effluent discharge and the intake of cooling water at any location and any depth in the computational field (advection-diffusion module);
- the effect of the heat flux through the free surface;
- online analysis of model parameters in terms of Fourier amplitudes and phases enabling the generation of co-tidal maps;
- drogue tracks;
- advection-diffusion of substances with a first order decay rate;

- online simulation of the transport of sediment (silt or sand) including formulations for erosion and deposition and feedback to the flow by the baroclinic pressure term, the turbulence closure model and the bed changes;
- the influence of spiralling motion in the flow (i.e. in river bends). This phenomenon is especially important when sedimentation and erosion studies are performed;
- modelling of obstacles like 2D spillways, weirs, 3D gates, porous plates and floating structures;
- wave-current interaction, taking into account the distribution over the vertical;
- many options for boundary conditions, such as water level, velocity, discharge and weakly reflective conditions;
- several options to define boundary conditions, such as time series, harmonic and astronomical constituents;
- online visualisation of model parameters enabling the production of animations.

Applications areas

Delft3D-FLOW can be applied to the following application areas:

- salt intrusion in estuaries;
- fresh water river discharges in bays;
- thermal stratification in lakes and seas;
- cooling water intakes and waste water outlets;
- sediment transport including feedback on the flow;
- transport of dissolved material and pollutants;
- storm surges, combined effect of tide and wind/typhoon;
- river flows, meandering and braided rivers;
- floodplains, with or without vegetation;
- reservoir siltation and degradation below dams;
- bottom vanes, spurs, groynes, bridges, weirs and levees.

Coupling with other modules

The results of the hydrodynamic module are used in all other modules of Delft3D. The results are dynamically exchanged between the modules through the use of a so-called communication file. Basic (conservative) water quality parameters like concentrations of dissolved material and pollutants, can be included in the computations. But, for more dedicated water quality simulations, the hydrodynamic module is coupled with the far-field water quality module (Delft3D-WAQ) , the nutrient phytoplankton module (Delft3D-ECO) and the near-field particle tracking module (Delft3D-PART). A coupling with the sediment transport module (Delft3D-SED) is available to simulate cohesive and non-cohesive sediment transport processes, e.g. in the case of erosion and sedimentation studies. For wave-current interaction a dynamic coupling is provided with the wave module (Delft3D-WAVE) and for morphodynamic simulations the hydrodynamic module is integrated with the wave module and a sedimentation and erosion module into a morphodynamic module (Delft3D-MOR).

To simulate a model defined on a curvilinear grid system, an orthogonal grid must be provided. To generate such a grid the program Delft-RGFGRID is provided, though the grid can be generated by any grid generator program as long as the grid is delivered in the prescribed (ASCII) file format. The generation of a curvilinear grid is an important and somewhat complex task. Along with the main model parameters, the grid will ultimately determine the accuracy of the final model results.

To prepare the bottom topography or other grid-related data, such as a non-constant initial condition file, the program Delft-QUICKIN is provided. This program interpolates the scattered, digitised chart data to depth-values at the grid points in the model. Many powerful interactive processing options to further adjust the topography are supported, e.g. manual adjustment of the values at individual points, selection of the domain of influence, group adjustments, and smoothing. The output of this program can be imported into other Delft3D modules.

Analysis and interpretation of a hydrodynamic simulation in terms of tidal quantities can be performed by the program Delft-TRIANA. Delft-TRIANA performs off-line tidal analyses of time-series of either water levels and/or velocities. The results from these analyses can be subsequently compared with observation data supplied by you.

In case the open boundaries of a (detailed) Delft3D-FLOW model are located within the model domain of a coarser Delft3D-FLOW model, the coarse model can generate the boundary conditions of the detailed, nested model. The offline generation of boundary conditions is done by Delft3D-NESTHD.

B.2 Water quality module

The transport of substances in surface and ground water is commonly represented by the so-called advection-diffusion equation. The water quality module, Delft3D-WAQ, is based on this equation and it offers different computational methods to solve it numerically (in one, two or three dimensions) on an arbitrary irregular shaped grid, on a grid of rectangles, triangles or curvilinear computational elements. In order to model waste loads and water quality processes the advection-diffusion equation is extended with an extensive water quality library of source/sink terms. The model is capable of describing any combination of constituents and is not limited with respect to the number and complexity of the water quality processes.

The water quality processes may be described by arbitrary linear or non-linear functions of the selected state variables and model parameters. For many water quality problems, these process formulations have been standardised in the form of a library, which smoothly interfaces with the water quality module. The library contains over 50 water quality processes routines covering 140 standard substances. A graphical user interface within the WAQ module enables you to select substances and associated water quality processes. Recently, the water quality processes are extended with formulations and processes from HydroQual, Inc, a US-based water quality expert consultant for fresh and salt water, with which WL | Delft Hydraulics has entered into a co-operation on advanced environmental modelling.

Water quality module description

In most practical cases Delft3D-WAQ models a physical system that consists of a surface or ground water body. Strictly speaking it models a body of a medium that is able to transport passive constituents. In this respect "passive" means that the influence of the concentration of the constituents on the transport coefficients may be neglected.

The transporting medium is characterised by its spatially and time dependent content (mass) of the modelled constituents. Some of these are transportable, some are non-transportable. An example of the latter is the material in the bottom sediment in a surface water model.

The concentration of the transportable constituents is computed by dividing the mass by the water volume. The mass is the state variable and the model is mass conserving by definition.

Waste disposals are specified either as mass units per time unit or as a combination of waste flow and concentration. They represent either point sources (urban, industrial, rivers) or diffuse sources (run-off, atmospheric deposition). The case of recirculating flows, as with cooling water studies, is also taken care of: the water that was let in, will have the same quality at the outlet.

The hydrodynamic characteristics of the transporting medium are expressed in terms of the volume and the flux of the transporting medium ("flow"). The combination of water volumes and flows must be consistent, i.e. an increase of the water volume must be balanced by a difference between inflow and outflow. As part of Delft3D, the coupling module can derive a set of consistent hydrodynamic flows automatically from Delft3D-FLOW, but the methods involved can be applied equally well to third-party hydrodynamic models outside Delft3D.

In many cases the water quality processes in the model are determined by meteorological conditions, by other (modelled or non-modelled) constituents or by other (modelled or non-modelled) processes. Examples are wind, water temperature, acidity (pH), primary production and the benthic release of nutrients. These entities are referred to as "forcing functions". Water quality process formulations are often of an empirical or semi-empirical nature and contain "model parameters" that are subject to tuning or calibration. Because of this, Delft3D-WAQ allows complete freedom in selecting the set of water quality processes and the relevant forcing functions and model parameters may vary between individual applications. It therefore provides flexible input facilities for constants, spatially varying parameters, functions of time and functions of space and time.

The physical system is affected by two types of processes:

- transport processes: these processes involve the movement of substances;
- water quality processes: these processes involve a transformation of one or more substances.

The transport of substances in surface and ground water is commonly represented by the so-called advection diffusion equation, which includes two basic transport phenomena: advection and diffusion. Advection is determined by the velocity field and dispersion by the dispersion coefficient. These basic transport processes operate on all transportable substances in the same way. Delft3D-WAQ offers the possibility to model other transport phenomena as well which may differ between individual substances. Examples are the gravity induced settling of particles and the autonomous motion of fish. These additional transport processes must be expressed as an extra, substance dependant, velocity or dispersion coefficient.

Water quality processes are incorporated in the advection diffusion equation by adding an additional source in the mass balance. Examples of water quality processes are:

- exchange of substances with the atmosphere (oxygen, volatile organic substances, temperature);
- adsorption and desorption of toxicants and ortho-phosporous;
- deposition of particles and adsorbed substances to the bed;
- re-suspension of particles and adsorbed substances from the bed;
- the mortality of bacteria;
- biochemical reactions like the decay of BOD and nitrification;
- growth of algae (primary production);
- predation (e.g. zooplankton on phytoplankton).

Special attention is paid to the treatment of the interaction with the bottom:

- all suspended sediment is modelled as cohesive sediment that can be transported with the water flow just like a dissolved substance;
- all particulate inorganic matter can be represented by three size fractions or components;
- all particulate organic matter is represented by separate components, namely detritus carbon, other organic carbon, diatoms, non-diatom algae (Green), adsorbed phosphorus and organic carbon from loads;
- the bottom sediment is modelled via two separate layers. Each layer is considered homogeneous (well mixed). The different layers can have different compositions. The density of a layer is variable depending on the sediment layer composition, which is also variable. The porosity within a given layer is constant (user-defined).
- a third (deeper) layer exists (but is not explicitly modelled) which can supply sediment for upward sediment transport 'digging';
- sedimentation and resuspension are modelled using the Krone-Partheniades approach (see the description of the sediment transport module Delft3D-SED).

Application areas water quality module

Delft3D-WAQ can be applied to the following application areas:

- bacterial decay processes;
- chemical processes;
- nutrient cycling and eutrophication processes;

- sedimentation and resuspension of particulates;
- interaction between water and bottom (including diffusive and benthic mixing);
- evaporation, re-aeration and other surface processes;
- transport and chemical processes regarding heavy metals and organic micropollutants;
- recirculation of cooling water.

These processes hold for such substances as:

- chloride/salinity;
- up to five different conservative substances;
- up to five different first order decaying substances;
- coliform bacteria (E.coli, faecal coliforms and total coliforms);
- oxygen and BOD;
- excess temperature;
- dissolved nutrients and nutrients in organic material;
- various fractions of inorganic phosphorus;
- up to three fractions of suspended sediment (both in water phase and bottom);
- up to three algae species (diatoms, greens, bluegreens);
- heavy metals like cadmium, copper, zinc, mercury, nickel, lead, chromium;
- organic micropollutants like PCB-153, HCB, lindane, fluoranthene and benzo(a)pyrene.

The processes always require input in the form of rate constants and/or simulation results from other substances. The input could come from:

- one of the other modelled substances;
- a user-specified spatially distributed time function;
- a user-specified time function for the whole area;
- a user-specified spatially distributed constant;
- a user-specified constant for the whole area;
- a process flux originating from one of the water quality processes from the library;
- output from one of the other processes in the library;
- a default value from the database containing default values.

The pre-processor will report the origin of the input for each process. If information for a process is missing, so that the process can not be evaluated, it will detail what information is actually required in addition.

B.3 Sedimentation and resuspension

Sedimentation

WAQ uses the sedimentation formula derived by Krone (1962). The rate of downwards mass is equal to the product of near bed velocity, the concentration and the probability that a settling particle becomes attached to the sea bed. The sediment flux derived by Krone (1962) is given by:

$$f_{sed} = \mathrm{P}_{sed} \cdot V_{set} \cdot C \tag{B.1}$$

With the limitation that the sedimentation in one model time step cannot exceed the available amount of substances in the water column.

$$\mathrm{P}_{sed} = \max\left(0, \frac{\left(\tau_{c,sed} - \tau\right)}{\tau_{c,sed}}\right) \tag{B.2}$$

With:

f_{sed}	:	sedimentation flux	[g.m^{-2}d^{-1}]
P_{sed}	:	sedimentation probability	[-]
V_{set}	:	settling velocity of SPM	[m.d^{-1}]
C	:	concentration of SPM	[g.m^{-3}]
P_{sed}	:	sedimentation probability	[-]
τ	:	bottom shear stress	[Pa]
$\tau_{c,sed}$	:	critical shear stress for sedimentation	[Pa]

In order to omit the probability term, the critical shear stress for sedimentation is set to a constant value of 100 Pa. This value is two orders higher then the bed shear stress that occur, by which the probability term in equation has the value one. Our aim is to analyse the influences of the different runs on the Humber estuary instead of the combination of the Humber estuary and the surrounding Sea, therefore in this study no sedimentation is allowed in the outer area. This can be achieved by modelling the critical shear stress for sedimentation outside the Humber mouth as a constant value of 1 10^{-6} Pa. As a result of which the probability term prevents erosion in the area outside the Humber mouth.

Resuspension

Erosion of bed material occurs when the bed shear forces exceed the resistance of the bed sediment. The resistance of the bed is characterised by a certain critical erosive strength (bottom shear stress). Erosion of sediment is induced by the bed stress due to tidal (and wind –induced advective flows and surface waves. The erosion is directly proportional to the excess of the applied shear stress over the critical erosive bottom shear stress. The formula for erosion of homogenous beds is based on Partheniades. The erosion and resuspension flux is limited by the available amount of sediment on the sea bed.

Upward mass transport of bed material is modelled in WAQ by:

$$f_{res} = \mathrm{P}_{res} \cdot E_0$$
$$\mathrm{P}_{res} = \max\left(0, \frac{\left(\tau - \tau_{cr}\right)}{\tau_{cr}}\right) \tag{B.3}$$

Equation B.3 has two limitations: (i) drying cells and the second and (ii) amount of dry mass:

$$(i) \quad \text{if } (H < H_{min}) \rightarrow f_{res} = 0$$
$$(ii) \; f_{res} = \min\left(f_{res}, \frac{DM}{\Delta t \cdot A}\right) \tag{B.4}$$

Depth averaged bed shear stress is calculated in WAQ by (no wave influence):

White Colebrook: $$C_{2D} = 18 \cdot \log_{10}\left(\frac{12H}{k_s}\right) \qquad \text{(B.5)}$$

$$\tau_{flow2D} = \frac{\rho_l \cdot g}{{C_{2D}}^2} \cdot \left|U\right|^2 \qquad \text{(B.6)}$$

With:

f_{sed}	:	sedimentation flux	[g.m^{-2}d^{-1}]
V_{set}	:	settling velocity of SPM	[m.d-1]
P_{sed}	:	sedimentation probability	[-]
τ	:	bottom shear stress	[Pa]
$\tau_{c,sed}$	:	critical shear stress for sedimentation	[Pa]

for 3D models (no waves influence):

$$C_{3D} = C_{2D} + \frac{\sqrt{g}}{\kappa} \cdot \left(1 + \ln\left(\frac{0.5 \cdot \Delta z_b}{H}\right)\right) \qquad \text{(B.7)}$$

$$\tau_{flow3D} = \frac{\rho_l \cdot g}{{C_{3D}}^2} \cdot \left|u_b\right|^2 \qquad \text{(B.8)}$$

With:

f_{sed}	:	sedimentation flux	[g.m^{-2}d^{-1}]
V_{set}	:	settling velocity of SPM	[m.d^{-1}]
P_{sed}	:	sedimentation probability	[-]
τ	:	bottom shear stress	[Pa]
$\tau_{c,sed}$	:	critical shear stress for sedimentation	[Pa]

When the depth and the bottom layer thickness are varied, the influence of the last part of equation B.7 becomes clear. A first check can be done by using a bottom layer of 100 % (actually depth averaged 2D mode) of the total water column, the adjustment is now zero. This is correct since a bottom layer of 100% corresponds with a 2Dh simulation.

C River discharges Ouse and Trent

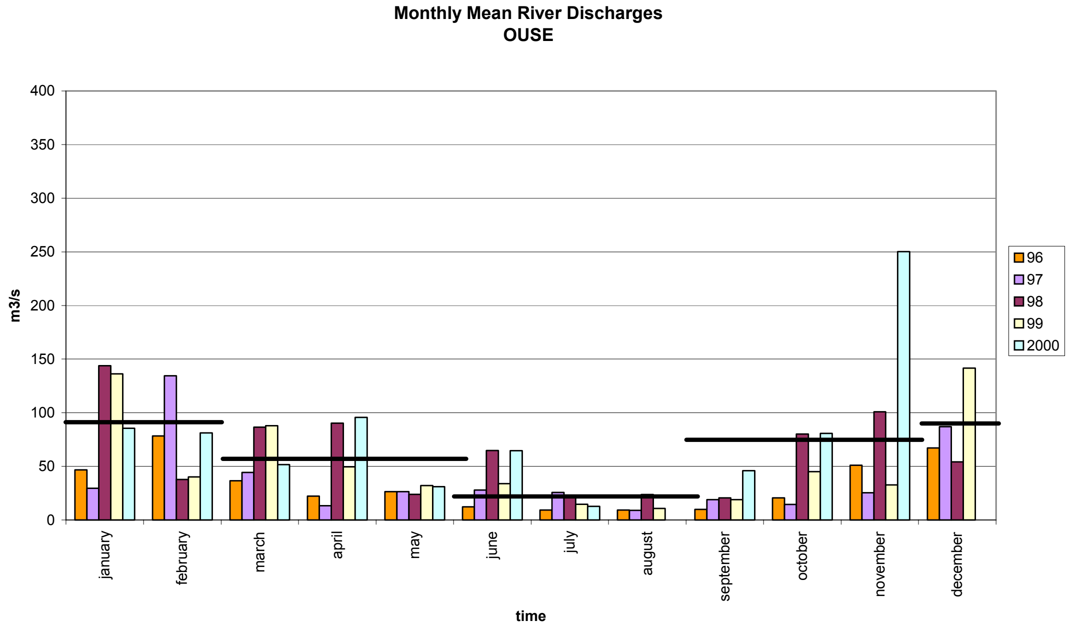

Figure C - 1 Average seasonal river discharges Ouse, Skelton [1996,2000]

Source Figure C - 1: Data WL | Delft Hydraulics (z3451)

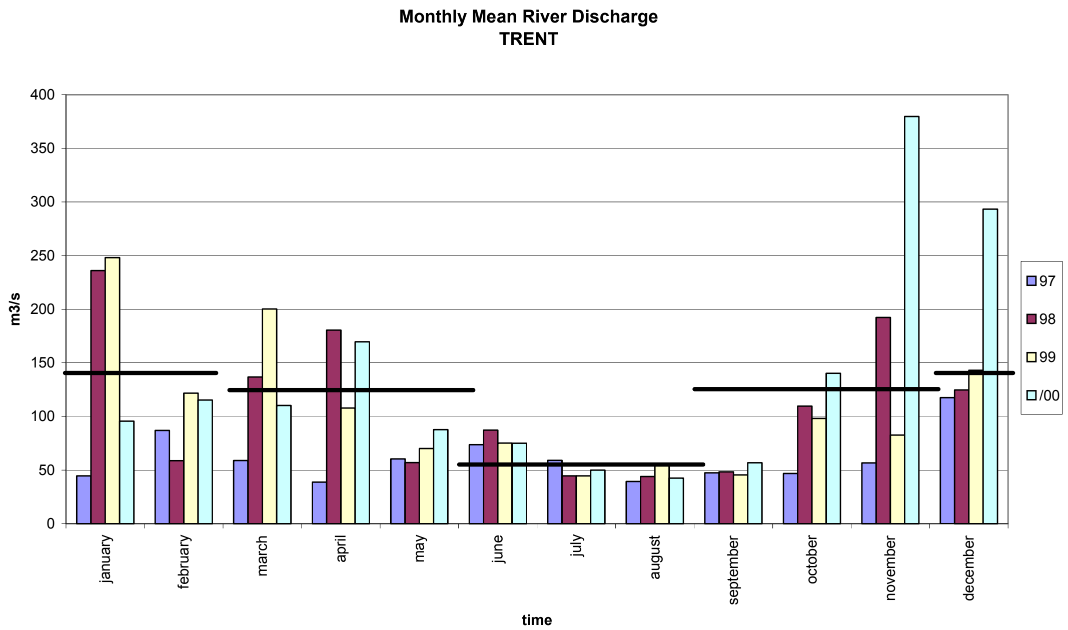

Figure C - 2 Average seasonal river discharges Trent, North Muskham [1996-2000]

Source Figure C - 2: Data WL | Delft Hydraulics (z3451)

Table C - 1 Average seasonal river discharges Trent an Ouse [01-12-1997,01-11-2000]

River:	winter	spring	summer	autumn	average
Ouse, Skelton	90	61	27	75	63
Trent, North Muskham	140	124	58	128	113

Source Table C - 1 Data WL | Delft Hydraulics (z3451)

Station (UK grid references)	Latitude	Longitude
Ouse, Skelton (SE568554)	53° 30’ 5.2’’N,	1° 59’ 29.2’’E
Trent, North Muskham (SK801601).	52° 36’ 10.22’’N	1° 59’ 17.4’’E

D Literature survey, tide induced residual fine sediment transport

D.1 Introduction tide induced residual sediment transport

Observations in the Dutch Wadden Sea, German Wadden Sea and Danish Wadden Sea have established the existence of gradients of fine-grained suspended sediments increasing from the tidal inlets, where concentrations are comparatively low, towards the coast. The suggested causes (Postma, 1954) of this increase are different in different localities. It has been assumed for the Northern Part of the Danish Wadden Sea and for part of the area near the mouth of the river Weser that large amounts of material are brought in suspension by the erosion of marshes and tidal flats. In the region under the immediate influence of fresh water from Elbe Weser and Ems on the other hand, high concentrations are found in the transition area from fresh water to salt water. For areas where no appreciable erosion occurs, and are not influenced by fresh water, and where the water masses are rapidly refreshed, such as those along the coast of the Dutch provinces of Friesland and Groningen, there must be a mechanism that causes up-estuary sediment transport. This mechanism must counterbalance the down-estuary flow of suspended matter by tidal and turbulent exchange (given by the observed down-estuary decrease of concentration and the high flushing rate). In attempt to explain this up-estuary transport, H. Postma (1954, 1961) was one of the first who wrote an article on ‘tide induced residual fine sediment transport’. Furthermore van Straaten & Kuenen (1957) and Dronkers (1985) delivered contributions to the knowledge on this mechanism.

D.2 ‘Hydrography of the Dutch Wadden Sea’, Postma (1954)

Postma suggested that accumulation of suspended matter is due to an up-estuary decrease of tidal current velocities and depths, combined with settling and scour lag effects. Assume that the mean current velocity at each point is the same for ebb and flood, but the magnitude decreases up-estuary. Part of the silt settles at the end of the flood tide in places where the current is too weak to carry it away. Hence the water mass, when travelling down-estuary, contains less silt than on it’s way up-estuary and a certain fraction of silt is left behind on the bed. This process repeats itself every tide

D.3 ’Accumulation of fine grained sediments in the Dutch Wadden Sea.’ Van Straaten & Kuenen, (1957)

Van Straaten & Kuenen further elaborated the theory of Postma (1954). One of the most important differences between the original theory and the version given by Van Straaten and Kuenen are the clear distinction by the latter authors between settling lag and scour lag. Furthermore the writer made a representation of the successive events in a given mass of water as it moves up-estuary and down-estuary under the influence of the tide. Van Straaten & Kuenen argue that in the Wadden Sea capacity conditions are not met, since the currents are always strongly undercharged with suspended matter. They therefore emphasize the importance of competency, assuming that every particle of a certain size is re-suspended as soon as sufficient flow velocity of the water has been reached. For a good understanding of their hypothesis, see Figure D-1 and its explanation.

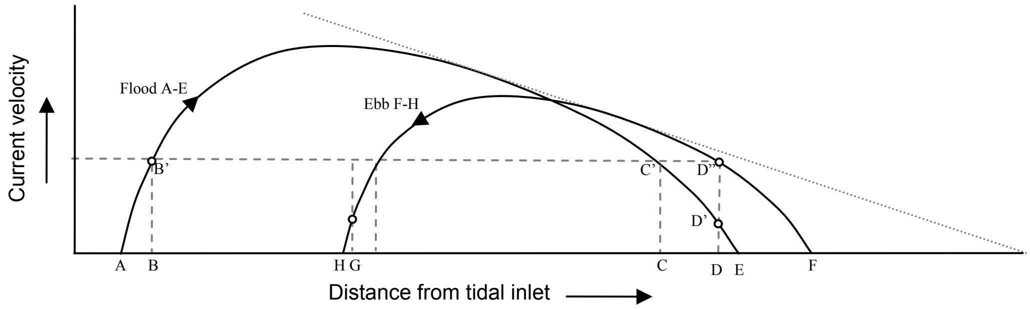

Figure D-1 Description transport of a silt particle during a single tide

Explanation Figure D-1: The construction of the silt transport paths is based on the simplifying assumption that current velocities at each separate point vary with time as a sinus function and that the current velocities at each stage of the tide decrease from point to point in direct, linear proportion to the distance from the inlet. A sediment particle brought in suspension at point B by a flood current velocity BB' is carried up-estuary to point C, where current velocity CC' equals BB'. Beyond this point the current velocity drops below the value at which the particle was brought into suspension. For two reasons, however, the particle is nevertheless transported farther up-estuary than point C. First, the velocity required to bring a particle in suspension is higher than the velocity necessary for keeping a particle in suspension (scour lag). Secondly after the current velocity has dropped below the latter value, it still takes some time before the particle reaches the bottom (settling lag). As a result the particle is assumed to reach the bottom at D. The water mass continues tot travel up-estuary to point E and then returns with the ebb to point A. When it passes point D again it is not able, however, to pick up the particle, since the current velocity DD' is smaller than BB'. At the end of the ebb tide this water mass deposits the particle at point G. Hence, over one tidal cycle the particle has been shifted up-estuary over the distance BG. The next tide will cause a further shift up-estuary.

Reviewers of the article wrote the following: Postma (1961); "In our opinion it has not yet been established with certainty that even if capacity in the strict sense does not play role, something very much like it should not be taken into account."… …"Increasing current velocities will locally cause deeper bottom scour, ripple movement etc., so that fine sediments will be exposed and are set in motion, which at lower current velocities were protected against transportation by sand and grains. When the current slackens, part of the finely divided suspended matter may be deposed in sheltered places before the main current has dropped below the critical value. The ultimate effect is a gradual change of the concentration of suspended material of virtually one grain size with the corresponding variation of current velocity, may be the same as in the case of capacity influence."

Groen (1967) on the other hand, mentioned a shortcoming in the argument of van Straaten & Kuenen that the behaviour of a particle is at any moment determined by the current velocity at that moment. "One cannot say that in a given current one particular particle can or cannot be 'sustained' by the current. In reality, only the statistics of the behaviour of the suspended particles is determined by the current."

D.4 'Transport and accumulation of suspended matter in the Dutch Wadden Sea' Postma, (1961)

In the later version of Postma (1961), special attention was paid to the important fact that there is a considerable asymmetry between the time interval of maximum flood to maximum ebb and maximum ebb to maximum flood. Postma concluded that the differences between the tidal phases are: first, the decrease of mean current velocities up-estuary (as discussed before) and, secondly, the asymmetrical shape of the ebb and flood curves in the small tidal channel, the velocity maximum of which, compared with the maximum of the sine wave are shifted towards low tide. “The reason for the different behaviour between high tide and low tide is the fact that the time span during which current velocities are sufficiently low to permit settling of fine material is much longer at high tide than at low tide.” Observations show that the up-estuary increase of sediment concentration only holds for material smaller than 64-128 microns. Larger particles under normal conditions probably show no concentration gradient, in a horizontal plane, or a slight decrease up-estuary. Postma suggests that the different behaviour of large particles in comparison with silt particles is mainly due to the fact that the former also settle at low tide, thus undergoing an down-estuary as well as an up-estuary shift.

D.5 Tide-induced residual transport of fine sediments’, Dronkers (1985)

For the residual transport of fine sediment, an approximate analytical expression has been derived by Dronkers (1985), based on a qualitative description by Postma (1961). In this derivation the excursion of sediment particles through the estuary is followed during a tidal cycle.

During the propagation of the tidal wave in shallow irregularly shaped basins harmonic overtides are generated, causing an asymmetry in the velocity variation between ebb and flood. As a consequence the time interval during which sediment particles can settle at slack water and remain on the bottom until resuspension may be different for HWS and LWS. Therefore the temporarily deposited sediment experiences a net residual displacement during a tidal cycle. The magnitude and direction of this residual sediment flux is mainly determined by the difference in the variation of the current velocity around LWS and HWS. This transport process only applies to fine sediment which is deposited and resuspended in a time interval in which current speed is small compared to its maximum value.

The evaluation of the tidally averaged transport is based on a simple bookkeeping method. A plane X(t) moving with the cross-sectional averaged velocity U is considered. The amounts of sediment passing through the plane during different stages of the tidal period are taken stoke of. Only sediment that has settled on the bottom passes the moving plane. Thus the amount of sediment passing through the moving plane X(t) during a tidal period equals the net amount passing through a fixed plane. The superscripts: + and - in the following formula refer to the HWS respectively LWS period.

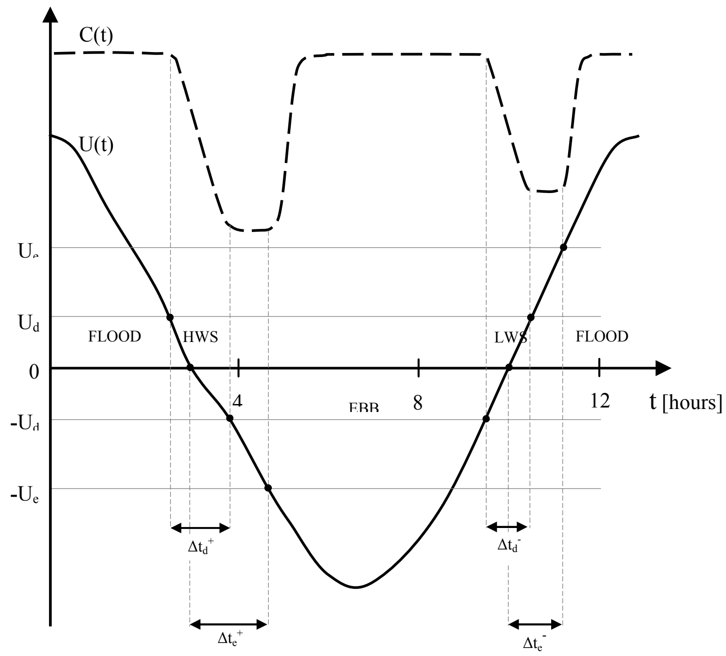

Figure D-2 Definition sketch of critical depth averaged current velocities Ud and Ue corresponding to treshholds for deposition and erosion. Definition of intervals $\Delta t_d^{+/-}$ and $\Delta t_e^{+/-}$.

The resulting expression for the net transported sediment mass through a cross section x ≈ ½*(x^+ + x^-) during a tidal cycle reads:

$$M(x) = \mu^+\lambda^+ - \mu^-\lambda^- \tag{D.1}$$

Where μ^+ (respectively μ^-) is the amount of sediment settled on the bottom at x^+ (resp. x^-) in the period of t^+, HWS (resp. t^-, LWS), and λ^+ (resp. λ^+) is the distance travelled by fluid parcels in the t^+ time interval Δt^+ (resp. t^- time interval Δt^-) during which the fine fraction remains on the bed. The quantities $\mu^\pm$ and $\lambda^\pm$ can be evaluated from the approximate expressions:

$$\begin{aligned} &\mu^\pm(x) \cong \omega^\pm(x)\cdot \max .susp.conc.(x) \\ &\omega^\pm(x) \approx A_s(x^\pm,t^\pm)[1-\exp(-w\frac{\Delta t_d^\pm(x^\pm)}{h(x^\pm,t^\pm)})] \\ &\lambda^\pm(x) \approx \frac{1}{2}U_e \Delta t^\pm(x^\pm) \end{aligned} \tag{D.2}$$

Variables: μ+ = amount of sediment settled on the bottom at x^+, *As* = stream cross-section, *w* = fall velocity, Δt_d = time interval for which |u| < u_d., λ^+ = the distance travelled by fluid parcels in the t^+ time interval Δt^+.

$$\left|du/dt\right|_{x^+,t^+} < \left|du/dt\right|_{x^-,t^-} \tag{D.3}$$

The physics behind these equations is obvious: the amount of sediment μ^+, which is settled per unit length in the period around t^+ (SBE, HWS), will not follow the tidal motion before the ebb current reaches the critical speed for erosion u_e. In this lapse of time the settled sediment is displaced with respect to the suspended sediment in landward direction over a distance, which on the average equals λ^+. Around t^- (SBF, LWS) a similar relative displacement will occur of a sediment mass μ^- in seaward direction over an average distance λ^-. The equations in D.3 show that a landward residual flux of fine sediment is favoured if:

- the channel depths decrease in landward direction (as demonstrated by Van Straaten & Kuenen.
- the velocity variation is slower around slack before ebb (high water slack): $|du/dt|x^+,t^+ < |du/dt|x^-,t^-$

This last condition can be realized by a distortion of the tidal wave or by a landward decrease of the current velocity. The latter aspect has been demonstrated by Van Straaten & Kuenen (1967).

The residual flux of fine sediment predicted by the analytical expression has been compared with field observations in two different tidal systems, the Wadden Sea-Ameland area and the Eastern Scheldt. The Wadden Sea-Ameland area behaves as a sediment trap and the reverse holds for the major part of the Eastern Scheldt. The order of magnitude and the direction of the sediment flux are in agreement with the observations.

It must be noted that in the tidal system which behaves as a sediment trap, the influence of a storm surges on the long term accumulation rate of sediment is very important. In storm surge circumstances the major part of the fine sediment accumulated during calm weather circumstances can be eroded and returned to the coastal shelf.

E Appendix Co-Tidal charts M_2 and S_2

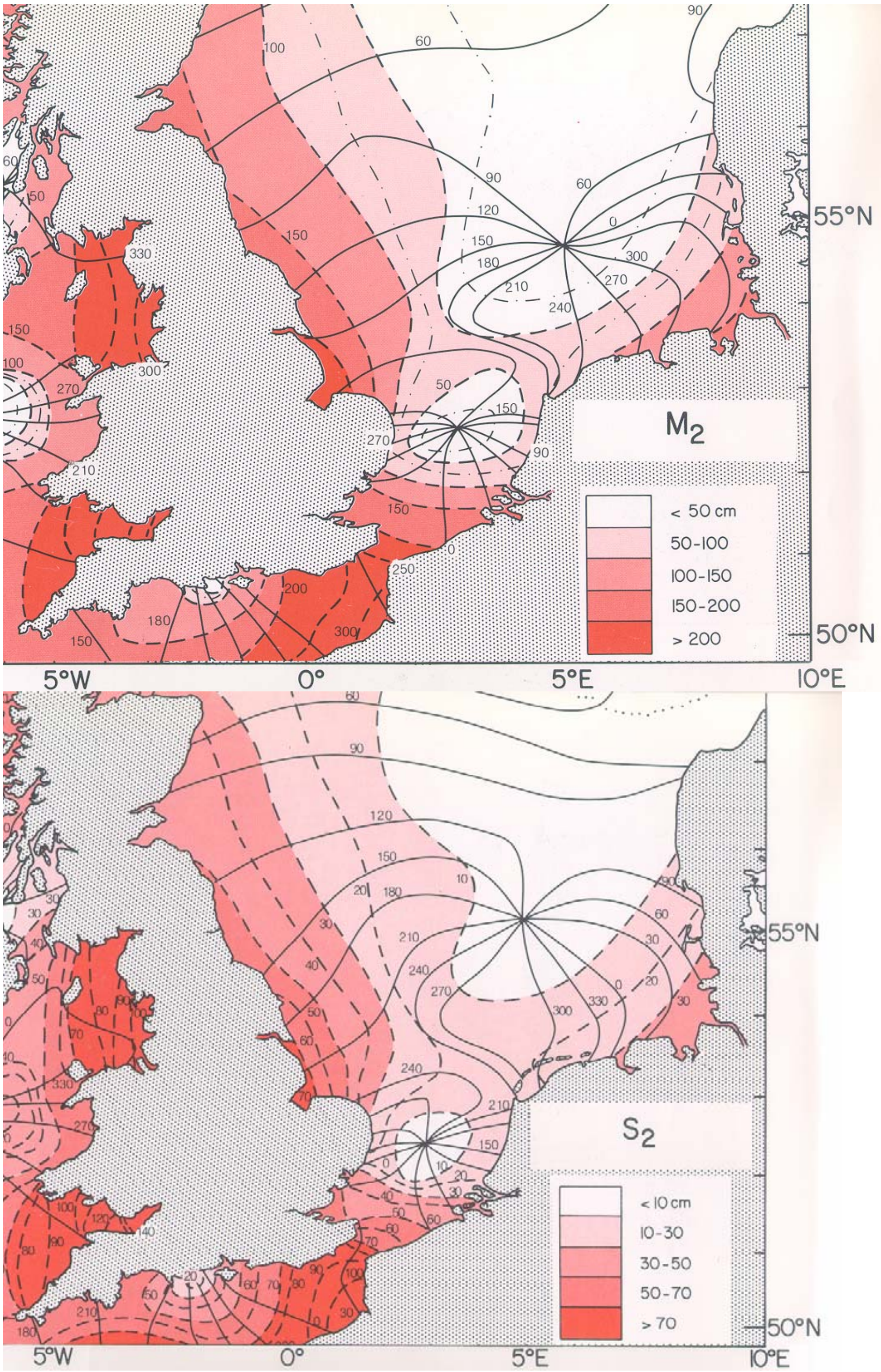

Figure E-1 Co-Tidal charts

F Computational grid

Hydrodynamic coarse grid, total area

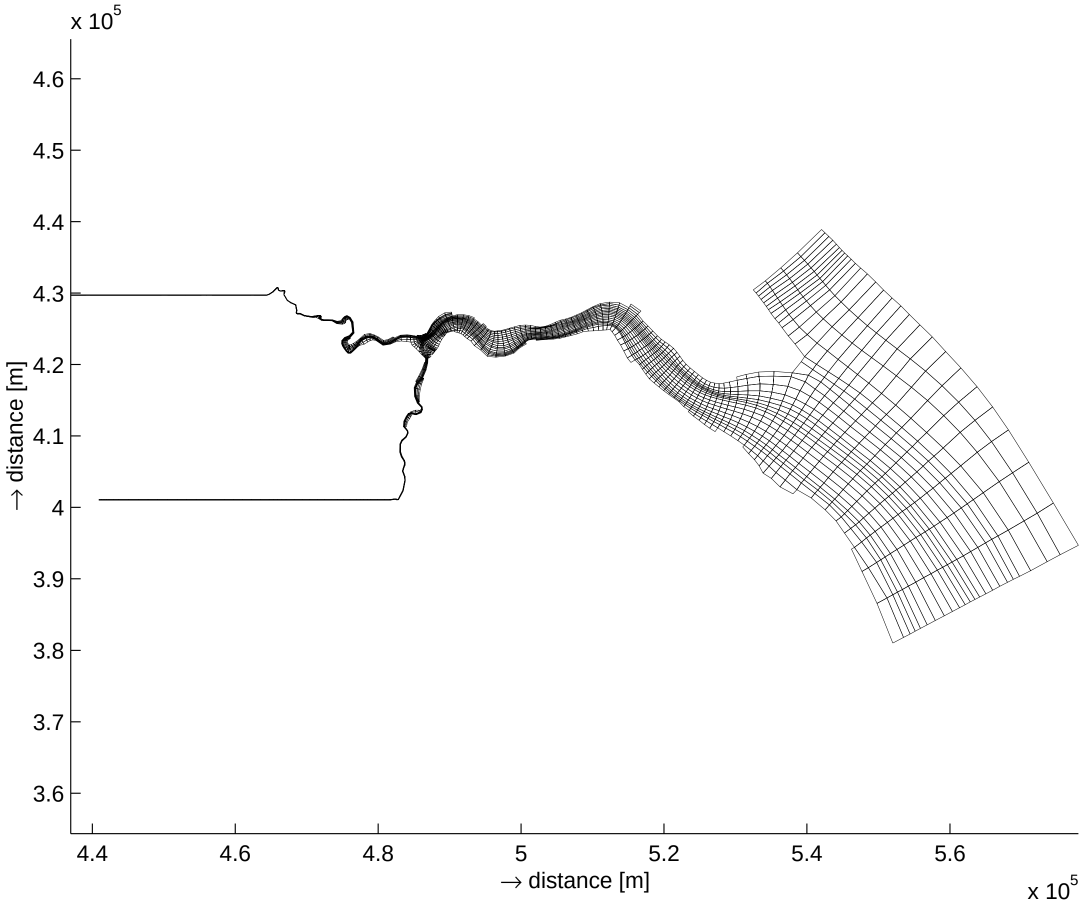

Figure F-1 Hydrodynamic coarse grid

Hydrodynamic coarse grid, areas of interest

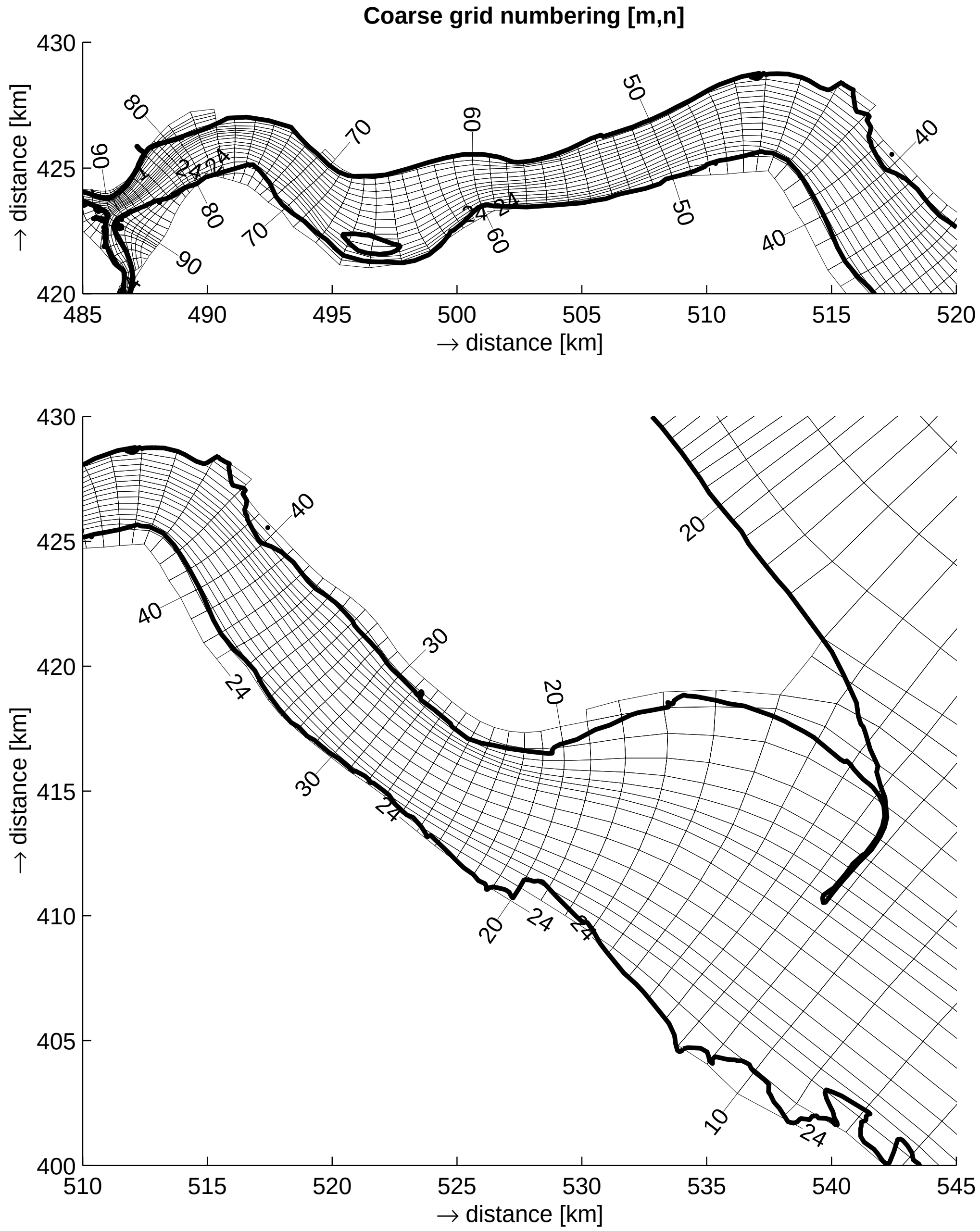

Figure F-2 Hydrodynamic coarse grid, area of interest

Explanation: Coarse grid including grid-numbering M and N values.

Morphological coarse grid, aggregated areas

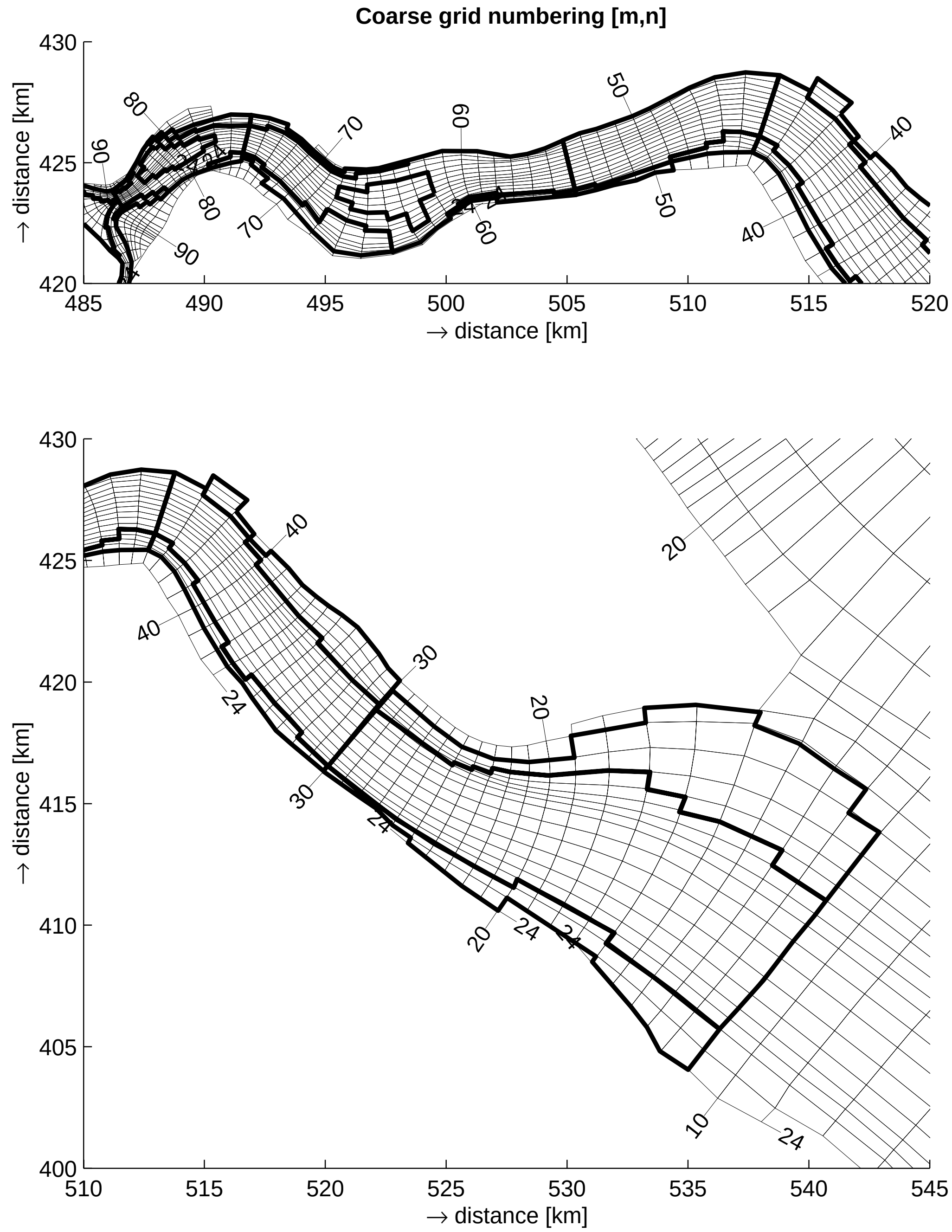

Figure F-3 Morphological coarse grid and aggregated grid

Explanation: The grid numbering of the coarse morphological grid are given.

Aggregated grid, area of interest

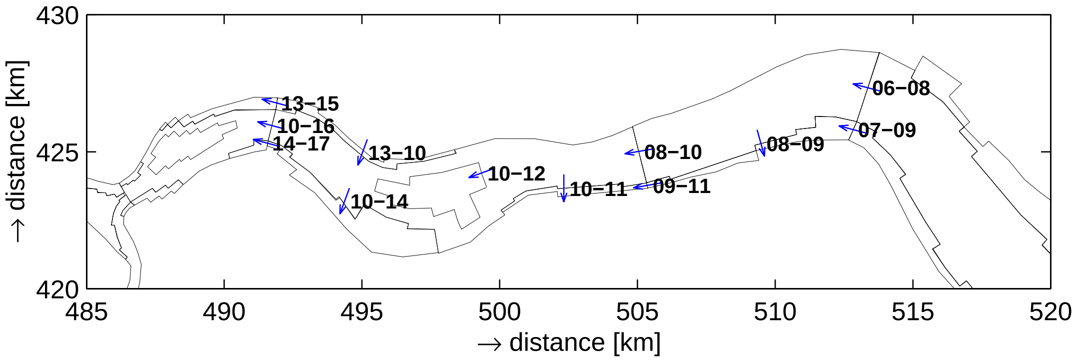

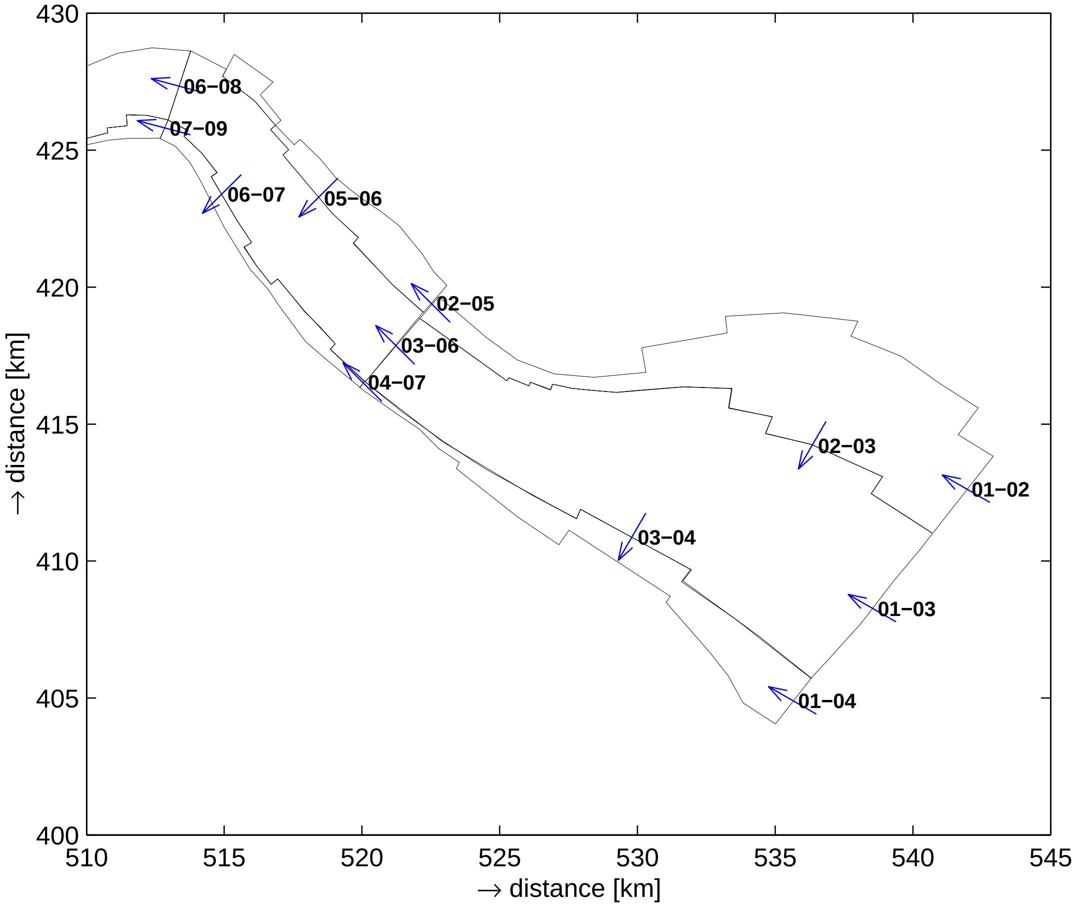

Figure F-4 Aggregated grid. area of interest including flux-numbering

G Hydrodynamic calibration

G.1 Observed and hindcast water levels

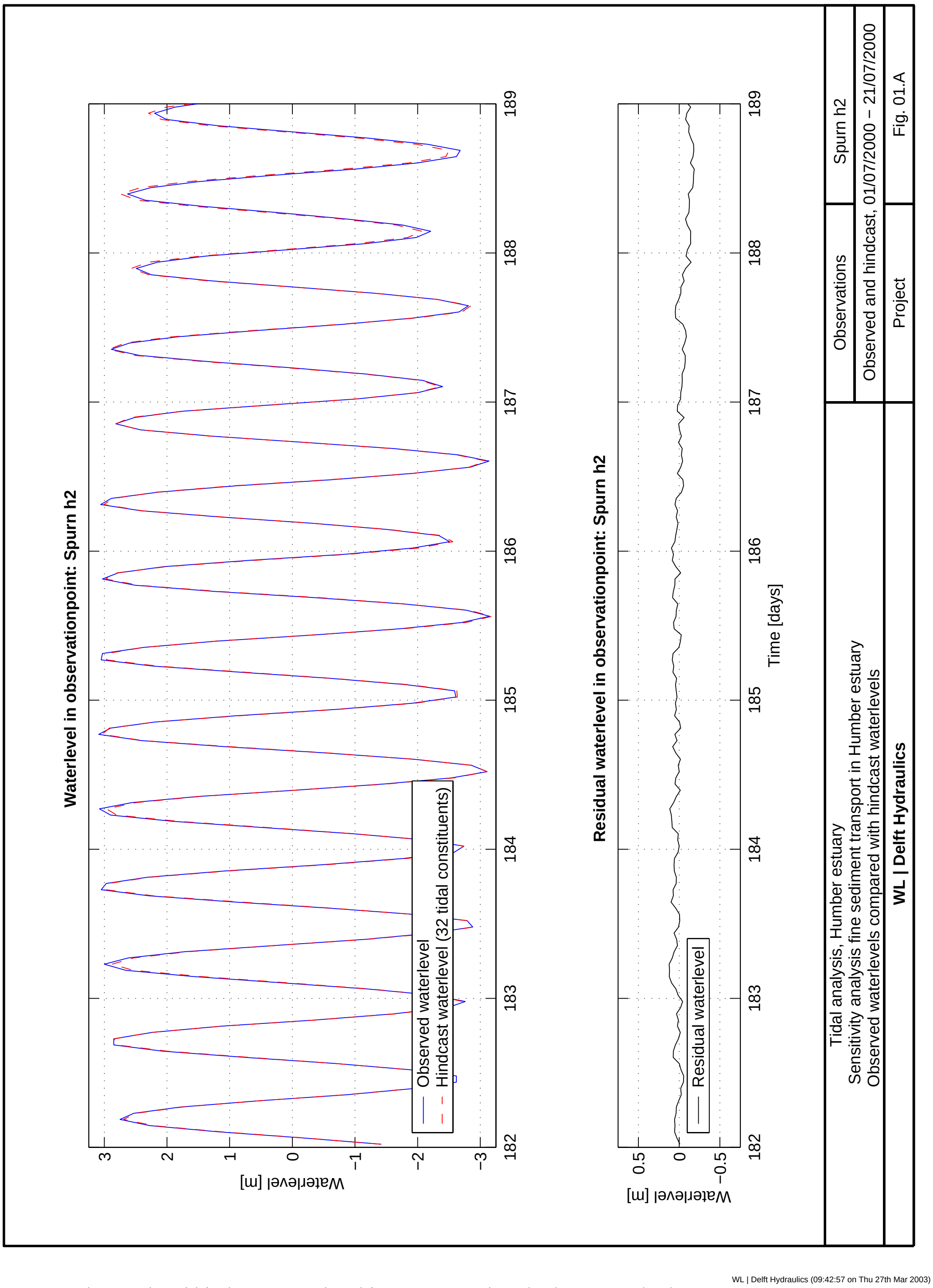

Figure G-1 Observed and hindcast water level in Spurn Head, 01/07/2000 - 07/01/2000

Source: Hindcast observations consisting of 32 tidal constituents derived from observations in June 2000.

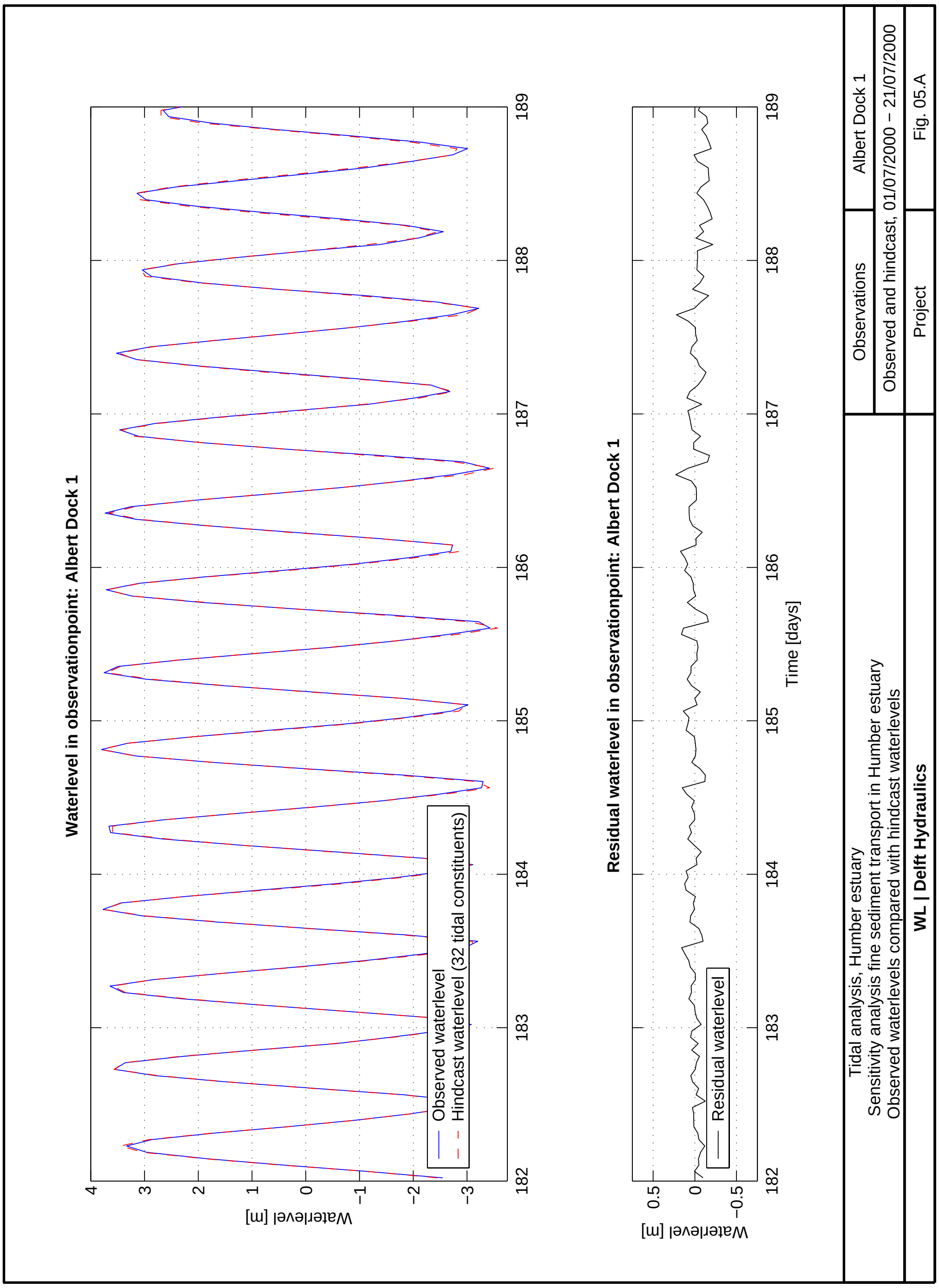

WL | Delft Hydraulics (09:43:13 on Thu 27th Mar 2003)

Figure G-2 Observed and hindcast water level in Albert Dock, 01/07/2000 - 07/01/2000

Source: Hindcast observations consisting of 32 tidal constituents derived from observations in June 2000.

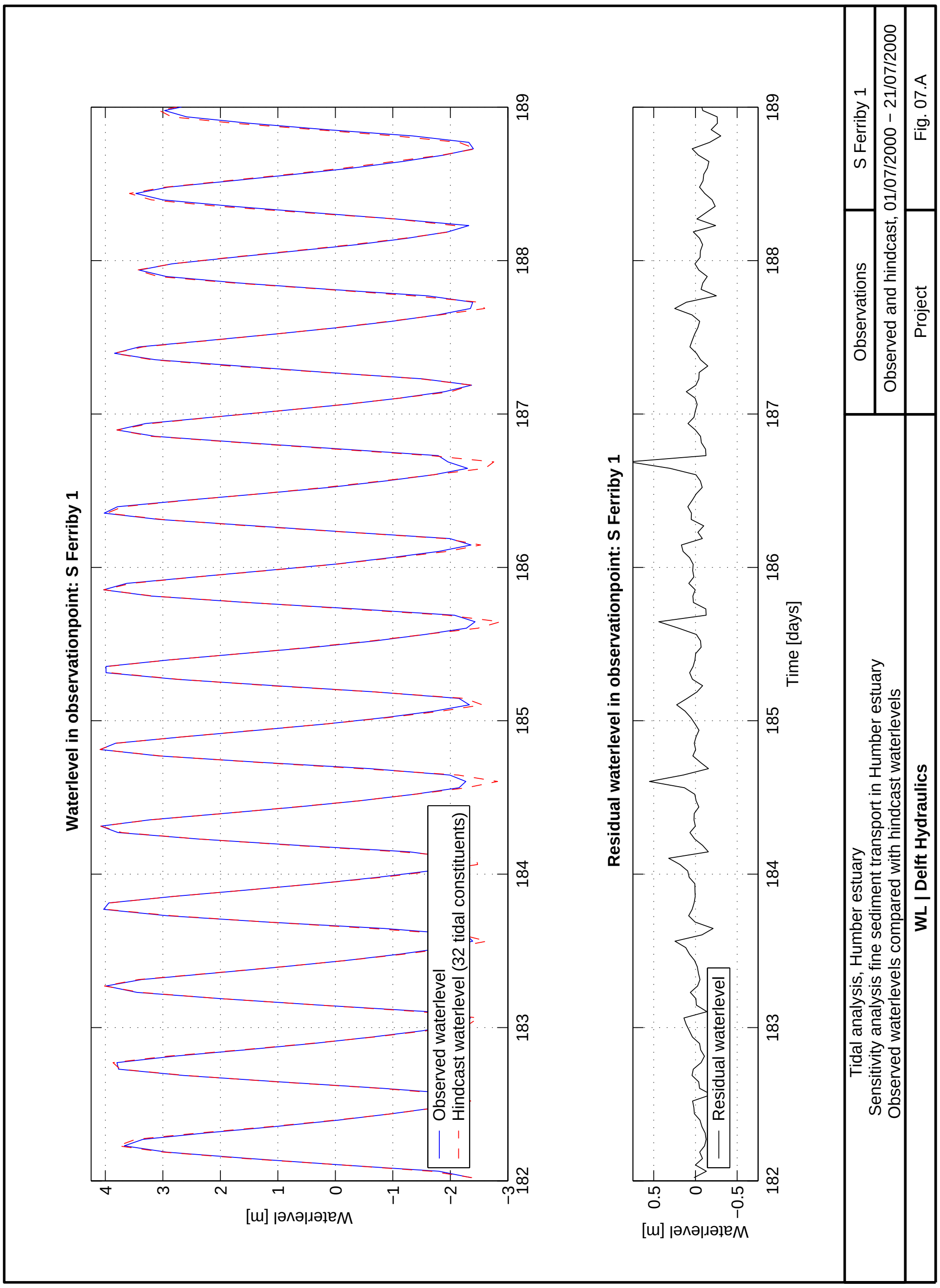

WL | Delft Hydraulics (09:43:19 on Thu 27th Mar 2003)

Figure G-3 Observed and hindcast water level in South Ferriby , 01/07/2000 - 07/01/2000

Source: Hindcast observations consisting of 32 tidal constituents derived from observations in June 2000.

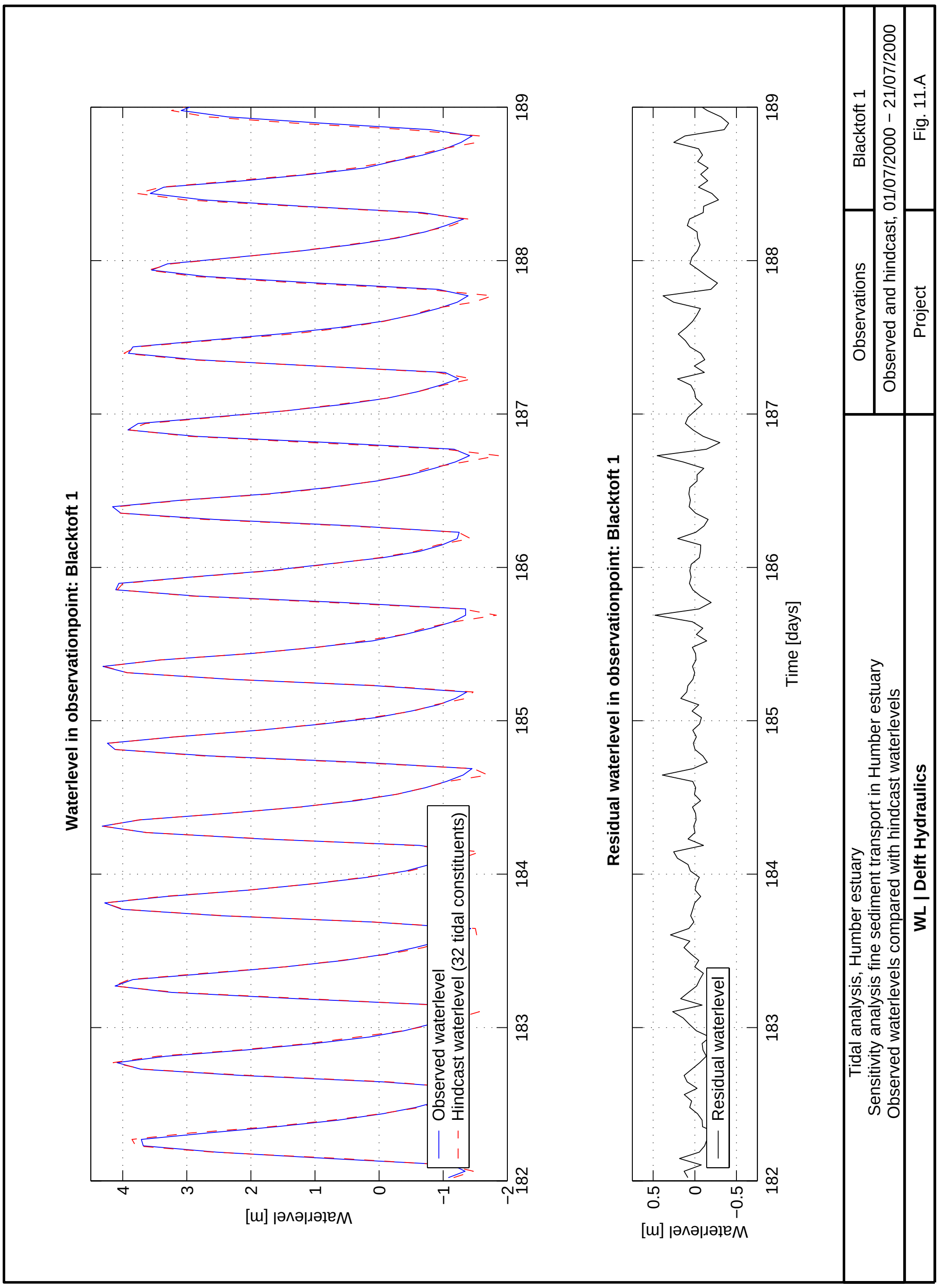

WL | Delft Hydraulics (09:43:32 on Thu 27th Mar 2003)

Figure G-4 Observed and hindcast water level in Blacktoft, 01/07/2000 - 07/01/2000.

Source: Hindcast observations consisting of 32 tidal constituents derived from observations in June 2000.

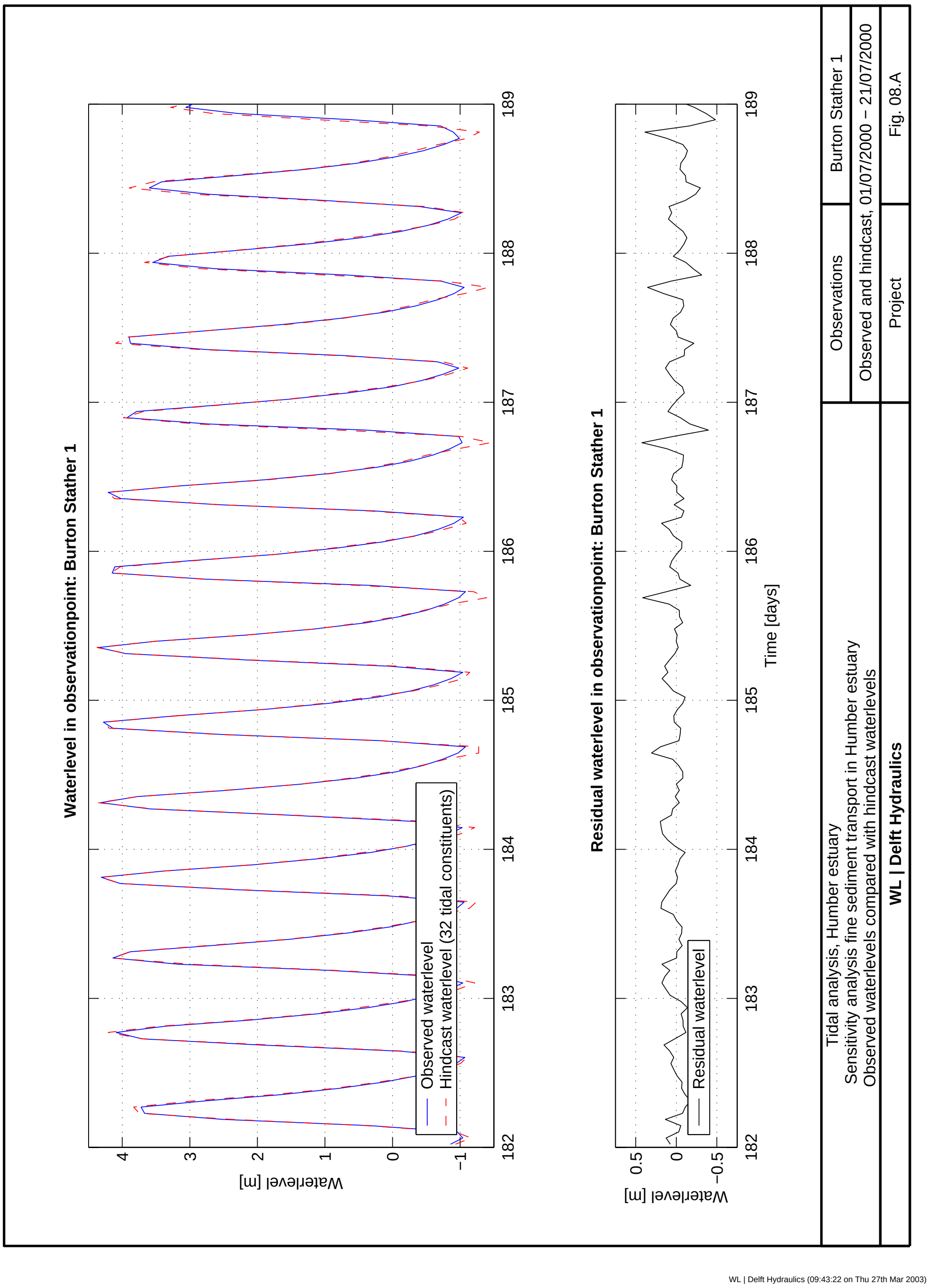

Figure G-5 Observed and hindcast water level in Burton Stather, 01/07/2000 - 07/01/2000.

Source: Hindcast observations consisting of 32 tidal constituents derived from observations in June 2000.

G.2 Computed waterlevels and hindcast observations

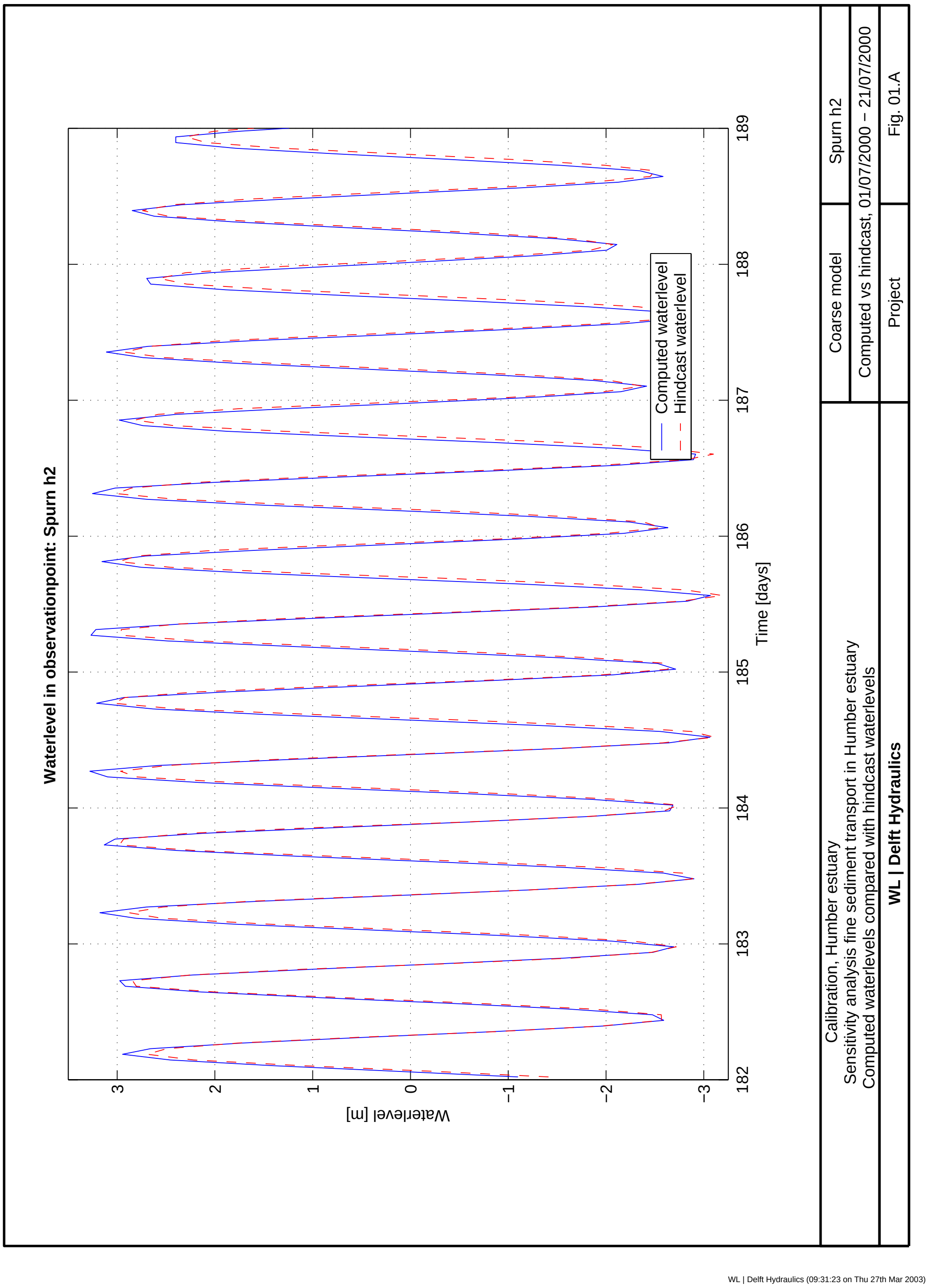

Figure G-6 Hindcast and computed water level in Spurn Head, 01/07/2000 - 07/01/2000.

Source: Hindcast observations consisting of 32 tidal constituents derived from observations in June 2000.

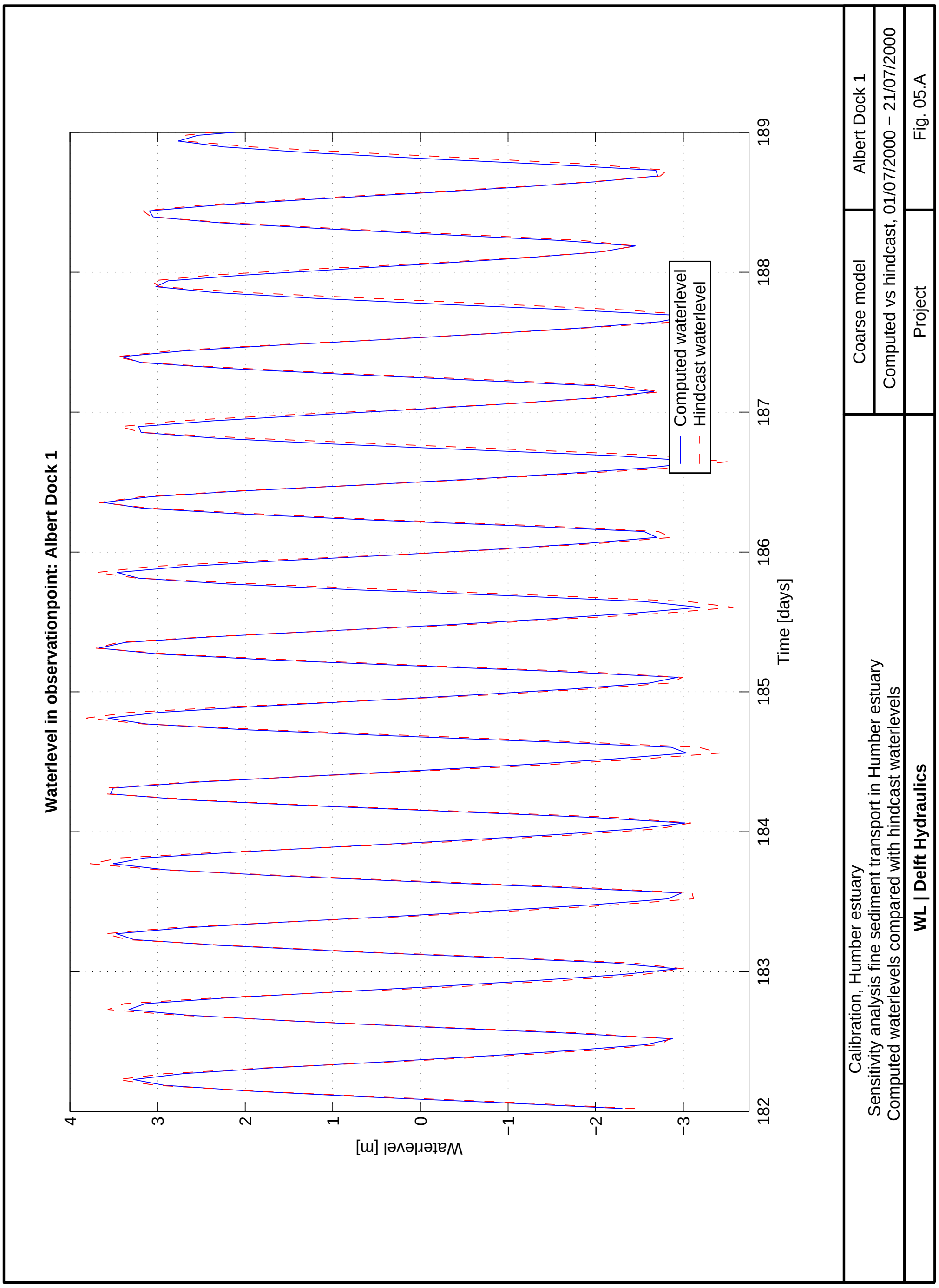

WL | Delft Hydraulics (09:31:31 on Thu 27th Mar 2003)

Figure G-7 Hindcast and computed water level in Albert Dock, 01/07/2000 - 07/01/2000.

Source: Hindcast observations consisting of 32 tidal constituents derived from observations in June 2000.

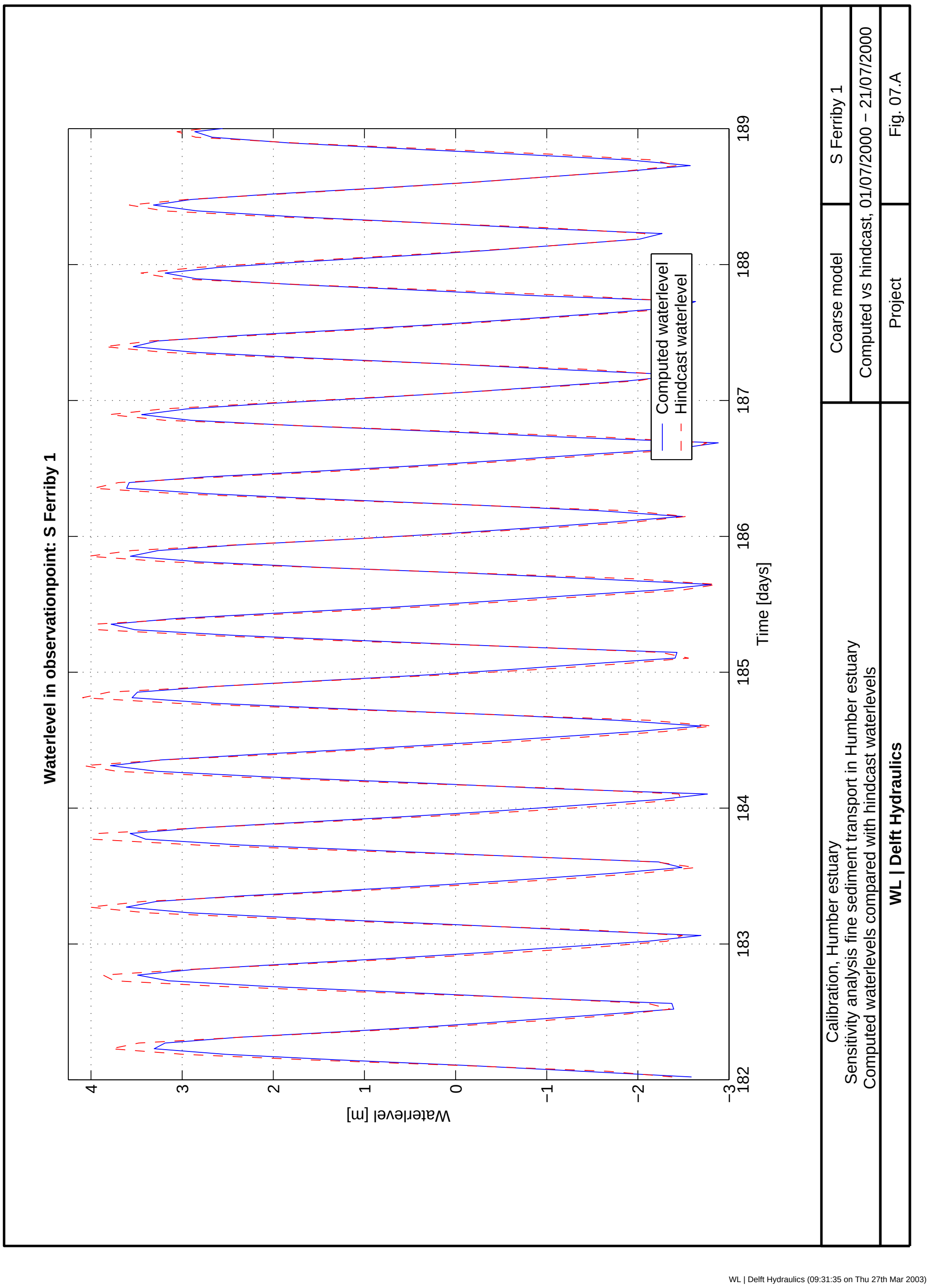

Figure G-8 Hindcast and computed water level in South Ferriby, 01/07/2000 - 07/01/2000.

Source: Hindcast observations consisting of 32 tidal constituents derived from observations in June 2000.

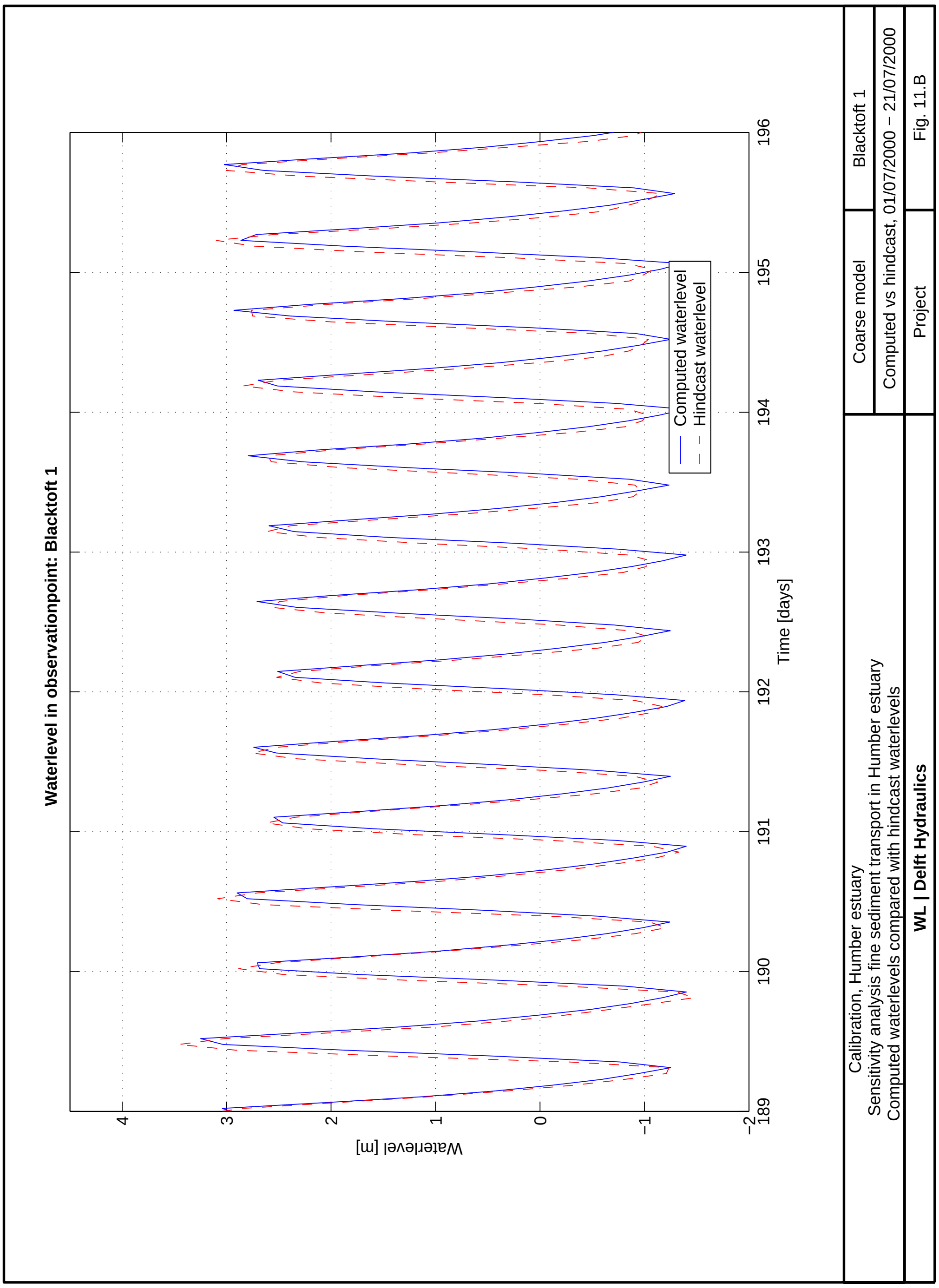

WL | Delft Hydraulics (09:31:45 on Thu 27th Mar 2003)

Figure G-9 Hindcast and computed water level in Blacktoft, 01/07/2000 - 07/01/2000.

Source: Hindcast observations consisting of 32 tidal constituents derived from observations in June 2000.

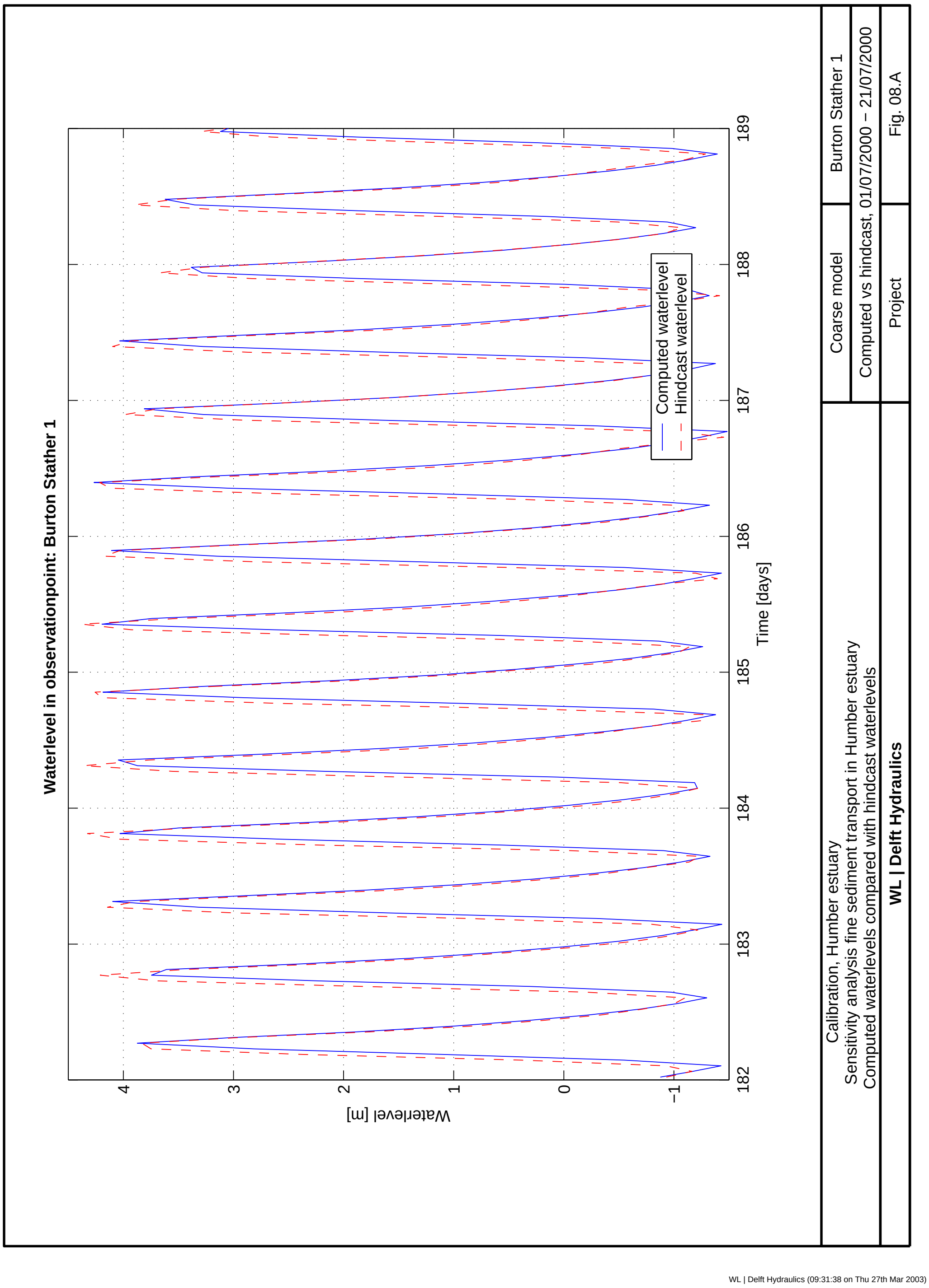

Figure G-10 Hindcast and computed water level in Burton Stather, 01/07/2000 - 07/01/2000.

Source: Hindcast observations consisting of 32 tidal constituents derived from observations in June 2000.

G.3 Calibration global roughness coarse model; -inner estuary-

A more detailed analysis is done by comparing tidal analysis of the computed and observed waterlevels in 2000. For four D3D coarse runs, phase and amplitude are calculated and compared with observations. The average errors of the seven water level stations in the estuary are plotted in Figure G-11 and Figure G-12.

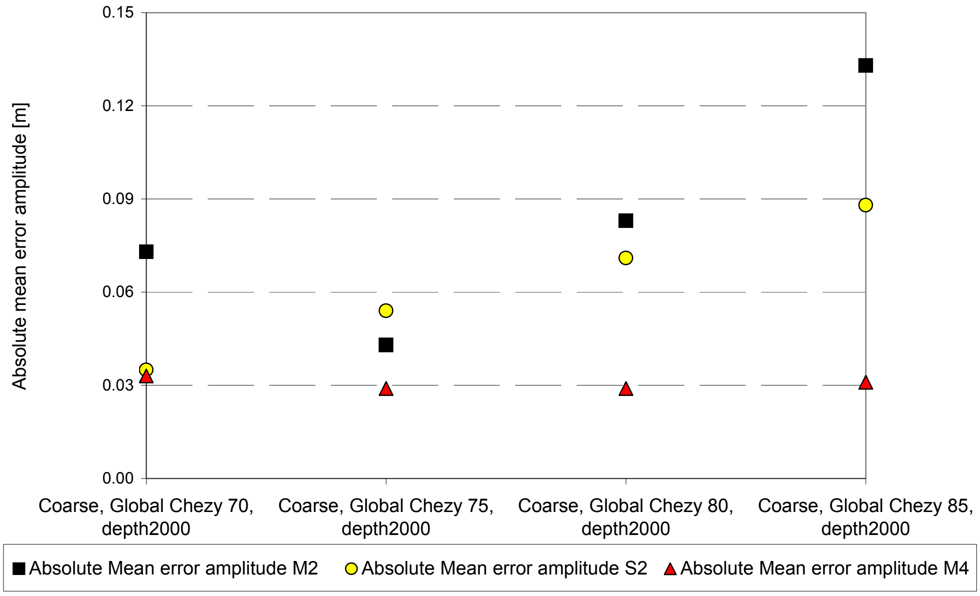

Figure G-11 Absolute mean error amplitude, coarse model, estuary

The amplitudes of M2 and M4 show an optimum for the run with a global Chezy of 75, a global Chezy of 70 shows better results for amplitude S2.

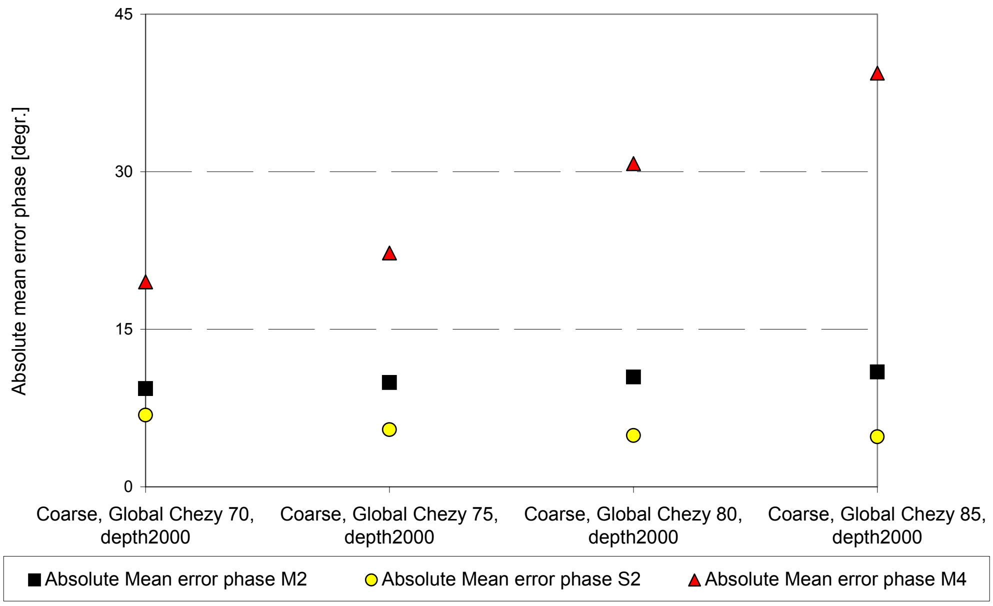

Figure G-12 Absolute mean error phase, coarse model, estuary
Source: Data analysis of D3D runs and observations in 7 water level-stations in Humber estuary.

A decreasing Chezy value from 85 to 70 shows a decreasing phase-error in M4, the phase-error in S2 on the other hand increases slowly. A global Chezy of 70 shows the most realistic results for phases of M2 and M4, but a global Chezy of 75 shows better results for phase S2.

G.4 Calibration global roughness coarse model; -total area-

The mean errors made in phase and amplitude, in the total area, are plotted for components M2, S2 and M4 in Figure G-13 and Figure G-14.

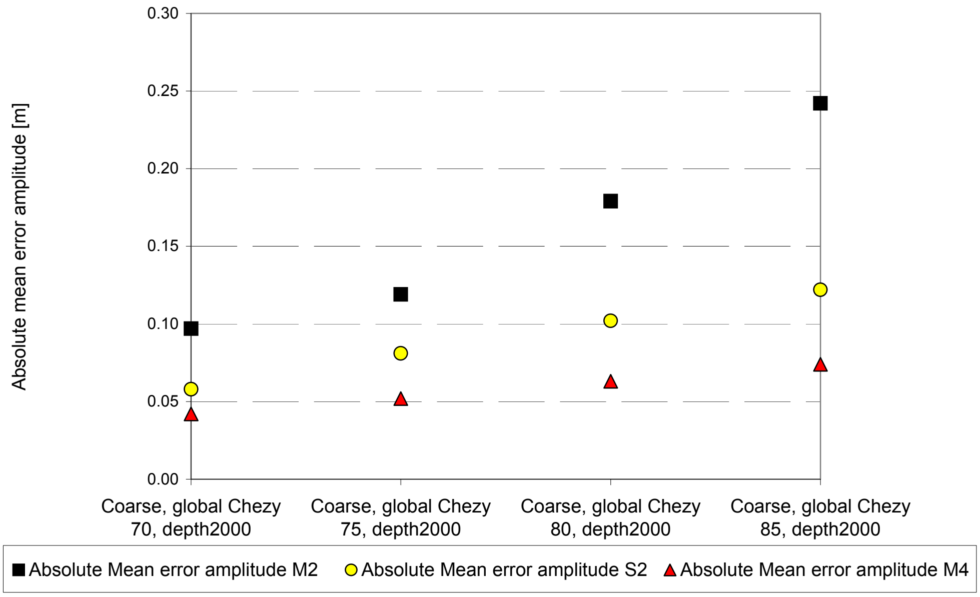

Figure G-13 Absolute mean error amplitude, total area

A decreasing Chezy value from 85 to 70 shows a decreasing amplitude-error in all three tidal constituents.

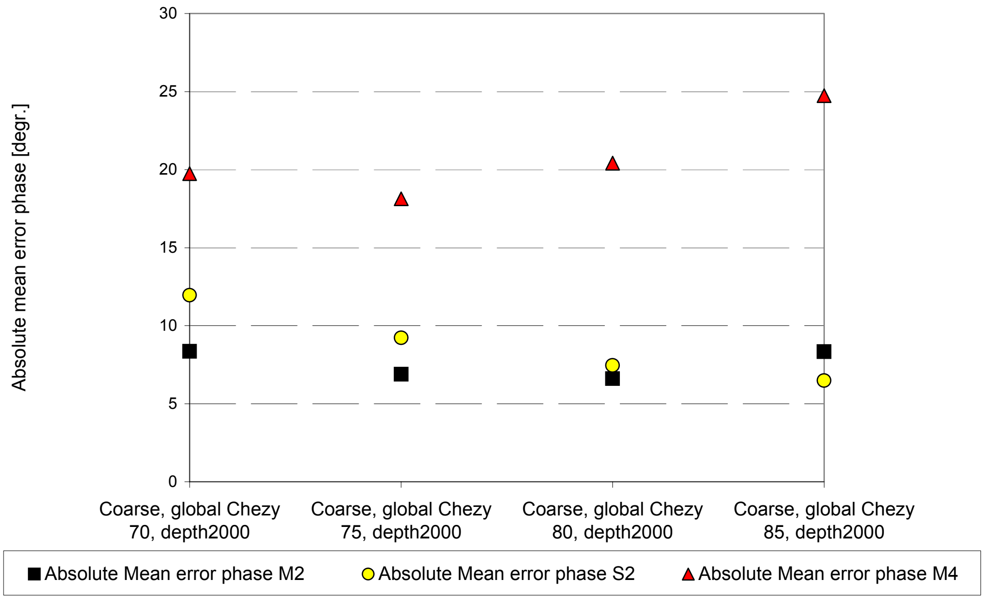

Figure G-14 Absolute mean error phase, total area
Source: Data analysis of D3D runs and observations in 12 water level stations in Humber estuary.

For the total area, the amplitudes are best represented by a global Chezy of 70, the phases by a global Chezy of 75.

G.5 Calibration global roughness fine model; -inner estuary-

For several D3D fine model runs, phase and amplitude are calculated and compared with observations. The average errors of the seven water level stations in the estuary are plotted in Figure G-15 and Figure G-16.

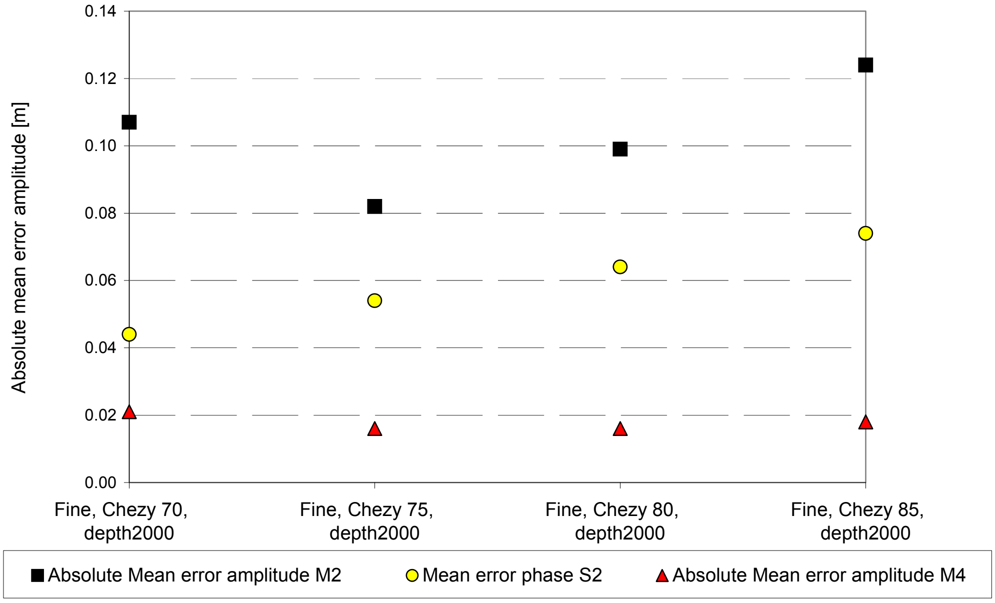

Figure G-15 Absolute mean error amplitude, fine model, inner estuary

The amplitude of M2 shows an optimum for the run with a global Chezy of 75, a global Chezy of 70 shows better results for amplitude S2.

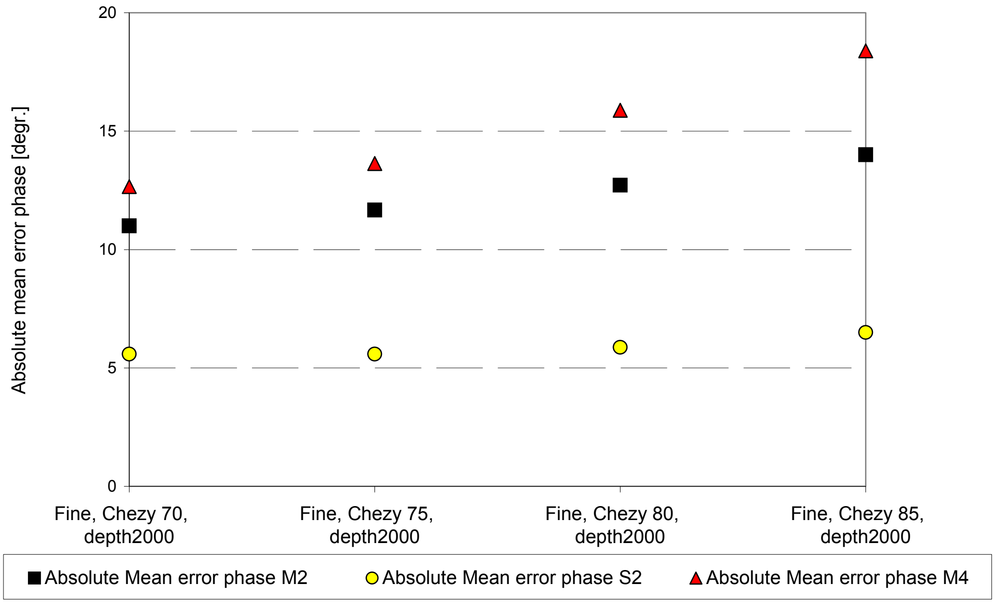

Figure G-16 Absolute mean error phase, fine model, inner estuary
Source: Tidal analysis in 7 water level stations in Humber estuary compared with several D3D model.

A decreasing Chezy value from 85 to 70 shows a decreasing phase-error in M2, S2 and M4.

G.6 Calibration global roughness fine model; -total area-

The mean errors made in phase and amplitude, in the total area, are plotted for components M2, S2 and M4 in Figure G-17 and Figure G-18.

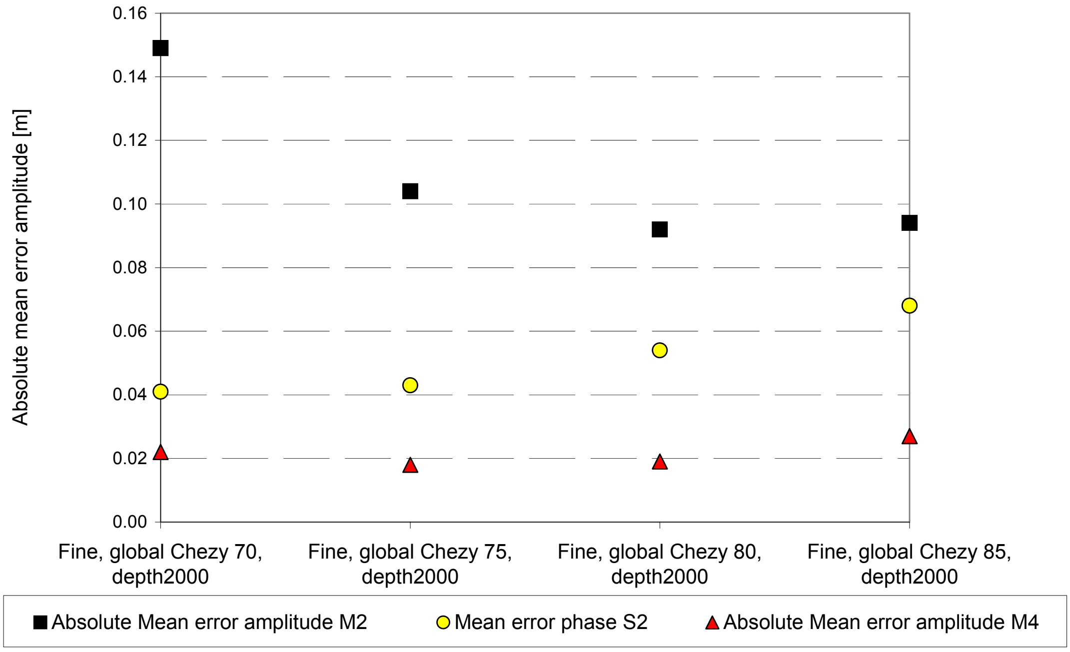

Figure G-17 Absolute mean error amplitude, fine model, total model area

The amplitude of M2 shows an optimum for the run with a global Chezy value of 80, S2 for a Chezy of 70 and M4 for a Chezy of 75.

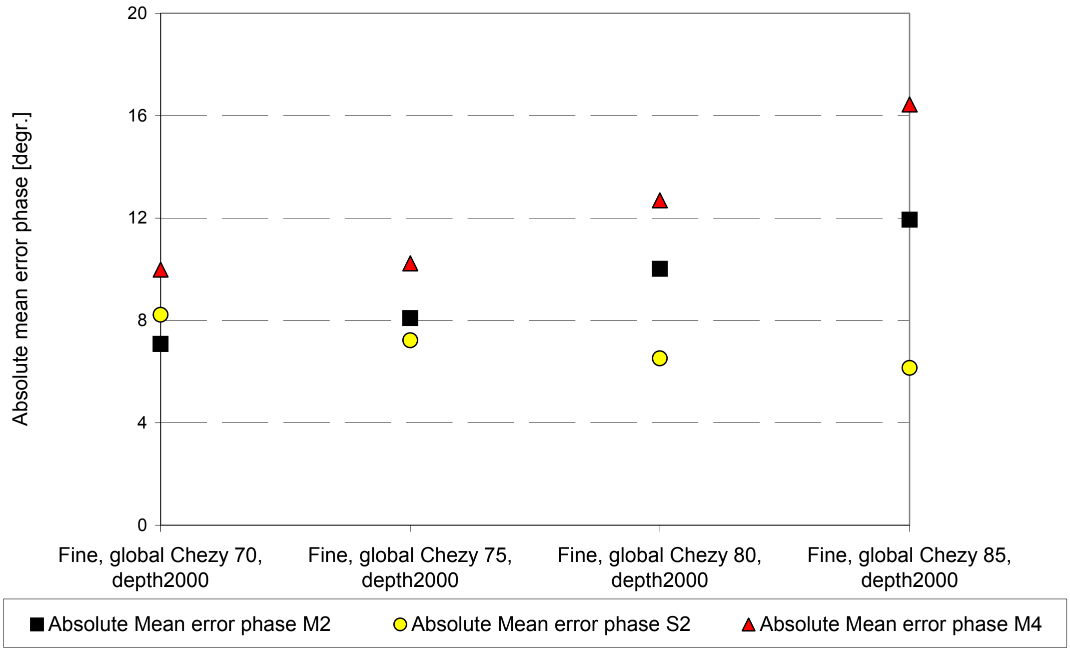

Figure G-18 Absolute mean error phase, fine model, total model area
Source: Tidal analysis in 12 water level stations in Humber estuary compared with several D3D runs.

For the total area, the amplitudes are best represented by a global Chezy of 70, the phases by a global Chezy value of 80.

G.7 Conclusion calibration global roughness coarse and fine model

In the above described comparison the errors of the runs with a global Chezy of 70 and 75 lie near each other. See Table G-1 for the values plotted above. The mean absolute relative error and the absolute error phase are within acceptable error-range for both Roughness values.

Table G-1 Mean error in tidal constituents M2, S2 and M4.

D3D-model:	Coarse,	Coarse,	Fine,	Fine,
Roughness:	Chezy70	Chezy75	Chezy70	Chezy75
Mean absolute relative error in amplitude M2	3%	2%	5%	4%
Mean absolute relative error in amplitude S2	5%	8%	7%	8%
Mean absolute error amplitude M2	0.073 m	0,043 m	0,107 m	0.081 m
Mean absolute error amplitude S2	0.035 m	0,054 m	0,044 m	0.054 m
Mean absolute error amplitude M4	0.033 m	0,029m	0,021 m	0.016 m
Mean absolute error phase M2	9°	10°	11°	12°
Mean absolute error phase S2	7°	5°	6°	6°
Mean absolute error phase M4	20°	22°	13°	14°

Source: Mean relative absolute error amplitude, mean(|Hc-Ho|)/Ho). With: Hc(/o): computed (/observed) amplitude.

Since the M4 is only a centimetre at Spurn Head a relative mean error in amplitude would not give useful information on the accuracy of the model, for this reason this value is not produced.

Conclusion
With the focus on the inner estuary a global Chezy of 70 has been chosen for the coarse model. Amplitudes and phases show acceptable results in the inner estuary as well as in the total area. A global Chezy of 75 has been chosen for the fine model, the output shows acceptable results in the both area as well.

H Relative phases

The relative phase difference between U_{M2} and U_{M4} can be calculated from the harmonic analysis as follows:

$$U_{M2} = a\cos(\omega t) + b\sin(\omega t) = \sqrt{a^2+b^2}\cos(\omega t - \varphi_{M2}) =$$
$$U_{M2} = \hat{U}_{M2}\cos(\omega t - \varphi_{M2}), \tag{H.1}$$
$$\varphi_{M2} = \arctan(\frac{b}{a})$$

$$U_{M4} = c\cos(2\omega t) + d\sin(2\omega t) = \sqrt{c^2+d^2}\cos(2\omega t - \varphi_{M4}) =$$
$$U_{M4} = \hat{U}_{M4}\cos(2\omega t - \varphi_{M4}), \tag{H.2}$$
$$\varphi_{M4} = \arctan(\frac{d}{c})$$

The relative phase difference between M4 and M2 is calculated with respect to the time of maximum positive M2 amplitude. Time (t') where UM2 reaches its maximum:

$$\frac{\delta U_{M2}}{\delta t} = -\omega \hat{U}_{M2}\sin(\omega t' - j_{M2}) = 0 + k2\pi, k=0,1,2,.$$
$$t' = \frac{j_{M2}}{\omega} + \frac{k2\pi}{\omega} \tag{H.3}$$

Minimum phase lag of U_{M4} maximum to U_{M2} maximum amplitude (k =0):

$$U_{M4}(t_{M2\max} = \frac{\varphi_{M2}}{\omega}) = \hat{U}_{M4}\cos(2\omega t - \varphi_{M4}) = \hat{U}_{M4}\cos(2\varphi_{M2} - \varphi_{M4}) \tag{H.4}$$

From now on the sum of UM2 and UM4 can be written as follows:

$$t = t'' + t' = t'' + \frac{\varphi_{M2}}{\omega},$$
$$U_{M2\&M4}(t) = \hat{U}_{M2}\cos(\omega t'') + \hat{U}_{M4}\cos(2\omega t'' - (\varphi_{M4} - 2\varphi_{M2})), \tag{H.5}$$
$$\Delta\varphi_{(M2\&M4)} = (\varphi_{M4} - 2\varphi_{M2})$$

The relative phase difference of UM4 is defined as derived in equation H.5. A similar calculation can be made for any combination of tidal constituents. In the further analysis relative phase differences of the constituents are all relatively to the M2 constituent and flow velocity is defined as positive when the direction is up-estuary.

I Tidal asymmetry

I.1 Astronomical component analysis M_2 and M_4

In this appendix the plots of the tidal analysis (as described in section 6.1) are given for runs TA01A to TA01I, see plots Figure I-1 to Figure I-9.

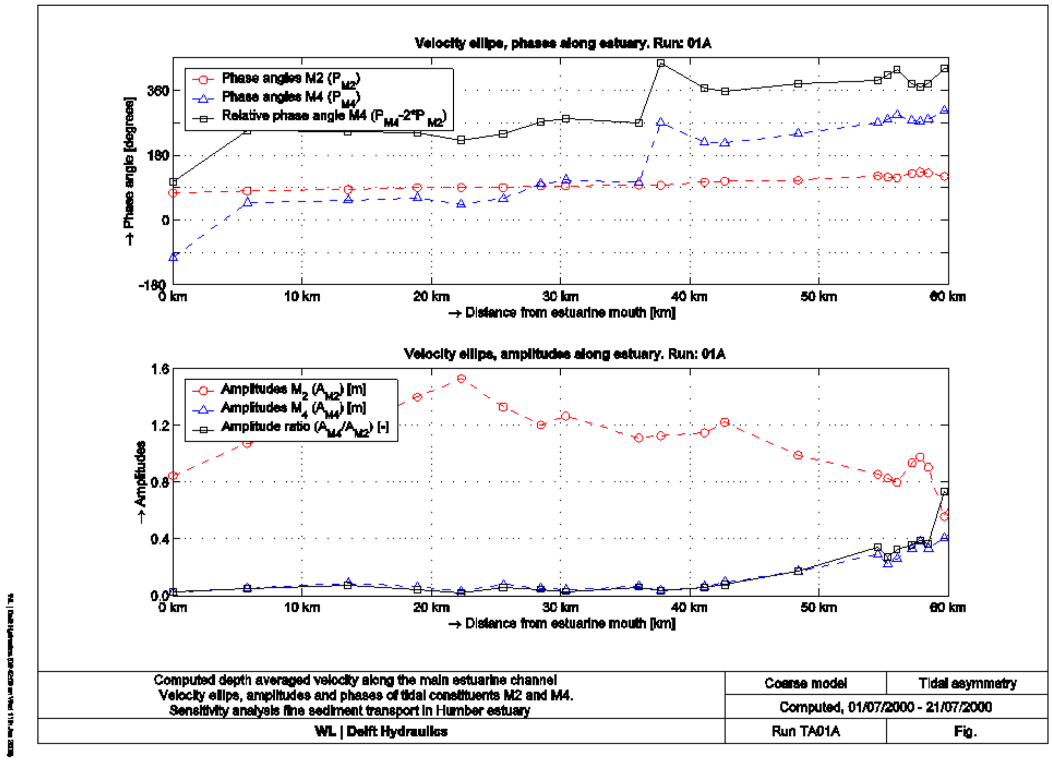

Figure I-1 Tidal asymmetry analysis run TA01A

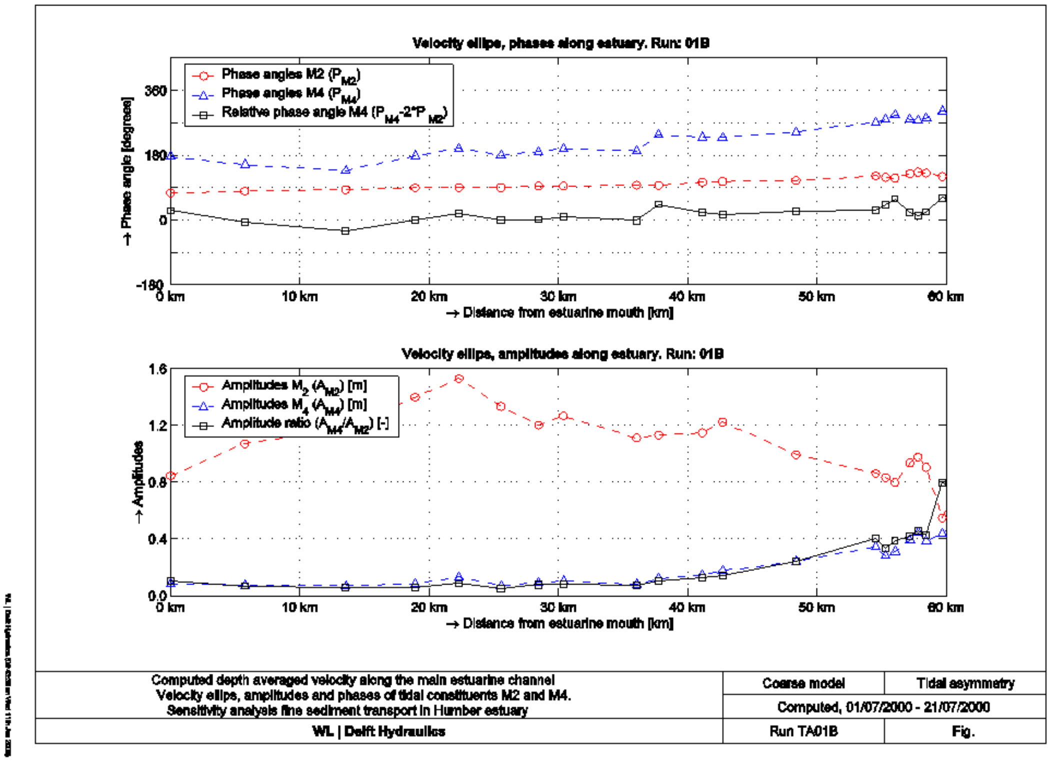

Figure I-2 Tidal asymmetry analysis run TA01B

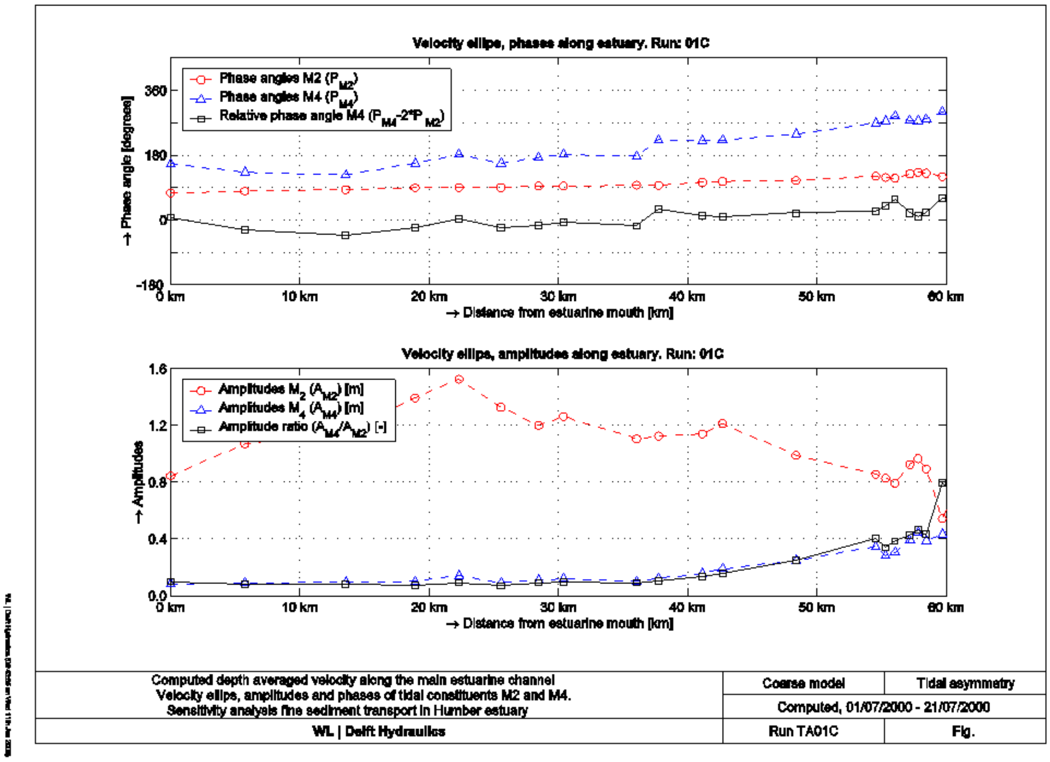

Figure I-3 Tidal asymmetry analysis run TA01C

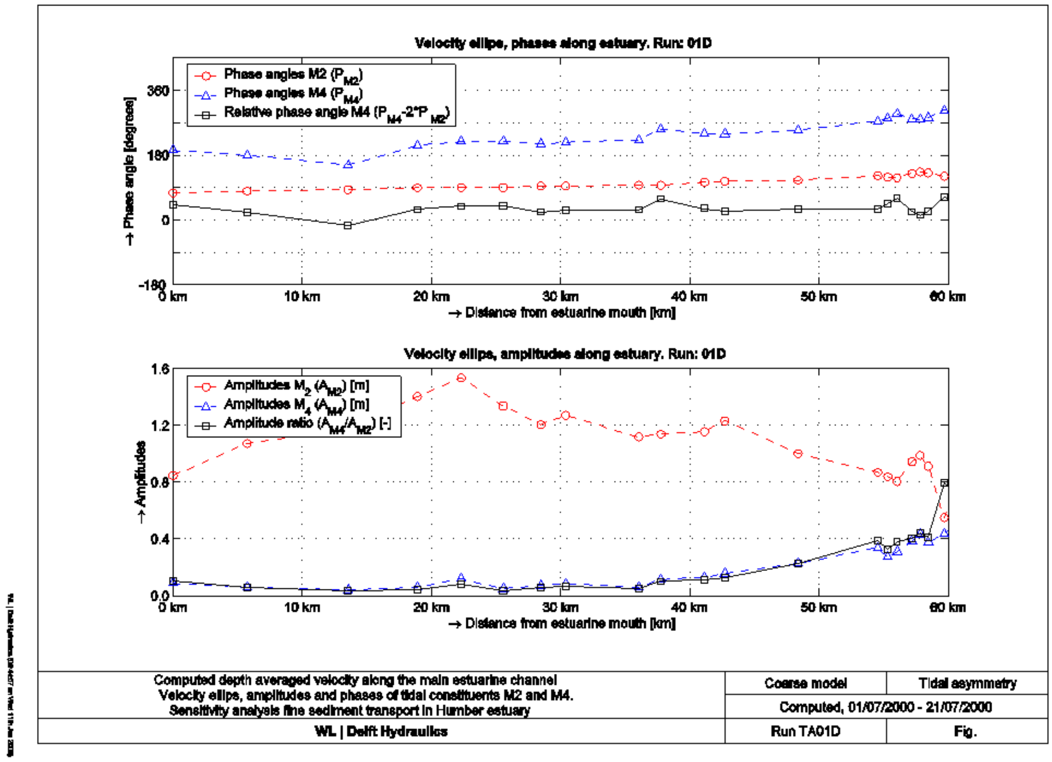

Figure I-4 Tidal asymmetry analysis run TA01D

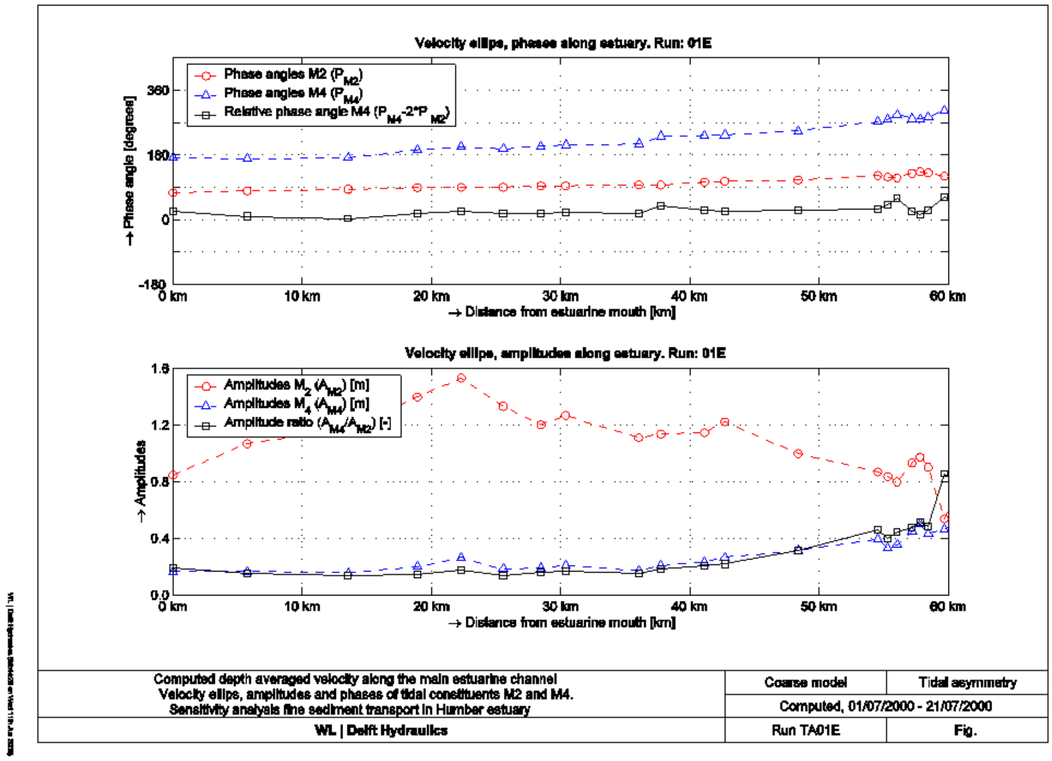

Figure I-5 Tidal asymmetry analysis run TA01E

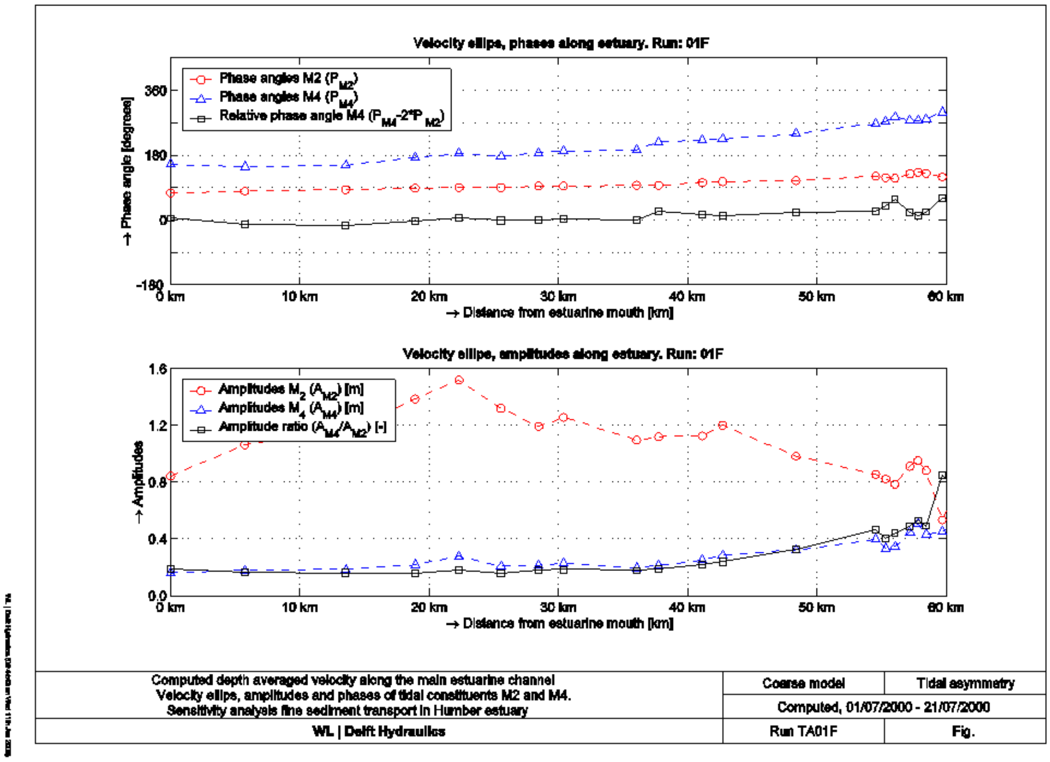

Figure I- 6 Tidal asymmetry analysis run TA01F

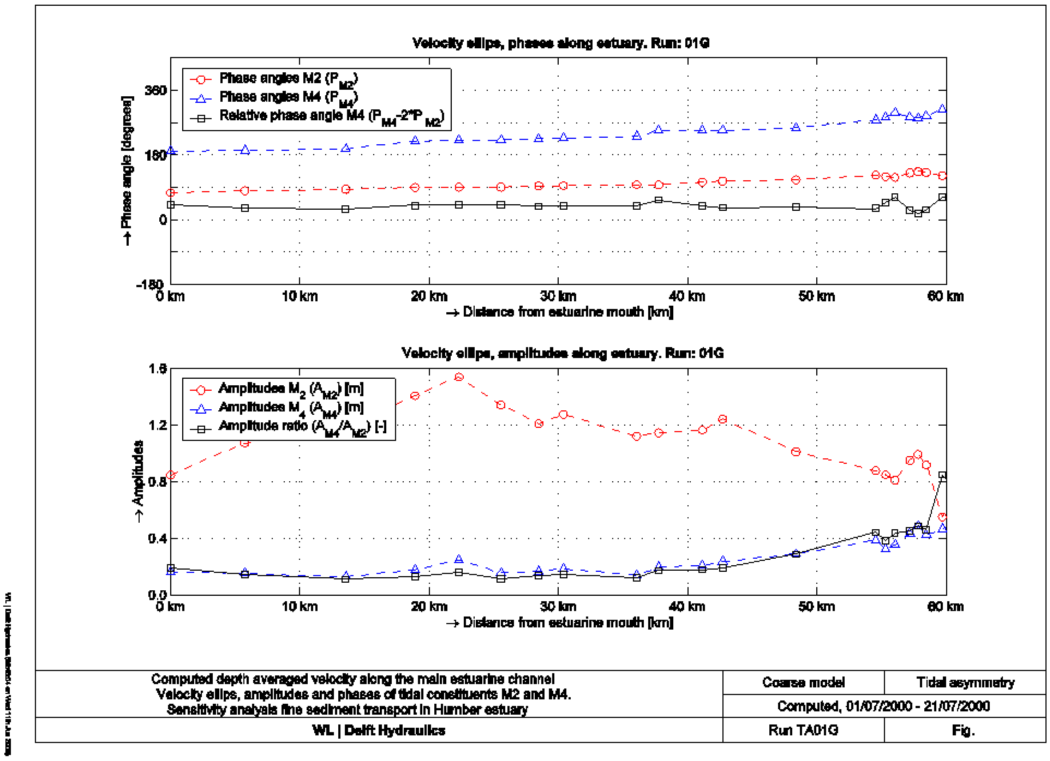

Figure I-7 Tidal asymmetry analysis run TA01G

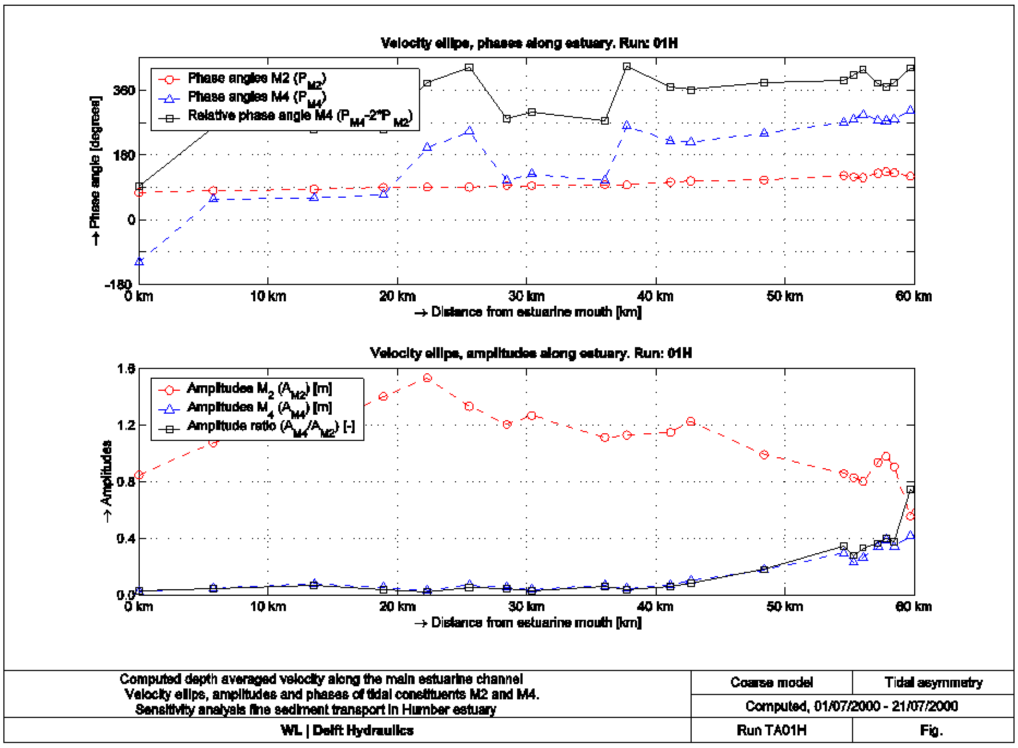

Figure I-8 Tidal asymmetry analysis run TA01H

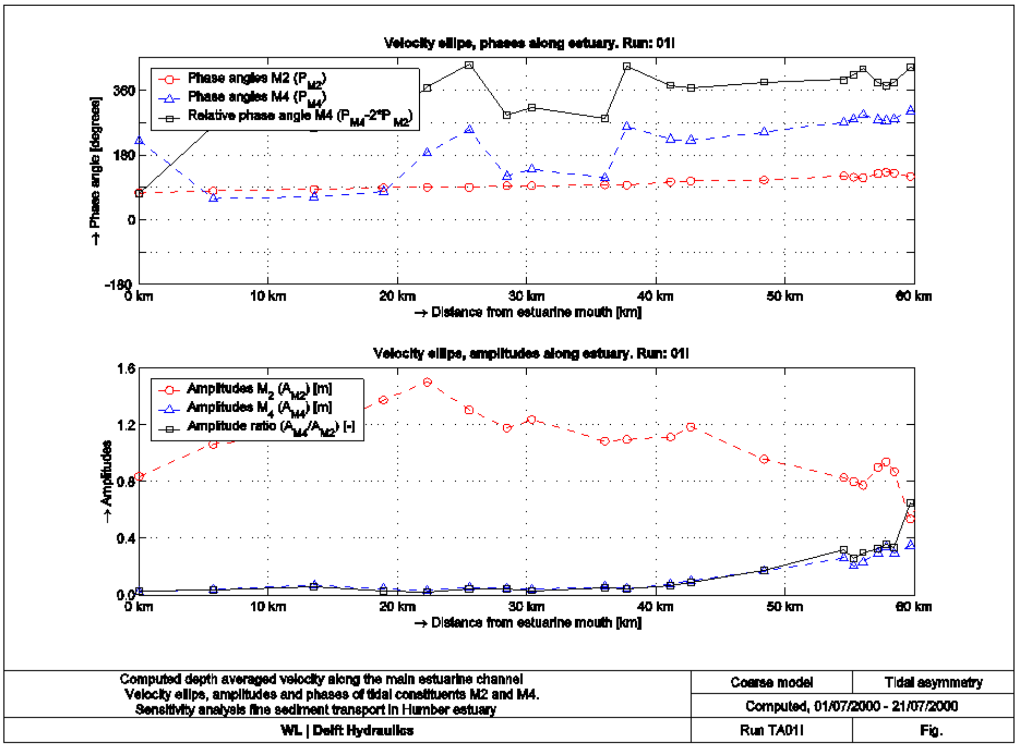

Figure I-9 Tidal asymmetry analysis run TA01I

I.2 Slack water period analysis

In the Figure I-10 to Figure I-12 the spring neap average slack water periods and the slack period ratio HWS / LWS are given as derived from the 2Dh runs TA01A to TA01I. For run TA01I that will be used in the sensitivity analysis, a snap shot (a period of 25hrs intead of 14.7 days) of the calculation of the HWS and LWS is given in Figure I-13 to Figure I-33.

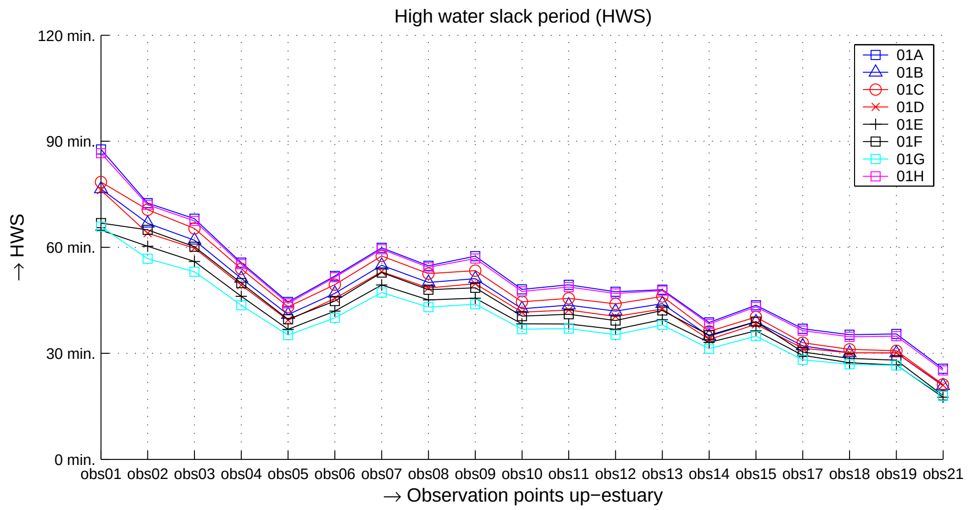

Figure I-10 Spring neap average high water slack

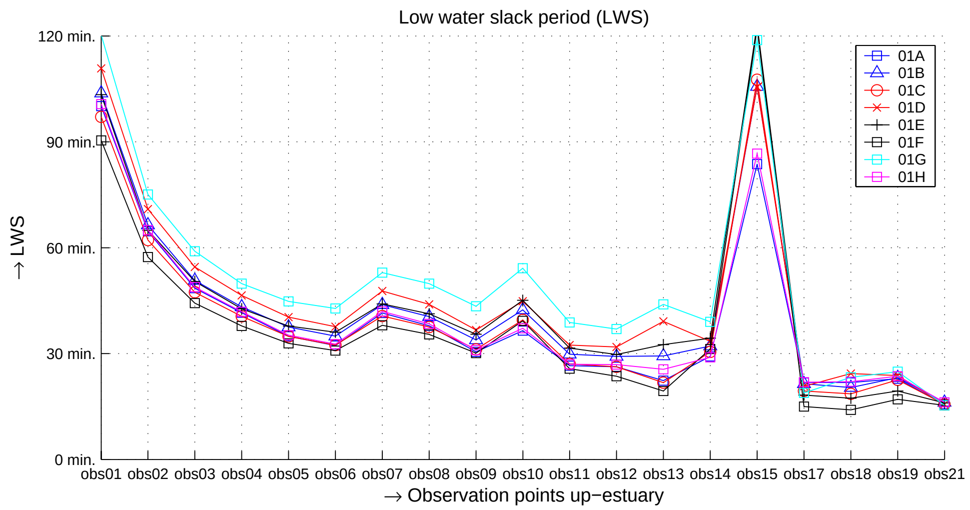

Figure I-11 Spring neap average low water slack

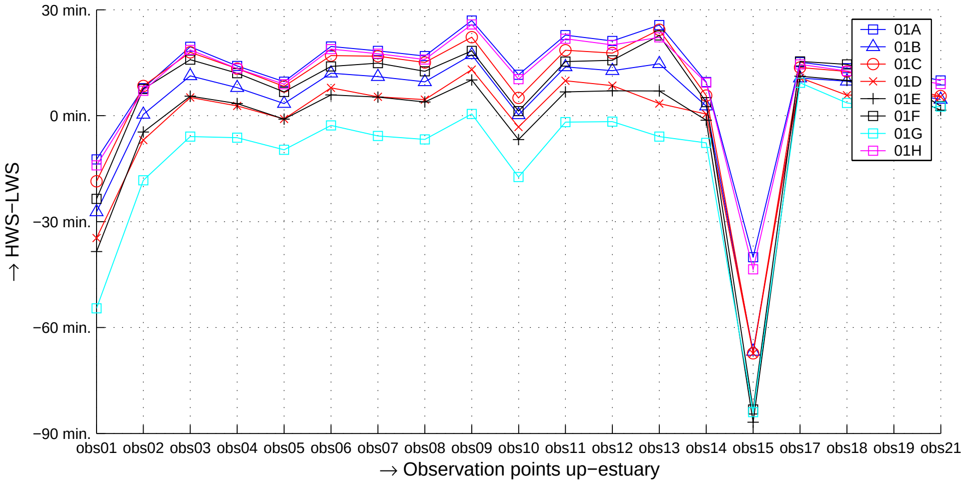

Figure I-12 Slack water period asymmetry along estuarine channel (ΔWS = HWS-LWS)

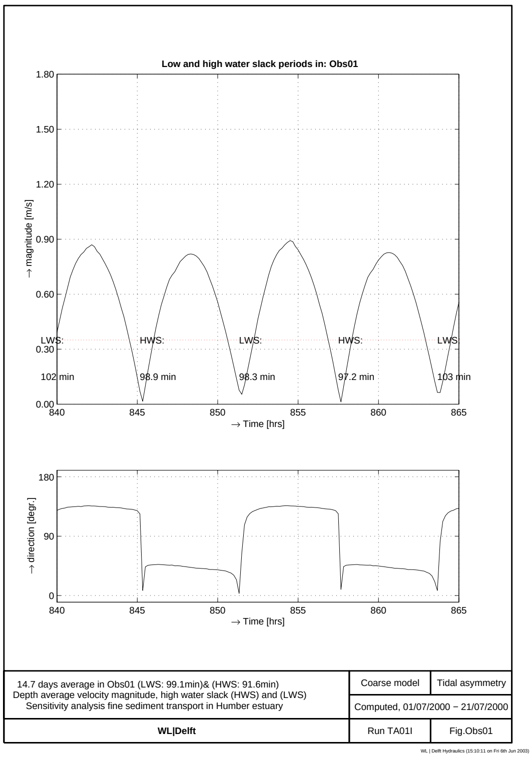

Figure I-13 Velocity magnitude TA01I, obs01

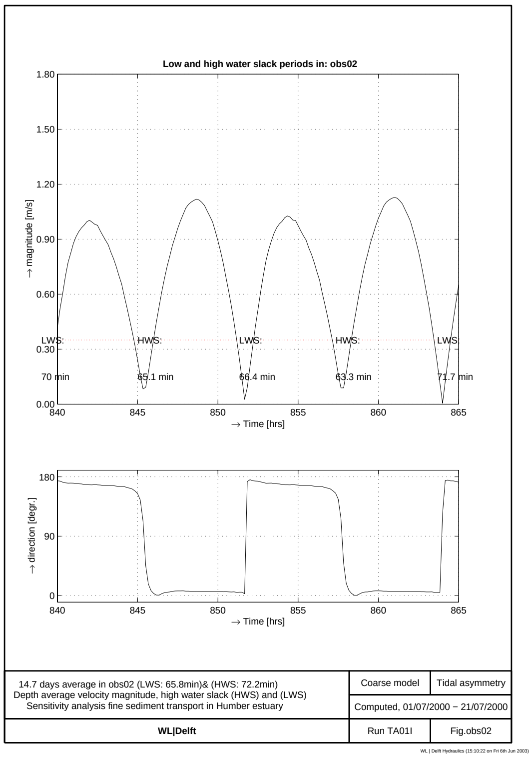

Figure I-14 Velocity magnitude TA01I, obs02

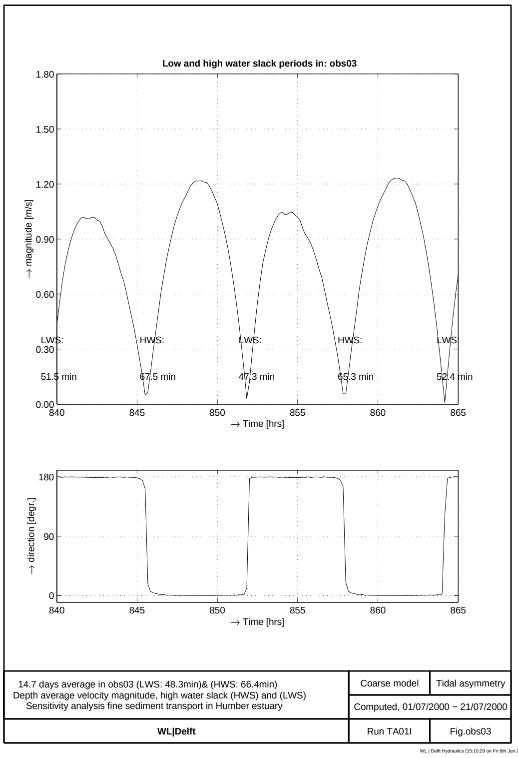

Figure I-15 Velocity magnitude TA01I, obs03

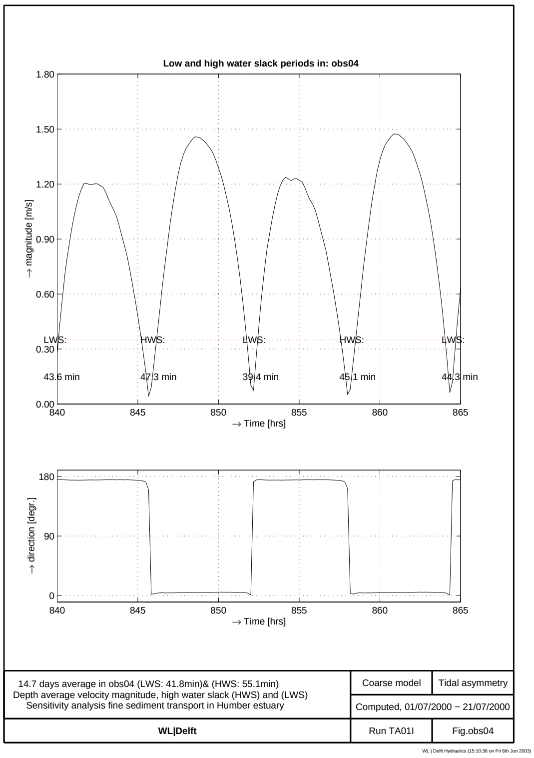

Figure I-16 Velocity magnitude TA01I, obs04

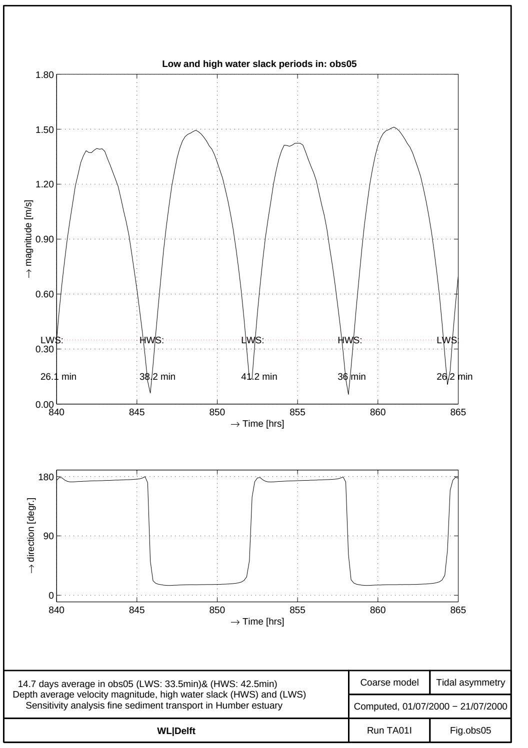

Figure I-17 Velocity magnitude TA01I, obs05

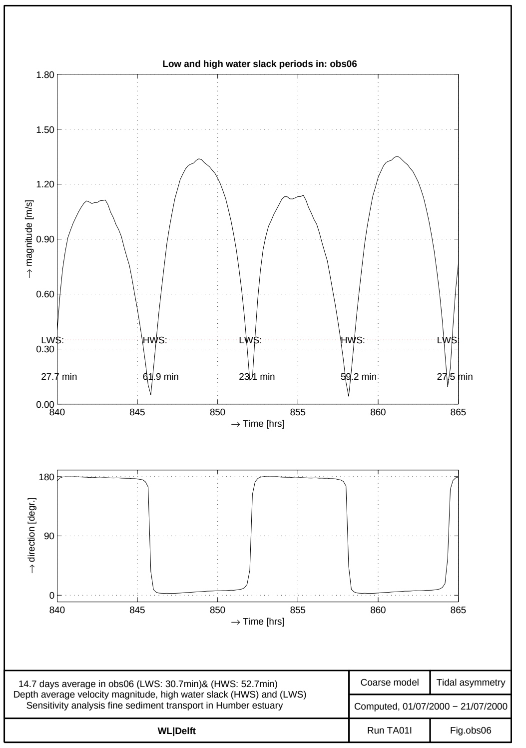

Figure I-18 Velocity magnitude TA01I, obs06

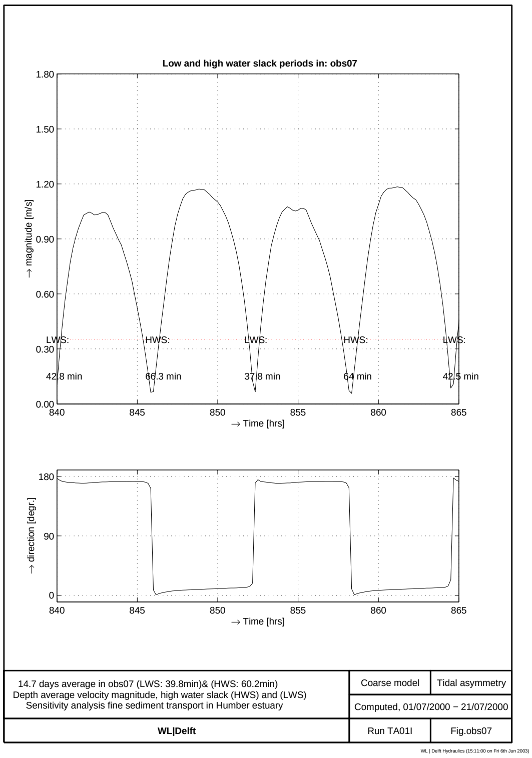

Figure I-19 Velocity magnitude TA01I, obs07

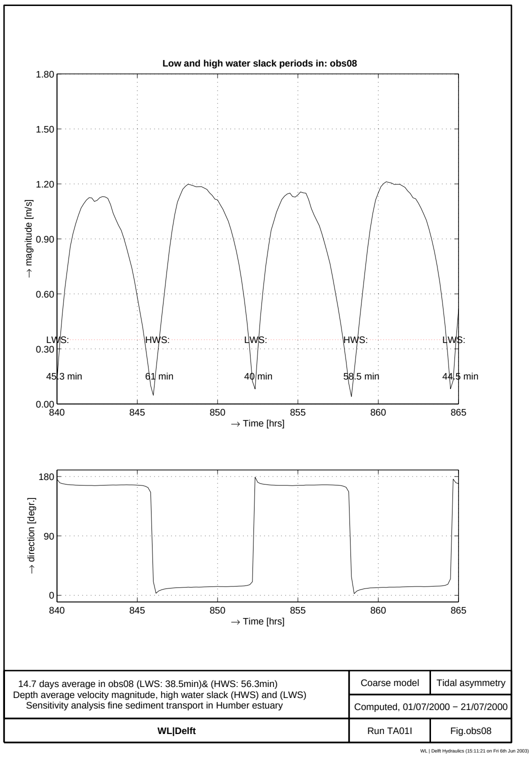

Figure I-20 Velocity magnitude TA01I, obs08

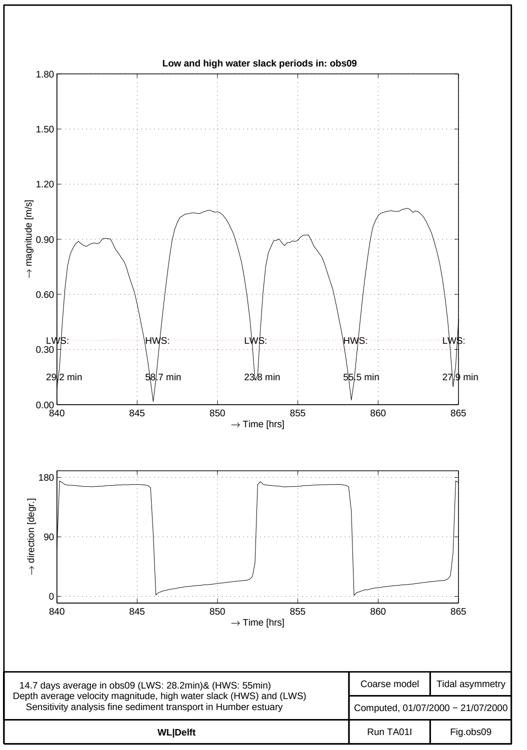

Figure I-21 Velocity magnitude TA01I, obs09

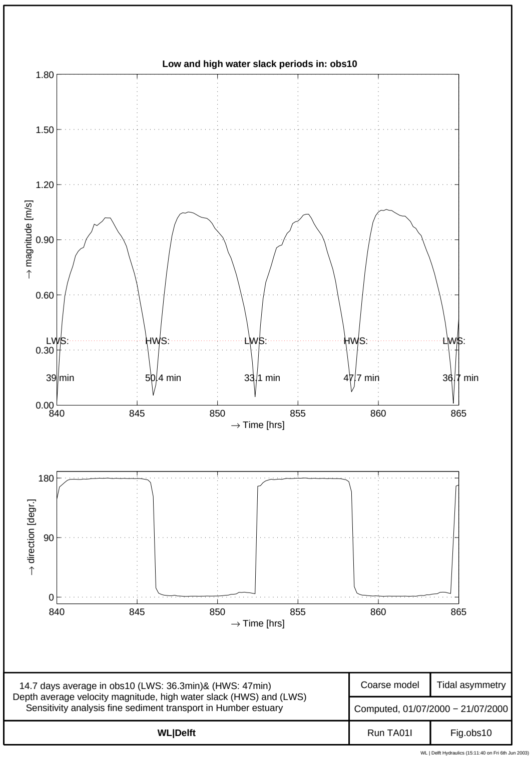

Figure I-22 Velocity magnitude TA01I, obs10

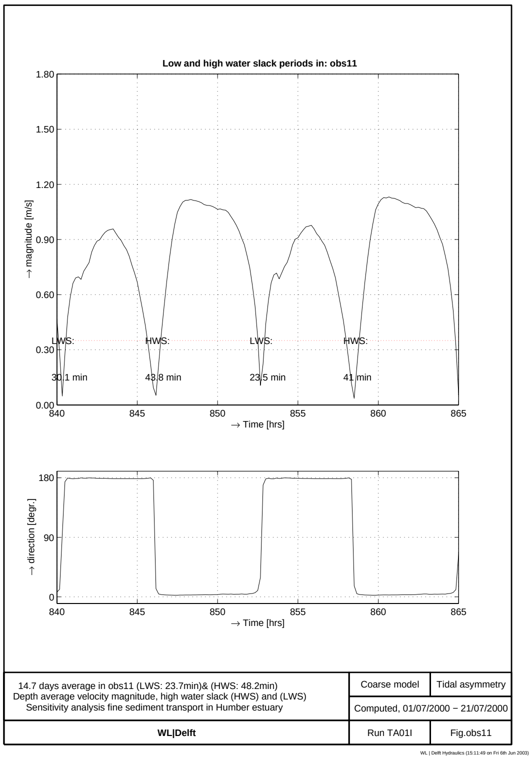

Figure I-23 Velocity magnitude TA01I, obs11

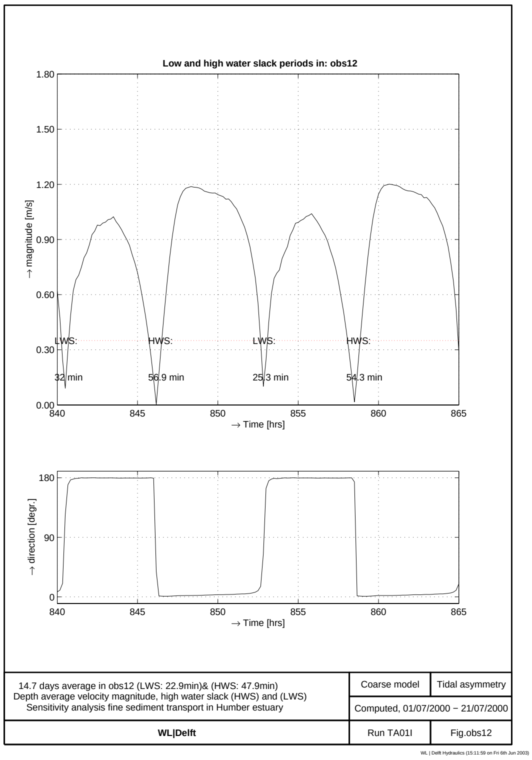

Figure I-24 Velocity magnitude TA01I, obs12

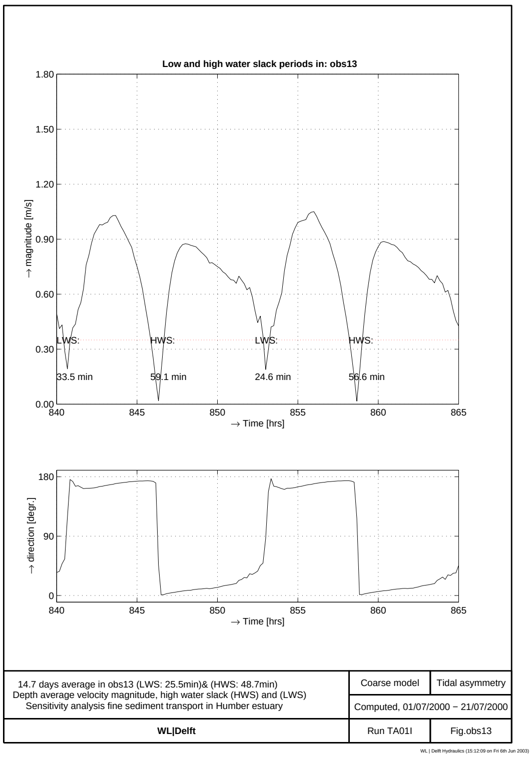

Figure I-25 Velocity magnitude TA01I, obs13

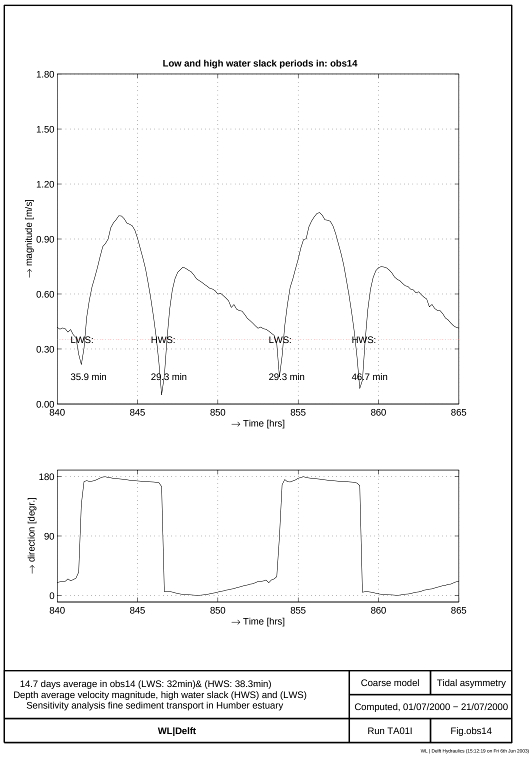

Figure I-26 Velocity magnitude TA01I, obs14

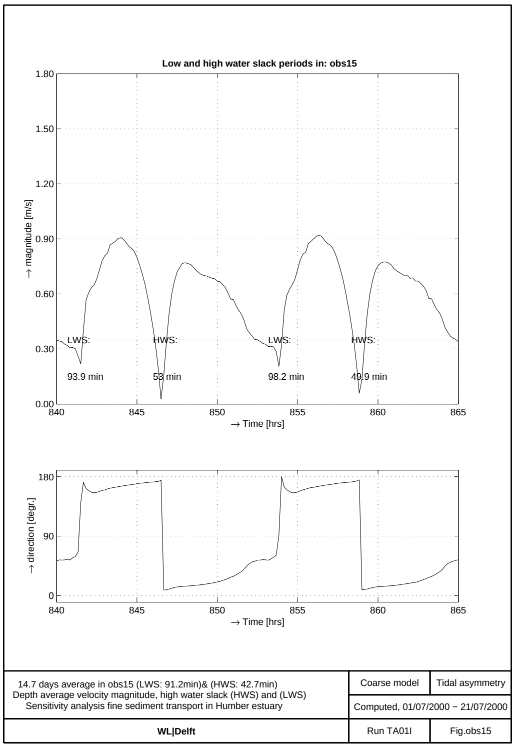

Figure I-27 Velocity magnitude TA01I, obs15

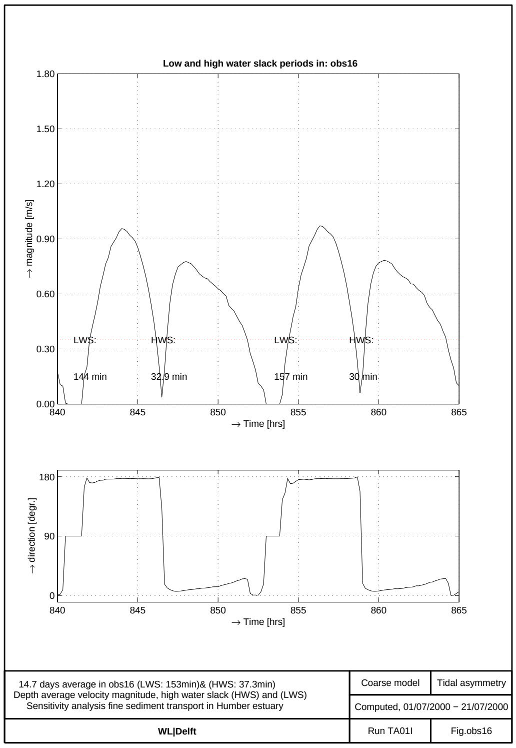

Figure I-28 Velocity magnitude TA01I, obs16

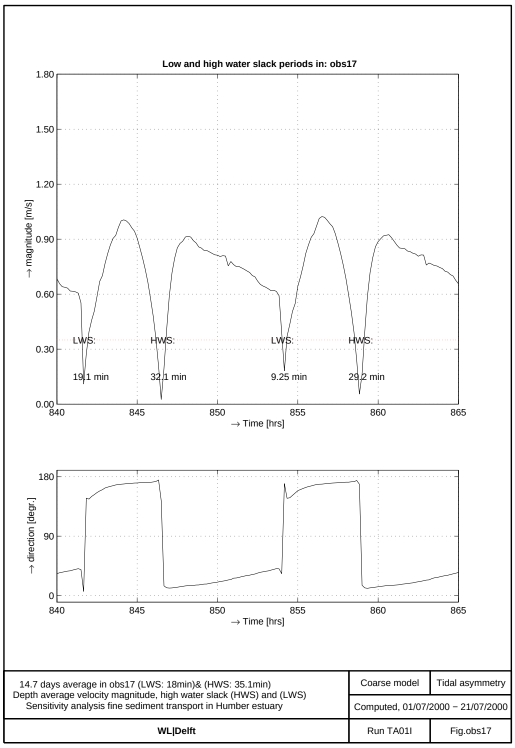

Figure I-29 Velocity magnitude TA01I, obs17

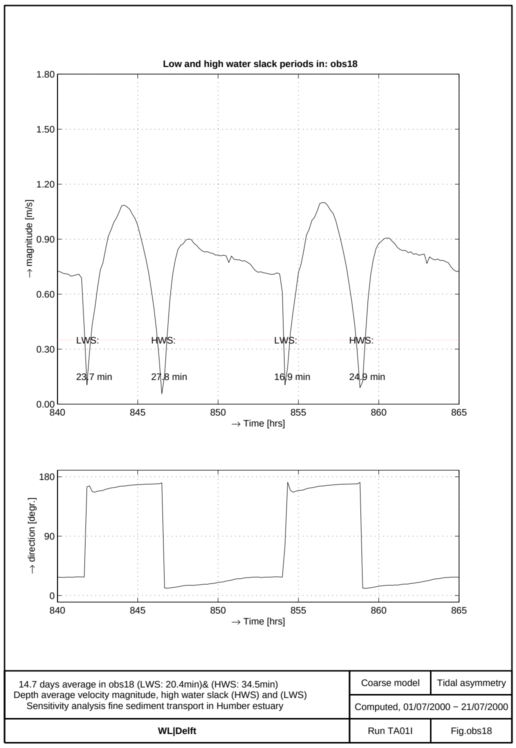

Figure I-30 Velocity magnitude TA01I, obs18

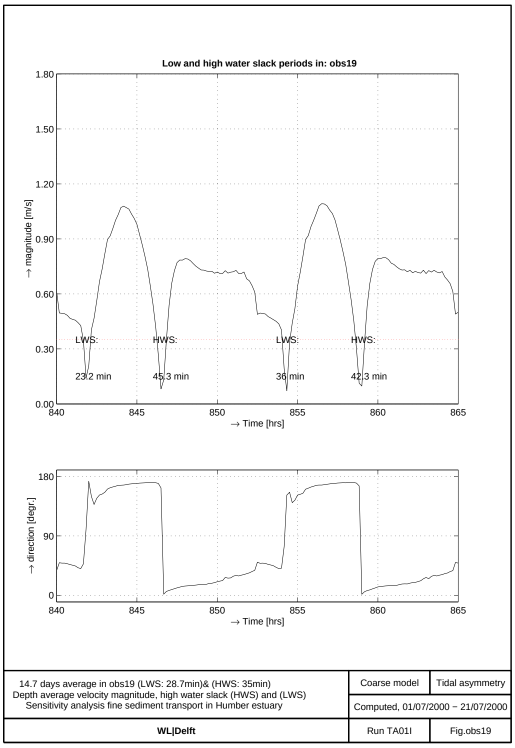

Figure I-31 Velocity magnitude TA01I, obs19

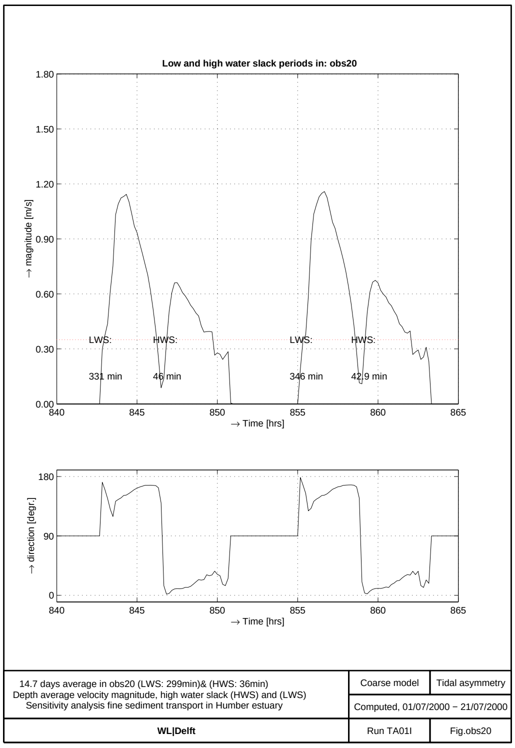

Figure I-32 Velocity magnitude TA01I, obs20

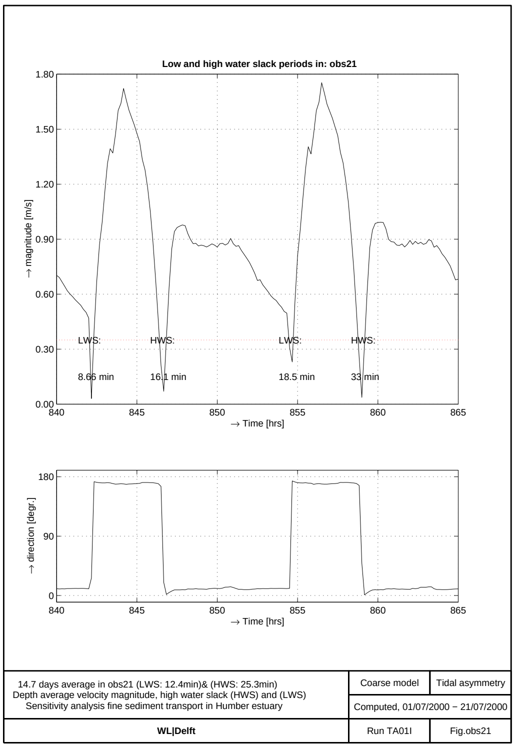

Figure I-33 Velocity magnitude TA01I, obs21

Slack water period phase-sensitivity

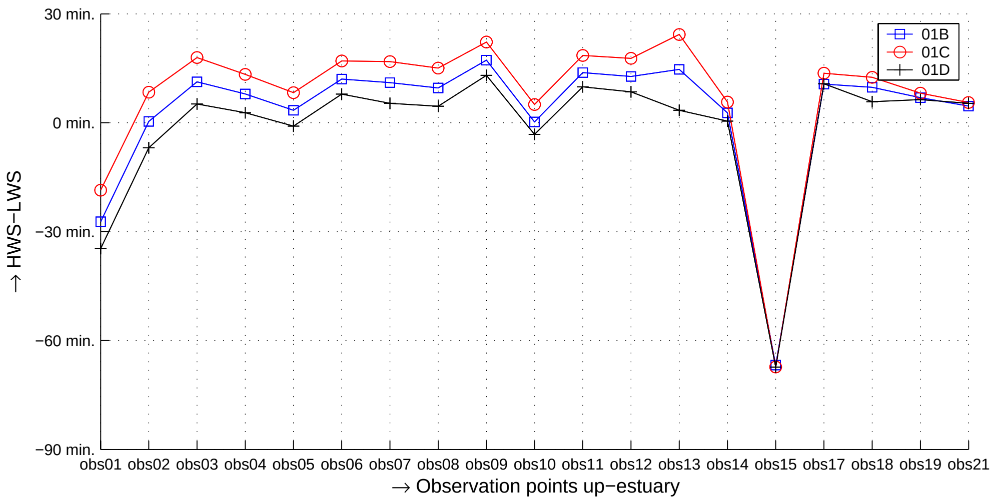

Figure I-34 Slack water asymmetry simulations TA01A, B, E and H
Explanation: TA01B(0°, 5%), TA01C(-20°, 5%), TA01D(+20°, 5%).

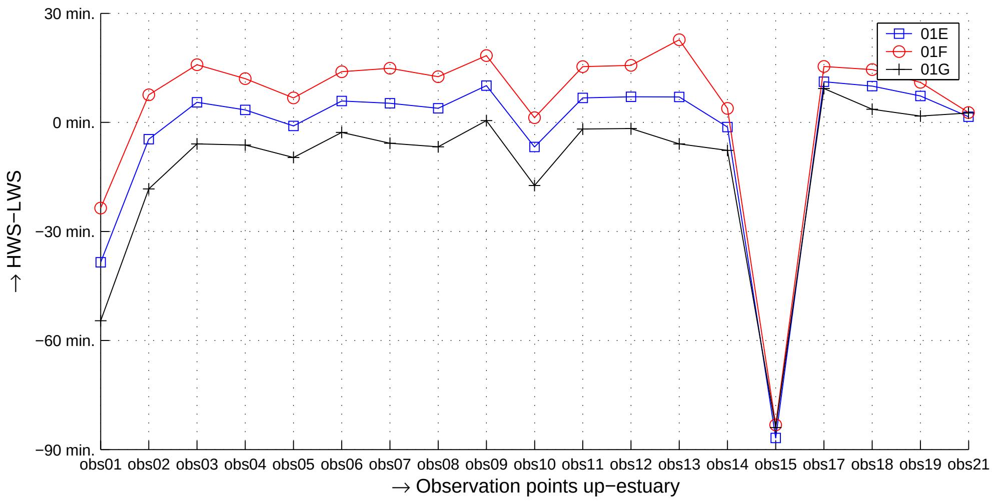

Figure I-35 Slack water asymmetry simulations TA01A, B, E and H
Explanation: TA01E(0°, 10%), TA01F(-20°, 10%), TA01G(+20°, 10%).

Slack water period amplitude-sensitivity

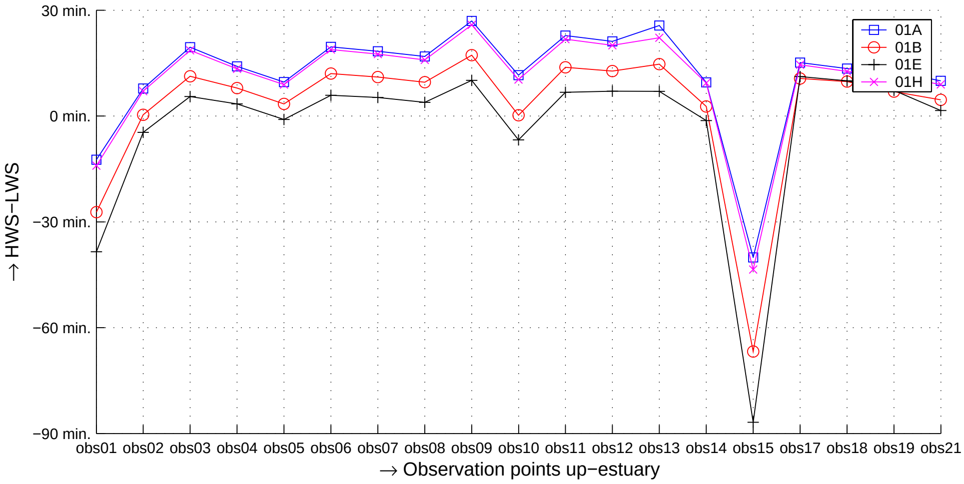

Figure I-36 Slack water asymmetry simulations TA01A, B, E and H
Explanation: TA01A(-°, -%), TA01B(0°, 5%), TA01E(0°, 10%) & TA01H(0°, 1 cm).

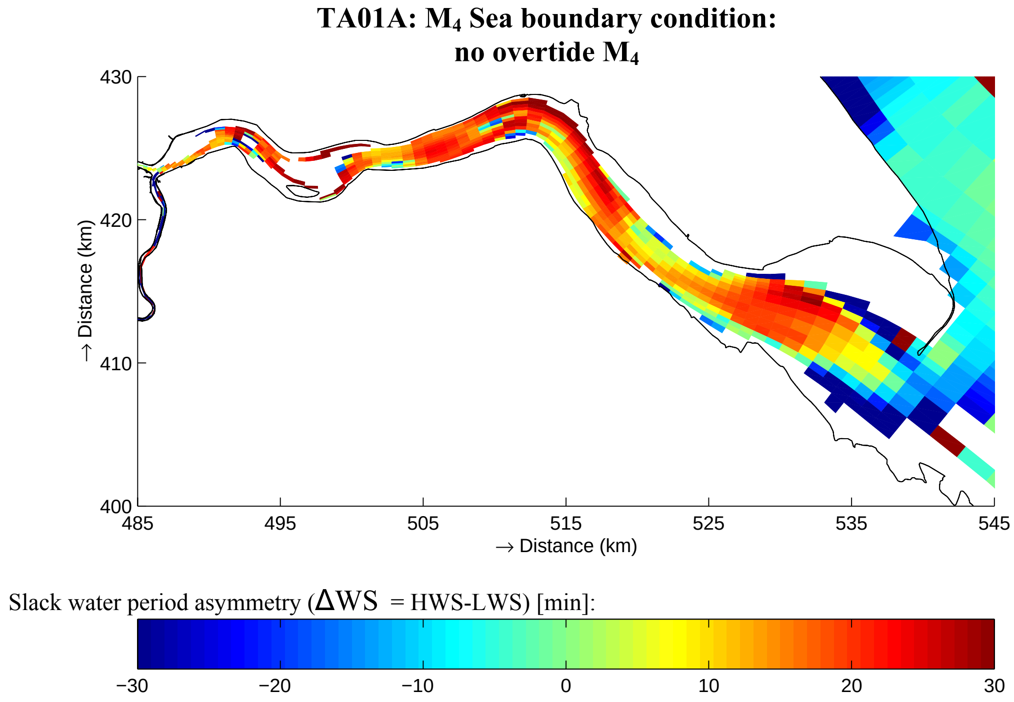

Figure I-37 Slack water period asymmetry of reference simulation TA01B.

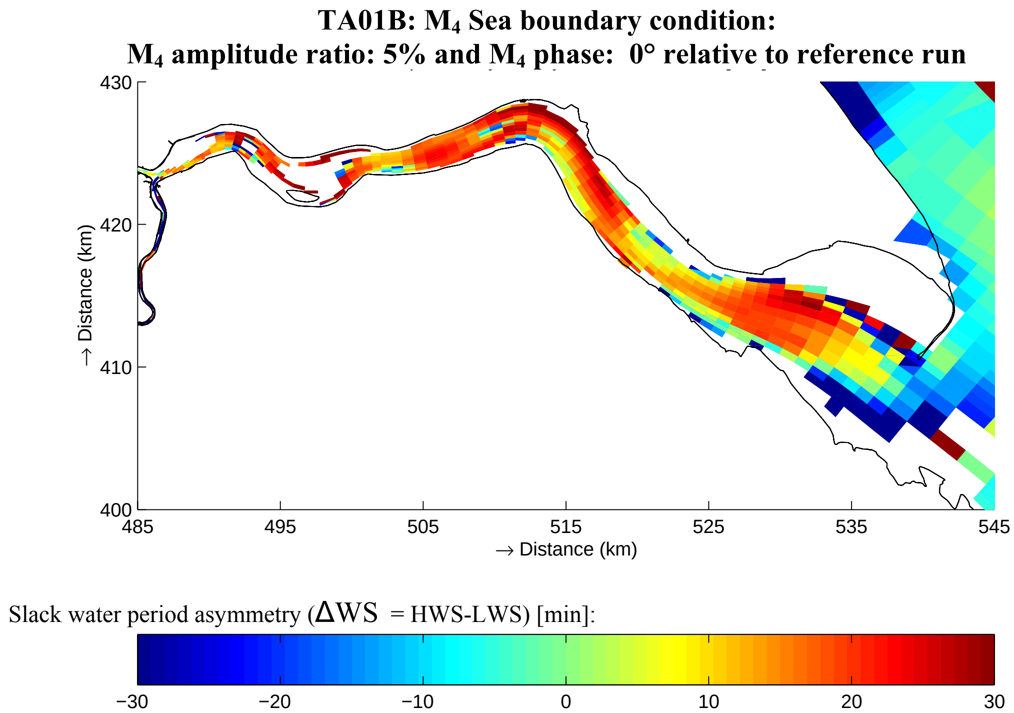

Figure I-38 Slack water period asymmetry of reference simulation TA01B.

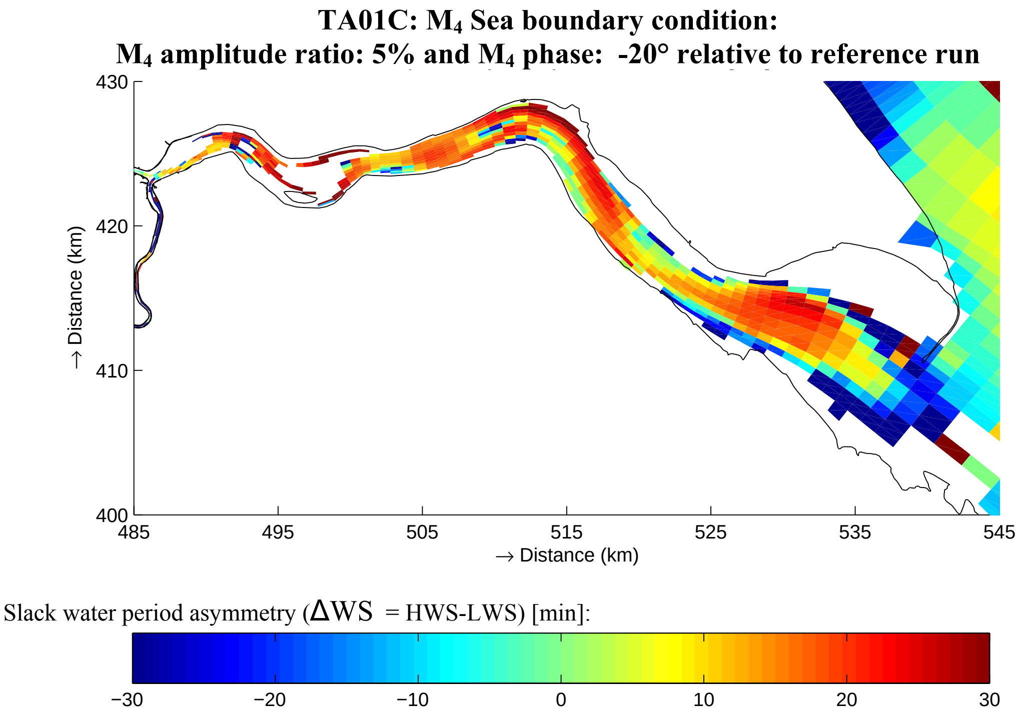

Figure I-39 Slack water period asymmetry of reference simulation TA01B.

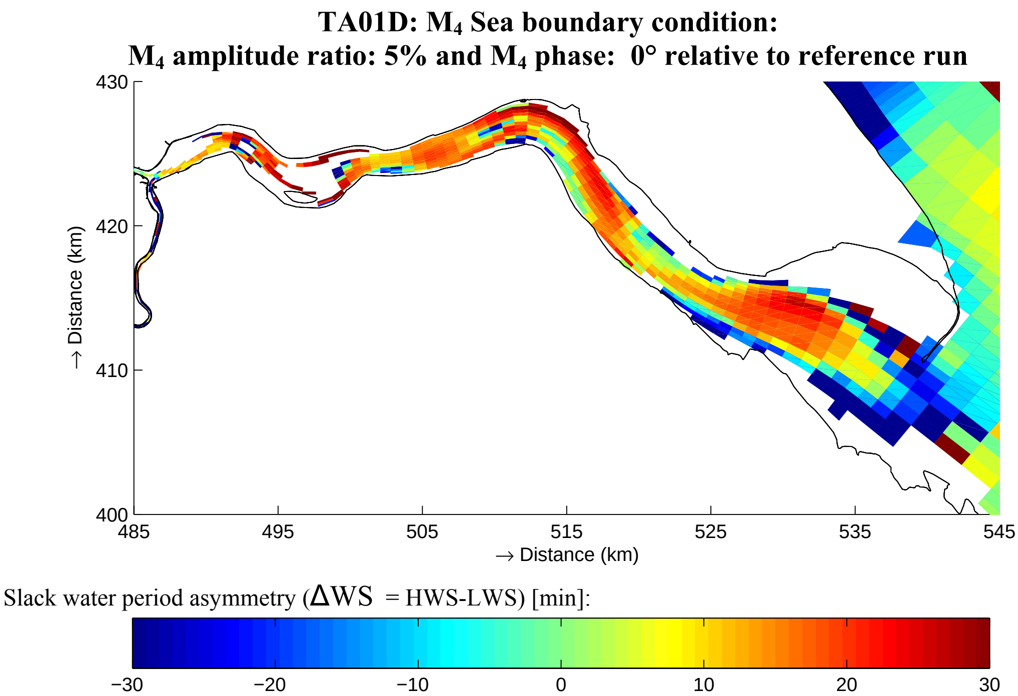

Figure I-40 Slack water period asymmetry of reference simulation TA01B.

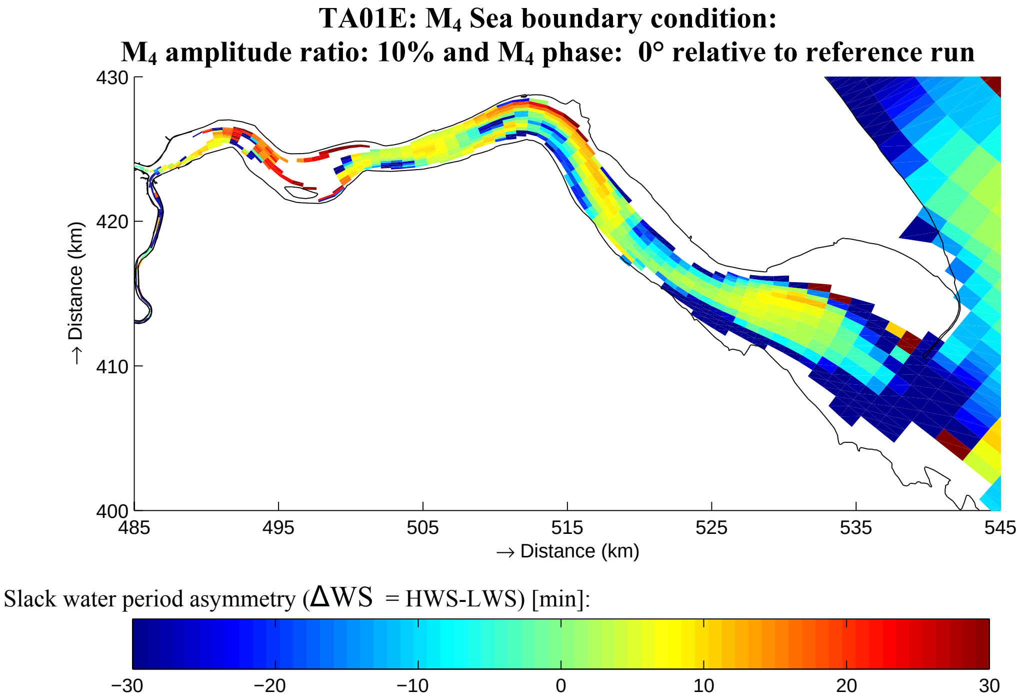

Figure I-41 Slack water period asymmetry of reference simulation TA01B.

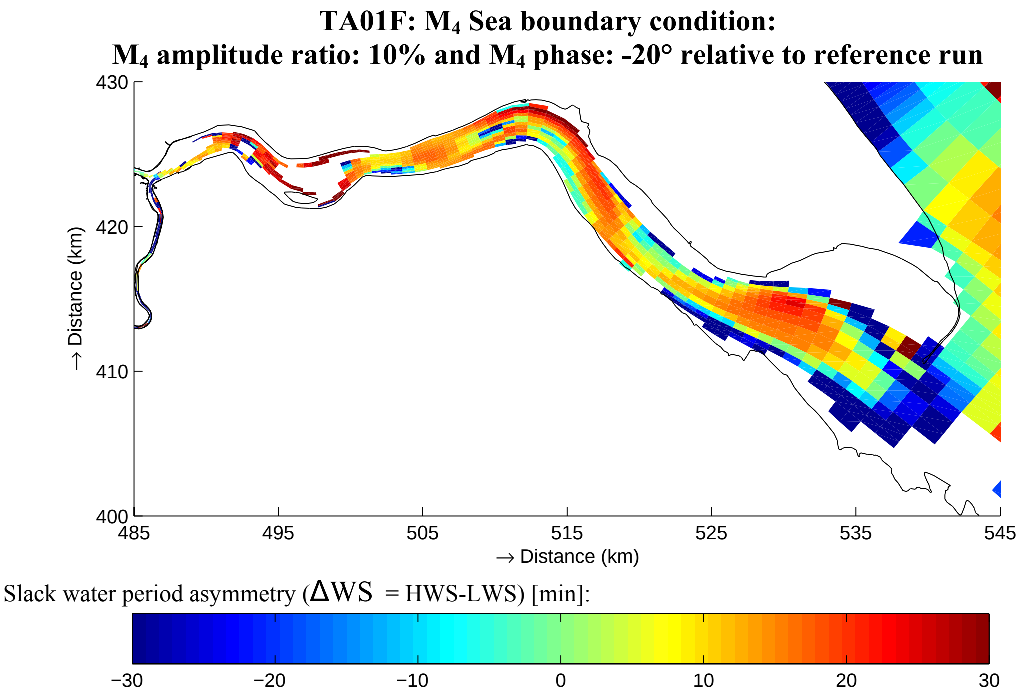

Figure I-42 Slack water period asymmetry of reference simulation TA01B.

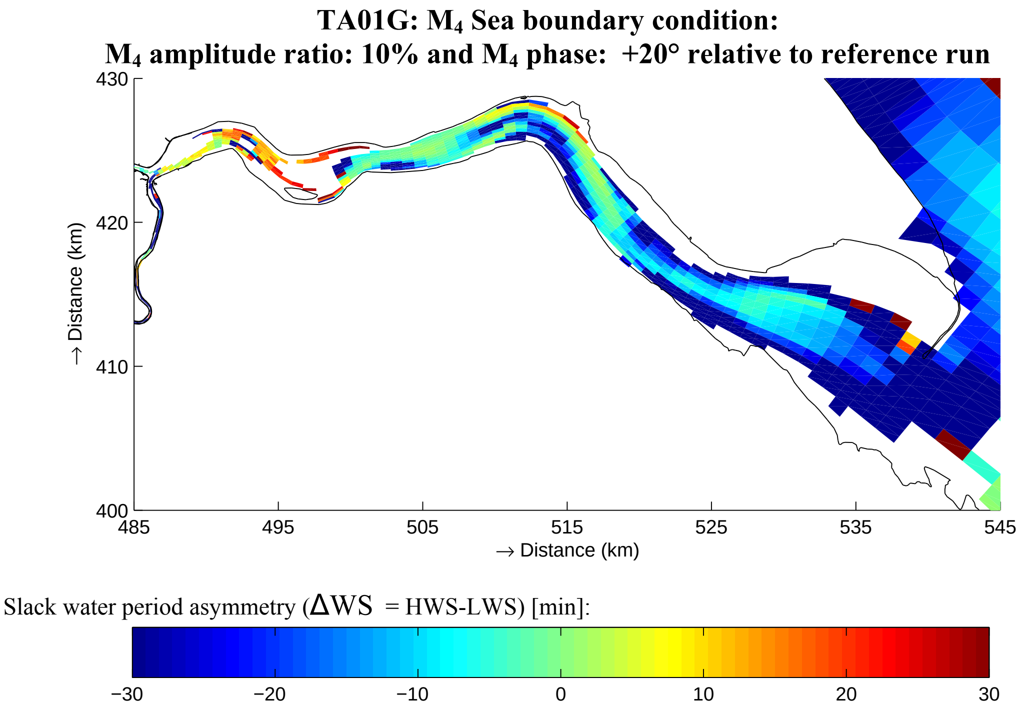

Figure I-43 Slack water period asymmetry of reference simulation TA01B.

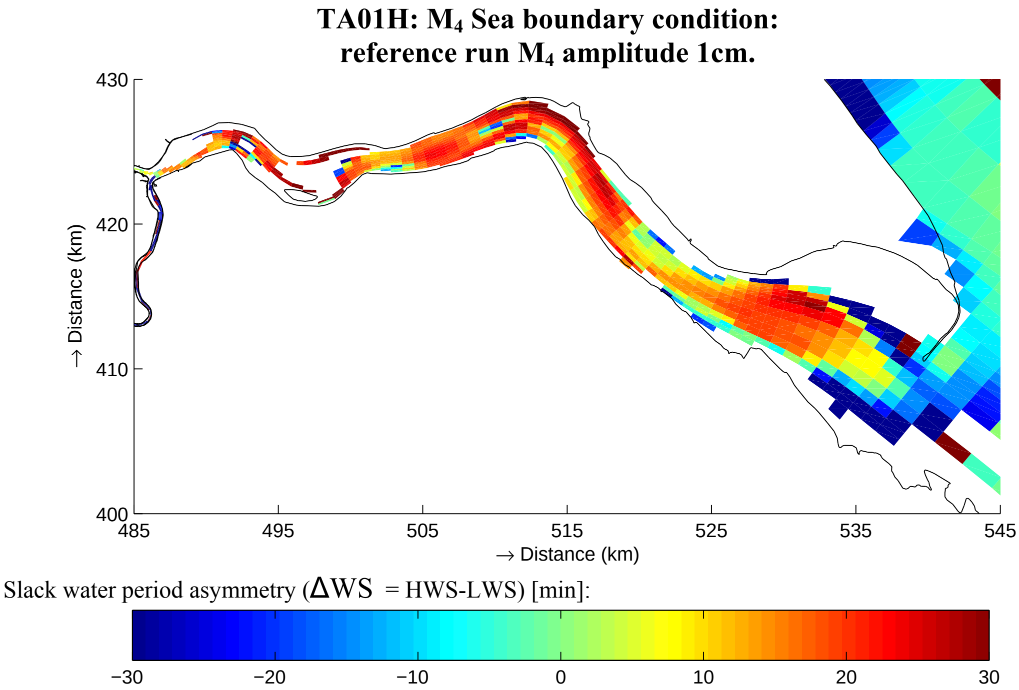

Figure I-44 Slack water period asymmetry of reference simulation TA01B.

J Gravitational Circulation

J.1 Gross discharge and transport

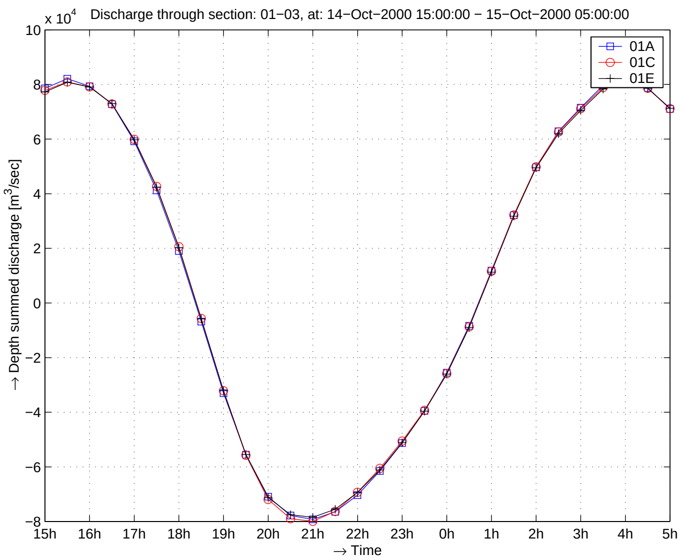

Figure J-1 2Dh and 3D gross discharge comparison in cross section 01 -> 03.

Gross transport of fine sediments

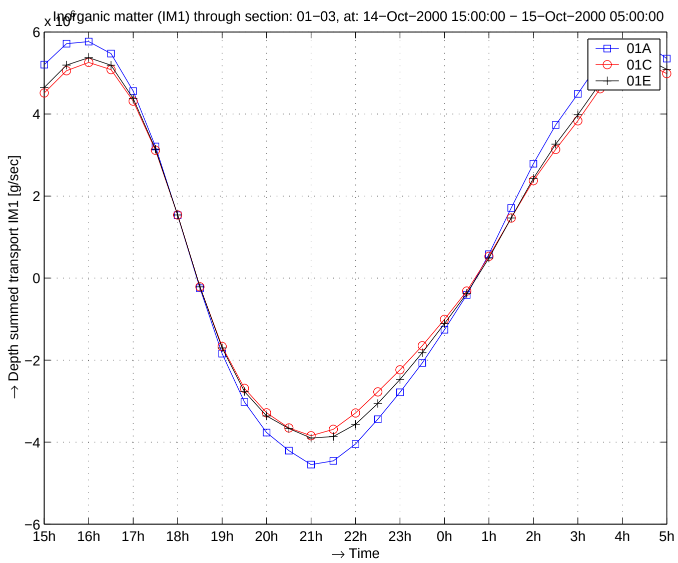

Figure J-2 Gross transport comparison in cross section 01 -> 03.

Explanation: For an explanation of the WAQ runs see Appendix A.

J.2 Experiment 2D and 3D transport

Experiment I

Suppose that the depth averaged concentration is equal in both the 2D as the 3D run. In formula:

$$\overline{c_{2D}} = \overline{c_{3D}} \tag{J.1}$$

a. The concentration-depth-profile in 3D run will show a higher value near the bottom than the depth averaged value.

$$c_{2D\text{bottom}} (= \overline{c_{2D}}) < c_{3D\text{ bottom}} \tag{J.2}$$

b. The gross deposition flux is modelled by the product of the fall velocity and concentration near the bottom. In the 3D run the deposition term will be larger than 2D due to the difference in concentration near the bed.

$$\begin{gathered} D = w_s c_{\text{bottom}}, \\ D_{3D} > D_{2D} \end{gathered} \tag{J.3}$$

Experiment II

Suppose that the averaged concentration and the depth averaged velocity are both equal in the 2D and the 3D run.

$$\overline{c_{2D}} = \overline{c_{3D}} \;\&\; \overline{u_{2D}} = \overline{u_{3D}} \tag{J.4}$$

a. When sediment fluid interaction does not play a role and the flow does not contain complicated three dimensional structures, the vertical velocity profile can be described as a logarithmic distribution. See equation J.5.

$$\text{u(z)} \;;\; \frac{u_*}{\kappa} \log(\frac{\text{z}}{\text{z}_0}) \tag{J.5}$$

b. If furthermore, the erosion and deposition rates are much smaller than the horizontal transport and the Rouse number is small (the Rouse number is generally small in cohesive sediment suspensions).

$$\text{c(z)} \;;\; \bar{c} \cdot \frac{\sin(\pi\beta)}{\pi\beta} \left(\frac{\text{1-z/h}}{\text{z/h}} \right), \text{ for } \beta = \frac{\sigma_T W_s}{\kappa u_*} < 1 \tag{J.6}$$

Note that the vertical concentration profile starts to deviate from equation when the deposition and erosion terms become relatively large.

Gross transport of matter is computed by the product of concentration and discharge. In the 3D run the depth averaged gross transport term will be smaller then the 2D due to the combination of developments of concentrations and velocity. This conclusion can be explained by extracting the depth averaged values from concentration and velocity (see the mathematical foundation).

For convenience we write the velocity and concentration as follows:

$$\begin{aligned} u(z) &= \bar{u} + u'(z) \\ c(z) &= \bar{c} + c'(z) \end{aligned} \tag{J.7}$$

Gross transport can now be written as:

$$\overline{uc} = \bar{u} \cdot \bar{c} + \overline{u'c'} \tag{J.8}$$

The difference between the two model types in calculation of the gross transport is given in the following equation.

$$\begin{aligned} T_{2D} &= \bar{u} \cdot \bar{c} \\ T_{3D} &= \bar{u} \cdot \bar{c} + \overline{u'c'} \end{aligned} \tag{J.9}$$

Thus difference between the two models can be described by equation J.10. When the integral over depth of the product is negative the gross depth averaged transport in two dimensional runs will be larger.

$$\overline{u'c'} \tag{J.10}$$

For most part of the relative depth counts the following conclusion, when the velocity is below (above) its depth averaged value, the concentration is higher (lower) then the depth average value. Thus the product as described in equation J.10 is mainly negative (note that values near change in sine are all low) and therefore sum of all depth values will be negative.

We can now conclude with:

$$\overline{u'c'} < 0, \qquad T_{2D} > T_{3D} \tag{J.11}$$

In order to visualize the experiment, see have been made of the velocity, concentration and transport according to Whitehouse et al (2000) see Figure J-3.

Visualization of mind experiment II

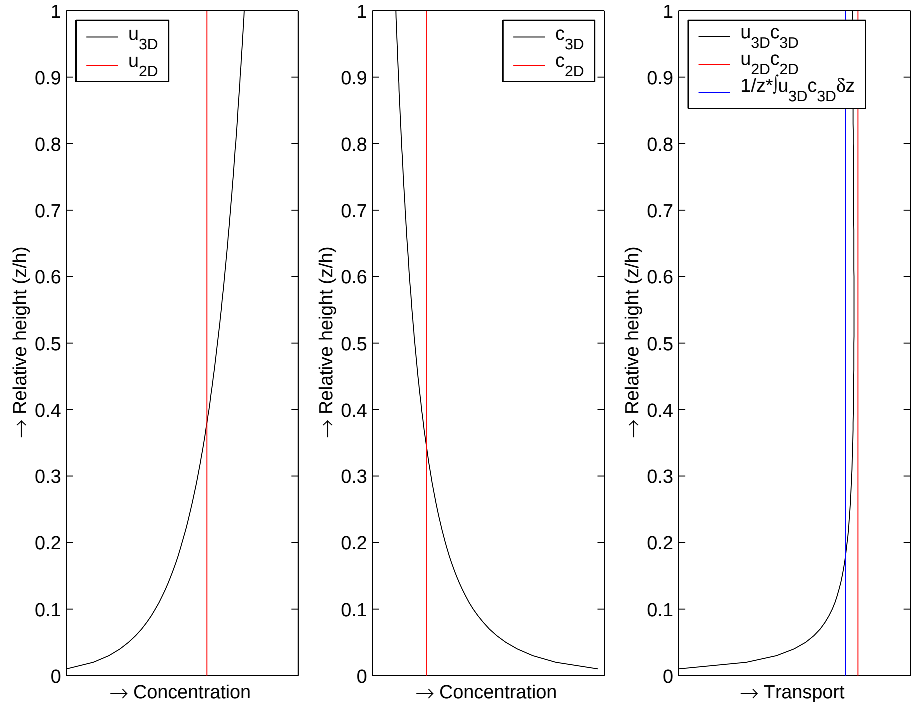

Figure J-3 Distribution of velocity, concentration and transport

J.3 Distribution of gross transport in the vertical

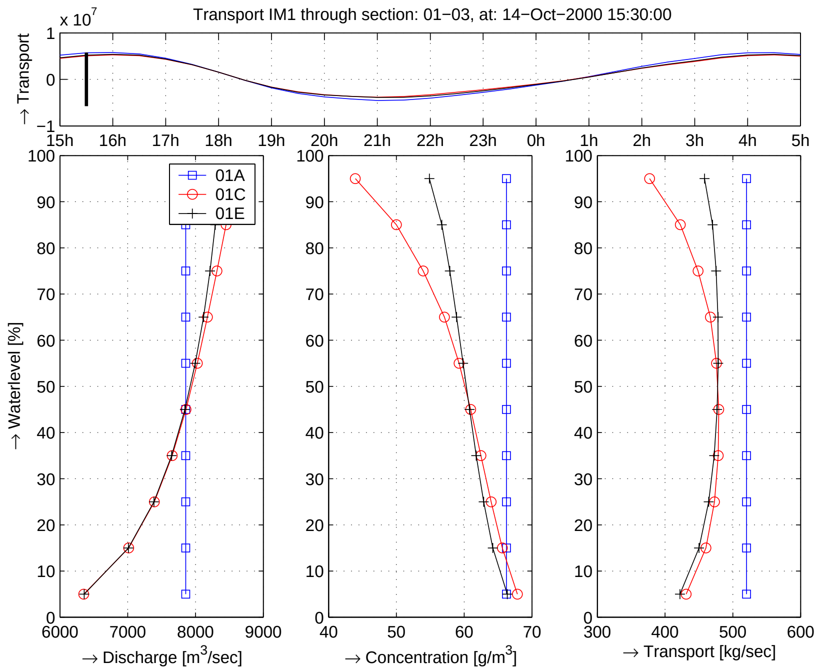

Figure J-4 profile of discharge, concentration and transport over depth in section 01-03 at maximum flood

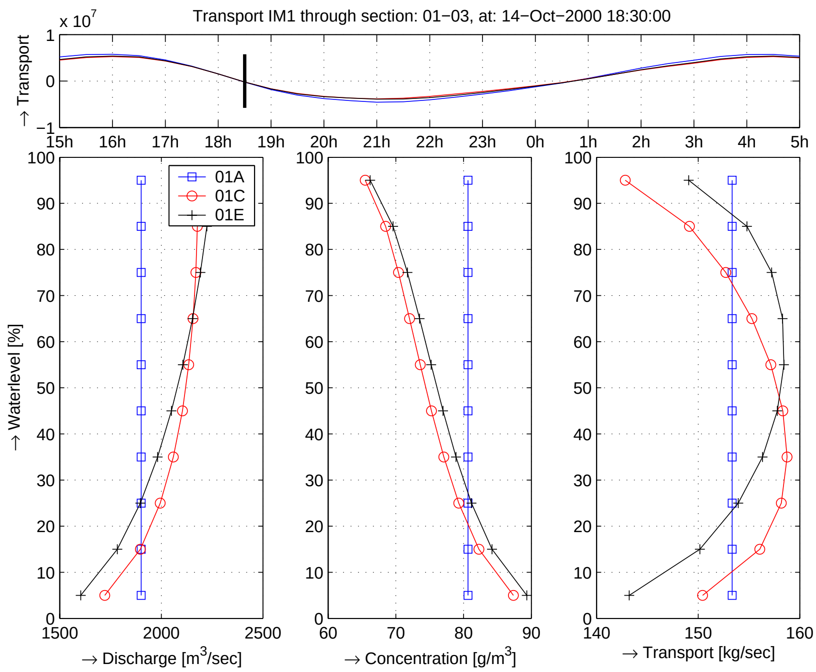

Figure J-5 Profile of discharge, concentration and transport over depth in section 01-03 approaching HWS.

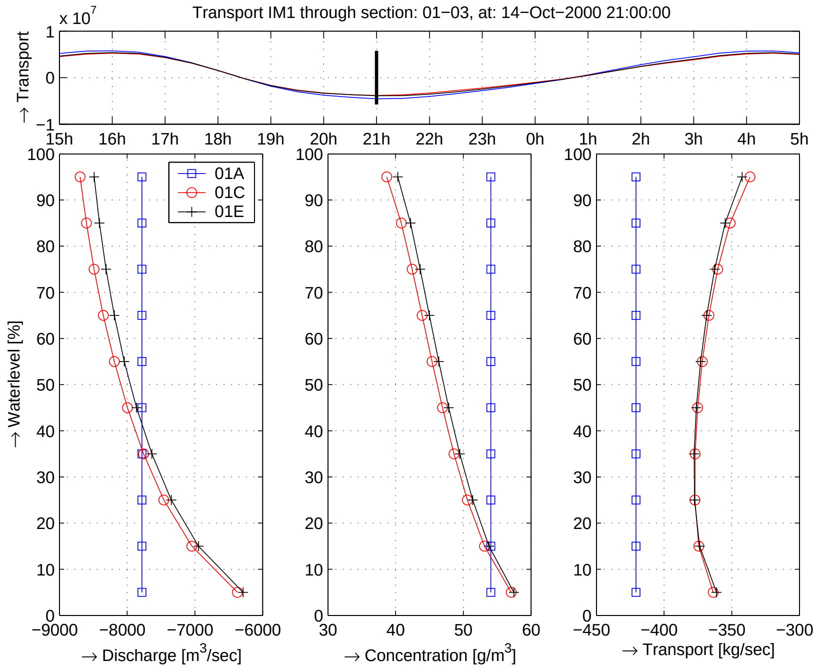

Figure J-6 Profile of discharge, concentration and transport over depth in section 01-03 at maximum ebb

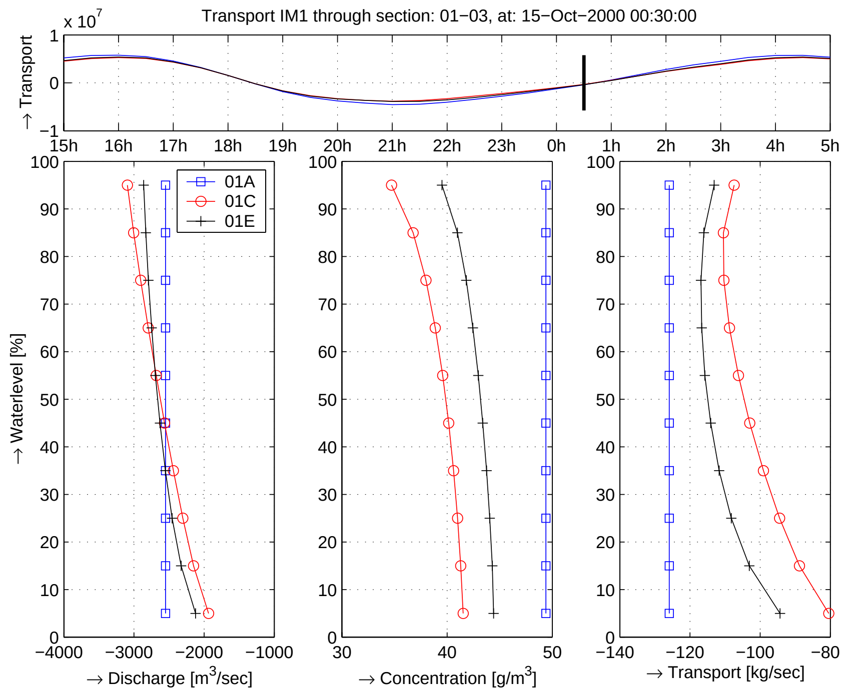

Figure J-7 Profile of discharge, concentration and transport over depth in section 01-03 approaching LWS.

J.4 Net transport distribution

Net discharge and transport distribution

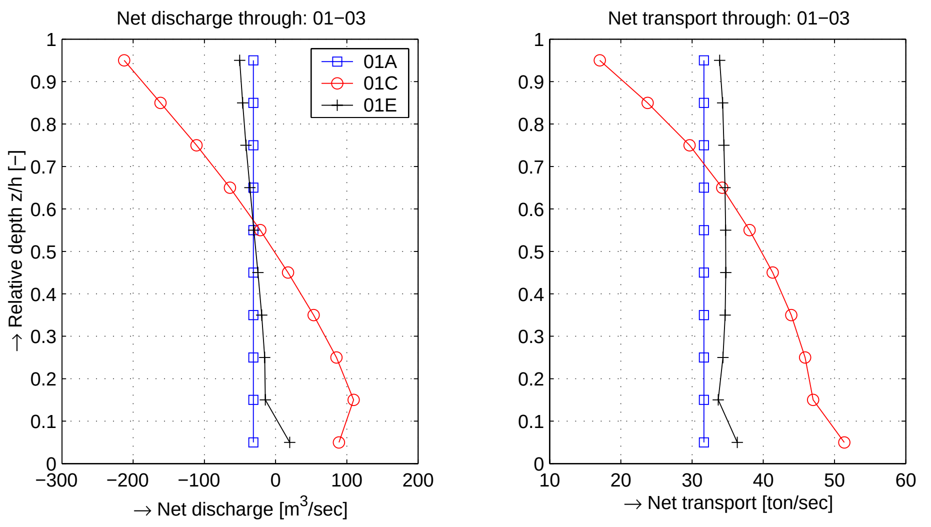

Figure J-8 Net discharge and transport profile section 01-03

Source: Accumulative discharges every 30min, integration period: 12-Oct-2000 02:00 to 15-Oct-2000 04:30.

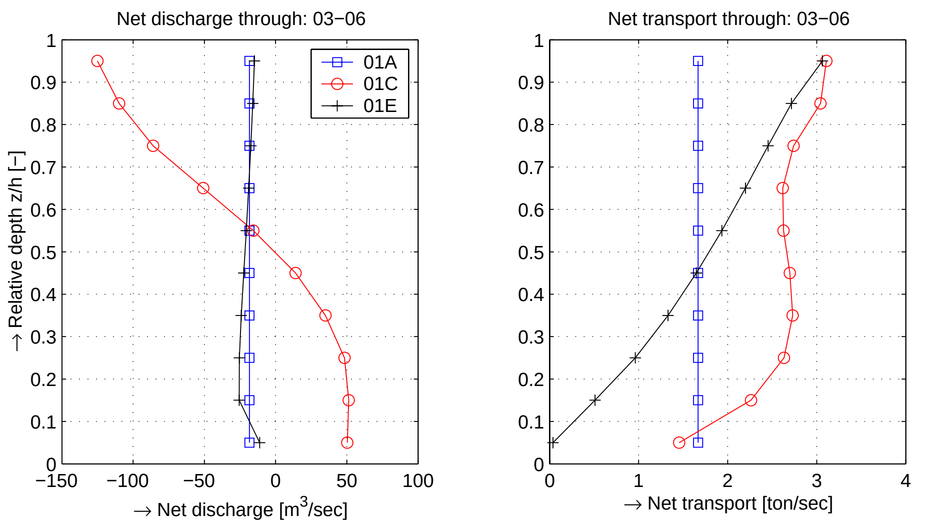

Figure J-9 Net discharge and transport profile cross-section 03-06

Source: Accumulative discharges every 30min, integration period: 12-Oct-2000 02:00 to 15-Oct-2000 04:30.

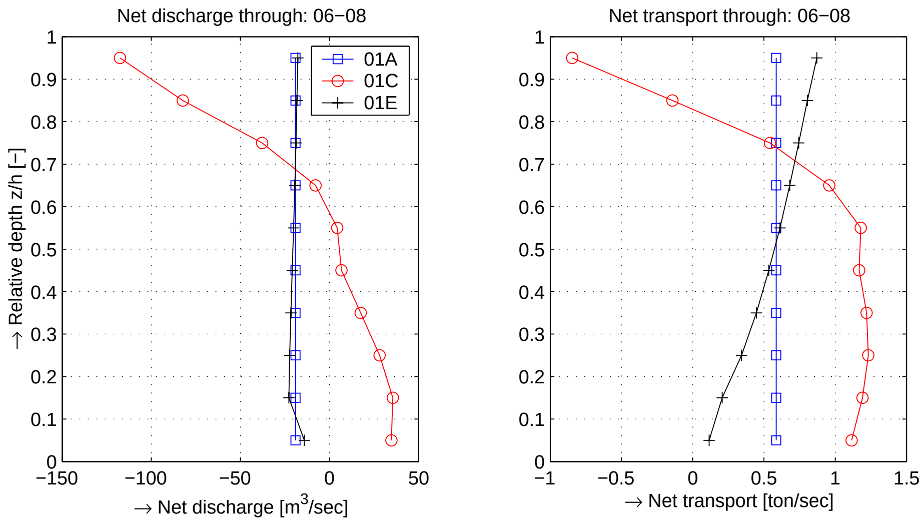

Figure J-10 Net discharge and transport profile cross-section 06-08

Source: Accumulative discharges every 30min, integration period: 12-Oct-2000 02:00 to 15-Oct-2000 04:30.

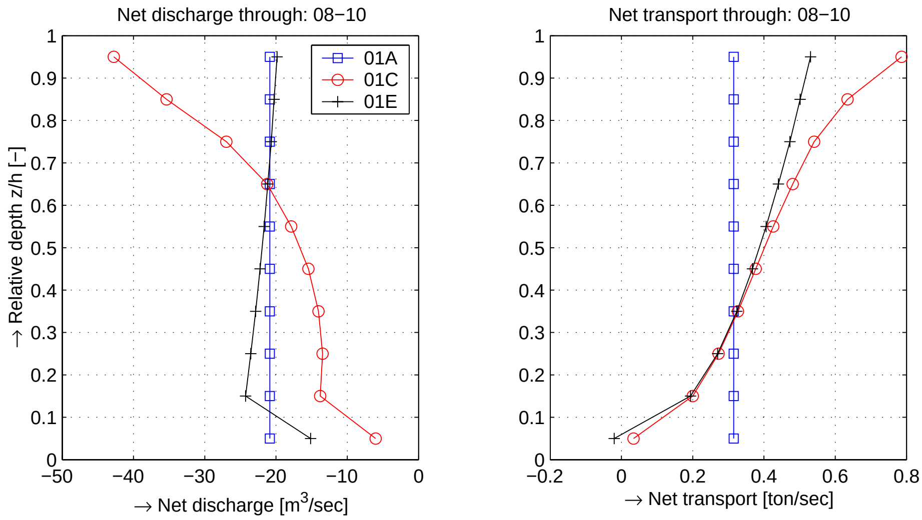

Figure J-11 Net discharge and transport profile cross-section 08-10

Source: Accumulative discharges every 30min, integration period: 12-Oct-2000 02:00 to 15-Oct-2000 04:30.

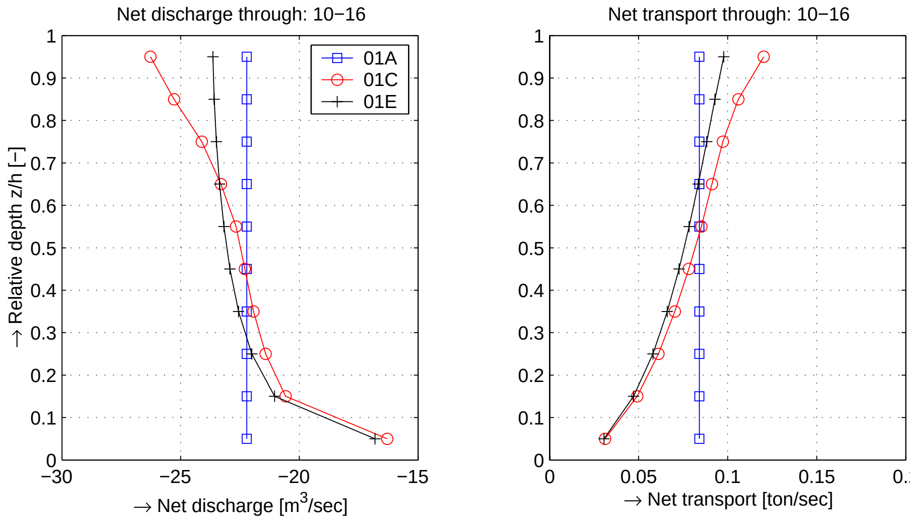

Figure J-12 Net discharge and transport profile cross-section 10-16

Source: Accumulative discharges every 30min, integration period: 12-Oct-2000 02:00 to 15-Oct-2000 04:30.

J.5 Sedimentation areas

GC01C: 3D, non-homogeneous density

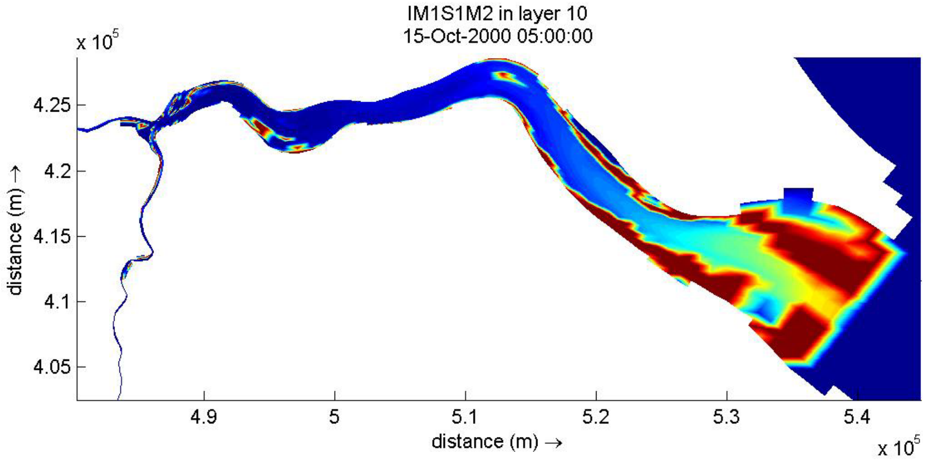

GC01E: 3D, homogeneous density

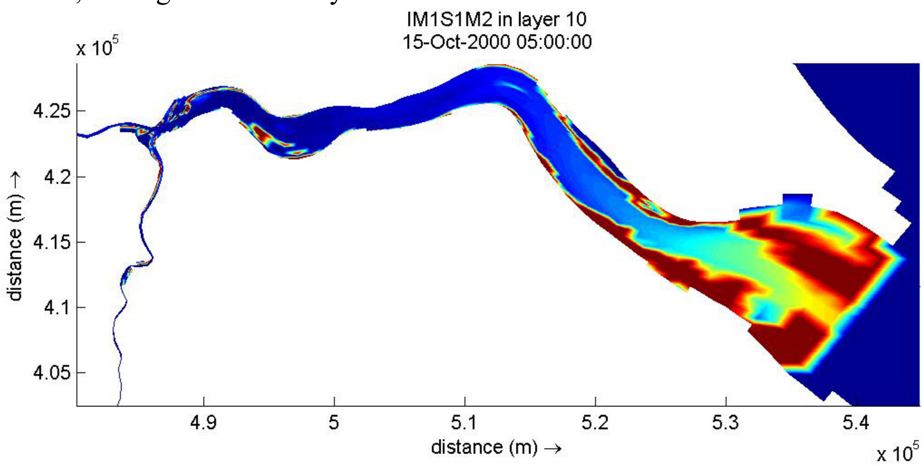

GC01A: 2Dh, homogeneous density

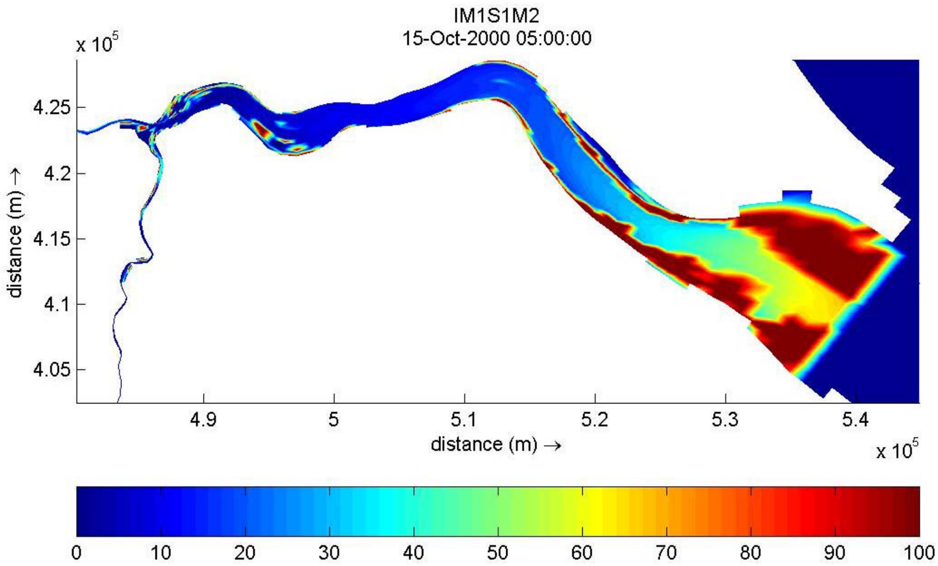

Figure J-13 GC01A, Sedimentation of Inorganic matter in bed layer (IM1S1M2) at 15 October 05:00.

GC01C: 3D, non-homogeneous density

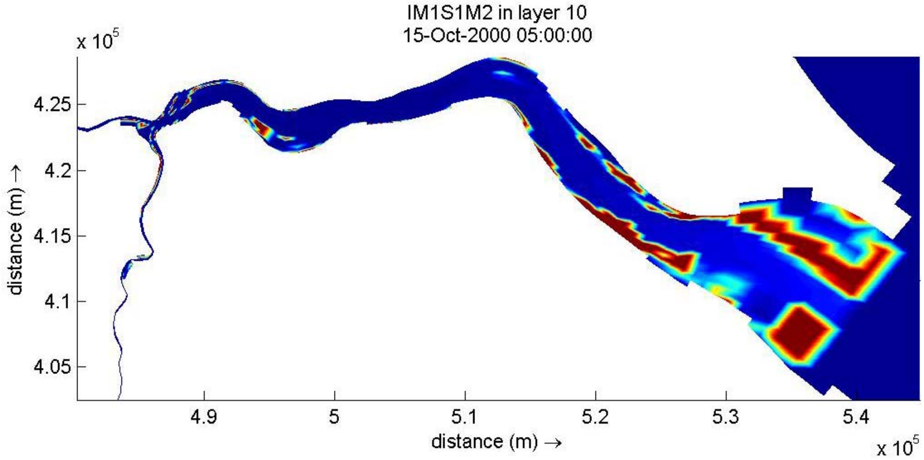

GC01E: 3D, homogeneous density

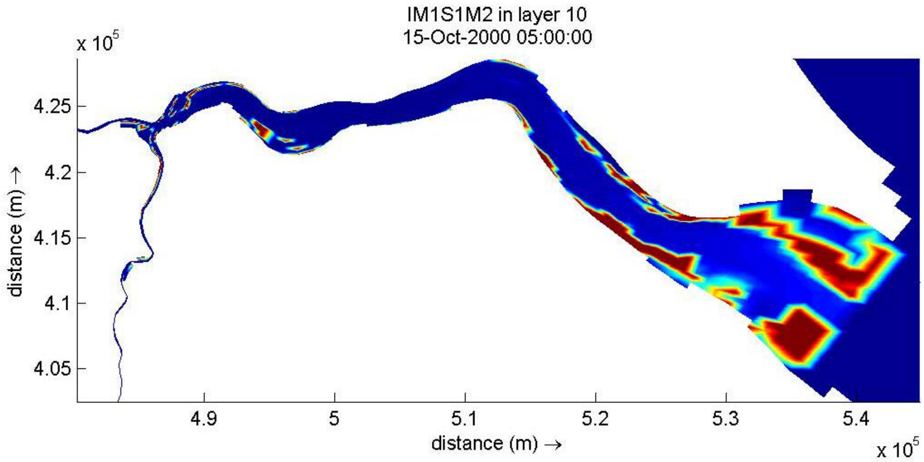

GC01A: 2Dh, homogeneous density

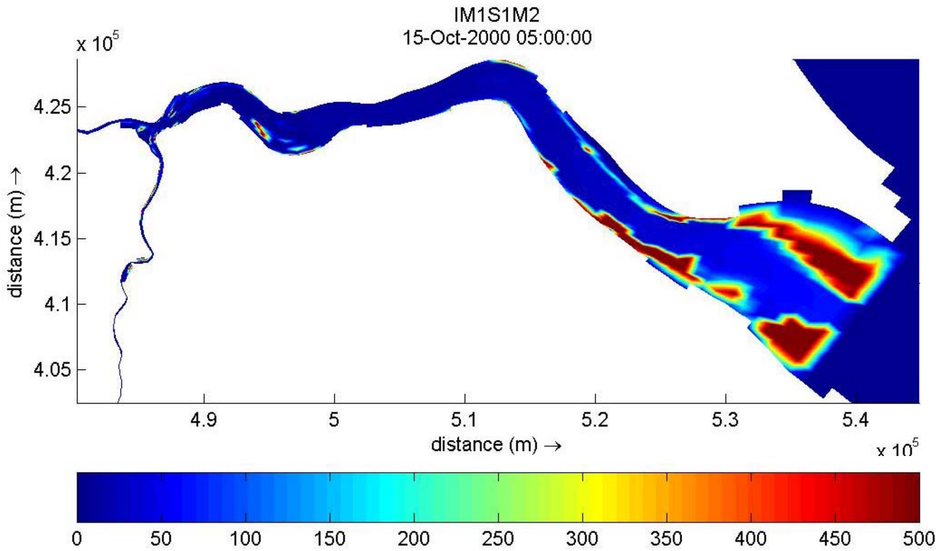

Figure J-14 GC01A, Sedimentation of Inorganic matter in bed layer (IM1S1M2) at 15 October 05:00.

J.6 Net fine sediment transport in aggregated grid

In the following figures the net transport is represented in the aggregated grid.

GC01C: 3D, Non-homogeneous density

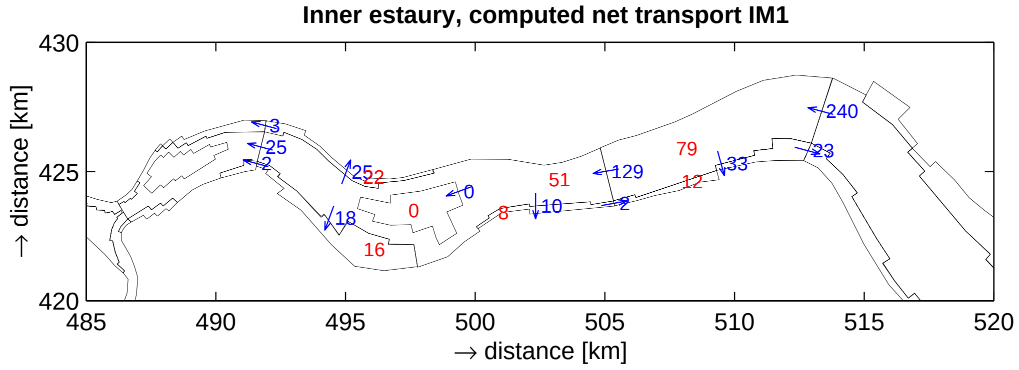

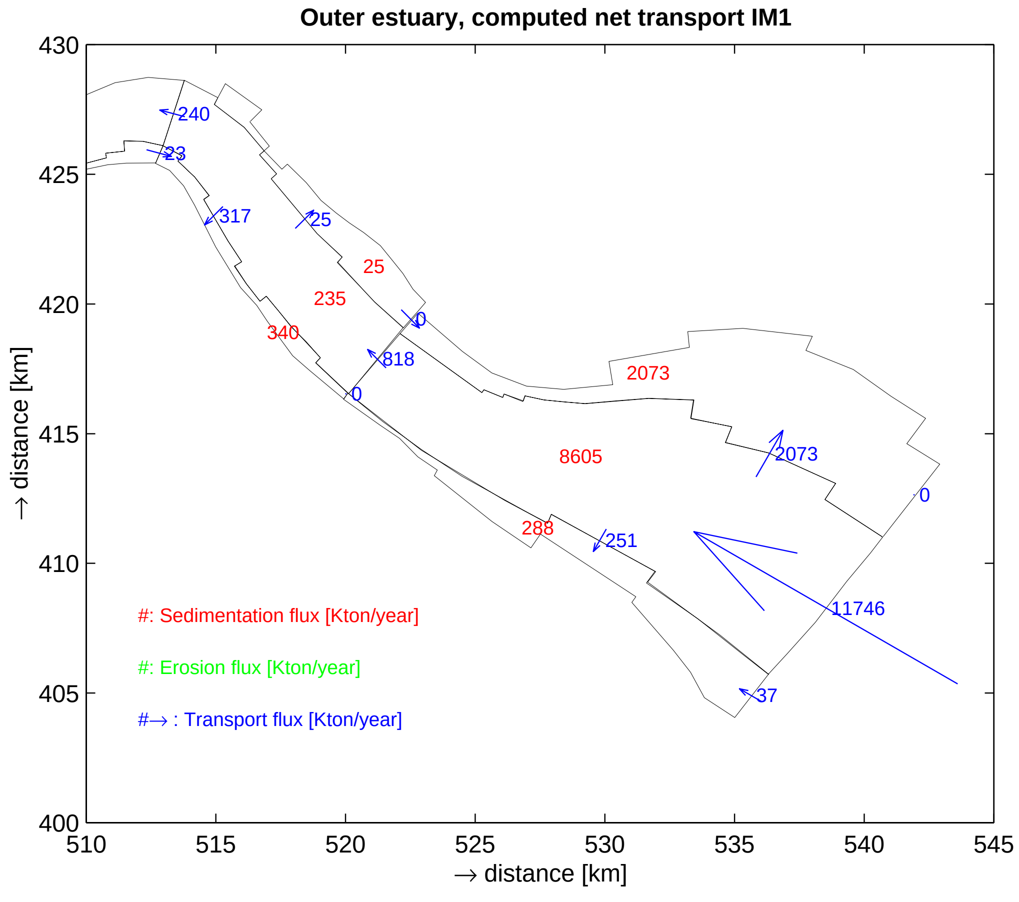

Figure J-15 Net transport of fine sediment in aggregated grid for run GC01C

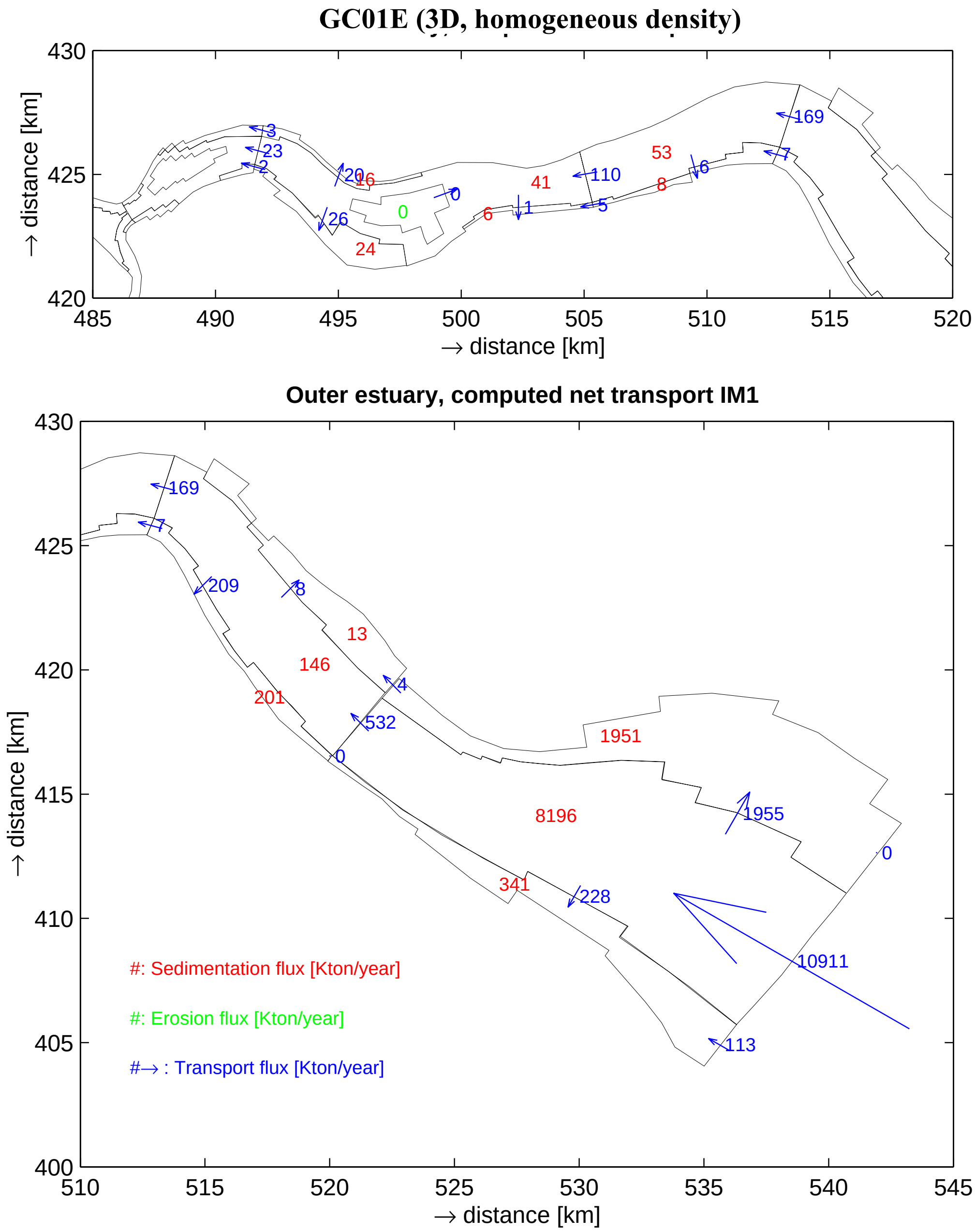

Figure J-16 Net transport of fine sediment in aggregated grid for run GC01E

GC01A: 2D, ks = 1mm

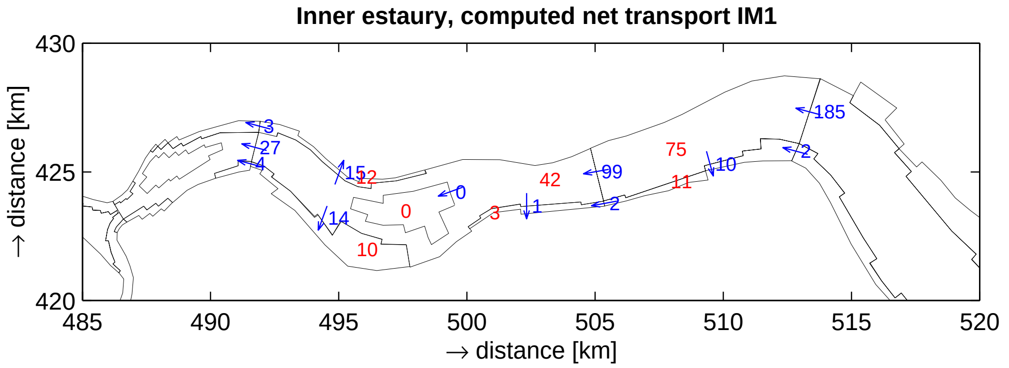

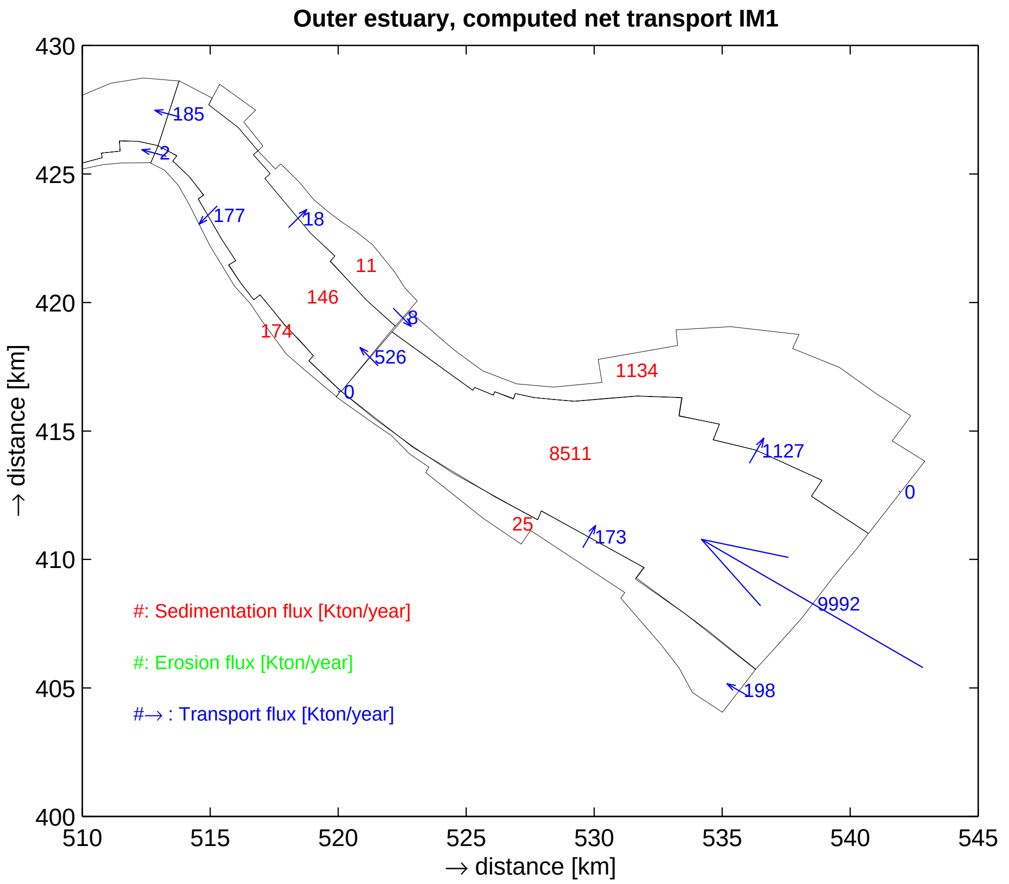

Figure J-17 Net transport of fine sediment in aggregated grid for run GC01A

J.7 Bed shear stress run GC01A, GC01C and GC01E

White Colebrook (ks=1mm)

01C Model description: 3D, ks = 1 cm, No homogeneous density	01E Model description: 3D, ks = 1 cm, No homogeneous density	01A Model description: 2D, ks = 1 cm, No homogeneous density
14-Oct-2000 15:00	(15:30 maximum flood current in Humber mouth)	
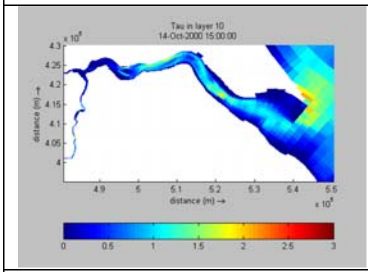	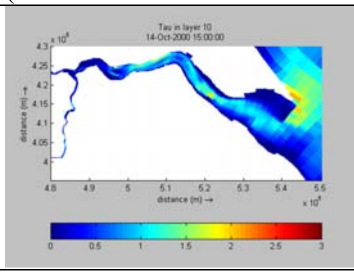	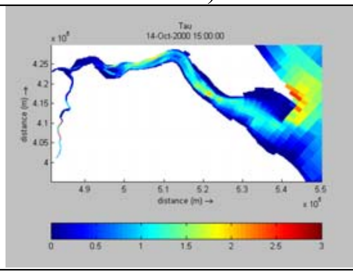
14-Oct-2000 17:00		
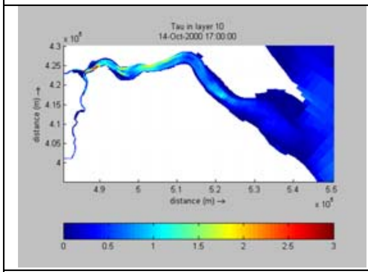	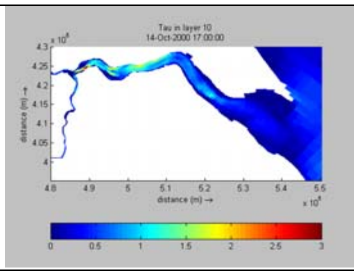	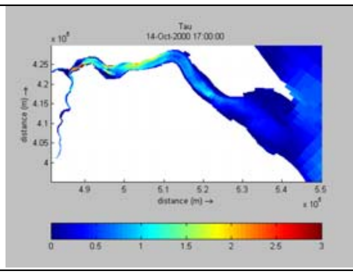
14-Oct-2000 19:00		
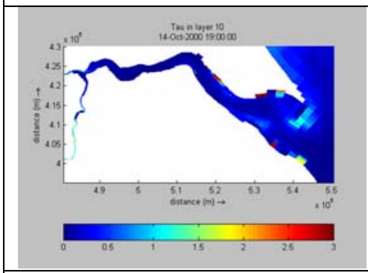	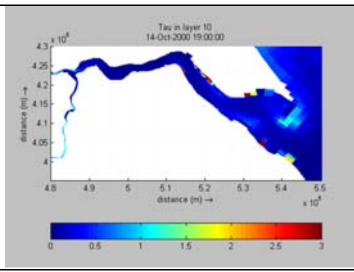	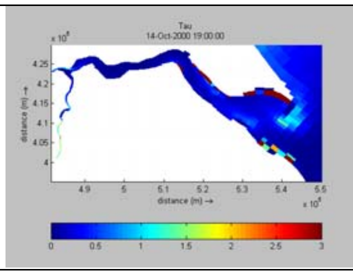
14-Oct-2000 21:00	(maximum ebb current)	
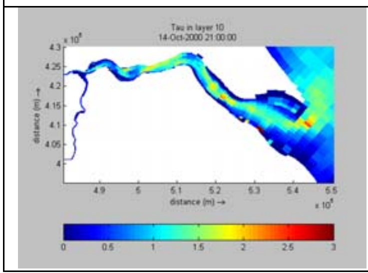	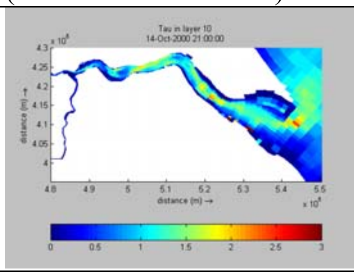	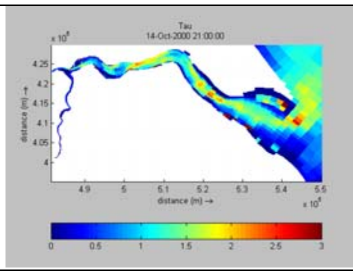

NEW WAQ version, White Colebrook (ks=1mm)

01C Model description: 3D, ks = 1 cm, no homogeneous density	01E Model description: 3D, ks = 1 mm, homogeneous density	01A Model description: 2D, ks = 1 mm, homogeneous density
14-Oct-2000 23:00		
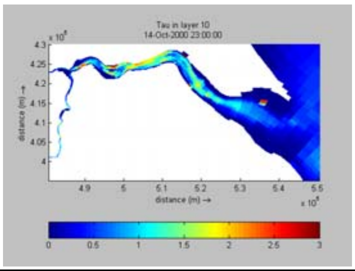	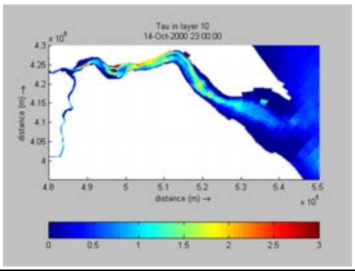	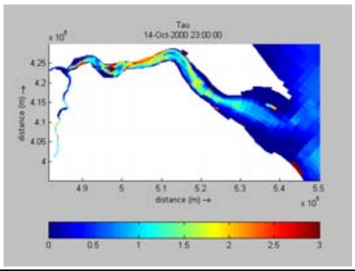
15-Oct-2000 01:00		
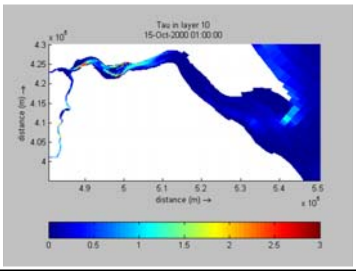	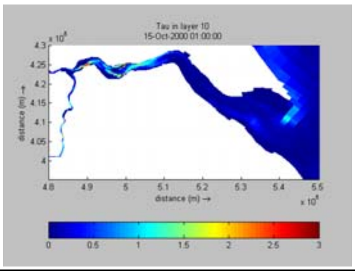	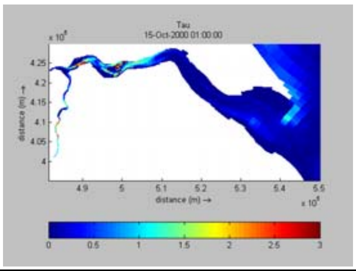
15-Oct-2000 03:00		
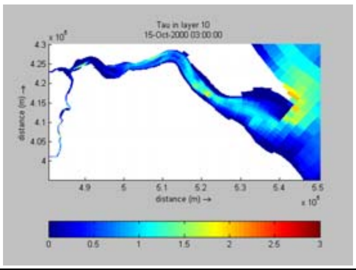	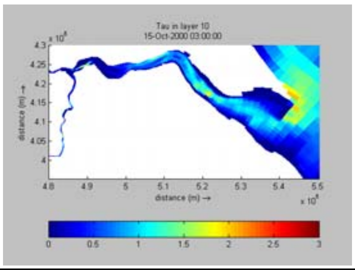	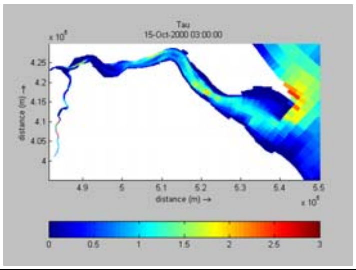
15-Oct-2000 05:00		
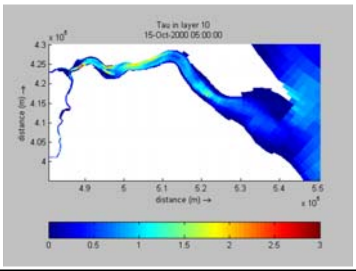	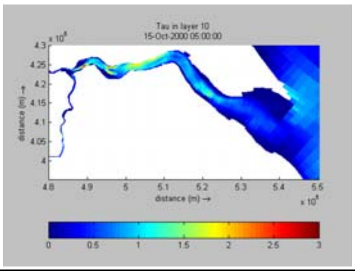	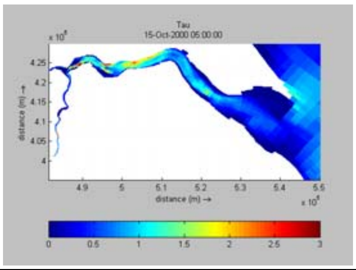

K Channel – Shoal interaction

K.1 Sedimentation areas 2D

GC01A: 2Dh, k_s = 1mm, homogeneous density

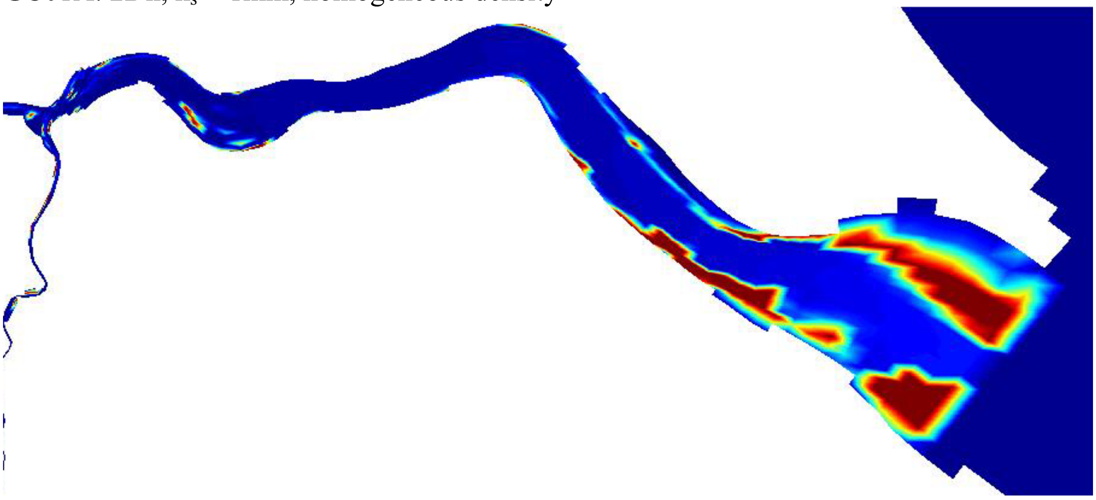

GC01B: 2Dh, k_s = 1cm, homogeneous density

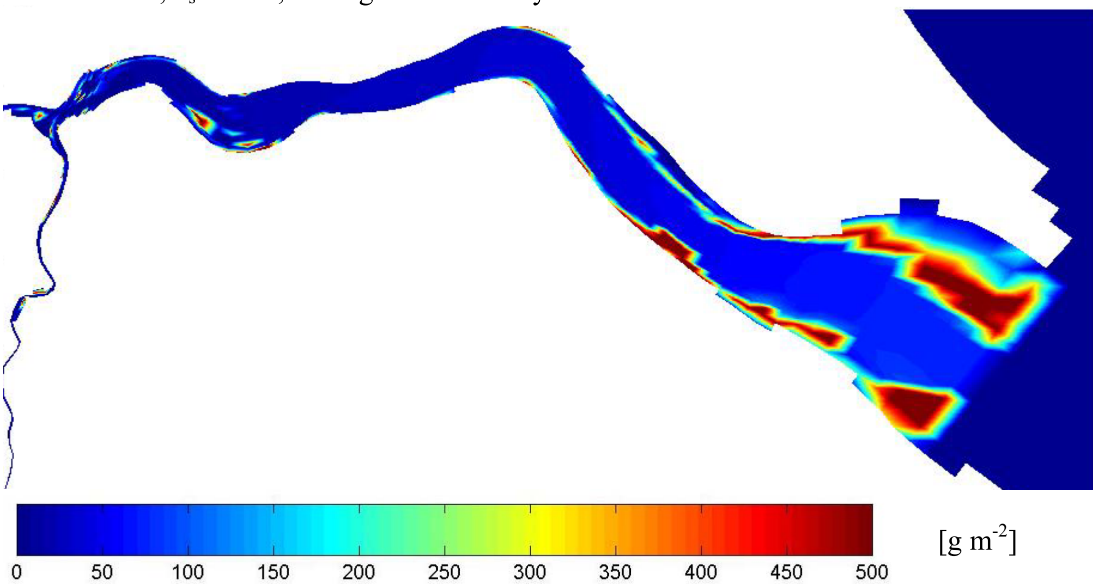

Gross sedimentation of inorganic matter in bed layer S1 (IM1S1M2).
Explanation: Sedimentation in grams m^{-2}, note that the values have been clipped above 50 T m^{-2}.

K.2 Net transport of fine sediments 2D

GC01A: 2Dh, k_s = 1mm, homogeneous density

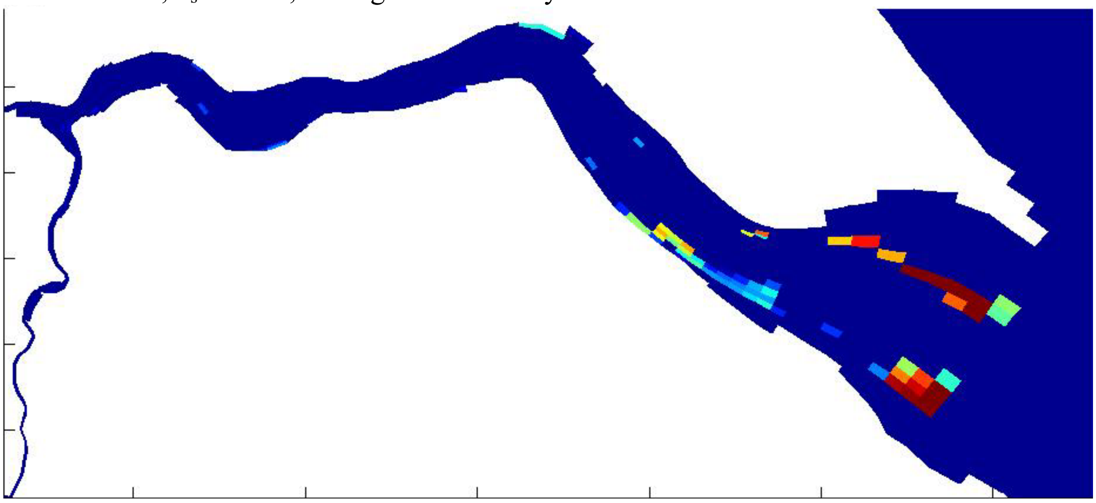

GC01B: 2Dh, k_s = 1cm, homogeneous density

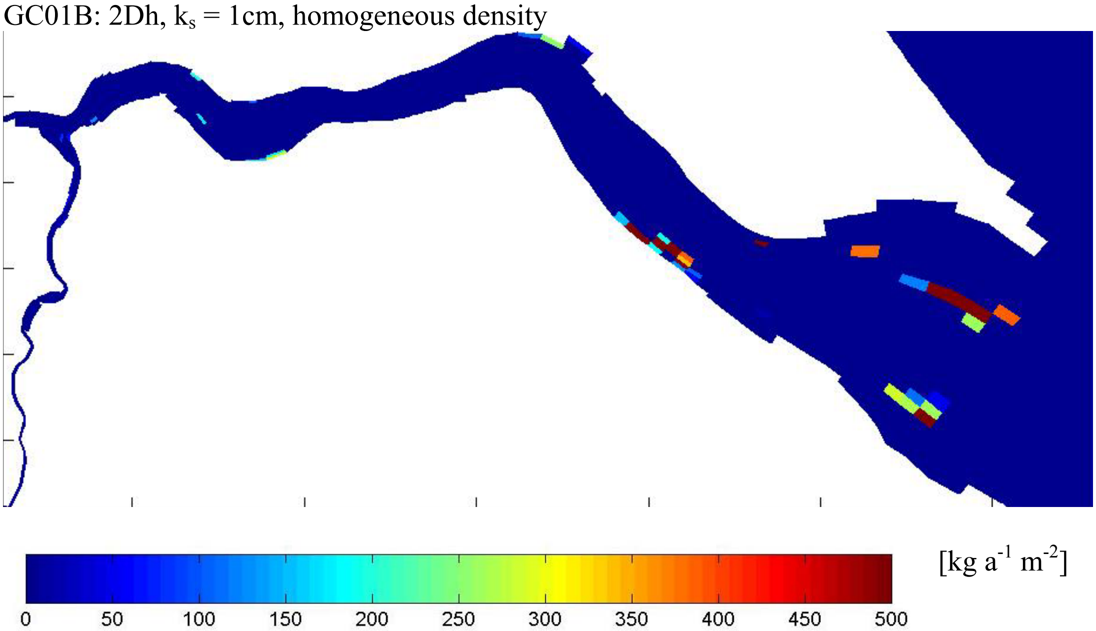

Figure K-1 Net sedimentation of inorganic matter in bed layer 2Dh (IM1S1M2) in [kg a^{-1} m^{-2}]

GC01B: 2D, ks = 1cm

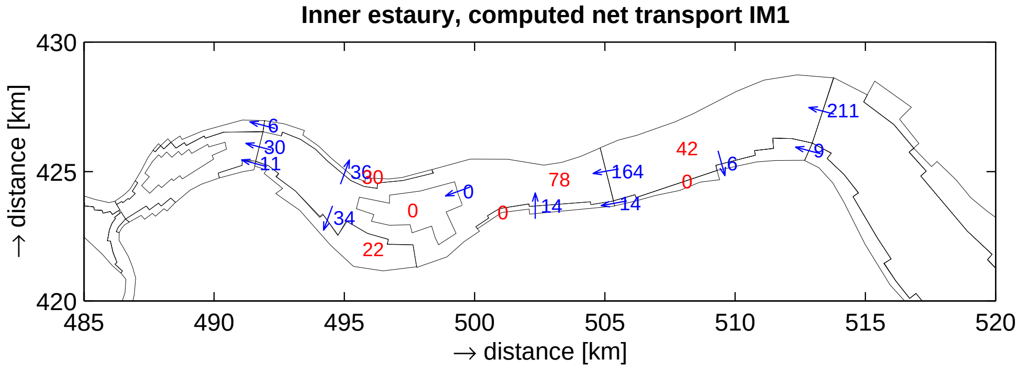

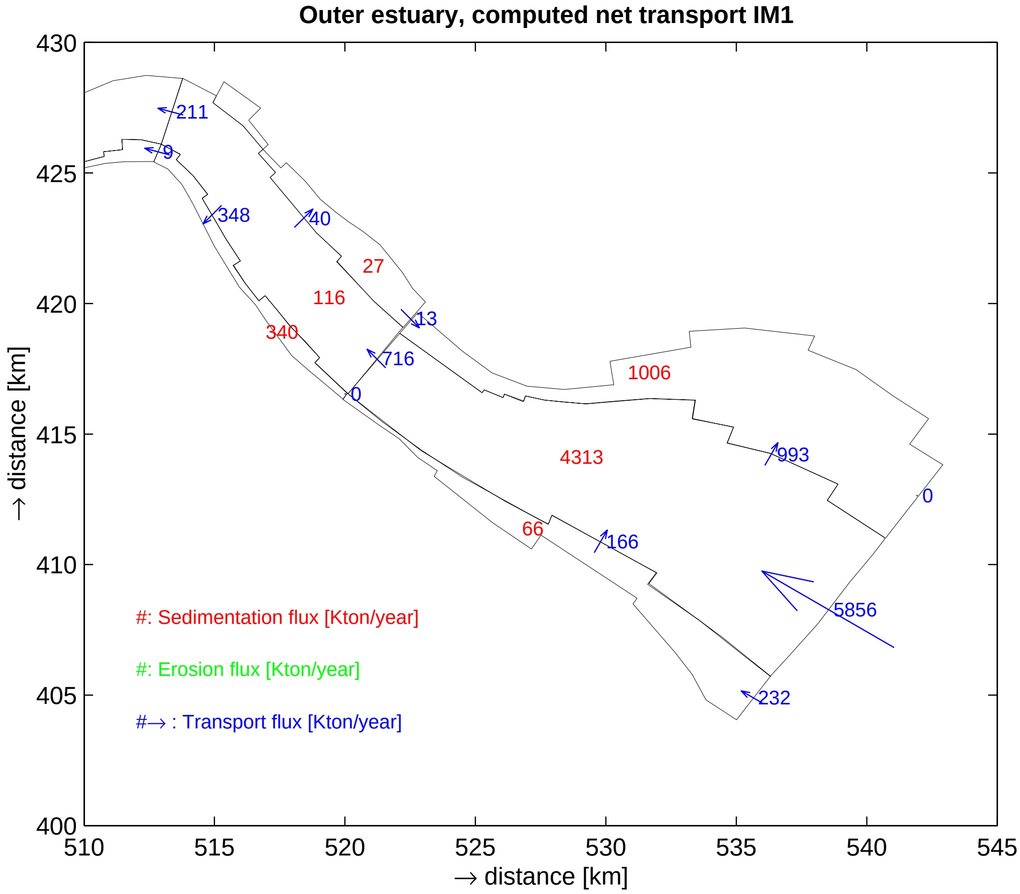

Figure K-2 Net transport of fine sediment in aggregated grid for run GC01B

GC01B: 2D, ks = 1cm

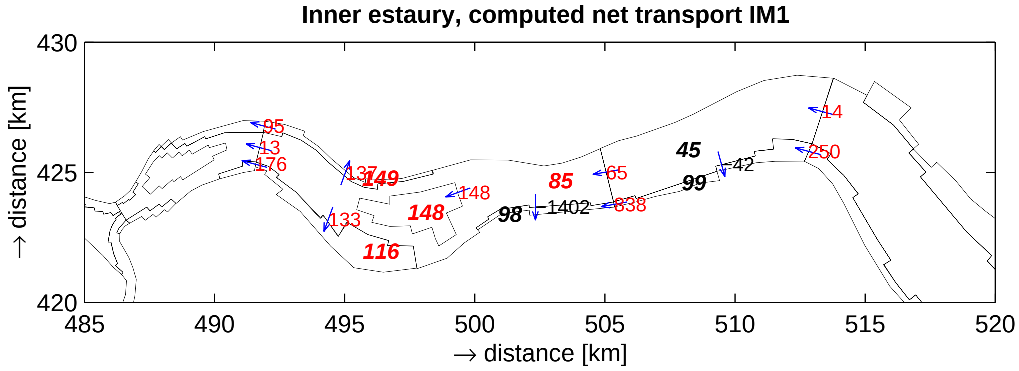

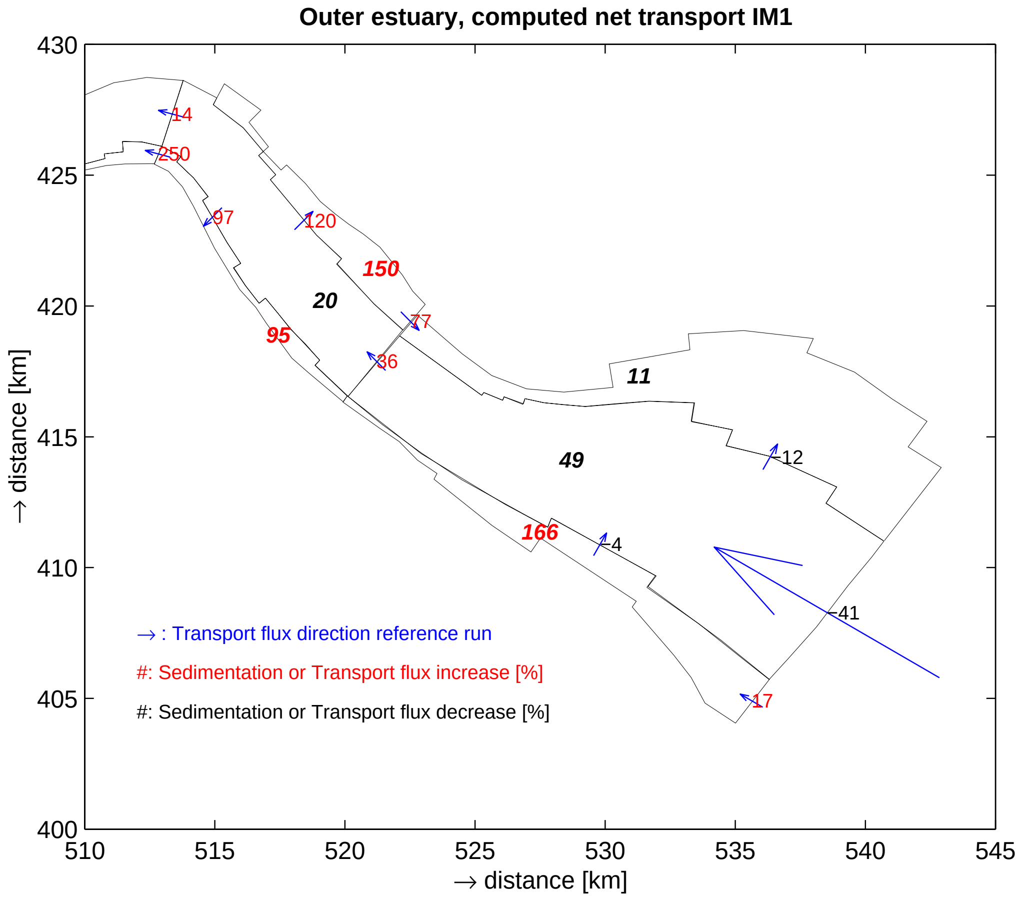

Figure K-3 Net transport of fine sediment in aggregated grid for run GC01B compared with run GC01A.

L Overview of sedimentation and erosion

L.1 Net fine sediment transport

Table L-1 Net fine sediment flux

Transect	01A	01B	01C	01D	01E	05A	16A	16C
1-> 2	0	0	0	0	0	0	0	0
1-> 3	9992	5856	11746	7541	10911	3042	8627	10132
1-> 4	198	232	37	26	113	124	179	21
2-> 3	-1127	-993	-2073	-1939	-1955	-291	-1022	-2259
3-> 4	-173	-166	251	433	228	-123	-162	222
2-> 5	-8	-13	0	-4	4	0	-6	-4
3-> 6	526	716	818	1249	532	16	274	463
4-> 7	0	0	0	0	0	0	0	0
5-> 6	-18	-40	-25	-30	-8	-1	-13	-24
6-> 7	177	348	317	621	209	12	125	216
6-> 8	185	211	240	437	169	2	69	105
7-> 9	2	9	-23	-55	7	0	2	-19
8-> 9	10	6	33	53	6	0	-3	22
8-> 10	99	164	129	254	110	0	30	43
9-> 11	2	14	-2	-2	5	0	-1	-4
10-> 11	1	-14	10	3	1	0	1	8
10-> 12	0	0	0	0	0	0	0	0
10-> 14	14	34	18	36	26	0	4	6
13-> 10	-15	-36	-25	-62	-20	0	-4	-8
13-> 15	3	6	3	4	3	0	1	1
10-> 16	27	30	25	38	23	0	7	7
14-> 17	4	11	2	5	2	0	1	0

Explanation: Net fine sediment transport through transects in kTon/year.

L.2 Net fine sedimentation

Table L-2 Net fine sedimentation

Transect	01A	01B	01C	01D	01E	05A	16A	16C
A-CH	8511	4313	8605	3920	8196	2857	7493	7188
A-NT	1134	1006	2073	1943	1951	291	1028	2263
A-ST	25	66	288	459	341	1	17	243
B-CH	146	116	235	161	146	3	67	117
B-NT	11	27	25	26	13	0	6	21
B-ST	174	340	340	676	201	11	123	235
C-CH	75	42	79	130	53	2	42	40
C-ST	11	0	12	0	8	0	0	7
D-CH	42	78	51	115	41	0	14	14
D-NT	12	30	22	58	16	0	4	8
D-IS	0	0	0	0	0	0	0	0
D-SET	3	0	8	1	6	0	0	4
D-SWT	10	22	16	31	24	0	3	5

Explanation: Net fine sedimentation in segments in Kton/year.

M Previous Delft3D DELWAQ version

M.1 Bed shear stress formulation in previous DELWAQ version

Comparison of runs GC01A and GC01C showed that the bed shear stress showed large differences. In order to explain these values a further analysis was done by comparing run 01A and 01E. Even in these runs a large difference was found in the bed shear stress. (See figures: “OLD WAQ version, White Colebrook (ks=1mm)”)

A calculation by hand showed that the bed shear stress in all 3D runs did not correspond with the values computed by DELWAQ.

White Colebrook:

$$C_{2D} = 18 \cdot \log_{10}\left(\frac{12H}{k_s}\right) \tag{M.1}$$

$$\tau_{flow2D} = \frac{\rho_l \cdot g}{C_{2D}^{\ 2}} \cdot |U|^2 \tag{M.2}$$

$$C_{3D} = C_{2D} + \frac{\sqrt{g}}{\kappa} \cdot \left(1 + \ln(\frac{0.5 \cdot \Delta z_b}{H}\right) \tag{M.3}$$

$$\tau_{flow3D} = \frac{\rho_l \cdot g}{C_{3D}^{\ 2}} \cdot |u_b|^2 \tag{M.4}$$

The uniform depth value (H) used to calculate the C_{2D} in 3D simulations was not the total depth (H) but the depth of the bottom layer (Δz_b). This results in an underestimation of the C_{2D}, and therefore an underestimation of C_{3D}. An underestimation of the Chezy value is equal to an overestimation of the bed roughness which results in a overestimation of bedshear stress as can be shown in figures: “OLD WAQ version, White Colebrook (ks=1mm)”.

M.2 Bed shear stress comparison in previous DELWAQ version between 2D and 3D homogeneous

01E, Model description: 3D, ks = 1 mm, No homogeneous density	01A, Model description: 2D, ks = 1 mm, No homogeneous density

14-Oct-2000 15:00

(15:30 maximum flood current in Humber mouth)

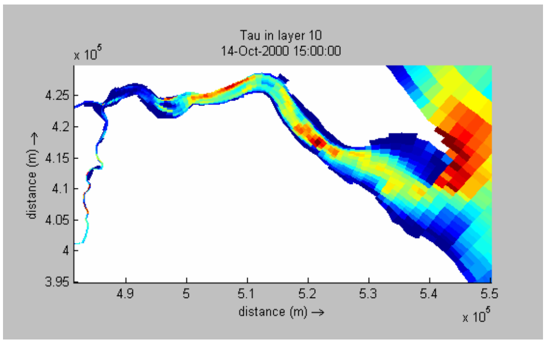

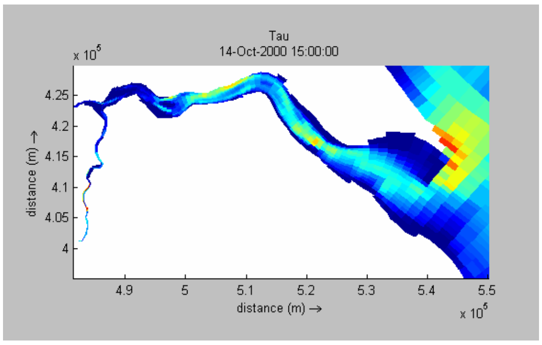

14-Oct-2000 17:00

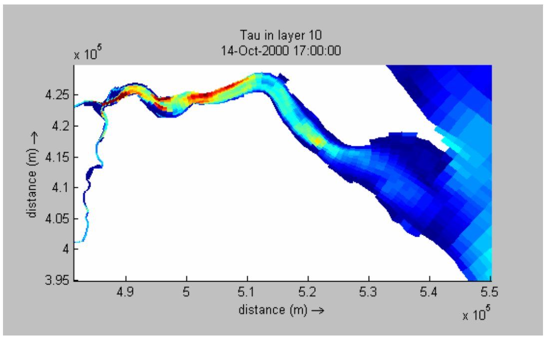

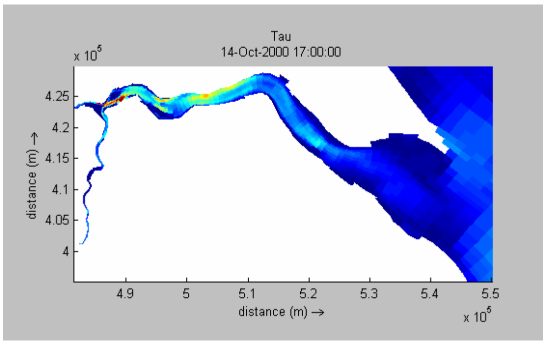

14-Oct-2000 19:00

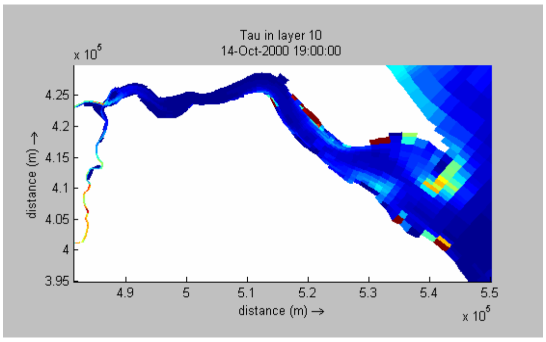

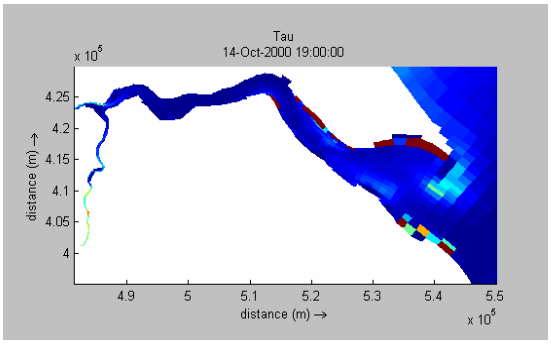

Bed shear stress [Pa]

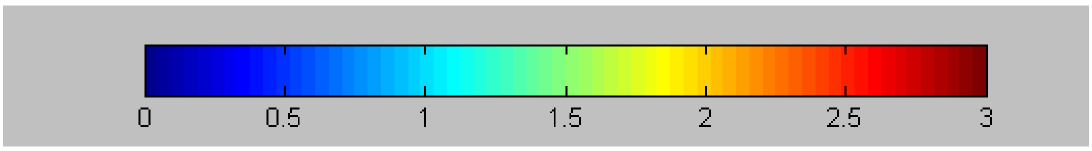

01E	**01A**
14-Oct-2000 21:00	
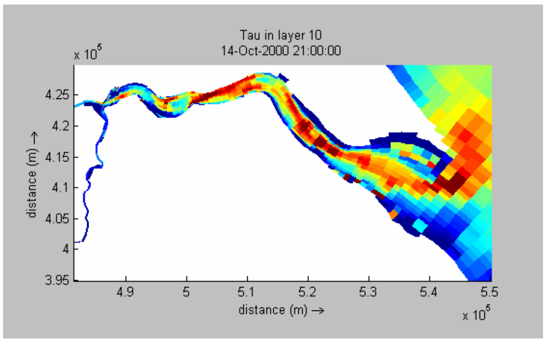	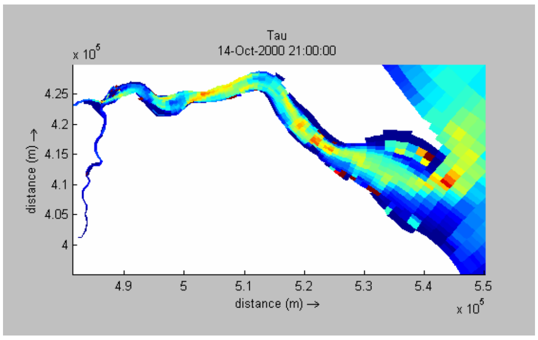
14-Oct-2000 23:00	
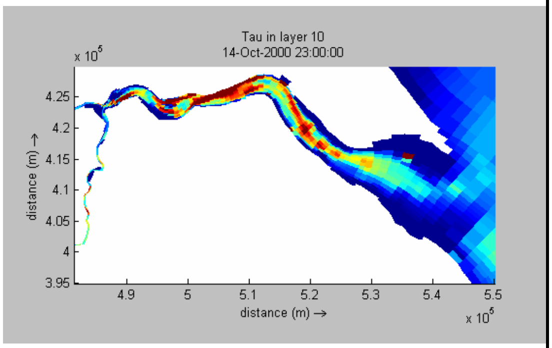	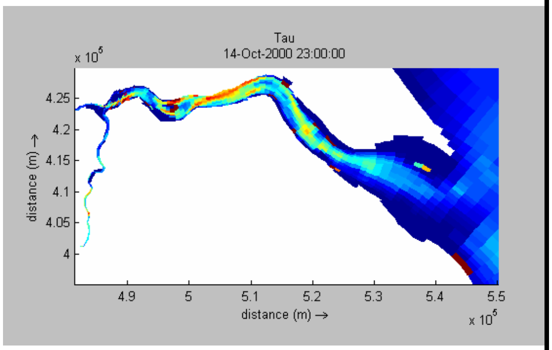
15-Oct-2000 01:00	
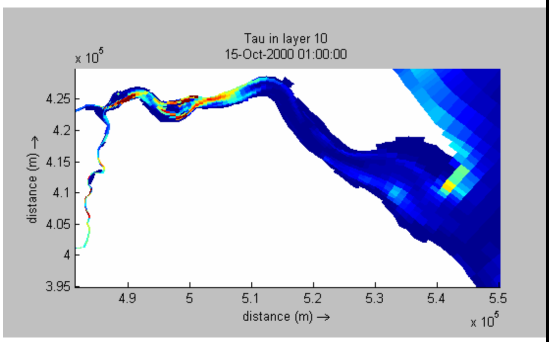	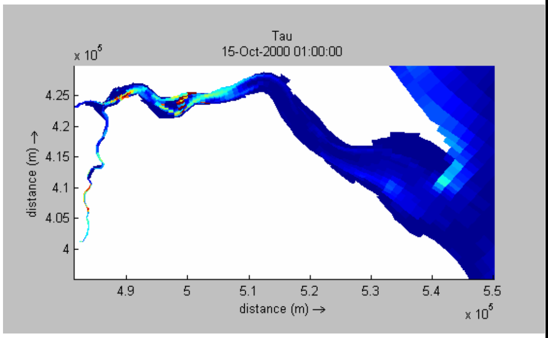
Bed shear stress [Pa]	
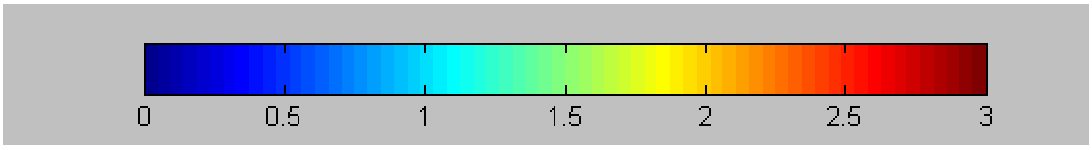	

01E	**01A**

15-Oct-2000 03:00

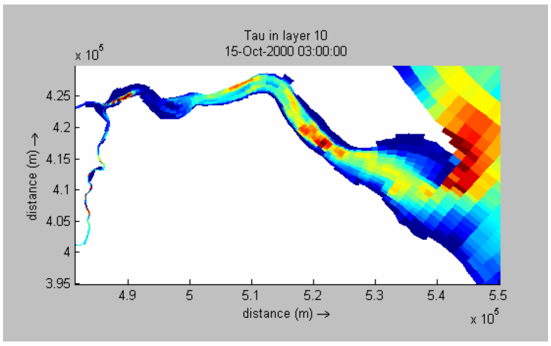

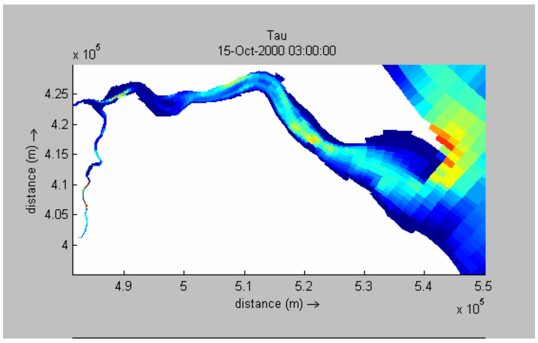

15-Oct-2000 05:00

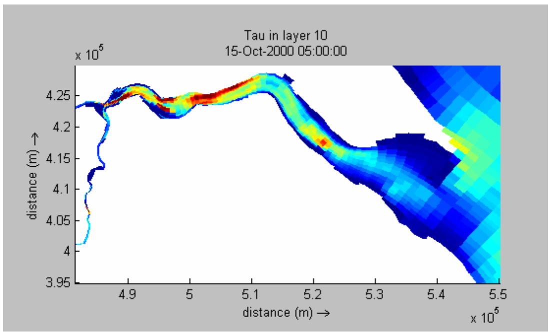

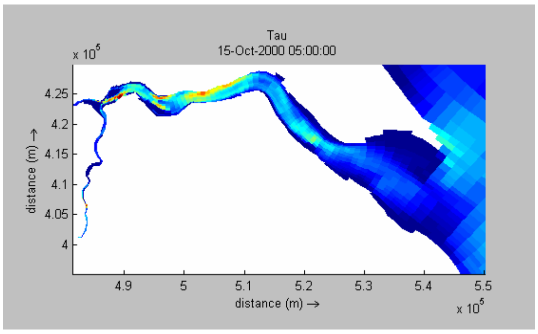

Bed shear stress [Pa]